

MOHAMADAMIN FOROUZANDEHMEHR

Mathematical Modeling of Cardiomyocytes Pathophysiology and Biomechanics

MOHAMADAMIN FOROUZANDEHMEHR

Mathematical Modeling of Cardiomyocytes
Pathophysiology and Biomechanics

ACADEMIC DISSERTATION

To be presented, with the permission of
the Faculty of Medicine and Health Technology
of Tampere University,
for public discussion in the auditorium TB109
of the Tietotalo building, Korkeakoulunkatu 1, Tampere,
on 16 February 2024, at 12 o'clock.

ACADEMIC DISSERTATION

Tampere University, Faculty of Medicine and Health Technology
Finland

<i>Responsible supervisor and Custos</i>	Professor Jari Hyttinen Tampere University Finland	
<i>Supervisors</i>	Adjunct professor Jussi Koivumäki Tampere University Finland	Docent Michelangelo Paci Tampere University Finland
<i>Pre-examiners</i>	Professor Eleonora Grandi University of California at Davis United States	Professor Beatriz Trenor Valencia Polytechnic University Spain
<i>Opponent</i>	PD Dr.-Ing. Axel Loewe Karlsruhe Institute of Technology Germany	

The originality of this thesis has been checked using the Turnitin OriginalityCheck service.

Copyright ©2024 author

Cover design: Roihu Inc.

ISBN 978-952-03-3302-7 (print)

ISBN 978-952-03-3303-4 (pdf)

ISSN 2489-9860 (print)

ISSN 2490-0028 (pdf)

<http://urn.fi/URN:ISBN:978-952-03-3303-4>



Carbon dioxide emissions from printing Tampere University dissertations have been compensated.

PunaMusta Oy – Yliopistopaino
Joensuu 2024

To Mohammad Bakhtiarpour Dashtbozorg

ACKNOWLEDGEMENTS

This doctoral thesis research was conducted in Computational Biophysics and Imaging Group (CBIG) of Faculty of Medicine and Health Technology (MET) at Tampere University during 2019-2023, as a part of Center of Excellence in Body-on-Chip Research. I wish to thank Prof. Tapio Visakorpi and Prof. Seppo Parkkila the former and present deans of the faculty for providing an excellent interdisciplinary research environment during my studies. Further, I appreciate all the scholarships supporting this thesis, including the MET Doctoral Program in Biomedical Sciences and Engineering and Pirkanmaa Fund of Finnish Cultural Foundation.

My undying gratitude to Prof. Jari Hyttinen, the principal investigator of CBIG, Head of BioMediTech, and my main thesis supervisor for the great research opportunity in his group since 2019. Working under your supervision and in such skilled environment was a great privilege. I wish to express my deepest thanks to Drs. Jussi T. Koivumäki and Michelangelo Paci, my co-supervisors, for their masterful supervision, worldclass research, invaluable inputs, magnificent leadership, and contribution to this thesis. I wish to extend my appreciation to the thesis follow-up group members Drs. Samuel Wall and Mari Pekkanen-Mattila for their expert opinions that assisted the structure of the progress of the thesis.

My special gratitude also goes to Prof. Katriina Aalto-Setälä and MSc. Mahmoud Gaballa for the helpful discussions that greatly assisted Study IV of this doctoral thesis. I wish to express my gratitude to the thesis pre-examiners Profs. Eleonora Grandi and Beatriz Trenor for their time and valuable comments.

My heartfelt appreciation to my parents for setting an example for my scientific carrier and their steadfast support throughout my whole life. I want to specially thank my wife Soudabeh for her unconditional love, support, and expert remarks that paved my way throughout conducting the research.

Tampere, October 2023

ABSTRACT

Resolving the ethical concerns regarding animal-based experiments, human induced pluripotent stem cell-derived cardiomyocytes (hiPSC-CMs) represent a virtually limitless pool of human *in vitro* models in cardiology. They open up new opportunities for patient-specific safety cardiac pharmacology as they share the same genotype with patients and exhibit the same pathological traits as their real-life counterparts. Computational models of hiPSC-CMs assist us in bridging important vital gaps. Namely, i) Enhancing our quantitative understanding of intracellular interactions in preclinical drug trials and exploring genotype-phenotype relationships; ii) High-throughput risk stratification and prediction of vulnerability to arrhythmia; iii) addressing electrophysiological, contractile, and biochemical differences between *in vitro* hiPSC-CMs and *in silico* human adult ventricular CMs, since the combination of *in vitro* hiPSC-CMs and *in silico* human adult ventricular cardiomyocytes (hV-CMs) has been proposed as a promising new paradigm in drug screening by the FDA (the comprehensive proarrhythmia assay).

The first aim of this thesis was to develop a robust whole-cell model of hiPSC-CMs electromechanics capturing the mechano-electric feedback by integrating a reparametrized contractile element (CE) into the ionic model of hiPSC-CMs. The second aim was proposing a computational approach toward deep-phenotyping mutation-specific hypertrophic cardiomyopathy (HCM), specifically MYH7^{R403Q/+} and exploring the effects and action mechanisms of Mavacamten (MAVA), Blebbistatin (BLEB), and Omecamtive mecarbil (OM). The final aim was refining the hiPSC-CMs model of electro-mechano-energetic coupling to explore the interorganellar crosstalks in ischemia/reperfusion (I/R). A novel oxygen dynamic formulation was introduced to link the capillary level to extracellular oxygen concentrations affected by Na⁺/K⁺ exchanger, sarcolemmal Ca²⁺ pump current, and the contractile ATPase rate. The common methodology in Studies I-IV of the thesis is use of a set of *in vitro* data for model calibrations and another set of *in vitro* data for quantitative/qualitative results validations prioritizing hiPSC-CMs *in vitro* findings.

Meeting the accurate fractional cell shortening (FCS), time from peak contraction to 50% of relaxation (CRT50), and active tension (AT) amplitude were introduced as the optimization goals of the cell electromechanical calibrations. The sensitivity

analysis on the CE machinery in Studies I & II offer a robust reparameterization roadmap from animal-based computational models to hiPSC-CMs phenotype. A correct categorization of inotropic effects of non-cardiomyocytes was recapitulated in accord with hiPSC-CMs experimental reports. In Study III, the metabolite-sensitivity in the CE played a key role in capturing the contractile dysfunction, in terms of hypercontractility and irregular CRT50, in MYH7^{R403Q/+} HCM and the cardioprotective effect of MAVA, through affecting myofilament crossbridge (XB) state transitions and Pi, MgATP, and MgADP. The therapeutic compounds in Study III were sarcomere targeting molecules; MAVA, BLEB, and OM. Therefore, their mechanism of action was modeled by CE optimizations accordingly, and the XB parameter governing the dose-dependence of OM and BLEB inotropic effect was identified. In Study IV, in accord with Levosimendan (Levo) inotropic data, the dose-dependent effect of Levo as an I_{KATP} agonist was included in the drug-induced calibration besides the channel-blockings for I_{Na}, I_{CaL}, and I_{Kr}. Explicitly, introducing the novel oxygen dynamic formulation with a contractile ATPase rate was a first step toward linking the cellular energetics to oxygen consumption rate (OCR). Based on the sarco/endoplasmic reticulum Ca²⁺-ATPase pump (SERCA) calibration in Study IV, increased affinity of proton binding for luminal-oriented Ca²⁺ docking sites was suggested as a mechanism of SERCA response to I/R condition leading to increased Ca²⁺ concentration in SR. Study IV predicted the upper hand of Ca²⁺ flux to the myofilament in comparison with SERCA Ca²⁺ uptake, also recapitulating the fact that Levo does not increase the inotropy at the expense of elevated oxygen demand. Study IV findings suggest that, mechanistically, SERCA contributes similarly in I/R and sepsis-induced heart failure conditions. Furthermore, Study IV suggested that the increase in proton leak in I/R, which results in elevated oxidative stress, may also contribute to the ischemic Ca²⁺ overload through disrupted competitive proton binding in SERCA, as a step toward establishing the connection between the elevation of oxidative stress and Ca²⁺ overload as the two main mechanisms of I/R injuries. Finally, Study IV linked the ameliorative effect of Levo on the contractile relaxation dysfunction to the drug's specific Ca²⁺ sensitizing mechanism, which involves Ca²⁺-bound troponin C and Ca²⁺ flux to the myofilament rather than SERCA phosphorylation inhibition.

To summarize, this thesis offers novel and robust computational frameworks of electro-mechano-energetic coupling in hiPSC-CMs, leveraging recent advances in human-based *in vitro* data acquisition. Ultimately, the presented models can serve as a platform to test advanced treatment ideas according to the temporal evolution of metabolites and molecular mechanisms in cardiomyocytes.

CONTENTS

1	Introduction	17
2	Literature review	21
2.1	Cellular physiology of healthy heart.....	21
2.2	Cellular pathophysiology of hypertrophic cardiomyopathy	26
2.3	Cellular pathophysiology of ischemia/reperfusion	30
2.4	Human induced pluripotent stem cell-derived cardiomyocytes.....	34
2.5	Computational frameworks of hiPSC-CMs	37
2.5.1	Paci lineage: dawn of hiPSC-CMs in silico models	38
2.5.2	Koivumäki model: the structural immaturity	40
2.5.3	Kernik model: phenotypic variability.....	41
2.5.4	A comparative review of the models	43
3	Aims of the study	47
4	Methods	48
4.1	Summary of the models	48
4.2	Integration of the contractile elements into the ionic model.....	49
4.3	Reparameterization of the contractile elements	50
4.4	HCM and the drug-induced calibrations	55
4.5	Integrating a metabolite-sensitive SERCA model into hiMCE	60
4.6	Modeling of ischemia/reperfusion	62
4.6.1	Ischemia.....	62
4.6.2	Reperfusion	66
5	Results	68
5.1	Biomarker evaluations of the models.....	68
5.2	The results of hiPSC-CM-CE model.....	71
5.2.1	Model response to Verapamil and Bay-K8644	71
5.2.2	Simulated inotropic effect of non-CMs in hiPSC-CM EHTs.....	73
5.3	The results of hiMCE model	74
5.3.1	Simulation of HCM-R403Q and MAVA mechanisms	74
5.3.2	Modeling OM and BLEB dose-dependent inotropy	76
5.4	The results of hiMCES model.....	78

5.4.1	Simulation of ischemia.....	78
5.4.2	Simulation of Levosimendan mechanism of action	83
5.4.3	Ischemic-induced arrhythmia simulation and I_{Ks}	84
5.4.4	Simulation of Levosimendan in ischemia and reperfusion	86
6	Discussion.....	89
6.1	The model of hiPSC-CMs electromechanics	89
6.2	Electro-mechano-energetics in HCM and drug mechanism	92
6.3	Electro-mechano-energetics in ischemia/reperfusion	95
6.4	Limitations and future perspectives	98
6.4.1	The hiPSC-CM-CE model (Study II).....	99
6.4.2	The hiMCE model (Study III)	99
6.4.3	The hiMCEs model (Study IV)	101
7	Conclusion.....	102
7.1	Biophysical modeling development and calibration maps	102
7.2	Extending the orthodox drug modeling formalism	103
7.3	Discovering cellular crosstalks in ischemia/reperfusion	103

ABBREVIATIONS

AP	Action potential
APA	Action potential amplitude
ADP	Adenosine diphosphate
AT	Active tension
ATP	Adenosine triphosphate
BLEB	Blebbistatin
CaT	Ca ²⁺ transient
CE	Contractile element
CICR	Calcium induced calcium release
CL	Cycle length
CM	Cardiomyocyte
cMyBP-C	Cardiac myosin binding protein C
ctn	Percent of cardiomyocytes in EHT
DAD	Delayed afterdepolarization
DRX	Disordered relaxed state
dV/dt max	Maximum upstroke velocity
EAD	Early afterdepolarization
EC coupling	Excitation-contraction coupling

EHT	Engineered heart tissue
FA	Fatty acids
FCS	Fractional cell shortening
HCM	Hypertrophic cardiomyopathy
hiPSC-CM	Human induced pluripotent stem cell-derived cardiomyocyte
hV-CM	Human adult ventricular cardiomyocyte
I_{CaL}	L-type Ca^{2+} current
I_f	Funny current
I_{K1}	Inward rectifying K^+ current
I_{Kr}	Rapid delayed rectifying K^+ current
I_{Ks}	Slow delayed rectifying K^+ current
I_{Na}	Fast Na^+ current
I_{NaL}	Late Na^+ current
I_{NaK}	Na^+/K^+ ATPase pump
I_{rel}	Release Ca^{2+} current from sarcoplasmic reticulum
I_{to}	Transient outward K^+ current
I_{up}	SERCA uptake Ca^{2+} flux
IHD	Ischemic heart disease
I/R	Ischemia-reperfusion
Levo	Levosimendan
MAVA	Mavacamten
MDP	Maximum diastolic potential

MI	Myocardial infarction
NCX	Na ⁺ /Ca ²⁺ exchanger
OCR	Oxygen consumption rate
ODE	Ordinary differential equation
OM	Omeamtiv mecarbil
Pi	Inorganic phosphate
RyR	Ryanodine receptors
RT50	Time from peak to 50% of relaxation
SA	Sinoatrial node
SERCA	Sarcoplasmic Ca ²⁺ ATPase
SL	Sarcomere length
SR	Sarcoplasmic reticulum
SRX	Super relaxed state
T-tubule	Transverse tubule
WT	Wild type
XB	Crossbridge in myofilament

ORIGINAL PUBLICATIONS

This dissertation is based on three original and peer-reviewed publications listed below and referred to as Studies I-IV in the text.

- I. **M. Forouzandehmehr**, N. Cogno, J. Koivumäki, J. Hyttinen, M. Paci, The Comparison Between Two Mathematical Contractile Elements Integrated into an hiPSC-CM In-silico Model, in: 2020 Comput. Cardiol., IEEE, 2020: pp. 1–4. doi: 10.22489/CinC.2020.055.
- II. **M. Forouzandehmehr**, J.T. Koivumäki, J. Hyttinen, M. Paci, A mathematical model of hiPSC cardiomyocytes electromechanics, *Physiol. Rep.* 9 (2021). doi:10.14814/phy2.15124.
- III. **M. Forouzandehmehr**, M. Paci, J.T. Koivumäki, J. Hyttinen, Altered contractility in mutation-specific hypertrophic cardiomyopathy: A mechano-energetic in silico study with pharmacological insights, *Front. Physiol.* 13 (2022). doi:10.3389/fphys.2022.1010786.

This dissertation is also based on the following unpublished manuscript.

- IV. **M. Forouzandehmehr**, M. Paci, J. Hyttinen, J. Koivumäki, An in silico model of hiPSC cardiomyocytes mapping the ionic and subcellular crosstalks onto oxygen deprivation and contractile dysfunction in ischemia/reperfusion, (Under Review).

AUTHOR'S CONTRIBUTION

In all of Studies I-IV, M. Paci, J. Koivumäki, J. Hyttinen, and M. Forouzandehmehr contributed to the study design. M. Paci, J. Koivumäki and J. Hyttinen supervised Studies I-IV and revised the manuscripts. M. Paci and J. Koivumäki contributed to sensitivity analysis in Study II and Study IV, respectively. M. Forouzandehmehr was responsible for majority of model calibrations, simulations, obtaining *in vitro* data for validations, and writing the manuscripts.

1 INTRODUCTION

Progressive development of precision cardiology demands inclusion of advanced and analytical methods to identify the underlying disease with higher accuracy and tailor optimal patient-specific treatments accordingly; a goal which is hard to reach with conventional empirical setups. This issue is addressed by progressive extension of computational models in cardiology which provide mechanistic and integrative insights to pathophysiology (Niederer et al., 2019). These biophysical models are based on causality and calibrated to simulate validated (patho)physiological datasets, which instill confidence in their capacities to make reliable and realistic predictions (Niederer et al., 2019). The resulting models in the scope of this thesis can serve as a platform to improve diagnosis and prognosis, test treatment ideas, and gradation of therapeutic interventions according to the temporal changes in metabolites and molecular mechanisms in cardiomyocytes.

On the other hand, the stem cell technology has opened a new window into cardiac pathophysiology research, specifically:

- by developing EHTs with potential to substitute akinetic parts of the heart e.g., in end-stage heart failure (Gunaseeli et al., 2010);
- by serving as an *in vitro* drug screening platform for the development of patient-specific therapeutics based on hiPSC-CMs derived from donor's somatic cells (Murata et al., 2010);
- by providing a human-based cardiotoxicity screening platform that can offer patient-specific proarrhythmic risk assessments (Murata et al., 2010).

Notably, hiPSCs hold the capacity of self-renewal and differentiating through gene manipulation methods into different cell types such as cardiomyocytes (Häkli et al., 2021a). Representing the patient's genotype, this remarkable technology bypasses the ethical concerns regarding animal experiments and provides a practically unlimited source of human-based *in vitro* models thus offering promising opportunities for patient-specific drug safety and efficacy investigations (Murata et al., 2010).

The combination of computational simulations with hV-CMs and *in vitro* simulations with hiPSC-CMs has been projected by FDA as a new paradigm for

evaluation of new molecular compounds, the comprehensive *in vitro* proarrhythmia assay (Sager et al., 2014; Strauss et al., 2019). This approach, enabling drug screening beyond hERG-based QT method in cardiac safety pharmacology, is backed by pharmaceutical industry and FDA (Paci et al., 2015). Given these, the following summarizes the key reasons for developing computational models of hiPSC-CMs alongside hV-CMs:

- A. The *in vitro* use of hiPSC-CMs enables studying of diverse drug-induced responses and other perturbations in cardiology. Nevertheless, the inability to employ a high throughput method to associate the fundamental ionic, genomic, and proteomic mechanisms to the detected whole-cell behavior is a grave disadvantage of the *in vitro* setting. HiPSC-CM computational modelling provides a powerful tool for closing this gap (Kernik et al., 2019).
- B. One of the problems in prediction of vulnerability to arrhythmia due to genetic diseases or drug effects is interpatient variability (Kernik et al., 2019). Developing *in silico* models of hiPSC-CMs is an effort in response to the pressing need to devise new drug development and treatment strategies that account for sex and genotype differences across patient populations. Specifically, computational models assist us in finding new therapeutic targets and predict patient-specific vulnerability to rare cardiac events such as arrhythmia in the presence of a genetic mutation (Forouzandehmehr et al., 2022; Margara et al., 2022).
- C. Computational models of hiPSC-CMs enhance our quantitative understanding of cellular, molecular, and interorganellar interactions, especially for preclinical drug tests and prediction of genotype-phenotype coupling where *in vitro* hiPSC-CMs are actively in use (Kernik et al., 2019).
- D. One aspect that has received insufficient attention is the potential impact of electrophysiological, contractile, and biochemical disparities between hiPSC-CMs and hV-CMs on differing reactions to pharmaceutical interventions. The identification of these differences is crucial in order to guarantee a precise interpretation of combined assays involving *in vitro-in silico* hiPSC-CMs and hV-CMs (Paci et al., 2015). For instance, hiPSC-CMs display greater sensitivity to selective current block (Paci et al., 2015). Thus, *in silico* models of hiPSC-CMs can facilitate the extrapolation of drug effects and proarrhythmic risk assessment from hiPSC-CMs to hV-CMs (Paci et al., 2015).
- E. Computational models of hiPSC-CMs provide us with a high throughput approach to study the mechanisms underlying phenotypic variability in

hiPSC-CMs *in vitro*, thus helping to design more effective *in vitro* maturation protocols and gain mechanistic insights on the translational challenges of hiPSC-CMs readouts (Huebsch et al., 2022; Kernik et al., 2019).

- F. The applicability of assessing the population level cell variability or the *in vitro* drug testing is limited by skilled manpower required for implementing current *in vitro* methods as they are not high throughput. In fact, *in vitro* measurements cannot be used efficiently to test all possible positive or adverse effects of drug candidates on the cardiac functions. Thus, there is a great need for developing new high-throughput predictive methods to gain mechanistic insights.
- G. Finally, in drug cardiotoxicity tests, the computational models have shown high regulatory impact. That is, simulation results can constitute the key source of evidence in analysis of drug's cardiotoxicity. They can replace part of the data traditionally generated in a pre-clinical trials (Musuamba et al., 2021).

Several mathematical models of hiPSC cardiomyocytes have been developed and used in drug studies (Kernik et al., 2019; Koivumäki et al., 2018; Paci et al., 2020). However, most models lack EC coupling and the mechanical feedback to the ion dynamics. When this doctoral project started in 2019, there was no whole cell models of hiPSC-CMs with strong mechano-electric coupling, and the adult CMs electromechanical models were scarce. Moreover, there have been no whole-cell computational models of hiPSC-CMs electro-mechano-energetics capable of capturing mutation-specific pathologies and I/R together with the relevant drug effects. These facts motivated me to incorporate the contractile function into the mainstream mathematical models of hiPSC-CMs (Study I) and complement the models toward the electro-mechano-energetic coupling (Study IV).

The main objective of this thesis was to establish robust and novel mathematical frameworks for hiPSC-CMs pathophysiological investigations and advancing the electro-mechano-energetic coupling at cell level. To this end, the first mathematical model of hiPSC-CMs electromechanics was developed by integrating a model of contractile element by Rice et al. (Rice et al., 2008) into Paci2020 model of hiPSC-CMs electrophysiology (Paci et al., 2020). I aimed for simulating key ionic biomarkers, the new contractile readouts, the inotropic effects of Verapamil and Bay-K 8644 and validating them against *in vitro* hiPSC-CMs data. The next objective was employing the established model as a computational basis and updating with a metabolite-sensitive contractile element, to investigate complex and less explored cellular pathologies such as mutation-specific HCM and the action mechanism and

effect of promising sarcomere-targeting drugs such as MAVA, OM, and BLEB. As the final objective, I aimed for complementing the model toward a more refined electro-mechano-energetic coupling by adding a mathematical model of metabolite-sensitive SERCA pump and a novel oxygen dynamic formulation. Facilitated by the emerging *in vitro* hiPSC-CM I/R data, the model was calibrated to explore the main ischemic mechanisms, (hypoxia, hyperkalemia, and acidosis), separately and combined. The model associates the metabolite and molecular dynamics to cell-level readouts to characterize the ionic and subcellular signature unique in I/R and the recently reported antiarrhythmic effect of Levo in ischemia.

Aside from the studied pathologies, the models developed withing this doctoral thesis rigorously investigate the action mechanisms and effects of promising drugs such as MAVA, OM, BLEB, and Levosimendan in light of the aforementioned diseases. Surpassing the orthodox IC50-based channel blocking formalism, the models propose novel mechanistic methods to explore the action mechanism and predict the effects of sarcomere-targeting drugs regarding interfilament kinetics.

All in all, the computational models developed in this doctoral thesis demonstrate deep-phenotyping and pharmacological potential. They can serve as platforms to test mutation-specific HCM and I/R treatment ideas according to the temporal evolution of metabolites and molecular mechanisms in cardiomyocytes.

2 LITERATURE REVIEW

2.1 Cellular physiology of healthy heart

Pumping oxygenated blood into systemic circulation and sending vital nutrients to the cells are main tasks of the heart muscle, myocardium. The cardiac conduction system synchronizes the cardiac contraction (Kennedy et al., 2016) which is regulated by metabolic dynamics (Kolwicz et al., 2013) and the autonomic nervous system as well (Habecker et al., 2016). Cardiomyocytes are the contractile units in the myocardium which consist only 20-30% of the total cell count but 70-85% of the whole myocardial space. The non-cardiomyocyte portion of the heart muscle consists of fibroblasts, endothelial cells, and leukocytes (Y. Guo & Pu, 2020).

Cardiac contraction begins with the SA node generated impulse rendering the cardiac conduction system (CCS) propagating the excitation all through the entire myocardium (Kennedy et al., 2016). Upon receiving the excitation wave by cardiomyocytes, the cells produce AP and active tension (AT) through a rapid communication called the EC coupling (Crocini & Gotthardt, 2021; Eisner et al., 2017). AP morphology can be categorized into five distinct phases which may appear dissimilar between different types of cardiomyocytes (Figure 1). This depends on the specific manifestation of the ion currents governing each phase of the AP (Nerbonne & Kass, 2005). In Figure 1, phase 0 denotes the rapid depolarization of CMs. In this phase, the resting (diastolic) membrane potential (-75 to -85 mV) rapidly rises to reach 20 to 40 mV which is succeeded by a fast repolarization period (phase 1) to 20 to 0 mV. Thenceforth, the ventricular AP enters a long plateau (phase 2) of 200 to 300 milliseconds length which is less obvious in nodal and atrial APs. Finally, the membrane potential returns to the diastolic state (phase 4) by a late repolarization (Kockskämper, 2016).

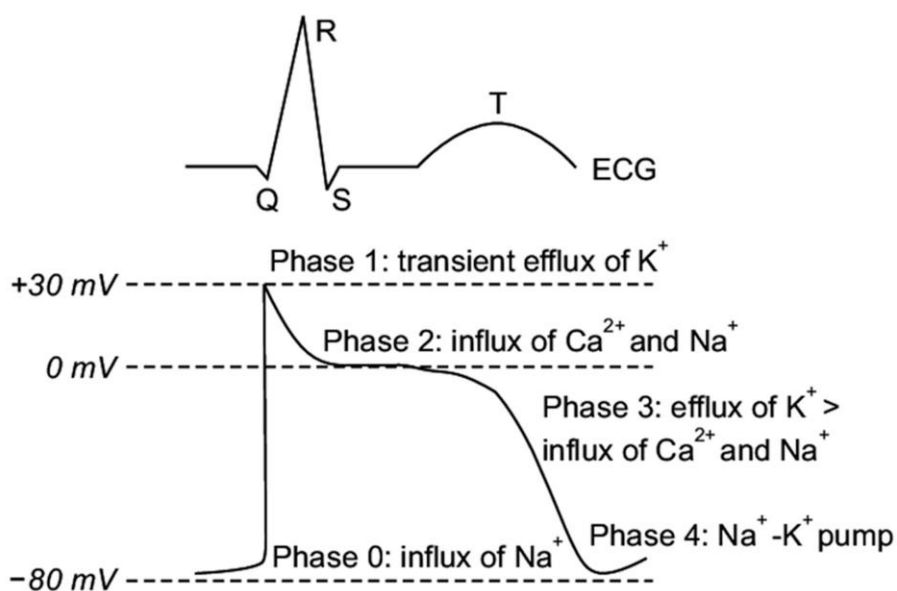


Figure 1. The phases of the cardiac action potential. This figure shows the main ion channels that impact the five distinct phases of the cardiac action potential, both in terms of inward and outward flow (adopted from (Lester et al., 2019) under CC BY license: <https://creativecommons.org/licenses/by/4.0/>). It should be noted that these phases correspond to time-dependent intervals that are determined by the entry and exit of different ions and their influence on the transmembrane voltage.

In the AP development, I_{K1} and I_{Na} are largely responsible for the negative resting membrane potential and the rapid depolarization, respectively. Inactivation of I_{Na} occurs at the end of phase 0 and the activation of I_{to} elicits the fast repolarization in phase 1. The plateau in phase 2 is mostly defined by the balance between I_{CaL} and outward K^+ currents, triggering the CICR mechanism where Ca^{2+} is released from SR into the cytoplasm. More pronounced in ventricular than atrial CMs, I_{Kr} and I_{Ks} cause the repolarization illustrated in phase 3 proportionately to the level I_{K1} is responsible for the resting membrane potential (Kockskämper, 2016; Nerbonne & Kass, 2005).

Upon AP depolarization which leads to the opening of L-type Ca^{2+} channels over the cell membrane and T-tubules the EC coupling triggers the cardiomyocyte contraction (Figure 2) (Eisner et al., 2017). T-tubules are invaginations of sarcolemma associated with large concentration of ion channels traversing to the center of cardiomyocytes while forming a communication network around long axis of myofibrils (Crocini & Gotthardt, 2021; Hong & Shaw, 2017). Ryanodine receptors of SR sense the elevated intracellular Ca^{2+} level due to the L-type funneled Ca^{2+}

influx and trigger CICR mechanism (Eisner et al., 2017; Kockskämper, 2016). Together with SR Ca^{2+} buffering, troponin C is also a main Ca^{2+} buffers in the cytosol (G. L. Smith & Eisner, 2019). When the released Ca^{2+} into the cytoplasm binds to the troponin of the myofibrils, the contractile units of CMs, the contraction takes place (Crocini & Gotthardt, 2021).

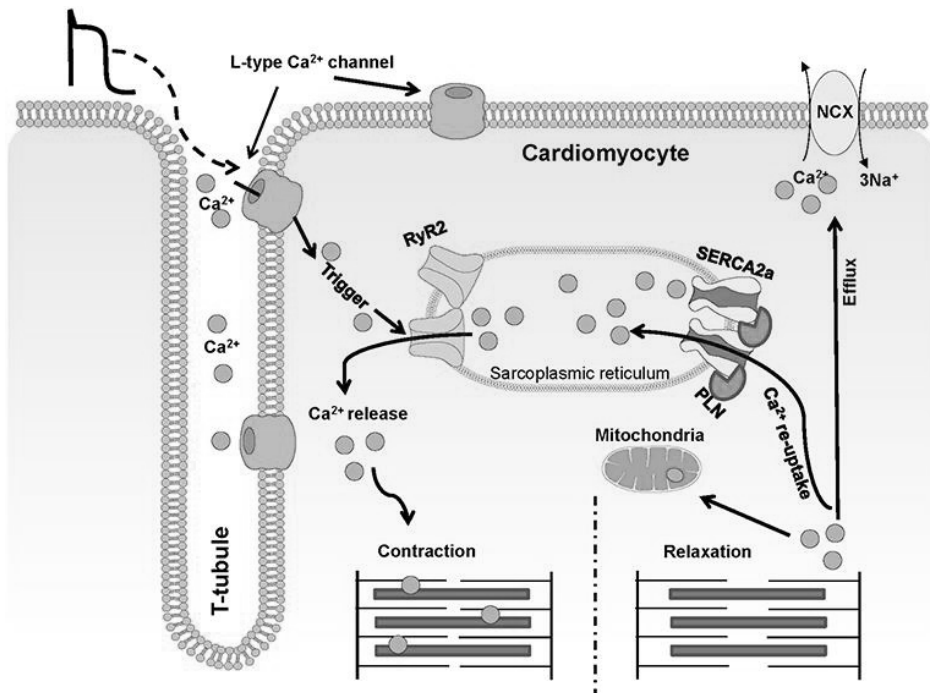


Figure 2. A schematic of Ca^{2+} dynamics during cardiac excitation-contraction adopted from (Mahmoodzadeh & Dworatzek, 2019) under CC BY license: <https://creativecommons.org/licenses/by/4.0/>. The occurrence of an action potential leads to the activation of L-type calcium channels, allowing the influx of Ca^{2+} into the cell. This Ca^{2+} influx then triggers the subsequent release of additional calcium ions from the sarcoplasmic reticulum (SR) through the activation of ryanodine receptors (RyR2). Intracellular Ca^{2+} interact with troponin within the myofibrils, resulting in the exposure of myosin binding sites on the actin filaments. The process of sarcomere contraction involves the binding of myosin to actin, followed by the movement of myosin along the filament. The process of relaxation takes place when the concentration of Ca^{2+} is reduced in the cytoplasm, either by being transported to the SR through the sarco/endoplasmic reticulum Ca^{2+} -ATPase (SERCA) or by being transported outside the cell through the sodium-calcium exchanger (NCX).

Sarcomeres, the contractile components of myofibrils, comprise of thin (actins) and thick (myosins) filaments (Figure 3). Actins and myosins are interconnected with each other and at each end of the sarcomere they attach to Z-disk (Sarantitis et al., 2012). A sarcomere also consists of a number of accessory proteins, namely, troponin, tropomyosin, cMyBP-C, and titin taking part in the contraction process (Sarantitis et al., 2012). Troponin has T, I, and C subunits with different functions. Troponin C acts as a binding dock for Ca^{2+} whilst troponin I is an inhibitory agent binding to actin harbors holding actin-tropomyosin in location and preventing actomyosin crossbridge formation. Troponin T, the largest of the subunits, plays mainly a structural role by facilitating the fixation of the troponin complex by binding to actin and tropomyosin (Gomes et al., 2002). Titin, attached to the Z-disk, contributes to the stability, structure, and flexibility of the sarcomere during contraction. It is connected to the myofilaments via cMyBP-C and serves as a mechanical spring during the contraction-relaxation cycle (Crocini & Gotthardt, 2021; Sarantitis et al., 2012).

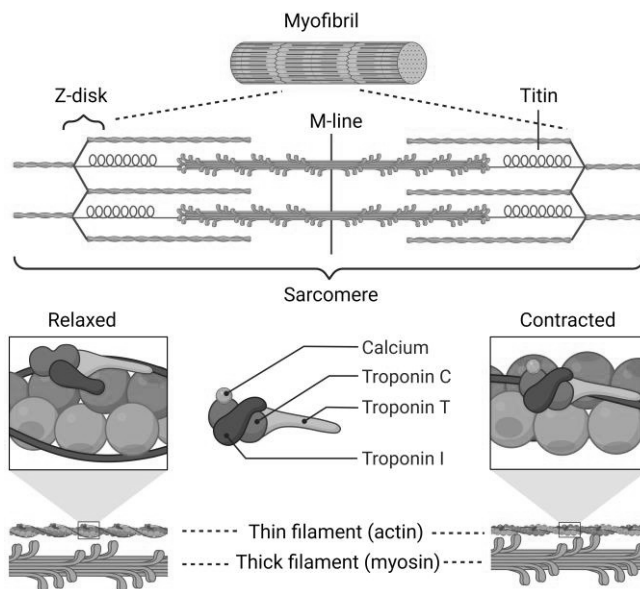


Figure 3. Schematics of sarcomere structure. Sarcomeres are the building blocks of myofibrils. Cardiac contraction is the product of actomyosin interaction toward the Z-disk. The sarcomere structure is stabilized by titins, functioning as a spring in contraction/relaxation (Created with BioRender.com).

The binding of cytosolic Ca^{2+} to troponin C and altering its conformation start the cardiomyocyte contraction process. Next, Troponin I and C interact with each other

and troponin I disconnects from the thin filaments. As binding of Ca^{2+} to troponin C triggers the conformational arrangement change, the myosin binding sites on the thin filaments become accessible for myosin heads as a result of tropomyosin and troponin relocation (de Tombe, 2003; Gomes et al., 2002). These biomechanical processes lead to binding of myosin heads to the docking sites on actins which is called the crossbridge formation. Upon dissociation of myosin heads from thin filaments, the myosin heads bind to ATPs where ATP hydrolyzation induce conformational change in myosin heads from super relaxed state (SRX) to disturbed relaxed state (DRX) rendering the next crossbridge forming cycle (Nag & Trivedi, 2021; Sarantitis et al., 2012). Finally, in the XB formation mechanism myosin heads thread toward the sarcomere Z-disks resulting in sarcomere shortening (contraction) and their retreat leads to the subsequent relaxation (Crocini & Gotthardt, 2021).

Only 10% of myosin molecules in sarcomeres are thought to be involved in the production of sarcomere force (Spudich, 2014); this observation suggests that there is/are some mechanism(s) by which unneeded myosins are prevented from forming inappropriate XBs, thus avoiding unnecessary energy expenditure. Recent structural data and biochemical analyses indicate that the energy-saving state is facilitated by dynamic conformational changes occurring between paired myosin molecules, thus serving as a structural mechanism (Alamo et al., 2017; Hooijman et al., 2011; Nag et al., 2017). The interaction between the head domains of paired myosin molecules is observed through an interacting-heads motif (IHM) in two conformations: the SRX conformation, where the ATP-binding domains are sterically inhibited and cannot bind actin, and the DRX conformation, where only one myosin head is accessible for ATP hydrolysis and interaction with actin (Alamo et al., 2017) (Figure 3). According to this model, the ratio of myosins in these conformations would affect both energy consumption and contractility. Additionally, this phenomenon offers a mechanism for maintaining a harmonious equilibrium between work output and metabolic expenditures, thereby facilitating sustained cardiac functionality throughout an individual's lifespan.

The sarcomere relaxation coincides with the steep decrease in cytosolic Ca^{2+} during each AP cycle (Kockskämper, 2016). A key contributor to Ca^{2+} removal is the SERCA pump which imports intracellular Ca^{2+} into the SR space. Another contributor to the Ca^{2+} removal is the sarcolemmal NCX which exports one Ca^{2+} to the extracellular matrix and imports three Na^+ . Depending on the transmembrane ion concentration gradients, NCX can function in forward or reverse mode, extruding Ca^{2+} in the former and intruding Ca^{2+} in the latter. In the initial AP depolarization phase, NCX functions in reverse mode as voltage-gated sodium

channels rapidly intrude Na^+ . The repolarizing outward current in phases 0 and 1 of AP development is due to influx of Ca^{2+} and efflux of Na^+ due to the reverse mode of NCX. Subsequently, NCX enters its forward mode during phases 2-4 of AP extruding Ca^{2+} from the cytosol leading to a depolarizing inward current (Figure 1).

Another key ion exchanger affecting AP development is Na^+/K^+ ATPase (NKA) that makes an outward current by actively extruding three Na^+ and intruding two K^+ into the cytosol maintaining the K^+ and Na^+ homeostasis. ATP hydrolysis fuels the active ion transport in NKA which contributes to AP repolarization (phase 3). It also decreases the diastolic membrane potential toward more negative values and shortens the plateau phase of AP (Eisner et al., 2017; Kockskämper, 2016; Shattock et al., 2015).

The complex electrophysiological, mechanical, and energetic processes that lead to the contraction of the heart place a high energy demand on the cardiac tissue. Explicitly, fatty acids (FA), glucose, ketone bodies, can be used by cardiomyocytes as a source of energy (Martínez et al., 2017). Despite glucose being the substrate with the highest energy efficiency, FAs assume the role of the predominant energy source under aerobic conditions and during periods of rest. Fatty acids contribute to 60-90% of the energy generated, whereas glucose only accounts for 10-40% of the energy produced (Martínez et al., 2017; Rosano et al., n.d.). Nonetheless, CMs are dependent on the influx of FA from the blood because they are unable to generate these molecules effectively on their own (Martínez et al., 2017). However, hiPSC-CMs rely upon glycolytic metabolism in contrast to FA-based mechanism of native adult CMs. Following the process of glycolysis, in conjunction with the assimilation of metabolites into the tricarboxylic acid cycle, ADP undergoes oxidative phosphorylation within the mitochondrial respiratory chain, resulting in the production of ATP. This ATP subsequently serves as a source of energy for muscle contraction (Martínez et al., 2017; Rosano et al., n.d.).

2.2 Cellular pathophysiology of hypertrophic cardiomyopathy

Hypertrophic cardiomyopathy (HCM) is the most commonly inherited cardiomyopathy with an autosomal dominant inheritance pattern. It is characterized by the thickening of the left ventricular wall, hypercontraction, impaired relaxation, and increased energy consumption that cannot be attributed to abnormal loading conditions (Gartzonikas et al., 2023). Obstructive HCM, the most common type, is

characterized by thickened septum and associates with obstruction of left ventricle outflow tract (Ho et al., 2020).

Between 34% and 60% of the time, a gene that causes a disease is discovered, and MYBPC3 and MYH7 are the two most often altered sarcomeric protein-encoding genes (Gartzonikas et al., 2023). The prevalence of HCM in the general adult population ranges from 1:344 to 1:625 according to numerous studies (Maron et al., 1995, 2004; Zou et al., 2004). There is no distinct geographic, racial, or sexual distribution of HCM. Several studies, however, show that men are diagnosed more frequently than women (Maron et al., 1995, 2004; Zou et al., 2004). People with HCM are often diagnosed when an irregular ECG is found during a routine test, a heart murmur is found during a physical examination, family screening studies of HCM probands are conducted, or when symptoms manifest.

According to the 2020 guidelines on HCM by the American Heart Association (AHA) and the American College of Cardiology (ACC), it is important to consider other systemic disorders that can lead to left ventricular hypertrophy in the differential diagnosis during the evaluation, even though they are not classified as HCM. HCM is a prevalent hereditary cardiac disorder primarily attributed to mutations in genes encoding sarcomere proteins (Ommen et al., 2020).

HCM has an autosomal dominant mode of inheritance and is a classic single gene disease (Maron et al., 2012). The genes that make sarcomeric proteins, particularly MYH7 (-myosin heavy chain), MyBPC3 (Ho et al., 2015), and TNNT2 (troponin T2) (Coppini et al., 2014), exhibit heterozygous missense or truncating mutations in around 35–60% of HCM patients. Despite some similarities, each mutation appears to produce a different pathophysiology, this mutation-specificity could account for the documented clinical phenotypic variety in HCM associated with sarcomeres (Limongelli et al., 2021). The association between the dysfunction of sarcomeric proteins and the adverse remodeling of the myocardium seems to be evident, given the frequent occurrence of diastolic dysfunction and heightened ventricular arrhythmogenesis (Olivotto et al., 2009).

In HCM, primitive functional changes occur at the sarcomere level, altering the actin-myosin interaction (Spudich, 2019) and impairing the thin filament's ability to switch off at low calcium concentrations (Tardiff et al., 2015). As a result, force generation requires more energy, contributing to the pathophysiology of the disease. Due to an increase in cytosolic Ca^{2+} buffering and an immediate impact on cardiac relaxation and energetics, the enhanced myofilament Ca^{2+} sensitivity is brought on by a direct effect of the mutation or post-translational modifications which secondarily causes electrical remodeling and increased arrhythmogenesis (Hoskins et

al., 2010). Aside from these main alterations, secondary alterations also happen when the sarcoplasmic reticulum and the sarcolemmal functions are negatively remodeled (Coppini et al., 2013). It has been shown that individuals with obstructive HCM experience changes in intracellular Ca^{2+} fluxes along with altered transmembrane ion currents (weaker K^+ currents, increased Ca^{2+} and Na^+ currents) (Coppini et al., 2013; Ferrantini et al., 2018). The measured active tension developed in HCM reveals a positive force frequency relationship (Coppini et al., 2013; Schotten et al., 1999). Additionally, the observed preservation of positive inotropic responses to β -adrenergic stimulation and stimulation pauses, as well as the sustained amplitude of CaTs and SR Ca^{2+} content measured in HCM cardiomyocytes, provides further evidence of the contractile reserve present in the ventricular muscle affected by HCM (Coppini et al., 2013; Ferrantini et al., 2018).

The vast majority of pathogenic variations responsible for HCM are located within the genes MYH7 and MYBPC3. These genes are responsible for encoding the primary isoform of adult cardiac myosin and myosin-binding protein C, respectively. A significant proportion of MYBPC3 HCM variants result in the production of truncated proteins, which enhance the contractile properties of myosin and alter the ratio of myosins in DRX phase (McNamara et al., 2016, 2017; Toepfer et al., 2019). In contrast, all MYH7 HCM variants encode missense residues, and it is unclear how these subtle modifications to myosin SRX and DRX conformations will affect cellular processes. In fact, previous biophysical and biochemical analyses of isolated single myosin head fragments with HCM variants do not always show gain of function, as might be predicted by a conformational shift toward DRX (Figure 3) (Ho et al., 2018; Kawana et al., 2017; Lowey et al., 2018; Moore et al., 2012; Mosqueira et al., 2018; Nag et al., 2015a; Sommesse et al., 2013).

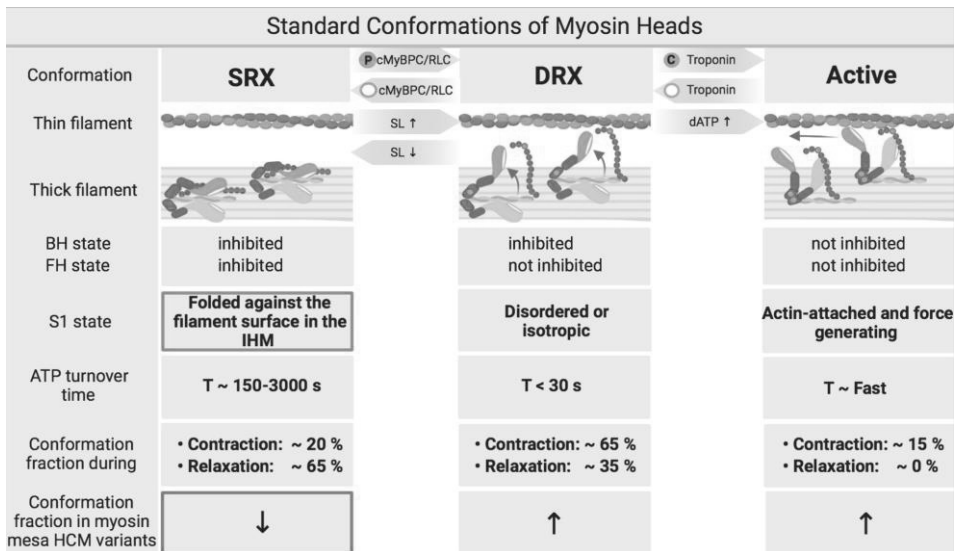


Figure 3. Myosin heads in different conformations adapted from (Schmid & Toepfer, 2021) under CC BY license: <https://creativecommons.org/licenses/by/4.0/>. The equilibrium between the myosin super-relaxed (SRX) and disordered-relaxed (DRX) states is subject to modulation by various regulatory mechanisms, including the phosphorylation of cardiac regulatory light chain (cRLC) and cMyBPC, as well as the length of the sarcomere (SL). The binding of myosin heads to actin occurs in the presence of calcium binding to troponin. The states of SRX, DRX, and active contraction undergo alterations throughout the contraction process. During the process of relaxation, a significant proportion of myosin heads maintain the SRX conformation (Brunello et al., 2020). BH: blocked head state, FH: free head state.

Arrhythmias, most often atrial fibrillation, are frequently brought on by HCM, and in a few cases, these arrhythmias result in cardiac failure and early death. A comprehensive examination of over 4500 patients diagnosed with HCM has demonstrated a stratification of heart failure and arrhythmic risks based on the specific genotype of sarcomere proteins. The highest risks were observed in patients harboring pathogenic or likely pathogenic variants, followed by an intermediate risk category comprising patients with variants of unknown clinical significance (VUS). Patients lacking sarcomere variants exhibited the lowest risks in this regard (Ho et al., 2018).

2.3 Cellular pathophysiology of ischemia/reperfusion

The most prevalent cardiovascular illness and a significant contributor to morbidity and mortality worldwide is IHD (Khan et al., 2020). In IHD, the blood supply to the cardiac tissue is diminished or blocked, depriving it of oxygen and nutrients and causing the buildup of metabolic waste. On the other side, this impairs heart function by causing damage to and/or death of the cardiomyocytes. IHD is most frequently caused by coronary artery disease. The coronary arteries that provide blood to the heart get clogged with plaque, which causes the arterial lumen to narrow and the blood flow to the myocardial to decline. If the plaque ruptures, it may result in an abrupt blockage of the artery that completely stops blood flow and causes CM mortality unless the blood flow is restored through prompt reperfusion (Ambrose & Singh, 2015). Acute IHD events may manifest abruptly, such as in instances of plaque rupture, or they may gradually evolve as a chronic state characterized by diminished blood supply to the heart, ultimately leading to heart failure (Libby & Theroux, 2005). Although prompt reperfusion is essential for salvaging the ischemic region, it initially induces additional tissue damage (Hausenloy & Yellon, 2013).

The electrophysiological, biochemical, and metabolic processes of CMs are altered as a result of oxygen and nutrient loss during ischemia (Figure 4) (Hausenloy & Yellon, 2013). Because oxidative phosphorylation cannot occur in the absence of oxygen, the heart switches from aerobic FA metabolism to inadequate and inefficient anaerobic glycolysis (María Sofía Martínez et al., 2017; Rosano et al., n.d.). The intracellular pH is lowered as a result of ATP depletion and a rise in lactate (Hausenloy & Yellon, 2013; Martínez et al., 2017). When H^+ builds up, the Na^+-H^+ exchanger (NHE) activates, releasing one H^+ ion in exchange for the import of one Na^+ , which causes intracellular Na^+ buildup. As NKA is unable to operate in the absence of ATP, NCX is activated in the reverse mode, releasing Na^+ and increasing intracellular Ca^{2+} levels (Garcia-Dorado et al., 2012; Kalogeris et al., 2016; Sanada et al., 2011). The reduced pH makes troponin C less sensitive to Ca^{2+} , which delays the appearance of the myosin binding site and, as a result, hampers CM contraction (Sanada et al., 2011).

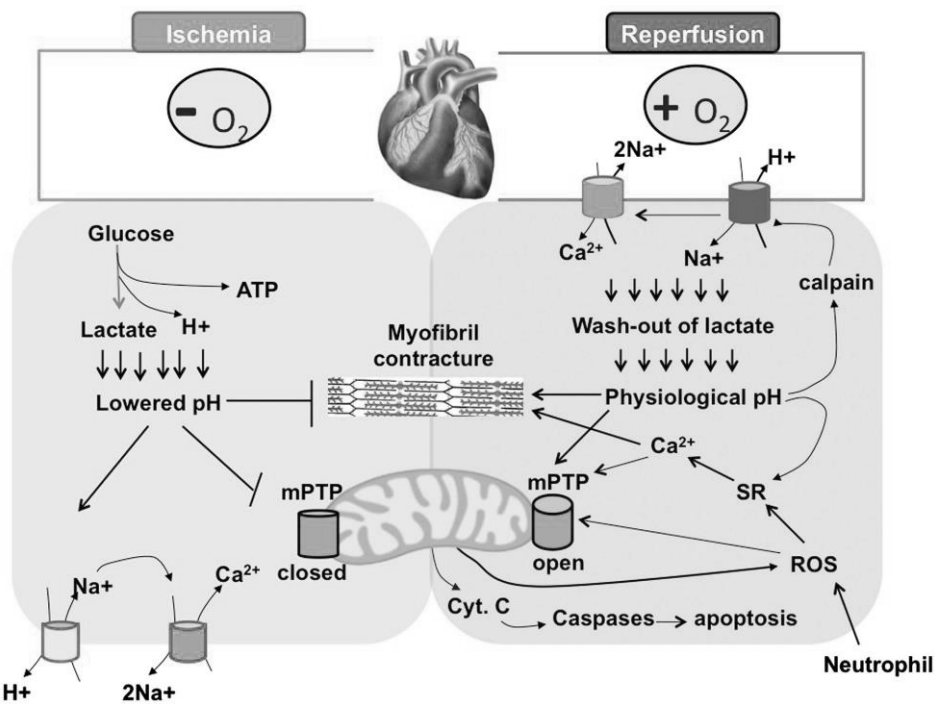


Figure 4. A schematic of key cellular mechanisms in myocardial ischemia-reperfusion injury adopted from (Li et al., 2016) under CC BY-NC-ND license: <https://creativecommons.org/licenses/by-nc-nd/4.0/deed.en>. An anaerobic glycolysis in ischemia leads to the lowered pH level causing an inhibited myofibrillar contracture. The reperfusion renders myofibrillar hypercontracture.

Ischemia alters the ion channel and pump functions, which affects the AP shape of the cardiomyocytes (Figure 5A). The surface electrocardiogram can exhibit different patterns depending on whether the ischemia affects the entire thickness of the heart wall (transmural) or is limited to the subendocardial layer (Figure 5B). Ion channels and pumps that depend on ATP hydrolysis are rendered inactive by the lack of ATP during ischemia. As a result of a drop in intracellular K^+ and a rise in extracellular K^+ after ischemia, the resting membrane potential of the CM becomes more depolarized (less negative). That depolarization further inactivates Na^+ channels, which cannot then produce the fast upstroke that would normally happen during AP phase 0 (Klabunde, 2017). The slower AP upstroke at the cell level directly slows down the conduction of the excitation wave at the tissue level, in conjunction with ischemia-induced gap junctional uncoupling of cells (De Vuyst et al., 2011; Garcia-Dorado et al., 2012). At a membrane potential of -55 mV, the rapid sodium (Na^+) channels undergo inactivation. Nevertheless, APs can still occur as a result of the

sluggish inward current of Ca^{2+} through L-type Ca^{2+} channels, albeit with a significantly slower depolarization rate. Furthermore, alongside the decelerated upstroke and decreased negative resting membrane potential during phase 0, the repolarization of the cardiac myocyte occurs earlier, leading to a reduction in the duration of the AP (as depicted in Figure 5). This is likely due to the activation of K^+ channels (Klabunde, 2017).

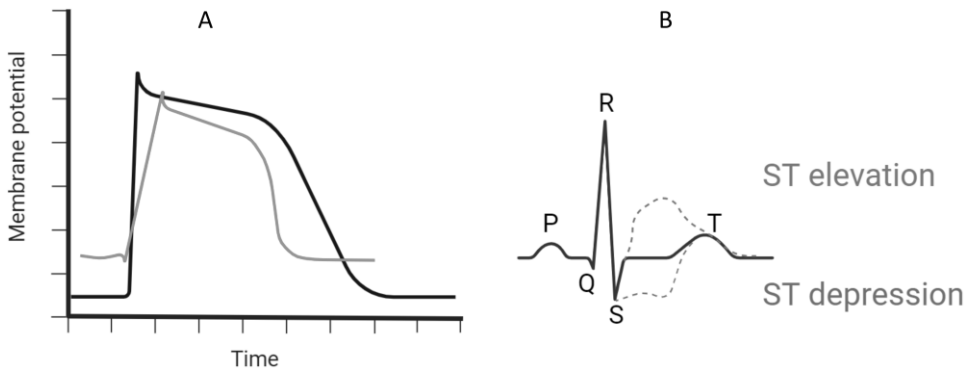


Figure 5. Action potential and ECG profiles change in ischemic condition (created with BioRender.com). (A) The upstroke velocity is decreased and resting membrane voltage is depolarized in ischemia (red line) in comparison to normal condition (black line). ST elevation occurs in transmural ischemia and ST depression is due to subendocardial ischemia (B).

As a result of the restoration of blood flow to the heart tissue during reperfusion, substrates, oxygen, and a normal extracellular pH are restored, enabling the synthesis of ATP by the oxidation of fatty acids (Hausenloy & Yellon, 2013). The depletion of H^+ from the extracellular milieu results in the establishment of a notable proton gradient across the cellular membrane, thereby enhancing the activity of NHE and NCX, consequently leading to an elevation in intracellular Ca^{2+} levels. Consequently, the elevation in intracellular Ca^{2+} levels also stimulates the release of calcium from SR, exacerbating the Ca^{2+} overload. (Wang et al., 2020). Arrhythmias, hypercontracture of myofibrils, and uncontrolled and persistent contraction of the CMs result from increased cytoplasmic Ca^{2+} and reestablished energy synthesis (Garcia-Dorado et al., 2012; Sanada et al., 2011). Reactive oxygen species (ROS), which are generated by the reactivated electron transport chain, cause oxidative stress and cause mitochondrial permeability transition pores (mPTPs) to open during reperfusion (Figure 4). These events also cause pH to return to normal (Turer & Hill, 2010). The extra Ca^{2+} in the cytoplasm can enter the mitochondria when the

mPTPs are opened, which lowers the levels of cytoplasmic Ca^{2+} . However, due to ROS generated in the mitochondria, its opening further causes oxidative stress (Hausenloy & Yellon, 2013). In turn, ROS can cause damage to mitochondrial and nuclear DNA. Additionally, although it may not always happen quickly or synchronously, the electrical changes in the CM electrophysiology are reversed upon reperfusion (Manning & Hearse, 1984).

Both reversible and irreversible kinds of damage can result from reperfusion in CMs. In the absence of enduring scarring, reperfusion has the potential to induce arrhythmias, which can be managed through the administration of antiarrhythmic drugs and are generally of a temporary nature (Hausenloy & Yellon, 2013). The AP heterogeneity at the boundary between previously ischemic and healthy tissue can lead to ventricular fibrillations (Manning & Hearse, 1984). Furthermore, Ca^{2+} release from the SR outside of the typical EC coupling cycle might cause DADs (S. Chen & Li, 2012). Additionally, capillary damage, external capillary compression from swollen cells, and microthrombosis can lead to microvascular obstruction, which is the inability to reperfuse the ischemic zone. Infarction-related intramyocardial bleeding can happen when there is substantial microvascular blockage. At the end of the ischemia phase, CMs that were still viable died as a result of lethal myocardial reperfusion injury. According to (Hausenloy & Yellon, 2013), this type of injury can account for up to 50% of the total size of the infarction and is brought on by oxidative stress, calcium excess, mPTP opening, and CM hypercontractility.

Myocardial stunning is a form of reversible injury characterized by prolonged dysfunction of the heart tissue and myocardial contractile apparatus. This condition arises due to intracellular Ca^{2+} overload and oxidative stress (Hausenloy & Yellon, 2013). Myocardial stunning occurs during the reperfusion phase following a brief ischemic episode, in contrast to myocardial hibernation which occurs during ischemia. Unlike infarction or cell death, myocardial stunning is characterized by a reduction in cardiac contractility. Myocardial stunning is a pathological state characterized by a prolonged recovery period, which can span multiple days. This condition arises due to dysregulated energy metabolism, the generation of ROS, disturbances in Ca^{2+} homeostasis, microvascular anomalies, and the accumulation of leukocytes in the affected region. Conversely, in cases of ischemic myocardium, characterized by a diminished blood supply, the phenomenon of myocardial hibernation occurs. The CMs are nonetheless functional despite having decreased contractile activity since this lowers the tissue's need for oxygen, which in turn protects the CMs (Richard Conti, 1991; Ytrehus, 2006).

2.4 Human induced pluripotent stem cell-derived cardiomyocytes

The capacity for self-renewal, differentiation into specialized cell types, and multicellularity are the characteristics that distinguish stem cells from other types of cells. Totipotent stem cells possess the ability to undergo differentiation into various cell types, encompassing those found in extraembryonic tissues. Pluripotent stem cells possess the capacity to undergo differentiation into cell types representative of the three primary embryonic lineages, while lacking the ability to differentiate into cell types specific to extraembryonic tissues. Multipotent stem cells possess the ability to undergo differentiation into a wide range of specialized cell types within a specific tissue, whereas unipotent stem cells are limited to differentiating into a single type of cell. Adult stem cells, which are multipotent or unipotent, are present in various locations within the body following the completion of embryonic development. Embryonic stem cells (ESCs) are a type of stem cell with pluripotent capabilities, derived from the inner cell mass of blastocysts (Daley, 2015). In contrast, induced pluripotent stem cells (iPSCs) refer to somatic cells that have been forced to express transcription factors associated with cellular pluripotency, specifically SOX2, OCT4, KLF4, and c-MYC (Takahashi et al., 2007; Takahashi & Yamanaka, 2006).

It is possible to create iPSCs from human somatic cells (Takahashi et al., 2007), and these cells have a variety of uses, involving tissue engineering, the treatment of immunodeficiency diseases, disease modeling, and the development and testing of pharmaceuticals (A. S. T. Smith et al., 2017; P. T. Yin et al., 2016) (Figure 6). These cells can be cultured *in vitro*, but to preserve the pluripotency of the cells, the culture environment must closely resemble the *in vivo* stem cell niche. The two most crucial tools for achieving this are the cell culture media and culture substrate. The iPSCs are normally grown in growth media that contains growth factors and cytokines that boost the cells' capacity for self-renewal and pluripotency. Additionally, the cells can be grown on feeder cells that help the iPSCs develop and avoid differentiation, e.g., from mouse embryonic fibroblasts. On the other hand, an alternative approach to feeder-dependent culture involves the utilization of extracellular protein matrices such as Matrigel, fibronectin, or laminin, which do not require the presence of feeder cells (van der Sanden et al., 2010). The cultivation of iPSCs in xeno-free environments is of utmost importance for therapeutic and translational applications, necessitating the use of culture components that are either derived from humans or artificially synthesized (Kaur et al., 2013).

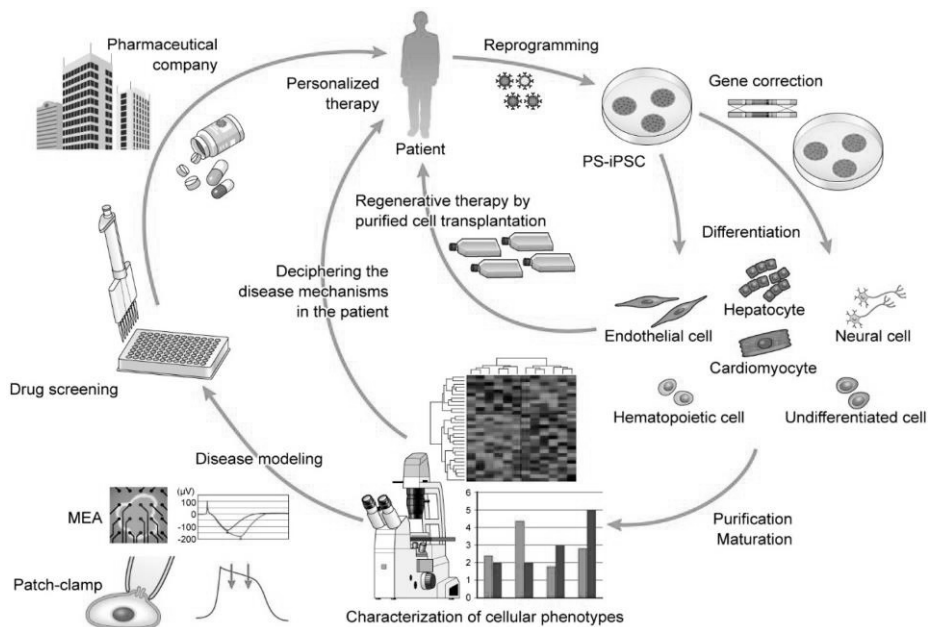


Figure 6. Different aspects of iPSC applications adopted from (Tanaka et al., 2015) under CC BY 4.0 license: <https://creativecommons.org/licenses/by/4.0/>. Pluripotent cells, commonly referred to as induced pluripotent stem cells (iPSCs), are generated through the reprogramming of somatic cells obtained from individuals with genetic disorders. This reprogramming process involves the induction of specific transcription factors. Subsequently, gene targeting methodologies are employed to discern cells that are pertinent to the disease or have undergone mutation correction from iPSCs. The utilization of purified and expanded cells holds potential for application in cellular transplantation procedures. In contrast, differentiated cells have the potential to be utilized *in vitro* for various purposes, including disease modeling and drug testing. Various experimental methods are employed to characterize cellular phenotypes in disease modeling, offering potential insights into the underlying disease mechanisms and potential avenues for therapeutic intervention. The assessment of drug efficacy and toxicity for candidate chemical compounds can be conducted by examining cellular characteristics. The utilization of pluripotent stem cell systems, specifically iPSCs, holds significant potential as a valuable platform for personalized medicine and the facilitation of efficient drug discovery. This potential collaboration between PSC systems, such as PS-iPSCs, and the pharmaceutical industry could prove to be advantageous in the future. MEA stands for multi-electrode array.

HiPSC-CMs exhibit distinct dissimilarities when compared to adult CMs, encompassing disparities in both morphology and physiological performance. Adult

CMs exhibit a rod-like morphology, characterized by organized sarcomeres and a highly developed system of T-tubules and SR. In contrast, hiPSC-CMs exhibit a smaller and more spherical morphology, characterized by shortened and disorganized sarcomeres, an underdeveloped SR, and a lack of a well-defined longitudinal axis and T-tubules (Ahmed et al., 2020). The underdeveloped SR and absence of T-tubules, combined with inadequate expression of crucial proteins that regulate CICR, contribute to the slower EC coupling observed in hiPSC-CMs compared to adult CMs (Veerman et al., 2015). Adult CMs only beat when stimulated, whereas hiPSC-CMs beat spontaneously. Furthermore, hiPSC-CMs exhibit significantly reduced contractile force, as well as slower conduction and upstroke velocities. Additionally, the morphological characteristics of their APs exhibit a wide range of variations, which can be categorized into atrial, nodal, or ventricular types (Karakikes et al., 2015). In addition, it should be noted that while hiPSC-CMs exhibit a functional pacemaker current, the current density alone is inadequate for the initiation of spontaneous APs and contractions. Instead, the spontaneous activity observed in hiPSC-CMs resembles that of nodal cells within the SA node, and it relies on the involvement of ryanodine and inositol-1,4,5 trisphosphate receptors. These receptors facilitate the spontaneous release of Ca^{2+} from the SR. The subsequent increase in intracellular Ca^{2+} concentration initiates a depolarizing current through NCX. This current, in conjunction with I_f , then elicits an AP (Koivumäki et al., 2018).

Due to the significant need for ATP and energy for healthy heart function, adult CMs have a high metabolic activity. As a result, adult CMs primarily produce energy through the oxidation of FAs, which is a reliable and efficient pathway for the synthesis of ATP. HiPSC-CM metabolism is more similar to that of fetal CM, which generates ATP mostly by the glycolysis of glucose (Ahmed et al., 2020; Hu et al., 2018; Ulmer & Eschenhagen, 2020). Adult CMs exhibit an increased abundance of mitochondria, along with a more compacted cristae network and tubular network. Subsarcolemmal mitochondria are located in close proximity to the sarcolemma, serving as a vital source of energy for facilitating the transportation of electrolytes and metabolites. In contrast, interfibrillar mitochondria traverse the SR and align themselves with sarcomeres, thereby providing ATP for the uptake of Ca^{2+} by the SR and the contractile system. In both fetal and hiPSC-CMs, the majority of mitochondria are located near the nucleus, exhibiting a reduced number of cristae and a less extensive tubular network (Ulmer & Eschenhagen, 2020).

2.5 Computational frameworks of hiPSC-CMs

In recent years, the significance of computational modeling in cardiac cell electrophysiology has grown in importance, allowing for a better understanding of CM function. This, together with increasing computer processing capacity, prompted the development of a wide range of mathematical models representing *in silico* versions of nearly all *in vitro* models utilized in experimental practice. As models of adult hV-CMs inadequately recapitulate the hiPSC-CM electromechanics and according to the reasons given in the first chapter, there have been efforts to develop new mathematical frameworks to capture the hiPSC-CMs (patho)physiology. However, mathematical models of adult hV-CMs (Grandi et al., 2009; ten Tusscher & Panfilov, 2006) provided the basis for the first computational models of hiPSC-CMs, for example, voltage-dependent time constants in I_{CaL} formulation in (Paci et al., 2013). In this section, the evolution of cell-level 0D mathematical models of hiPSC-CMs based on ODEs is addressed. The review of computational models of adult hV-CMs has been thoroughly detailed elsewhere (Niederer et al., 2019; Zile & Trayanova, 2018) and resides out of the scope of this thesis. In general, these 0D models follow the classic Hodgkin-Huxley framework modeling the membrane potential as:

$$\left\{ \begin{array}{l} C \frac{dV}{dt} + I_{ion}(V, \mathbf{g}, \mathbf{c}) = I_{apd} \\ \frac{d\mathbf{g}}{dt} = G(V, \mathbf{g}) \\ \frac{d\mathbf{c}}{dt} = L(V, \mathbf{g}, \mathbf{c}) \\ V(0) = v_0, \mathbf{g}(0) = \mathbf{g}_0, \mathbf{c}(0) = \mathbf{c}_0 \end{array} \right. \quad (2.1)$$

Where, V is the membrane potential, C is the membrane capacitance, \mathbf{g} is the vector of gating variables, \mathbf{c} denotes the vector of ion concentration variables, G is the general gating variable equation, L represents the general ionic concentration dynamic equation, and I_{apd} denotes an applied stimulus current.

There are several types of ionic models: (i) phenomenological models, which are designed to replicate the overall behavior of the cell in relation to V ; (ii) first generation models, which aim to replicate the macroscopic behavior and physiology of the cell by incorporating the most significant ionic currents; and (iii) second generation models, which offer an intricate depiction of the cell's behavior by providing a highly detailed description. The cardiac physiology modeling can also be categorized under static and dynamic (virtual live cells) approaches. In the former

approach, the ion concentrations do not vary, and the virtual cell is considered always in a constant homeostatic. However, the latter approach (dynamic/live approach) the intracellular concentrations are variables and ion dynamics are required to generate AP. The models reviewed in the subsequent sections are all 2nd generation and dynamic.

2.5.1 Paci lineage: dawn of hiPSC-CMs in silico models

Starting from the hV-CM model by (ten Tusscher & Panfilov, 2006), Paci et al. (Paci et al., 2013) developed the first *in silico* model of hiPSC-CMs electrophysiology in 2013 based on hiPSC-CMs experimental electrophysiology data available (Ma et al., 2011). The first version of Paci model lineage, *Paci2013*, considered both atrial-like and ventricular-like phenotypes of hiPSC-CMs observed in hiPSC-CMs EHTs. In *Paci2013* model, for each of the ionic currents, shown in Figure 7, first a basic literature-based data fitting was done to simulate the voltage-clamp protocol used *in vitro*. As the recordings were obtained from a combination of atrial-, and ventricular-like hiPSC-CMs, the basic fitting parameters rescaled to account for the phenotypical differences influencing the voltage-clamp outputs. Of note, the key modeling threshold adopted to distinguish between atrial-like and ventricular-like phenotypes was *rappAPD*, defined below, as an AP shape factor:

$$rappAPD = \frac{APD_{30} - APD_{40}}{APD_{70} - APD_{90}} \quad (2.2)$$

Where APD_{30} , APD_{40} , APD_{70} , and APD_{90} denote AP duration at 30%, 40%, 70%, and 90% of repolarization, respectively. This modeling approach changed in the later evolved versions, *Paci2018* (Paci et al., 2018) and *Paci2020* (Paci et al., 2020), which only focused on the ventricular-like AP phenotype inspired by the fact that the atrial-like and node-like AP phenotypes had been rarely observed in the dense syncytia of new commercial hiPSC-CMs cell lines (iCell²) (Paci et al., 2020). This modeling adaptation was also acknowledged in the other mathematical models of hiPSC-CMs, namely, by Koivumäki et al. and Kernik et al. (Kernik et al., 2019; Koivumäki et al., 2018).

The conventional initial stage involves utilizing a revised iteration of prior models of adult human CMs, which adhere to the classical second-generation formulation as outlined in Equation 2.1. This formulation characterizes the membrane potential through the utilization of the generalized Cauchy problem. The evolution of Paci models mostly contributed to ionic equations, comprising an improved calcium

dynamic formulation, updating the late Na current I_{NaL} model, the Na^+ contribution to the funny current I_f , reformulated release current from RyR channels (I_{rel}) thus enabling the simulation of DADs in *Paci2018* model. *Paci2018* model also benefited from a new parameter optimization based on a search for a minimum technique using Nelder-Mead Simplex algorithm given in (Fabbri et al., 2017). Briefly, the cost function method in Fabri et al. would result in zero cost if the evaluated biomarker sit within the experimental average value $\pm SD$, otherwise, it is increased linearly (Paci et al., 2018). Finally, in *Paci2018*, new Ca^{2+} recording *in vitro* data from the heart group of BioMediTech unit of faculty of medicine and health technology of Tampere University, was added to the pool of previous hiPSC-CMs data used before for calibration of *Paci2013* model (Paci et al., 2013).

In *Paci2020* model (Paci et al., 2020), the enhancement of the AP automaticity was one of the main improvements compared to the previous versions. Furthermore, the inability of *Paci2018* in simulating the termination of the spontaneous activity due to an I_{NCX} strong blockade, observed in earlier *in vitro* investigations, was a limitation resolved in *Paci2020* model. The authors identified the large window in the fast Na^+ current of *Paci2018* as the responsible factor for maintaining the automaticity when the cell is subject to significant I_{NCX} inhibition. Other important updates in *Paci2020* model of hiPSC-CMs electrophysiology included updating the I_{Na} and I_f by adopting the equations from Koivumäki2018 model (Koivumäki et al., 2018). The improvements resulted in the activation of the spontaneous beating by I_f and SR Ca^{2+} sequentially contributing to AP depolarization through I_{NCX} .

As the models are developed based on a system of ODEs, in a time-evolution manner, the models reach a steady-state from generic initial values obtained either by data fittings, calibrations, experimental data in the literature, or model optimizations (Paci 2013, 2018, 2020). Figure 7 illustrates the schematics of Paci latest model, *Paci2020*, in which the components that have been improved overtime are in red.

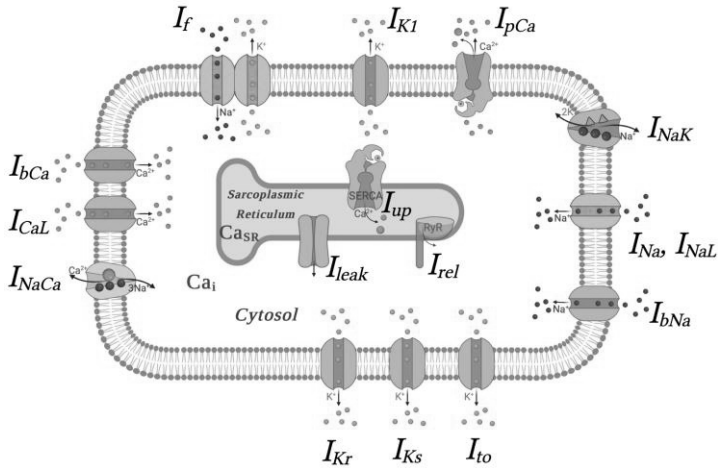


Figure 7. Schematics of the first 0D computational model of hiPSC-CMs, Paci et al. lineage, addressing only the electrophysiology of the cell adopted form (Botti, Sofia, 2022) with permission. The red components denote the key evolved formulations since Paci2013 model (Paci et al., 2013).

2.5.2 Koivumäki model: the structural immaturity

The second generation of computational models of ventricular hiPSC-CMs electrophysiology was introduced by Koivumäki et al., in 2018 (Koivumäki et al., 2018). The model was developed based on *Paci2013* (Paci et al., 2013), integrating a novel cell geometrical structure accounting for the heterogeneous Ca^{2+} dynamics. Specifically, *Koivumäki2018* model could capture the spontaneous SR Ca^{2+} release in hiPSC-CM which were not addressed in the previous *in silico* models at the time (Paci et al., 2013, 2015). As the red components in Figure 8 also denote, the three main updates of *Koivumäki2018* model with respect to *Paci2013* (Paci et al., 2013) and *Paci2015* (Paci et al., 2015) models can be summarized as:

- An improved I_{Na} formulation adopted from (Skibsbbye et al., 2016) and calibrated regarding hiPSC-CMs *in vitro* data of (Ma et al., 2011);
- A new I_{CaL} formulation from (Koivumäki et al., 2014) was adopted to optimize the fitting to the *in vitro* hiPSC-CMs recordings presented in (Koivumäki et al., 2018);
- The calibration of the activation component of I_{f} in order to reach an accurate consistency with the *in vitro* data by (Sartiani et al., 2007).

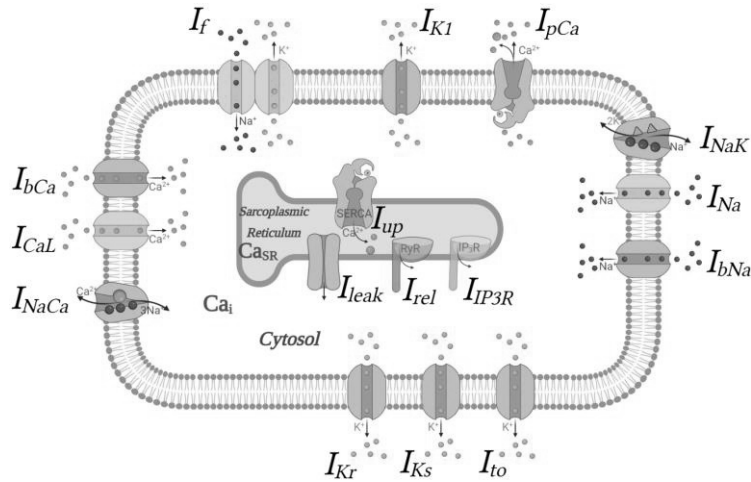


Figure 8. Schematics of *Koivumäki2018* computational model of hiPSC-CMs electrophysiology adopted form (Botti, Sofia, 2022) with permission. The red components denote the updated formulations with respect to Pacı2013 model.

Equipped with a refined subcellular Ca^{2+} formulations, *Koivumäki2018* model focused on the structural immaturity of hiPSC-CMs and by comparison with a hV-CMs computational model (Grandi et al., 2010) provided insights into the translational challenges of hiPSC-CMs investigations. Specifically, Koivumäki et al. reported that hiPSC-CMs show poor translation of the pathological phenotypical characteristics associated with Brugada syndrome and catecholaminergic polymorphic ventricular tachycardia (Koivumäki et al., 2018). Furthermore, based on a sensitivity test, they reported that in spite of sharing some properties with hV-CMs, hiPSC-CMs are functionally categorized closer to prenatal CMs. Finally, Koivumäki et al. concluded that the translational power of hiPSC-CM is mostly challenged by the immature cytosolic Ca^{2+} handling and advancing the mathematical platforms are vital in increasing our understanding of the optimizing the translational capability of hiPSC-CMs (Koivumäki et al., 2018).

2.5.3 Kernik model: phenotypic variability

Kernik and colleagues in 2019 introduced a whole-cell computational model of hiPSC-CMs taking into account interlab variability of hiPSC-CMs *in vitro* data by developing population of models and novel parametrizations to fit the experimental

readouts (Kernik et al., 2019). *Kernik2019* model construction follows H-H formalism based on Eq. 1.13 (Cauchy generalization) and considers the time rate of membrane potential equal to sum of transmembrane and stimulation currents (Kernik et al., 2019). The schematics of the model components and an example current formulation is given in Figure 9. *Kernik2019* model offers reformulations of I_{CaL} , I_{Na} , I_{Ks} , I_{Kr} , I_{to} , I_{K1} , and I_f , based on H-H formalism where a single exponential rate is optimized to fit *in vitro* data of hiPSC-CMs. Other currents were adopted from works of (Maltsev & Lakatta, 2009; Shannon et al., 2004; ten Tusscher et al., 2004) and calibrated to fit the experimental readouts. Notably, the *Kernik2019* model captures the CICR phenomenon in hiPSC-CMs which is comparable to *Koivumäki2018* model.

Finally, the optimization procedure of *Kernik2019* model consisted of a stepwise process of building the ionic current framework and a subsequent whole-cell level optimizations (Kernik et al., 2019). The optimization included evaluation of AP morphology biomarkers, namely, MDP, dV/dt_{max} , APD_{90} , and AP amplitude (Kernik et al., 2019). In summary, the discrepancy between the voltage-dependent characteristics of a specific gate's steady-state and time constants, as predicted by the model and observed experimentally, was reduced by performing a parameter optimization for each current. Optimizing other maximal conductances and rates involved examining every current, then considering the morphology markers for AP and CaT as described in (Kernik et al., 2019). This study aimed to explore the subcellular phenotypic mechanisms in hiPSC-CMs and establish a connection between the molecular mechanisms and cellular readouts through discovering unique set of model parameters related to reported hiPSC-CMs phenotypes.

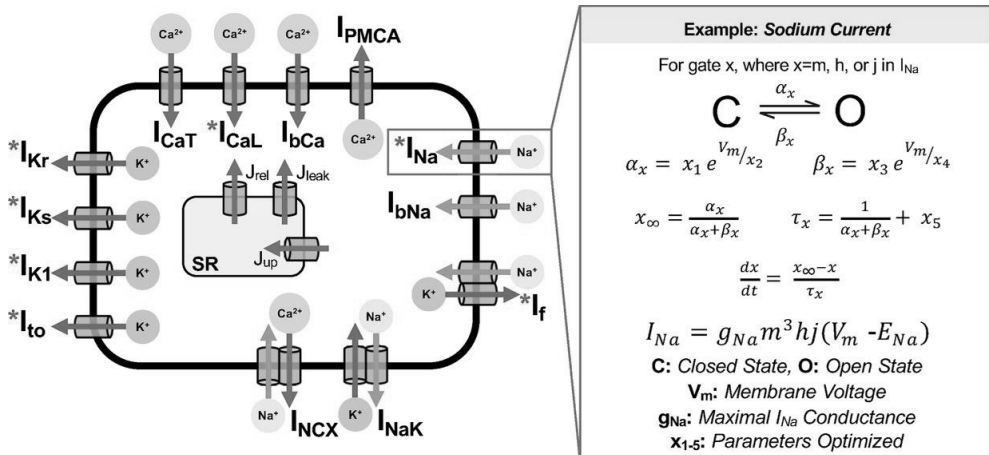


Figure 9. Schematics of Kernik2019 computational model of hiPSC-CMs electrophysiology adopted form (Kernik et al., 2019) under CC BY-NC license: <https://creativecommons.org/licenses/by-nc/4.0/>. The red stars denote the reformulated currents based on exponential voltage-dependent rate constants. On the right panel, the underlying equations of I_{Na} model are given. Of note, this example formulation also represents the gating variable modeling adopted in all the starred currents (Kernik et al., 2019).

2.5.4 A comparative review of the models

In 2021, Paci et al. reported a comparative study on the three main computational models of hiPSC-CMs electrophysiology i.e., *Paci2020*, *Koivumäki2018*, and *Kernik2019* which all were parametrized on hiPSC-CM *in vitro* data (Paci, Koivumäki, et al., 2021). Paci et al., gave an overview of the modeling paradigm for each component of the cell based on the formulation used (Table 1). Furthermore, the models show their differences in recapitulating hiPSC-CMs transmembrane currents, APs, and fluxes (Figure 11).

Table 1. The formulation paradigm of the currents and fluxes in *Kernik2019*, *Koivumäki2018*, and *Paci2020* models. HH denotes Hodgkin and Huxley, HH, R represents resistive Hodgkin and Huxley current/flux, HH, GHK indicates Hodgkin and Huxley with gates incorporating Goldman-Hodgkin-Katz driving force, M denotes Markov, and TT means adoption from ten Tusscher model. Refs: ¹(Shannon et al., 2004), ²(Keizer & Levine, 1996), ³(Sneyd & Dufour, 2002).

Currents	Kernik2019	Koivumäki2018	Paci2020
<i>Sarcolemmal</i>			
I_{Na}	HH	HH	HH
I_{NaL}	-	-	HH
I_f	HH	HH	HH
$I_{CaL} Ca^{2+}$	HH, GHK	HH	HH, GHK
$I_{CaL} Na^+$	HH, GHK	-	-
$I_{CaL} K^+$	HH, GHK	-	-
I_{CaT}	HH, GHK	-	-
I_{Kr}	HH	HH	HH
I_{Ks}	HH	HH	HH
I_{K1}	HH	HH	HH
I_{to}	HH	HH	HH
I_{NCX}	TT	TT	TT
I_{NaK}	TT	TT	TT
I_{pCa}	TT	TT	TT
I_{bNa}	HH, R	HH, R	HH, R
I_{bCa}	HH, R	HH, R	HH, R
<i>SR</i>			
J_{RyR}	M ¹	M ²	HH, R
J_{SERCA}	TT	TT	TT
J_{leak}	HH, R	HH, R	HH, R
J_{IP3}	M ³	-	-
Compartments	2	61	2
ODE #	23	26	23

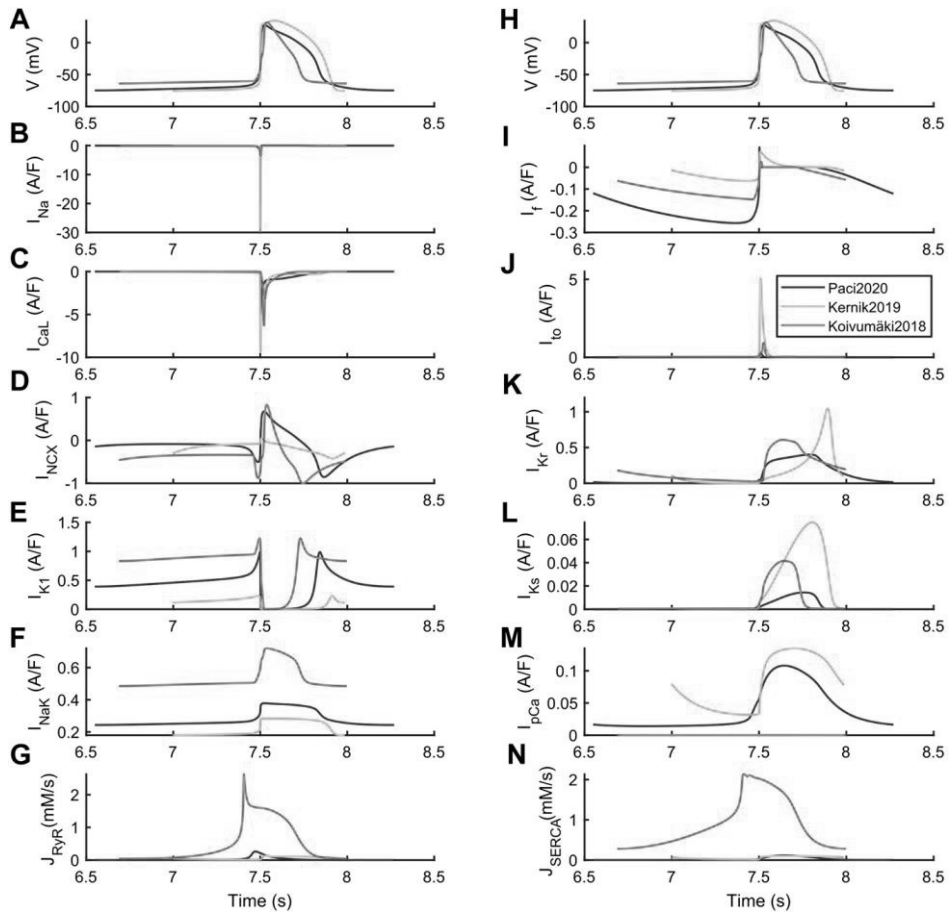


Figure 11. The steady-state membrane potentials and currents of *Paci2020*, *Kernik2019*, and *Koivumäki2018* models adopted from (Paci, Koivumäki, et al., 2021) under CC BY license: <https://creativecommons.org/licenses/by/4.0/>. *Kernik2019* simulates the highest I_{Na} , I_{CaL} , I_{to} , I_{Kr} and I_{Ks} , and the smallest I_{K1} . *Paci2020* and *Koivumäki2018* demonstrate a striking resemblance in the I_{NCX} shape. This similarity arises from the shared characteristic of both models wherein the automaticity is sustained by the pre-upstroke inward component of I_{NCX} , albeit to a lesser extent in the case of *Paci2020*. The *Kernik2019* study lacks the inclusion of the pre-upstroke inward component of the I_{NCX} .

In short, the models were evaluated in response to a number of compounds, specially through quantification of CaT duration at 90% of the initial base value (CTD90) and the frequency of occurrence of arrhythmic events. In addition, the sensitivity of each model to varying degrees of I_{Na} , I_{CaL} , and I_{Kr} current blockage was subsequently assessed. Finally, the impacts of drug-induced effects on CTD90 were compared with the findings obtained from *in vitro* experiments.

The observed changes in CTD90 were generally consistent among the *in silico* models, with all three models showing smaller magnitude changes compared to the *in vitro* measurements. Sparfloxacin at a concentration of 10 M was found to induce a 42% prolongation of CTD90 *in vitro*. Additionally, *in silico* models *Koivumäki2018*, *Kernik2019*, and *Paci2020* reported increases of 17%, 6%, and 9% respectively. After the administration of drugs, a range of arrhythmic events were observed, particularly for drugs that have an impact on I_{Kr} . *Paci2020* and *Kernik2019* models exclusively demonstrated repolarization failure. In contrast, *Koivumäki2018* exhibited both EADs and DADs. *Koivumäki2018* and *Paci2020* demonstrated that the utilization of Na^+ blockers and pharmacological agents that exhibit comparable effects on I_{CaL} and I_{Kr} effectively inhibited spontaneous activity, whereas only strong I_{CaL} blockers, such as nisoldipine, suppressed spontaneous activity in *Kernik2019*. The sensitivity analysis confirmed these findings.

On a computational note, the structural differences between the three models also were mirrored in their running times. *Paci2020* and *Kernik2019* were faster due to their simpler structure and compartmentalization (210 s simulations taking 22 s). *Koivumäki2018*, on the other hand, is more than 100 times slower due to its higher complexity (210 s simulations taking 2,331 s). Matlab 2017b was used to run these benchmark simulations on a computer (i7 @2.80 GHz and 32 GB memory).

On the whole, all the key computer whole-cell models of hiPSC-CMs had addressed only the electrophysiology. This also has been the dominating focus in computational models of adult hV-CMs (Bartolucci et al., 2020; Grandi et al., 2010; Kernik et al., 2019; O'Hara et al., 2011; ten Tusscher & Panfilov, 2006; Tomek et al., 2019). The phenomenon of myofilament contraction is observed in certain non-human multi-scale mathematical models, specifically those pertaining to the mouse and rat (Campbell et al., 2010; Land et al., 2013; Land & Niederer, 2015; Rice et al., 2008; Sheikh et al., 2012). Using such models allow linking the changes in intracellular properties to overall organ mechanical outcomes. Efforts have been made to develop human biophysical models that can accurately represent tension production and be integrated into a comprehensive framework for studying whole organ contraction. These models aim to incorporate the mechanical properties of cardiomyocytes (Land et al., 2017). In addition, some models of hV-CM electromechanics simulating active tensions and sarcomere dynamics were introduced (Margara et al., 2020; Margara, Wang, et al., 2021). Nevertheless, there was a dearth of biophysical models that encompassed the entirety of hiPSC-CM electromechanics and had the capability to accurately forecast active tension, cell shortening, and the inotropic impact of non-cardiomyocytes (Iseoka et al., 2018).

3 AIMS OF THE STUDY

The overall aim of this thesis was progressing mathematical models of hiPSC-CMs electrophysiology toward a more refined and comprehensive description of electro-mechano-energetic coupling at cell level. Therefore, the main objectives were defined as follows:

1. Developing a robust computational model of hiPSC-CMs electromechanics by integrating a reparametrized CE into Paci2020 model of hiPSC-CMs electrophysiology and quantitative and qualitative validation of the model against *in vitro* data (Study I & II).
2. Deep-phenotyping mutation-specific HCM by integrating a metabolite-sensitive model of CE into the established electromechanical model and investigating the mechanism of action and effects of sarcomere-targeting compounds, MAVA, BLEB, and OM on the disturbed actomyosin balance in HCM (Study III).
3. Characterizing the ionic and subcellular signature unique in I/R and action mechanism of Levo through designing a model capable of associating the hiPSC-CM metabolite and molecular dynamics to cell-level readouts (Study IV).

4 METHODS

4.1 Summary of the models

A brief overview of the models and the data based on which they were developed is given in Table 2.

Table 2 Summary of the modeling methods in each study. The detailed list of *in vitro* studies used are given in Tables 4, 7, and 8.

Study	Methods	Data
I	Integrating Negroni2015 and Rice2008 models of CE into Paci2020 model of hiPSC-CMs electrophysiology; simulating the developed tensions, tension-Ca ²⁺ relationships, and tension vs SL to study the calibration potentials of the models; ionic and contractile biomarker evaluations	Original values of model parameters from Negroni2015 (Negroni et al., 2015), Rice2008, and Paci2020 models.
II	Integrating Rice2008 CE into Paci2020 model of hiPSC-CMs electrophysiology and reparameterization of the CE; Sensitivity analysis of CE to identify the parameters governing CRT50 and FCS; A new passive force formulation as a function of percent of CMs in the EHTs to capture inotropic effects of non-CM components as an inter-scale analysis. EAD trigger due to 95% of I _{Kr} blockade; Channel-block IC50 based simulations of Verapamil and Bay-K 8644 compounds. The developed model was named hiPSC-CM-CE.	hiPSC-CMs <i>in vitro</i> data of FCS, CRT50, CRT25, categorizing inotropic effects of non-cardiomyocytes, contractile velocity profiles, and AT amplitude were used for CE reparameterization.
III	Integrating a metabolite-sensitive model of Rice2008 into Paci2020 model and reparametrizing the CE to fit hiPSC-CMs data in control and R403Q-HCM condition; MAVA-induced CE reparameterization and identifying the XB parameter(s) featuring in MAVA mechanism of	CRT50s, FCSs, AT amplitudes, pCa50s, Hill coefficients, and Tension vs drug dose relationship were calibrated using hiPSC-CMs <i>in</i>

	<p>action consistent with <i>in vitro</i> data. OM- and BLEB-induced CE reparameterizations and finding the XB parameter(s) governing the dose-dependent effects of OM and BLEB. The developed model was named hiMCE.</p>
<p>IV Optimizing the <i>in silico</i> protocol of ischemia simulation by considering oxygen deprivation and SERCA and CE metabolic changes in ischemia; Integrating a metabolite sensitive mathematical SERCA model into hiMCE model as SERCA responds significantly to ischemia; SERCA and CE calibrations for two severities of ischemia; Introducing an oxygen dynamic formulation considering the contractile ATPase rate and linking the effect of oxygen deprivation to I_{NaK} and I_{pCa} and vice versa; Expanding the channel-blocking formalism in modeling Levo mechanism of action by accounting for the role of I_{KATP} associating its inotropic effect to Ca^{2+}-bound to troponin transition rate in XBs in accord with <i>in vitro</i> data.</p>	<p><i>in vitro</i> data of control and R403Q-HCM and <i>in vitro</i> data from human, murine, and rat.</p> <p>Values of parameters used to model ischemia at two severities were derived from obtained from human based <i>in vitro</i> and <i>in silico</i> human-based works. SERCA and CE metabolite parameters change in accord with time courses of MgATP, MgADP, Pi, and pH calculated based on guinea pig hearts in the first 20 minutes of ischemia. SERCA sensitivity analyses of Ca^{2+} sensitivity and lup amplitude to identify the optimized calibration for I/R simulations.</p>

4.2 Integration of the contractile elements into the ionic model

The schematic representation of the hiPSC-CM-CE model is depicted in the middle panel of Figure 13. This diagram illustrates the various cell compartments, ion channels and pumps, as well as the CE component. The model consists of two distinct cellular compartments, namely the cytosol and the SR. According to Paci2020 model, both the I_f current and the pre-upstroke inward component of I_{NCX} play a role in sustaining spontaneous electrical activity. The electrophysiological basis is elucidated by the classical Hodgkin-Huxley formalism, which provides a description of the membrane potential as follows:

$$C \frac{dv}{dt} = -(I_{Na} + I_{NaL} + I_{CaL} + I_f + I_{K1} + I_{Kr} + I_{Ks} + I_{to} + I_{NaCa} + I_{NaK} + I_{pCa} + I_{bNa} + I_{bCa} - I_{stim}) \quad (4.1)$$

In this context, C represents the capacitance of a cell, I_{stim} denotes the stimulus current, and V represents the membrane potential. The simulations were conducted under the assumption of a temperature of 37°C, with extracellular concentrations of 151, 5.4, and 1.8 mM for Na^+ , K^+ , and Ca^{2+} , respectively.

In the CE by (Rice et al., 2008), there exist two distinct forms of Ca^{2+} binding: regulatory calcium binding, which exclusively impacts the activation of thin filaments, and apparent calcium binding, which exerts influence over the cytosolic CaT, representing the Ca^{2+} binding that is detected by the cell. In this study, I incorporated the CE into the Paci2020 electrophysiology model through two main steps. Firstly, I calculated the net Ca^{2+} concentration available for binding to troponin by subtracting the total troponin concentration from the overall concentration of buffered Ca^{2+} . Secondly, I determined the apparent Ca^{2+} binding by subtracting the Ca^{2+} flux towards the myofilaments from the cytosolic Ca^{2+} concentration. The latter is characterized by:

$$\begin{aligned} \frac{d}{dt} [Trop_{Apr}Ca] &= [Troponin] \times \frac{d}{dt} Trop_{Apr}(s) \quad (4.2) \\ \frac{d}{dt} Trop_{Apr}(s) &= -\frac{d}{dt} SOVF_{thin}(s) \times Trop_L + (1 - SOVF_{thin}(s)) \times \\ &\frac{d}{dt} Trop_L + \frac{d}{dt} SOVF_{thin}(s) \times (Frct_{SBXB} \times Trop_L + (1 - Frct_{SBXB}) \times \\ &Trop_L) + SOVF_{thin}(s) \times \left(\frac{d}{dt} Frct_{SBXB} \times Trop_L + Frct_{SBXB} \times \frac{d}{dt} Trop_H - \right. \\ &\left. \frac{d}{dt} Frct_{SBXB} \times Trop_L + (1 - Frct_{SBXB}) \times \frac{d}{dt} Trop_L \right) \quad (4.3) \end{aligned}$$

The total buffer concentration of troponin, $[Troponin]$ in Equation 4.2 was set to 70 μM according to (Rice et al., 2008). Also, the flux from cytosolic Ca^{2+} toward the myofilament is given by Equation 4.3. Here, $SOVF_{thin}(s)$ denotes the thin filament overlap which depends on sarcomere length s . The Ca^{2+} bindings to troponin with low and high affinity are represented by $Trop_L$ and $Trop_H$, respectively. Lastly, the fraction of strongly attached XBs is represented by $Frct_{SBXB}$. The equations and specificities of the CE utilized in the hiPSC-CM-CE computational model have been comprehensively described in the study conducted by (Rice et al., 2008).

4.3 Reparameterization of the contractile elements

The basis for the development of the Rice et al. CE was *in vitro* rabbit data. Consequently, I modified the CE to align with the hiPSC-CM Ca^{2+} and tension data from existing literature through the adjustment of XB cycling and Ca^{2+} -based thin

filament activation parameters. The primary approach employed in reparametrizing the CE involved identifying a specific set of parameters that would enable the model to accurately replicate essential contraction-related protocols of hiPSC-CMs within the documented experimental ranges at a temperature of 37°C and an extracellular Ca²⁺ concentration of 1.8 mM (refer to Table 4). Specifically, the percentage of FCS at a pacing frequency of 1Hz and the CRT50 (the duration from the peak of contraction to half of the relaxation) (Pioner et al., 2020), along with the magnitude of the generated active tension (Ruan et al., 2016).

The calibrated parameters of the CE primarily control the binding of Ca²⁺ ions to troponin. However, there are two additional parameters that play a role in the CE model. The first is m , as shown in Table 3, which serves as a tuning parameter aimed at enhancing the model's response times. The second parameter is $xbmodsp$, which is species-specific and influences the regulation of the thin filament and cross-bridge cycling (Rice et al., 2008). Table 3 presents the adjusted and initial values of the parameters for the CE integrated into different computational models of this thesis.

A sensitivity analysis was conducted to examine the behavior of hiPSC-CM-CE in relation to mechanical biomarkers, as outlined in the methodology described by (Romero et al., 2011). The percentage of change $D_{b,p,a}$, sensitivity $S_{b,p}$, and relative sensitivity $r_{b,p}$, are given as follows, where b denotes biomarker and p represents the model parameter:

$$D_{b,p,m} = \frac{(b_{p,m} - b_{ctl})}{b_{ctl}} \times 100 \quad (4.4)$$

$$S_{b,p} = \frac{\Delta D_{b,p,m}}{\Delta m} = \frac{D_{b,p,+15\%} - D_{b,p,-15\%}}{0.3} \quad (4.5)$$

$$r_{b,p} = \frac{S_{b,p}}{|S_{b,p}|_{max,b}} \quad (4.6)$$

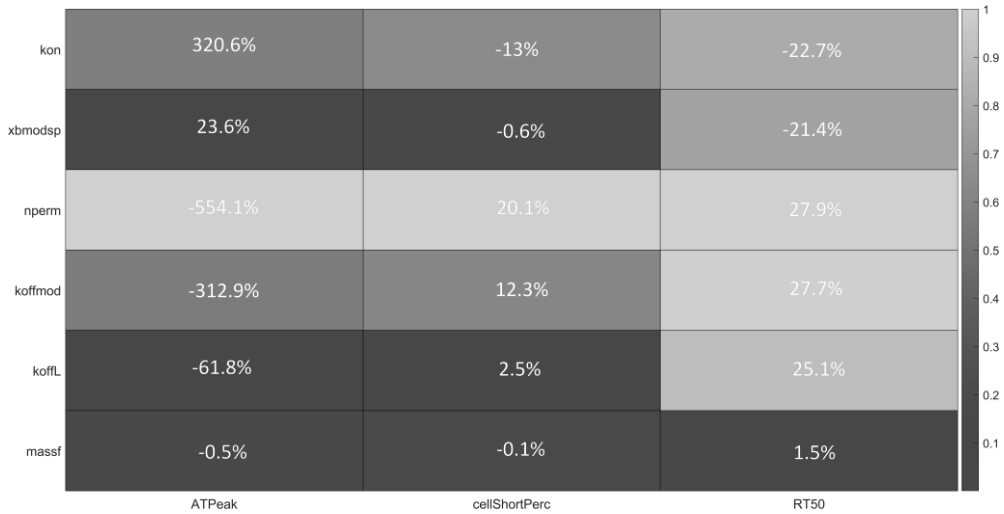


Figure 12. The sensitivity analysis performed on hiPSC-CM-CE model adopted from (Forouzandehmehr, Koivumäki, et al., 2021) under CC BY license: <https://creativecommons.org/licenses/by/4.0/>. The parameter alterations were within $\pm 15\%$ of the calibrated values. The color bar shows the relative sensitivity and the percents in each rectangle denote the maximum absolute sensitivity of the biomarker to the related parameter. ATPeak: Active Tension Peak, cellShortPerc: fractional cell shortening (%).

Tran et al. (Tran et al., 2017) proposed a mathematical model of a CE that integrated metabolite-sensitivity, building upon the work of (Rice et al., 2008). The aforementioned accomplishment was realized through the expansion of the Rice et al. model (Rice et al., 2008), wherein additional parameters were introduced to accommodate the competitive interaction between metabolic protons (H^+) and Ca^{2+} binding sites on troponin C. Furthermore, the model incorporates the binding kinetics of MgADP in the XB cycling process, as shown in Figure 13. The extended mechanistic description involves the division of the strongly bound state post isomerized rotation (XB_B) into two substates, AM1 and AM2, which are in rapid equilibrium. This division is done in order to accurately represent the kinetics of MgADP binding in the XBs, as depicted in Figure 13. The metabolite-sensitive model of XB kinetics and Ca^{2+} activation comprises four distinct states, namely, a non-permissive (N), a permissive (P), a pre power stroke state (XB_A), and a post power stroke state (XB_B) as shown in Figure 13 (Tran et al., 2017). XB_A and XB_B states both indicate the condition wherein myosin heads are firmly attached to actin filaments. (Rice et al., 2008; Tran et al., 2017). During the diastole phase, XBs exist in a non-interacting (N) state. However, upon activation by Ca^{2+} ions, XBs transition

into a high-energy state known as the permissive state (P). In this state, XBs are capable of engaging in the attaching and detaching of myosin heads, which is essential for the generation of tension within the muscle fibers (refer to Figure 13) (Tran et al., 2017). The active tension generated during the process is equivalent to the multiplication of myosin head strain and the fractional occupancy of strongly bound states (Tran et al., 2017).

In Studies III & IV, I have utilized the metabolite-sensitive CE model introduced by (Tran et al., 2017), and made adaptations to integrate active contraction mechanisms into the Paci2020 model of electrophysiology (Paci et al., 2020). In Study III, the extended CE model was adjusted manually by incorporating data from a prior sensitivity analysis (Figure 12) and a new set of sensitivity tests (Figures S2-S5 in (Forouzandehmehr et al., 2022) conducted on the contractile machinery and (Forouzandehmehr, Koivumäki, et al., 2021) (Table 3). I calibrated the model to accurately represent the AP, CaTs, and contractile experimental biomarkers observed in hiPSC-CMs under normal conditions, as outlined in Table 9.

In order to account for the influence of non-CM components in the model, and in line with the observed biphasic pattern of contraction-relaxation velocities for various cardiomyocyte ratios in EHTs as reported by (Iseoka et al., 2018), I introduced a piecewise function as the CE passive force (Eq. 4.7). In order to simulate the observed trend in Figure S7 of (Forouzandehmehr, Koivumäki, et al., 2021), an initial estimate using an exponential function was employed. The error was subsequently minimized through manual adjustments. This approach aimed to ensure that the simulated contraction-relaxation velocities accurately reproduced the data presented in (Iseoka et al., 2018). The passive force in this context refers to the influence exerted by the non-CM components on the dynamics of the sarcomere and the contractions of the cell, defined as:

$$F_{passive}(x) = \begin{cases} F_{titin}(x), & ctn = 100 \\ \frac{1}{0.54 \times (4.66 \times e^{-3.05c^{4.9}})} \times (F_{titin}(x) + F_{collagen}(x)), & 100 > ctn \geq 70 \\ (6 \times e^{-6.17c^{2.91}}) \times (F_{titin}(x) + F_{collagen}(x)), & 70 > ctn > 0 \end{cases} \quad (4.7)$$

Where c is equal to $ctn/100$ and ctn represents the percent of CMs in the EHT and x represents the length of the sarcomere.

Table 3 The values of the contractile element parameters for hiPSC-CM-CE (Forouzandehmehr, Koivumäki, et al., 2021) hiMCE, and hiMCES models. F1 and F2 represent DRX:SRX/(DRX:SRX)_{control} ratio in the XB cycling. K_{on} , K_{np} and K_{pn} respectively indicate the rate constants for Ca^{2+} binding to troponin and the forward and backward transition rates between Pxb and Nxb states (Rice et al., 2008). n_{perm} and $perm_{50}$ respectively represent the Hill coefficient and the half-activation constant, communicating the nonlinearity of the cooperativity in Ca^{2+} activation of XBs (Rice et al., 2008). K_{offL} and K_{offH} respectively represent the rate constants controlling Ca^{2+} unbinding from low and high affinity sites on troponin (Rice et al., 2008). m denotes the mass term in the Rice CE model (Rice et al., 2008). kxb denotes the tension scaling coefficient described in (Forouzandehmehr, Koivumäki, et al., 2021). $xbmodsp$ represents a species-dependent XB cycling rate scaling coefficient (Rice et al., 2008). The rate constant in the forward transition between XB_{preR} and XB_{pstR} is represented by h_f (Rice et al., 2008).

#	Parameter	Rice2008	hiPSC-CM-CE	hiMCE & hiMCES
1	F1	1	1	1
2	F2	1	1	1
3	K_{on} ($s^{-1} mM^{-1}$)	50×10^3	62.5×10^3	62.5×10^3
4	K_{offL} (s^{-1})	250	200	200
5	K_{offH} (s^{-1})	25	25	25
6	$perm_{50}$	0.5	0.6	0.6
7	n_{perm}	15	11.28	11.55
8	K_{np} (s^{-1})	500	550	550
9	K_{pn} (s^{-1})	50	50	50
10	K_{offmod}	1	0.5	0.5
11	m ($s^2 \mu m^{-1}$)	5×10^{-5}	2×10^{-5}	2×10^{-5}
12	kxb	120	12	13.1
14	$xbmodsp$	1.33, 1, 0.2	0.2	0.2
15	h_f (s^{-1})	2000	2000	2000

The experimental data obtained from hiPSC-CMs, which were used to reparametrize the computational CE model, consisted of the percentage of FCS, representing the preserved contractility of the CM (Pioner et al., 2020), the CRT_{50} (Clark et al., 2021), and the magnitude of active tension (Ruan et al., 2016).

Pioner et al. provided contractile *in vitro* data of % of FCS of hiPSC-CMs single cell lines with long term maturation paced at 0.5, 1, or 2 Hz through field stimulation (Pioner et al., 2020). Ruan et al. offered collagen-based hiPSC-CMs EHTs encapsulating single cell lines, and reported the developed active tensions in spontaneous and paced beating, based on digital measurements of sarcomere length and force signals and normalization of force over the circular cross-section area of

EHT constructs (Ruan et al., 2016). Table 4 provides a succinct overview of the model reparameterization, specifically regarding the experimental findings of hiPSC-CMs as documented in the referenced literature.

Table 4 The hiPSC-CM experimental data behind the reparameterization of the hiPSC-CM-CE model.

#	Experimental Paper	[Ca ²⁺] _e	Temperature (°C)	Target biomarkers of the calibration/results validations
1	Pioner et al., 2020 (Pioner et al., 2020)	1.8 mM	37	% of FSC
2	Clarks et al., 2021 (Clark et al., 2021)	1.8 mM	37	Contraction RT ₅₀
3	Yang et al., 2018 (Yang et al., 2018)	1.8 mM	37	% of FCS, Contraction RT ₂₅ ,
4	Ruan et al., 2016 (Ruan et al., 2016)	1.8 mM	Mechanical Measurements and drug tests at 37, Histological Measurements and microscopy at room temp.	Active tension amplitude and Verapamil and Bay-K 8644 inotropy
5	Iseoka et al., 2018 (Iseoka et al., 2018)	N/A	37	Inotropic effects of non-cardiomyocytes on the hiPSC-CM FCS and contraction-relaxation velocity
6	Hayakawa et al., 2014 (Hayakawa et al., 2014)	N/A	37	Contraction velocity profile
7	Rodriguez et al., 2014 (Rodriguez et al., 2014)	N/A	37	Contraction velocity profile

[Ca²⁺]_e denotes the extracellular Ca²⁺ concentration.

4.4 HCM and the drug-induced calibrations

In Study III, the baseline metabolite-sensitive CE of the hiPSC-CM model incorporates the primary influences of contractile metabolic substances, including

MgATP, MgADP, Pi, and H⁺, on the mechanism of tension development, as observed in the original Tran et al. model. (Tran et al., 2010, 2017). I calibrated the baseline model to construct a model of MYH7^{R403Q/+} HCM, which exhibits modified myofilament kinetics. The model variant was developed by adjusting certain metabolic parameters in order to simulate a state that aligns with experimental findings of MYH7^{R403Q/+} HCM, as outlined in Table 5.

The HCM model variant was derived by modifying the F1 and F2 values, as described in (Margara, Rodriguez, et al., 2021) and guided by the sensitivity tests previously reported in (Forouzandehmehr et al., 2022). Additionally, the concentration of MgADP was elevated, along with the reference value of Pi. The ap2 coefficient value was modified with regard to the hiMCE model sensitivity, as presented in Figure S2 of (Forouzandehmehr et al., 2022).

Table 5 The parameters used in the HCM model variant. Pi_ref represents the reference value for inorganic phosphate (Pi) in the simulations. The variable ap2 plays a significant role in the XB detachment. The coefficients F1 and F2 play a key role in influencing pre-rotational states in XB cycling, as demonstrated in the study conducted by (Margara, Rodriguez, et al., 2021).

#	Parameter	Control value	Value in HCM model variant
1	Pi_ref (mM)	2	18.9
2	MgADP (mM)	36×10 ⁻³	72×10 ⁻³
3	ap2 coef.	1	0.315
4	F1	1	1.3
5	F2	1	1.3

In a computational study conducted by (Margara, Rodriguez, et al., 2021), it was postulated that the primary influence of MAVA is on the transitions between XB_A and P states (Figure 13). This assumption is based on a disturbed DRX:SRX theory reported by (Toepfer et al., 2020). Following (Margara, Rodriguez, et al., 2021), I defined F1 and F2 coefficients denoting (DRX:SRX)/(DRX:SRX)_{control} ratio which take 1 as the control value. Changing F1 and F2 indirectly affect the CE ATPase dynamics (Figure 13) in the model and maps the HCM-induced disturbed interfilament state onto the transition between the permissive state and the strongly attached myosin pre-isomerization state (Forouzandehmehr et al., 2022).

In completion, I simulated the effect of MAVA expanding the affected parameter domain to achieve a thorough and precise analysis of the effect of 0.5 μM MAVA on the MYH7^{R403Q/+} HCM variant (Table 6). Experimental reports by (Awinda et al., 2020), (Alsulami & Marston, 2020), and (Green et al., 2016) guided the trends

taken in the MAVA-induced manual calibration regarding the effect of MAVA on Ca^{2+} activation and binding kinetics, P_i , and CE ATPase activity, respectively.

Of note, the CE parameter sensitivity analysis done previously in (Forouzandehmehr, Koivumäki, et al., 2021) informed the alterations made in K_{on} and n_{perm} values. Similarly, the CE sensitivity analysis reported in Fig. S4. of (Forouzandehmehr et al., 2022) guided the calibration of F1 and F2 coefficients. Further, *ap1* and *ap3* coefficients and A-E, in Equations 4.8-4.12, values were found through trial and error.

Table 6 The hiMCE model contractile element calibration to simulate the effect of Mavacamten.

A, B, C, D, and E are coefficients in Equations. 4.8-4.12 affecting P- XB_A interaction, P_i -dependent transition in P- XB_A , XB_A - XB_B regulation, Proton-dependent transition in XB_B - XB_A , and MgATP-dependent transition from XB_B -P, respectively. BL represents the baseline value given in Table 3. The baseline values of A-E, *ap1*, *ap3*, F1, and F2 are equal to 1.

#	Parameter	Values in 0.5 μM MAVA
1	$K_{on}(\text{mM}^{-1} \text{s}^{-1})$	BL \times 1.048
2	n_{perm}	BL \times 0.688
3	A	0.26
4	B	0.4
5	C	5.4
6	D	0.4
7	E	2.39
8	<i>ap1</i> coef.	1.45
9	<i>ap3</i> coef.	0.28
10	F1	0.1
11	F2	0.1

To demonstrate, A regulates the transition from P to XB_A , B modulates the P_i -dependent transition from XB_A to P, C adjusts the transition from XB_A to XB_B , D regulates the H^+ -dependent transition from XB_B to XB_A , and E impacts the MgATP-dependent transition from XB_B to P states (Forouzandehmehr et al., 2022). Correspondingly, the proposed modulations (A to E in Table 6) to Equations. 4.8-4.12, are in line with a disturbed interfilament state that impacts the tension-generating states of the XB as suggested in the etiology of MYH7^{R403Q/+} HCM (Nag et al., 2015b). My motivation for using A-E coefficients was the role of *xbmodsp* parameter in CRT50 observed in the sensitivity study before (Forouzandehmehr, Koivumäki, et al., 2021). In order to achieve a more precise simulation of the

impaired relaxation restored by 0.5 μM MAVA, I found that solely modifying $xbmodsp$ would not suffice. Therefore, the A-E values were employed to provide an optimized distribution of $xbmodsp$ effect on the contractile machinery.

$$f_{apt} = f_{ap} \times A \times xbmodsp \times Q_{f_{ap}}^{((T_{mpc}-37)/10)} \quad (4.8)$$

$$g_{apt} = g_{ap} \times g_{apstmd} \times B \times xbmodsp \times Q_{g_{ap}}^{((T_{mpc}-37)/10)} \quad (4.9)$$

$$h_{ft} = h_f \times h_{fmd} \times C \times xbmodsp \times Q_{h_f}^{((T_{mpc}-37)/10)} \quad (4.10)$$

$$h_{bt} = h_b \times D \times xbmodsp \times Q_{h_b}^{((T_{mpc}-37)/10)} \quad (4.11)$$

$$g_{xbt} = g_{xb} \times \max(g_{xbmd}, 1) \times E \times xbmodsp \times Q_{g_{xb}}^{((T_{mpc}-37)/10)} \quad (4.12)$$

The thin filament regulation and XB cycling parameters h_b , g_{ap} , g_{apstmd} and temperature dependences Q_{h_b} , $Q_{g_{xb}}$, $Q_{g_{ap}}$ values were directly adopted from (Rice et al., 2008). Also, g_{xbmd} regulates the strain-dependent rate of myosin heads defined in (Rice et al., 2008).

In Study III, the parameters of the hiMCE model were modified to simulate the impact of 5 μM BLEB and 1 μM OM, as well as to recapitulate the dose-dependent influence of BLEB and OM on the normalized tension. The specific values of these parameters can be found in (Forouzandehmehr et al., 2022).

Table 7 summarizes the *in vitro* data used for calibration and validations of the hiMCE model (Study III) readouts (Forouzandehmehr et al., 2022).

Calibration	(Green et al., 2016; Toepfer et al., 2020)	hiPSC-CMs Murine	The fractional cell shortening in R403Q	Corrected tension relaxation due to MAVA	33% increase of tension relaxation in R403Q	Fig. 3F	Fig. 3C	hiPSC-CM cell lines at day 30 post-differentiation,
	Reduction in fractional cell shortening due to MAVA		hiPSC-CMs	hiPSC-CM cell lines at day 30 post-differentiation, isolated adult rat ventricular cardiomyocytes treated with increasing concentrations of MAVA				

Table 7 Summary of the *in vitro* data behind the hiMCE *in silico* model.

Validation				
(Bakkehaug et al., 2015; Utter et al., 2015)	Murine Porcine	ATPase basal value increase due to OM	Fig. 5B	Ex vivo mouse and in vivo pig hearts
(Szentandrássy et al., 2016)	Canine	Change in APD due to 1 μ M OM	Fig. 5A	Left ventricular single canine myocytes
(Kawas et al., 2017)	Human & Bovine	Slowed relaxation in ATPase rate due to MAVA	Fig. 3D	Human and bovine cardiac myosins
(Rohde et al., 2018) (Kawas et al., 2017) (Green et al., 2016) (Gollapudi et al., 2021)	Human, Porcine, Bovine, and Murine	Reduction in ATPase rate due to MAVA	Fig. 3D	Human β -cardiac myosin, Porcine and Bovine ventricular myosin, mouse cardiac myofibrils
(Green et al., 2016)	Murine	Unchanged Cat and pCa ₅₀ in Tension-pCa curve due to MAVA	Fig. 3B, Fig. S1	Isolated adult rat ventricular cardiomyocytes
(Nag et al., 2015b; Sarkar et al., 2020)	Human, hiPSC-CMs	Negligible change in ATPase in R403Q	Fig. 3D	Human β -cardiac myosin
(Sewanan et al., 2019)	hiPSC-CMs	The unaffected CaT in R403Q	Fig. 3B	Engineered heart tissues made of hiPSC-CMs on decellularized porcine left ventricular tissue blocks
(Kampourakis et al., 2018)	Rat	OM and BLEB dose-dependent contractile response	Fig. 4D&E	Demembrated rat ventricular trabeculae
(Awinda et al., 2020; Green et al., 2016)	Murine, Human	Reduction in maximum tension due to MAVA	Fig. 3C	Isolated adult rat ventricular cardiomyocytes, skinned human myocardial strips

Type	Experiment	Cell/tissue type	Observation	Figure/Table in the paper	Preparation data
------	------------	------------------	-------------	---------------------------	------------------

4.5 Integrating a metabolite-sensitive SERCA model into hiMCE

In Study IV, an expansion of the model was undertaken to incorporate a more sophisticated electro-mechano-energetic coupling. This was achieved by integrating a thermodynamic 2-state model of the SERCA pump (Tran et al., 2009) into the hiMCE framework. The resulting model, referred to as hiMCES, was then utilized to investigate the pathophysiology of I/R, arrhythmia, and the impact of Levosimendan (Simdax®, Orion Corporation). The selection of the 2-state SERCA pump over the 3-state variant was determined by the findings presented in (Tran et al., 2009). The data provided in (Tran et al., 2009) demonstrated that both models exhibit identical behavior within the micromolar range of MgATP, which aligns with the working range of Study IV as indicated in Table 7.

The schematic representation of the hiMCES model, which includes the essential states and transitions of the CE and SERCA, is depicted in Figure 13. The SERCA pump is an enzyme classified as a P-type ATPase, which plays a crucial role in the functioning of skeletal (SERCA1a) and cardiac (SERCA2a) muscles (Tran et al., 2009). The previous literature has extensively discussed the equations that describe the ionic and contractile components of hiMCES (Forouzandehmehr et al., 2022; Forouzandehmehr, Koivumäki, et al., 2021; Paci et al., 2018). In this section, the mathematical formulation of the SERCA pump utilized in the hiMCES model is presented.

Tran et al., (Tran et al., 2009), developed a thermodynamic model of the SERCA that incorporates rapid equilibrium assumptions relevant to physiological and ischemic conditions. This model is based on the E1-E2 model of Ca^{2+} transport in SERCA proposed by (Makinose, 1973; Meis & Vianna, 1979). Additionally, the model includes proton (H^+) binding kinetics to account for pH-dependent effects. The apparent forward rates, as given in Figure 13, are explicitly defined as:

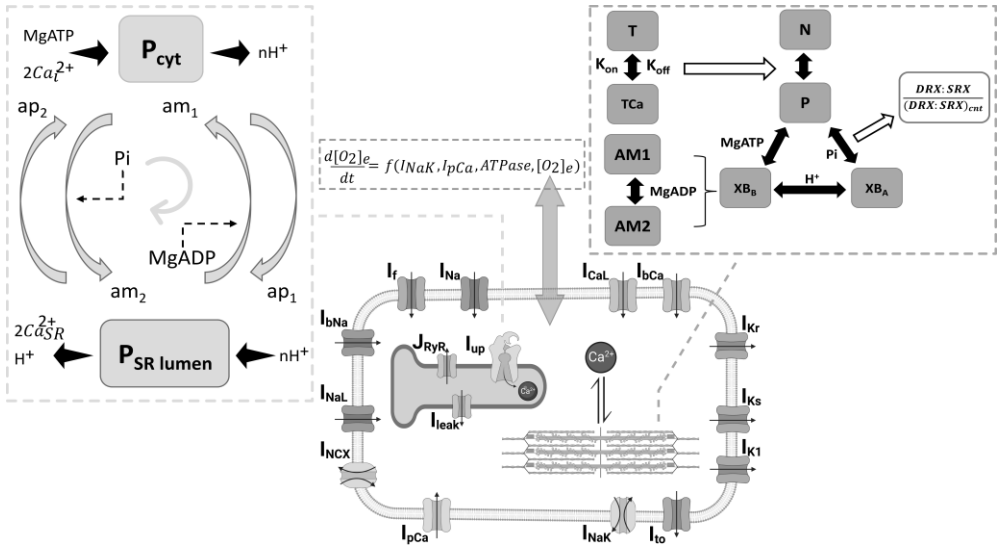


Figure 13 Schematics of the hiMCES model in Study IV. Left: SERCA pump 2-state model capturing the release of APD and Pi. The apparent rate constants, namely, ap_1 , ap_2 , am_1 , and am_2 are contingent upon the concentrations of cytosolic and SR Ca^{2+} , protons, and SERCA dissociation constants. P_{cyt} : lumped states of MgATP, H^+ , and Ca_i binding in cytosol. $P_{SR\text{Lumen}}$: lumped states of MgADP, H^+ , and Ca^{2+} binding in SR (Tran et al., 2009). Center: schematic of hiMCES main cell compartments, the ionic currents, and the model extracellular oxygen dynamics. Right: Schematic of the 4-state myofilament crossbridge (XB) cycling of hiMCES. T: troponin, TCa: Ca^{2+} bound troponin, N: off state prohibiting XB formation, P_{XB} : XB formation permissive state, XB_A : strongly bound XBs prior to isomerized rotation, XB_B : XBs in strongly bound post isomerized rotation state, AM1 and AM2 denote strongly-bound rapid equilibrium substates equally contributing to the generation of tension (Tran et al., 2010), DRX: Disordered relaxed state, SRX: Super relaxed state.

$$ap_1 = \frac{k_2^+ MgATP \widehat{Ca}_i^2}{MgATP \widehat{Ca}_i^2 + \widehat{H}_i (1 + MgATP (1 + \widehat{H}_1 + \widehat{Ca}_i^2))} \quad (4.13)$$

$$ap_2 = \frac{k_3^+ \widehat{H}_{SR}}{\widehat{H}_{SR} (1 + \widehat{H}) + \widehat{H} (1 + \widehat{Ca}_{SR}^2)} \quad (4.14)$$

The apparent backward rates are given as:

$$am_1 = \frac{k_2^- [MgADP] \widehat{Ca}_{SR}^2 \widehat{H}}{\widehat{H}_{SR} (1 + \widehat{H}) + \widehat{H} (1 + \widehat{Ca}_{SR}^2)} \quad (4.15)$$

$$am_2 = \frac{k_3^- [Pi] \widehat{H}_i}{MgATP \widehat{Ca}_i^2 + \widehat{H}_i (1 + MgATP (1 + \widehat{H}_1 + \widehat{Ca}_i^2))} \quad (4.16)$$

where

$$\widehat{Ca}_i = \frac{[Ca^{2+}]_i}{K_{d,Ca_i}}, \widehat{H}_i = \frac{[H^+]^{n_H}}{K_{d,H_i}}, \widehat{H}_1 = \frac{[H^+]}{K_{d,H_1}},$$

$$\widehat{Ca}_{SR} = \frac{[Ca^{2+}]_{SR}}{K_{d,CaSR}}, \widehat{H}_{SR} = \frac{[H^+]^{nH}}{K_{d,Hsr}}, \widehat{H} = \frac{[H^+]}{K_{d,H}}, \widehat{MgATP} = \frac{[MgATP]}{K_{d,ATP}}$$

$$K_{d,ATP} = \frac{k_1^-}{k_1^+} = \frac{k_2^+ k_3^+ K_{d,CaSR}^2 K_{d,Hi} K_{d,H}}{k_2^- k_3^- K_{d,Cai}^2 K_{d,Hsr} e^{\Delta G_{MgATP}^0 / RT}} \quad (4.17)$$

The values of the constants have been provided in Table 11. The rate at which the cycling SERCA pump operates, measured in units of s^{-1} , is defined as:

$$v_{cle} = \frac{ap_1 ap_2 - am_1 am_2}{ap_1 + ap_2 + am_1 + am_2} \quad (4.18)$$

According to (Liu et al., 2016, 2019), the flux of the SERCA pump, denoted as I_{up} , can be determined by multiplying the rate of calcium uptake into the SR (v_{cle}) by a scaling factor, S . This scaling factor, as described in Equation 4.19, is equivalent to the ratio of the maximum I_{up} simulated using the original formulation in the hiMCE model to the maximum v_{cle} simulated under control conditions.

$$I_{up} = S \times v_{cle} \quad (4.19)$$

4.6 Modeling of ischemia/reperfusion

4.6.1 Ischemia

In accordance with a well-established framework (Dutta et al., 2017; Ledezma et al., 2019; Rodriguez et al., 2006; Weiss et al., 2009), the severity of ischemia was classified into two distinct stages, namely SEV1 and SEV2. SEV1 represents a mild model, encompassing the period from the onset of the insult to 5 minutes post-insult. On the other hand, SEV2 corresponds to a severe model, occurring between 10 and 12 minutes after the ischemic insult. I simulated the ischemia at two different severity levels by utilizing the data provided in Table 7. The induction of hyperkalemia was achieved by changing the extracellular K^+ concentration, specifically by consistently increasing it to 6.25 and 9 mM. This methodology aligns with the approach utilized in previous studies conducted by (Kazbanov et al., 2014; Ledezma et al., 2019). Acidosis was simulated by reducing the maximum conductances of I_{Na} and I_{CaL} by 12.5% and 25% respectively, consistently with (Kazbanov et al., 2014; Ledezma et al., 2019). Likewise, I also attenuated I_{NaL} . The hiMCES model incorporated an ATP-sensitive potassium current (I_{KATP}) using the formulation proposed by (Kazbanov et

al., 2014). The maximum conductance of I_{KATP} was rescaled by the factor f_{KATP} under control, SEV1, and SEV2 conditions, as indicated in Table 7. The calculation of f_{KATP} values was based on an approach reported in (Ferrero et al., 1996). In this approach, the function of f_{KATP} is determined by the intracellular concentrations of MgATP and MgADP:

$$f_{KATP} = \frac{1}{1 + \left(\frac{[MgATP]}{K_{ADP}}\right)^h} \quad (4.20)$$

$$K_{ADP} = 35.8 + 17.9[MgADP]^{0.256} \quad (4.21)$$

$$h = 1.3 + 0.74e^{-0.09[MgADP]} \quad (4.22)$$

The values of f_{KATP} were determined using the concentrations of MgATP and MgADP under various conditions, as presented in Table 8.

Finally, a novel model of *in vitro*-based oxygen transport linking $[O_2]_e$ to cardiomyocyte ATP consumption was introduced based on methods in (Wan Ab Naim, Mohamed Mokhtarudin, Bakir, et al., 2021; Wei et al., 2014). The deprivation of oxygen in myocardium is simulated by reducing the oxygen source $[O_2]_s$, as the transport of oxygen in this context is a diffusion phenomenon. This reduction is done in order to model the extracellular oxygen concentration $[O_2]_e$ (Wan Ab Naim, Mohamed Mokhtarudin, Chan, et al., 2021). The oxygen formulation establishes a connection between two levels of oxygen concentration. One level is the oxygen concentration derived from the nearby capillary, referred to as $[O_2]_s$ (also known as source, supply, or bath). The other level is the oxygen concentration in the immediate extracellular space surrounding a single cell, denoted as $[O_2]_e$ (Wan Ab Naim, Mohamed Mokhtarudin, Bakir, et al., 2021) (Eq. 4.23). In addition, I took the contractile energetics into account by incorporating the contractile ATPase rate (measured in mM/s) into the simulations of oxygen dynamics. This decision was made based on the notable impact of contraction on myocardial oxygen consumption, as documented in studies on ischemia (Bo et al., 2021; Laslett et al., 1985; McDougal & Dewey, 2017). Here, the time rate of change in $[O_2]_e$ is calculated as:

$$\frac{d[O_2]_e}{dt} = -\Omega\gamma\beta(0.2I_{NaK} + I_{pCa}) - \Omega ATPase + \varepsilon([O_2]_s - [O_2]_e) \quad (4.23)$$

Where, the value of Ω was set to 1.6, based on the finding that the production of 1 mM/s ATP necessitates 1.6 mM/s oxygen through the complete oxidation of ATP, as reported by (Wei et al., 2014).

Table 8 The simulation of control, as well as the two severities of ischemia conditions with their respective pathology, involve the utilization of hiMCES model parameters and their corresponding references. f_{inh} is an scaling coefficient reducing the maximum conductances of I_{Na} and I_{CaL} ; f_{NaK} , f_{pCa} , and f_{KATP} are scaling coefs for reducing the maximum conductances of I_{NaK} , I_{pCa} , and I_{KATP} , respectively.

Item	Parameter	Control	SEV1	SEV2	Pathology	Reference
Ionic/extracellular concentrations	K_o (mM)	5.4	6.25	9	Hyperkalemia	(Kazbanov et al., 2014; Ledezma et al., 2019)
	$[O_2]_s$ (mM)	0.133	0.0551	0.0376	Hypoxia	(McDougal & Dewey, 2017)
	f_{inh}	1	0.875	0.75	Acidosis	(Kazbanov et al., 2014; Ledezma et al., 2019)
	f_{NaK}	1	0.8	0.69	Hypoxia	(Michailova et al., 2005)
	f_{pCa}	1	0.8	0.69		
	f_{KATP}	0.0041	0.0092	0.0128		
CE & SERCA metabolites	MgATP (mM)	5	4.2	3.1		(Tran et al., 2010)
	MgADP (mM)	36×10^{-3}	0.33	0.25		
	Pi (mM)	2	15.5	22		
	pH	7.15	6.5	6.3		

CE denotes contractile element. SEV1 & SEV2 represent the two severities of ischemia.

The charge utilization factor, denoted as γ , is a conversion factor that transforms the units of A/F (amperes per faraday) to mM/s (millimoles per second), defined as:

$$\gamma = \frac{C_m}{FV_c} \quad (4.24)$$

The cell capacitance, denoted as C_m , is equal to 98.7109×10^{-12} F. The unit F represents Farads, which is equivalent to 96485.3415 (C/mol). Additionally, the cell

volume, V_c , is equal to $8800 \times 10^{-18} \text{ m}^3$. The term ATPase refers to the rate at which contractile ATPase hydrolyzes ATP, measured in millimoles per second (mM/s). The value of β was assigned as 0.2658 based on the analysis of experimental data obtained from rat heart samples. These findings suggest that roughly 79% of the energy consumed by cardiomyocytes is attributed to contraction, while the remaining 21% is allocated to cell maintenance (McDougal & Dewey, 2017; Rolfe & Brown, 1997). The oxygen diffusion rate, denoted as ε , was determined to be $5 \text{ (s}^{-1}\text{)}$ using Fick's law, as described in (Cressman et al., 2009; Endeward, 2012):

$$\varepsilon = \frac{2D}{\Delta x^2} \quad (4.25)$$

The diffusion coefficient of O_2 in the I/R model of rat CMs, as reported in (Uchida et al., 1992), is denoted as $D = 2.5 \times 10^{-10} \text{ (m}^2\text{/s)}$. Additionally, the average distance between CMs in intact human cardiac tissues, as stated by (Endeward, 2012) is represented as $\Delta x = 10 \text{ }\mu\text{m}$. The baseline oxygen concentration in the source (bath) was $[\text{O}_2]_s = 0.133 \text{ mM}$, according to (McDougal & Dewey, 2017).

The impact of oxygen dynamics on I_{NaK} and I_{pCa} is mediated by the regulation of f_{NaK} and f_{pCa} , which are determined by a sigmoid function ρ (Petrushanko et al., 2007). This sigmoid function is subsequently multiplied by the maximum conductance of the currents (Wan Ab Naim, Mohamed Mokhtarudin, Bakir, et al., 2021; Wei et al., 2014). Indeed, ρ represents an O_2 dependent function which simulates the impact of oxygen deprivation on I_{NaK} and I_{pCa} , and vice versa. The coupling of oxygen dynamics to cell electrophysiology is done by ρ , expressed as:

$$\rho = \frac{a}{(1 + (\frac{[\text{O}_2]_e}{b})^c)} \quad (4.26)$$

Where, $a = 1.215$, $b = 0.215$, and $c = -1$. The utilization of ouabain-sensitivity has proven to be an effective indicator in the examination of the relationship between oxygen dependence and hypoperfusion (Chang et al., 2013; Petrushanko et al., 2007). Here, the values of variables a , b , and c were chosen in order to accurately simulate the oxygen deprivation effects, resembling the characteristic curve observed in I_{NaK} during hypoperfusion, as reported in (Chang et al., 2013; Sepp et al., 2014) (Figure 14A). Briefly, the values of a and b were determined to ensure that the IC_{50} of the curve would correspond to 15% of the maximum concentration, consistently with Ouabain $\text{IC}_{50} = 15 \text{ nM}$ within the dose-response curve range of 0-100 nM (Butt et al., 2000). Additionally, it was established that the hill coefficient, denoted as c , would

be a negative ouabain hill coefficient, $c = -1$, (Ferrandi et al., 1997). In light of the absence of direct measurement data, I derived the values of $[O_2]_s$ for SEV1 and SEV2 of ischemia by estimating the levels corresponding to 20% and 31% inhibition of I_{NaK} , as outlined in Table 7. This estimation was based on the ouabain-like curve presented in Figure 14A, which bidirectionally maps the oxygen deprivation onto I_{NaK} activity (Petrushanko et al., 2007). Figure 14B illustrates the temporal variation in the concentration of oxygen $[O_2]_s$ during simulations of I/R.

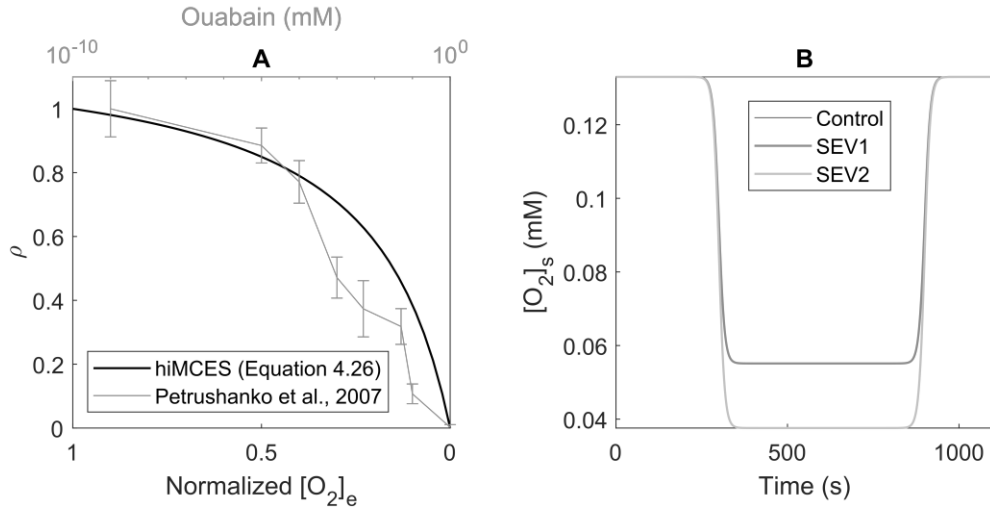


Figure 14 The rho function demonstrates a relationship between the inhibition of I_{NaK} and I_{pCa} and oxygen deprivation, which is in line with the inhibitory effect of ouabain on I_{NaK} activity (A). The variation in $[O_2]_s$ over time for different levels of ischemia severity, SEV1 and SEV2, is illustrated (B). ρ represents normalized activity of I_{NaK} .

4.6.2 Reperfusion

In order to incorporate I/R-induced arrhythmia into the I/R simulations, my initial step was adapting the methodology previously employed to simulate early EADs as described in (Forouzandehmehr, Koivumäki, et al., 2021). The maximum conductances and currents of the hiMCES model were adjusted using a coefficient SET, which was found to induce EADs in Paci2020 electrophysiology model (Paci, Koivumäki, et al., 2021). The occurrence of EADs following 95% inhibition of the I_{Kr} current was anticipated by the Paci2020 (Paci et al., 2020) and hiPSC-CM-CE (Forouzandehmehr, Koivumäki, et al., 2021) models. In the ischemic phase in I/R simulations, specifically during seconds 350-850 as shown in Figure 2B, I

consistently suppressed two significant factors that contribute to the repolarization reserve, namely I_{Kr} and I_{Ks} , by 85%. This aligns with findings from experimental studies on I/R conducted by (Y. Chen et al., 2017; C. Yin et al., 2017), as well as computational reports on ischemia by (Dutta et al., 2017). In the conducted I/R simulations, SEV1 values of ischemia were utilized, as indicated in Table 1. The simulation involved modeling the transitions of parameters from the oxygenated phase (0-350 s) to the ischemic phase (350-850 s), and subsequently returning to physoxia (850-1100 s), based on the calculated *in vivo* oxygen level of blood vessels (McDougal & Dewey, 2017). To achieve more realistic results, an ouabain-like behavior was employed, as depicted in Figure 14A, particularly during the transition to and from ischemia. In other words, rather than undergoing an abrupt switch from a concentration of 5 mM to 6.25 mM, the change in extracellular K^+ exhibited a pattern similar to the changes observed in $[O_2]_s$ at SEV1, as shown in Figure 14B.

In Study IV, the attainment of the steady state was achieved by reporting the results following a simulation run time of 800 seconds. Figure 14B depicts the model's control output after reaching the steady state (an 800-second run). Furthermore, it is worth noting that in Figure 14B, a duration of 500 seconds was simulated during the model's operation under ischemic conditions. This period was necessary to establish a steady state following the transition to SEV1/SEV2. The parameters SEV1 and SEV2 are indicative of the two levels of severity associated with acute ischemia. Therefore, in the context of computational simulations, the duration of the simulation (as shown in Figure 14B) is aimed at achieving a steady state condition and does not need to 1:1 correspond to the time protocols utilized in *in vitro* ischemic experiments. All of the results were observed in a state of spontaneous beating, unless otherwise specified.

To summarize, hiPSC-CM-CE was the first developed model of hiPSC-CMs electromechanics integrating a calibrated CE. The hiMCE, was the version upgraded with a reparametrized metabolite-sensitive CE, and it was used to study R403Q-HCM pathophysiology and the sarcomere-targeting drugs. Ultimately, building upon hiMCE, the hiMCES was the model incorporated a metabolite-sensitive model of SERCA reparametrized to fit ischemia/reperfusion condition and was adopted to map the ionic and subcellular crosstalks onto oxygen deprivation and contractile dysfunction in I/R. In the next chapter, a summary of the key results of this thesis is given.

5 RESULTS

5.1 Biomarker evaluations of the models

In the first stage, each developed computational model was validated against hiPSC-CMs *in vitro* data, by calculating a list of electrophysiological and contractile biomarkers (Table 9). The biomarkers were simulated in spontaneous beating and control condition except for percent of FCS and CRT50 which were computed at 1 Hz pacing matching the *in vitro* experiment (Clark et al., 2021; Pioner et al., 2020). Moreover, as Table 9 and Figure 15 confirm, the electromechanical models developed within this thesis were reparametrized to recap the key biomarkers accurately and maintain the electrophysiological and contractile traces morphology with respect to experiments.

Table 9 Action potential (AP), Ca²⁺ transients (CaT), and biomechanical biomarkers of Paci2020 (Paci et al., 2020), hiPSC-CM-CE (Forouzandehmehr, Koivumäki, et al., 2021), hiMCE (Forouzandehmehr et al., 2022), and hiMCES model computed in spontaneous condition in comparison with the experimental values (Forouzandehmehr, Koivumäki, et al., 2021; Paci et al., 2018, 2020).

No.	Biomarker	Paci2020	hiPSC-CM-CE	hiMCE	hiMCES	Experimental (Mean±SD)	Value
1	APA (mV)	102	103	103	103	104±6	
2	MDP (mV)	-74.9	-75.0	-75.0	-75.2	-75.6±6.6	
3	AP CL (ms)	1712	1644	1644	1694	1700±548	
4	dV/dt max (V/s)	20.5	23.9	24.0	10.7	27.8±26.3	
5	APD ₁₀ (ms)	87.0	95.0	95.1	91.6	74.1±26.3	
6	APD ₃₀ (ms)	224	238	238	238	180±59	

7	APD ₉₀ (ms)	390	403	403	413	415±119
8	AP Tri	2.8	2.9	3	2.9	2.5±1.1
9	CaT DURATION (ms)	691	693	693	693	805±188
10	CaT tRise _{10, peak} (ms)	184	163	163	197	270±108
11	CaT tRise _{10,50} (ms)	54.9	46.2	45.9	54	82.9±50.5
12	CaT tRise _{10,90} (ms)	118	102	102	125	167±70
13	CaT tDecay _{90,10} (ms)	341	343	343	317	410±100
14	AT magnitude (kPa)	-	0.055	0.055	0.0557	0.055±0.009
15	RT ₅₀ (ms)	-	161	158	154	158±12.1
16	%FCS	-	3.45	3.23	3.43	3.27±0.37

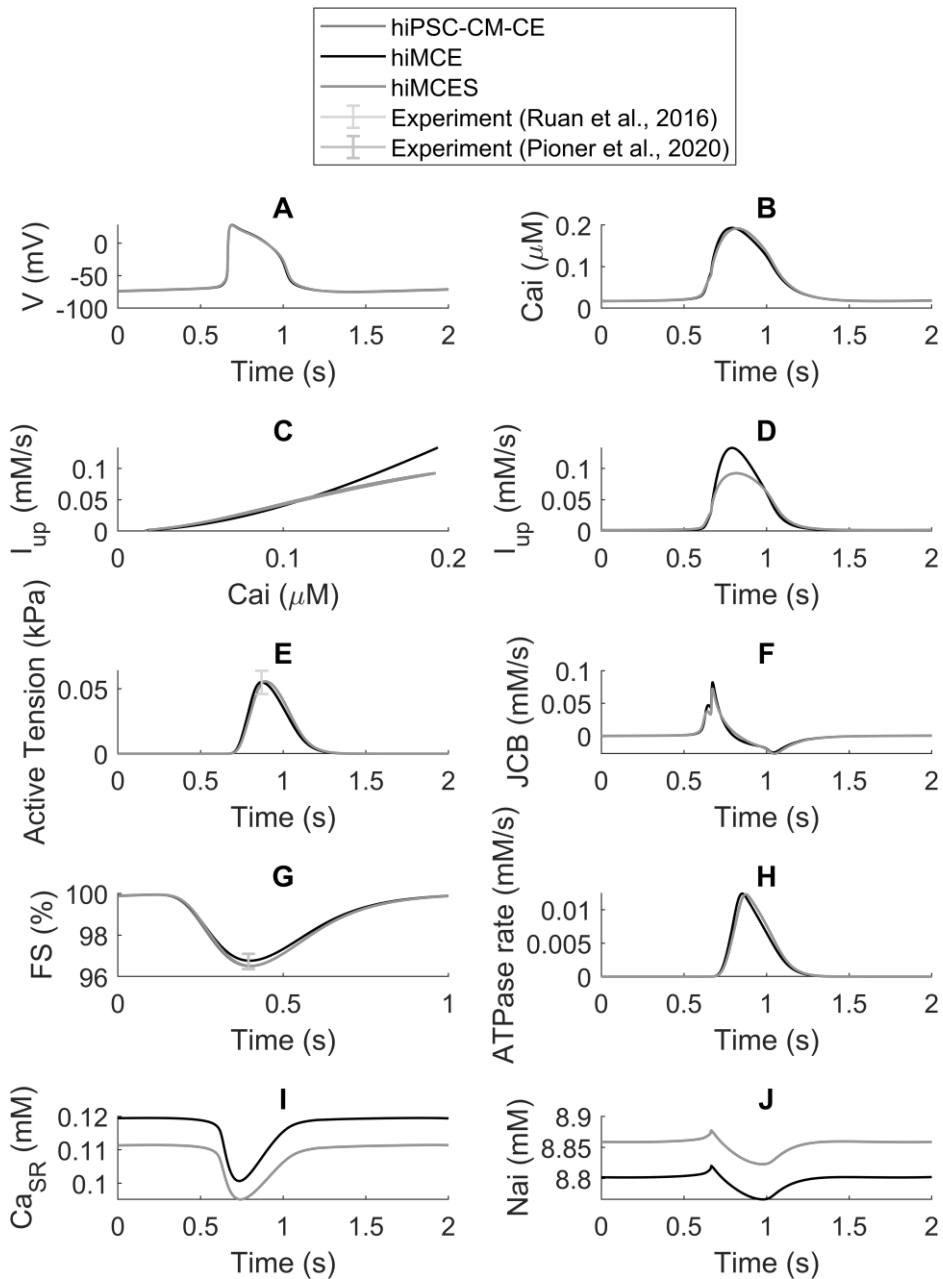


Figure 15 Standard outcomes of the hiMCEs model in control condition compared to hiPSC-CM-CE (Forouzandehmehr, Koivumäki, et al., 2021) and hiMCE (Forouzandehmehr et al., 2022) models. Action Potentials (A), Ca^{2+} Transients (B), SERCA uptake (I_{up}) (C & D), active tensions (E), flux of Ca^{2+} toward the contractile element (F), fractional cell shortening (G), contractile ATPase rate (H), sarcoplasmic reticulum Ca^{2+} concentration (I), and intracellular Na^+ concentrations (J). Panel G data are at 1 Hz pacing.

5.2 The results of hiPSC-CM-CE model

5.2.1 Model response to Verapamil and Bay-K8644

The model response to 90 nM Verapamil, as a multichannel action compound, was simulated following (Kramer et al., 2013), and the effect of 1 μ M of Bay-K 8644, with a previously reported positive inotropic effect for hiPSC-CMs (Ruan et al., 2016), was simulated as an agonist solely impacting I_{CaL} (Forouzandehmehr, Koivumäki, et al., 2021).

The simulation results of the hiPSC-CM-CE model demonstrated that the administration of Bay-K 8644 leads to the prolongation of AP, as shown in Figure 16A. Additionally, the compound induced an elevation in the CaT, as illustrated in Figure 16C. Consequently, there was an observed increase in the active tension, as given in Figure 16D. The results of this study are consistent with the AP prolongation observed in the research conducted by (Sicouri et al., 2007) and the reported positive inotropic effect of Bay-K 8644 in hiPSC-CMs *in vitro* experiments as documented by (Ruan et al., 2016). As shown in Figure 16D, the findings accurately align with the previous studies that categorize Verapamil as a negative inotropic agent in hiPSC-CMs (Ruan et al., 2016) and hV-CMs (Nguyen et al., 2017). The relaxation kinetics of the hiPSC-CM-CE model were examined by analyzing the RT80, which represents the time interval from peak contraction to 80% relaxation. The observed trends and ranges of RT80 in our study align with those reported for both commercially available and laboratory-generated hiPSC-CMs (Mannhardt et al., 2016), as depicted in Figure 16E.

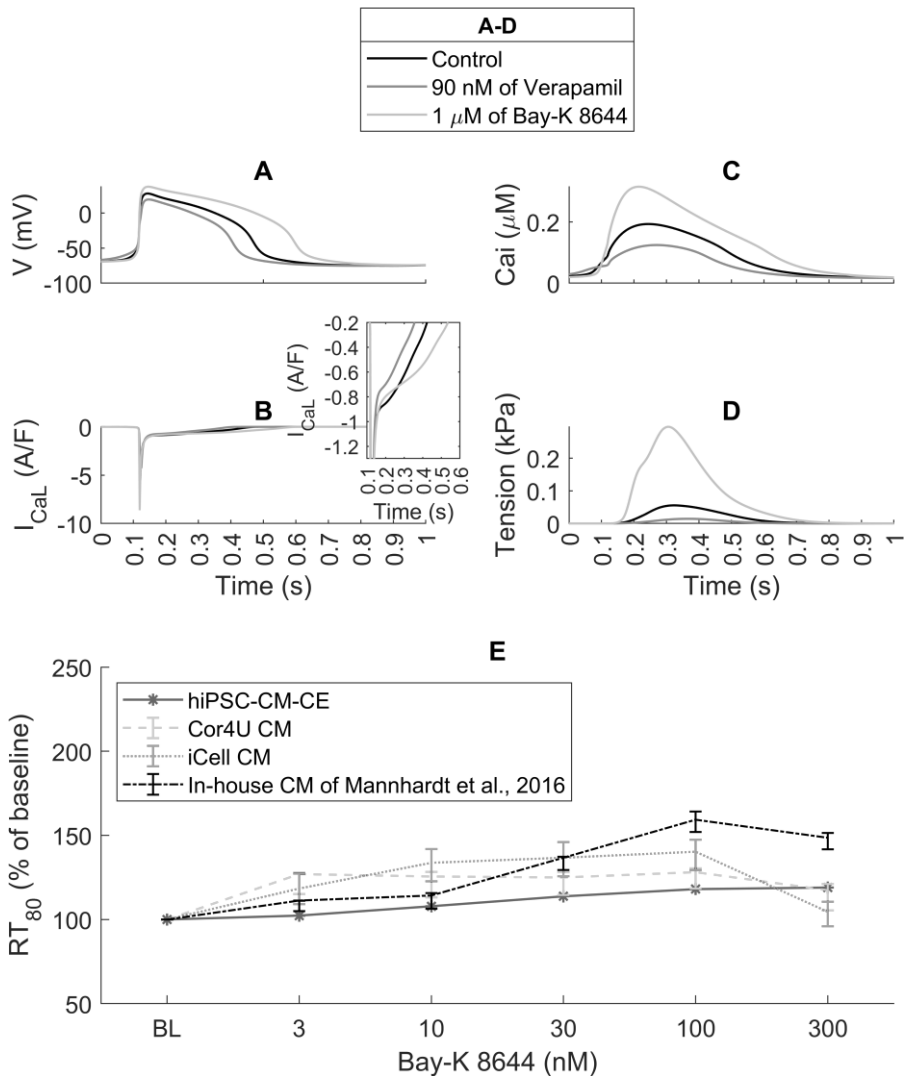


Figure 16 The hiPSC-CM-CE model outcomes in control and in response to inotropic drugs adopted from (Forouzandehmehr et al., 2021) under CC BY license: <https://creativecommons.org/licenses/by/4.0/>. (A) Action potentials, (B) L-type Ca^{2+} currents. (C) Cytosolic Ca^{2+} transients, (D) Active tensions, (E) RT_{80} (time interval from peak contraction to 80% of relaxation). The commercial cardiomyocytes, Cor4U and iCell, have been sourced from the data provided by (Mannhardt et al., 2016). The presented cases A-D exhibit data obtained under spontaneous conditions, while case E demonstrates the model results obtained under a pacing frequency of 1.5 Hz. It is worth mentioning that the tests conducted in panels A-D were also carried out under paced conditions (1Hz), and no significant differences were observed compared to the results presented in this figure. BL represents baseline.

5.2.2 Simulated inotropic effect of non-CMs in hiPSC-CM EHTs

Based on the observed biphasic pattern of contraction-relaxation velocities for various *ctn* ratios in hiPSC-CMs EHTs as reported by (Iseoka et al., 2018), I reformulated the CE passive force as a piecewise function (Equation 4.5). The incorporation of the passive force into the CE resulted in an accurate classification of the inotropic effects of non-CMs, as illustrated in Figure 17. Study II involves an inter-scale analysis of the behavior exhibited by hiPSC-CM tissues, as facilitated by the hiPSC-CM-CE simulations. In a comprehensive manner, the term "inter-scale" refers to the utilization of simulations conducted within a 0D framework to simulate and forecast the behavior of a domain consisting of multiple dimensions (1D or 2D) in a simplified manner.

Upon modifying the *ctn* parameter (Equation 4.5), the model exhibited both positive and negative inotropic effects, as indicated by the *in vitro* data presented in the study conducted by (Iseoka et al., 2018). These effects were observed in terms of contraction-relaxation velocity and FCS. The simulation results in Figure 17A demonstrate that the combination of 70% CMs and 30% non-CMs exhibit the greatest FCS. The velocities obtained from simulations conducted with 90% CMs in the EHT were observed to be lower compared to the velocities obtained from simulations involving 70% CMs in the EHT, as reported in the experimental study by (Iseoka et al., 2018). Significantly, the model accurately predicts the poorest contractile response consistently with the reported non-CMs effects suggesting the greatest electrical propagation inhibition for *ctn* = 25% (Iseoka et al., 2018).

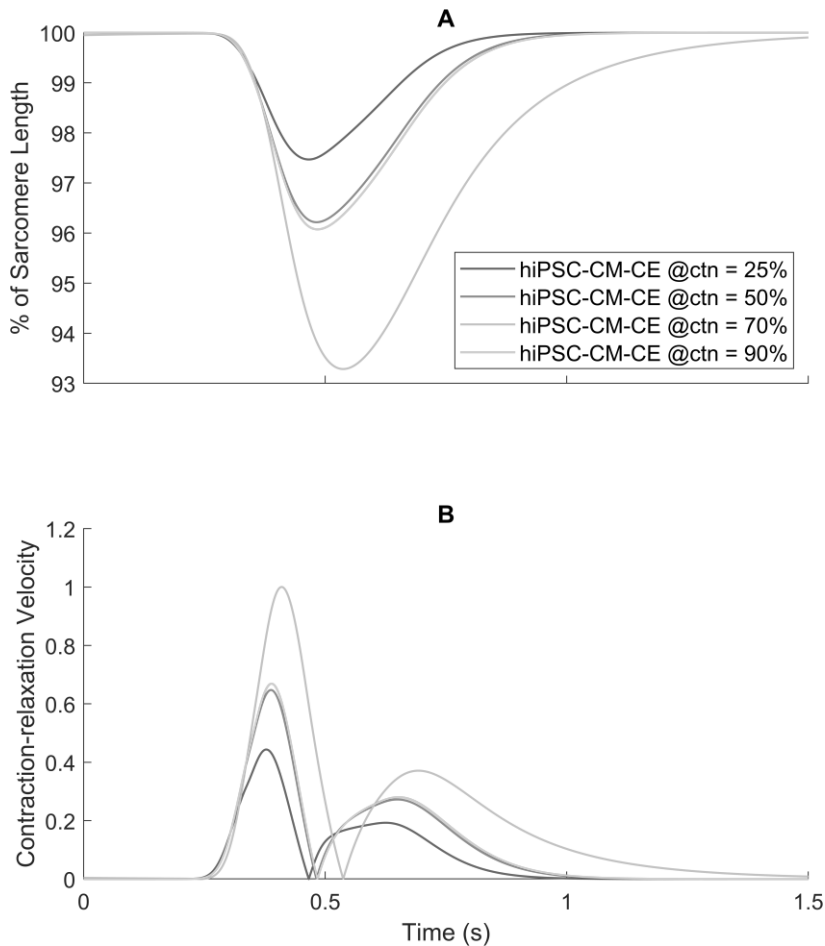


Figure 17 The simulated contractile performance regarding non-cardiomyocytes components in an engineered heart tissue adopted from (Forouzandehmehr et al., 2021) under CC BY license: <https://creativecommons.org/licenses/by/4.0/>. Normalized fractional cell shortenings (A) and contraction-relaxation velocities (B) at the simulated different percents of cardiomyocytes in an engineered heart tissue.

5.3 The results of hiMCE model

5.3.1 Simulation of HCM-R403Q and MAVA mechanisms

Based on the parameter values provided in Table 5 and in accordance with the metabolic data outlined in section 4.4, I performed a simulation to assess the active tension and ATPase rate in the MYH7^{R403Q/+} HCM model variant, as described in

Study III (Forouzandehmehr et al., 2022). The morphology of the CaT in the MYH7^{R403Q/+} HCM mode (Figure 18B) exhibited no alterations, which is in line with the findings reported by (Sewanan et al., 2019) for hiPSC-CMs. The findings depicted in Figure 18C provide intriguing evidence that incorporating energetics into the CE responds to the pathological alterations caused by MYH7^{R403Q/+} cardiomyopathy and can accurately forecast the extended relaxation in the generated active tension, with a similar magnitude of approximately 33%. These results align with the *in vitro* data of hiPSC-CMs reported by (Toepfer et al., 2020). Furthermore, the observed augmentation of FCS by approximately 40% resulting from the MYH7^{R403Q/+} cardiomyopathy aligns with the hiPSC-CMs *in vitro* findings reported in (Toepfer et al., 2020). It is worth mentioning that the model accurately predicts the minimal alteration in ATPase activity, as illustrated in Figure 18D, which aligns with the experimental findings presented in Table 9 (Nag et al., 2015b; Sarkar et al., 2020).

In order to replicate the electro-mechano-energetic impact of 0.5 μ M MAVA, I employed the model calibration values specified in Table 6. I hypothesized that the administration of MAVA would induce a restoration of the elevated metabolites, namely Pi and MgADP, toward their respective baseline levels in the MYH7^{R403Q/+} cardiomyopathy model variant. Of note, an unimpacted CaT in response to MAVA was accurately predicted by the hiMCE model in accord with experimental data (Green et al., 2016). Moreover, the observed decrease in simulated ATPase rate by 19.3% as a result of the presence of 0.5 μ M MAVA, as depicted in Figure 18D, falls within the range of reductions (17.9 to 28.5%) reported in previous experimental measurements of ATPase activity (Gollapudi et al., 2021). Also, the observed decrease in the ATPase rate relaxation phase is consistent with previous *in vitro* data (Figure 18D) (Kawas et al., 2017). Markedly, the simulations demonstrated a reduction of 14.6% in FCS and a prolongation of 20.9% in tension relaxation in response to 0.5 μ M MAVA in quantitative agreement with hiPSC-CMs *in vitro* data (Toepfer et al., 2020). Finally as shown in Fig. S1 of (Forouzandehmehr et al., 2022), when subjected to the effect of 0.5 μ M MAVA, the CE model accurately responded by simulating an unaffected pCa₅₀ in the tension-Ca²⁺ relationship in agreement with a previous experimental report (Green et al., 2016).

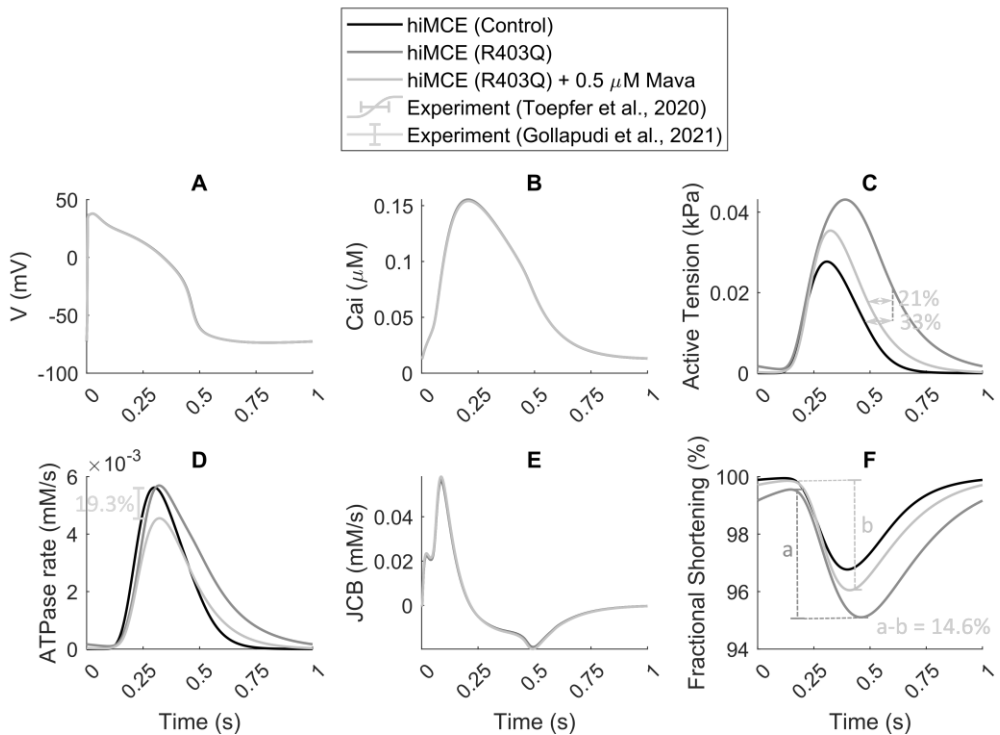


Figure 18 The hiMCE electro-mechano-energetic results in control, HCM, and under MAVA effect adopted from (Forouzandehmehr et al., 2022) under CC BY license: <https://creativecommons.org/licenses/by/4.0/>. The simulated results include the action potential (A), calcium transients (B), active tensions (C), ATPase rates (D), Ca^{2+} flux toward the myofilament (E), and fractional cell shortenings (F). These simulations were conducted with a pacing frequency of 1Hz. The percentages of prolonged tension relaxation in MYH7^{R403Q/+} mode (C), the decrease in tension relaxation attributed to MAVA (C), the decrease in fractional shortening in MYH7^{R403Q/+} mode caused by MAVA (F), and the decrease in ATPase rate due to MAVA (D) align with the empirical hiPSC-CMs observations (Gollapudi et al., 2021; Toepfer et al., 2020).

5.3.2 Modeling OM and BLEB dose-dependent inotropy

Employing the CE parameter values provided in Table 4 of Study III (Forouzandehmehr et al., 2022), the model response to 5 μM BLEB and 1 μM OM was simulated. According to the data presented in Table 10, the hiMCE model successfully predicted the Ca^{2+} sensitive effects of 5 μM BLEB and 1 μM OM, which aligns with the experimental findings reported by (Kampourakis et al., 2018). This agreement is further supported by the qualitative confirmation provided in Figure

19A. Furthermore, the coefficients of the tension governing variables in the CE, denoted as ap_2s were carefully chosen based on the information provided in Figure 19B&C and Tables S1 and S2 in (Forouzandehmehr et al., 2022). These selected coefficients successfully resulted in accurate dose-dependent predictions for BLEB and OM, as depicted in Figure 19D&E. Moreover, the predicted inverse Hill curves align with the experimental findings reported by (Kampourakis et al., 2018).

Table 10 The Ca^{2+} -dependent experimental ranges and the corresponding results of Study III in response to 1 μM OM and 5 μM BLEB. pCa_{50} denotes the negative logarithm of the concentration of Ca^{2+} ions at 50% of the maximum tension. The *in vitro* data presented in (Kampourakis et al., 2018) are based on the E-helix of cardiac troponin C (cTnC), and a probe that was linked to the myosin regulatory light chain (RLC).

#	Item	Kampourakis et al. 2018	hi-MCE Model
1	Increase in pCa_{50} due to 1 μM OM	5.4-6.9% (cRLC-E) 3.8-6.4% (cTnC-E)	5.8%
2	Decrease in pCa_{50} due to 5 μM BLEB	2.1-5.5% (cRLC-E) 2.6-5.7% (cTnC-E)	4.8%
3	Reduction of Hill coef. due to 1 μM OM	53.2-64.5% (cRLC-E) 57.1-68.1% (cTnC-E)	58.9%
4	Reduction of Hill coef. due to 5 μM BLEB	59.5-73.5% (cRLC-E) 44.8-58.3% (cTnC-E)	49.9%
5	Reduction in max tension due to 1 μM OM	0-29% (cRLC-E) 18-47% (cTnC-E)	25.3%
6	Reduction in max tension due to 5 μM BLEB	66-90% (cRLC-E) 64-80% (cTnC-E)	76.4%

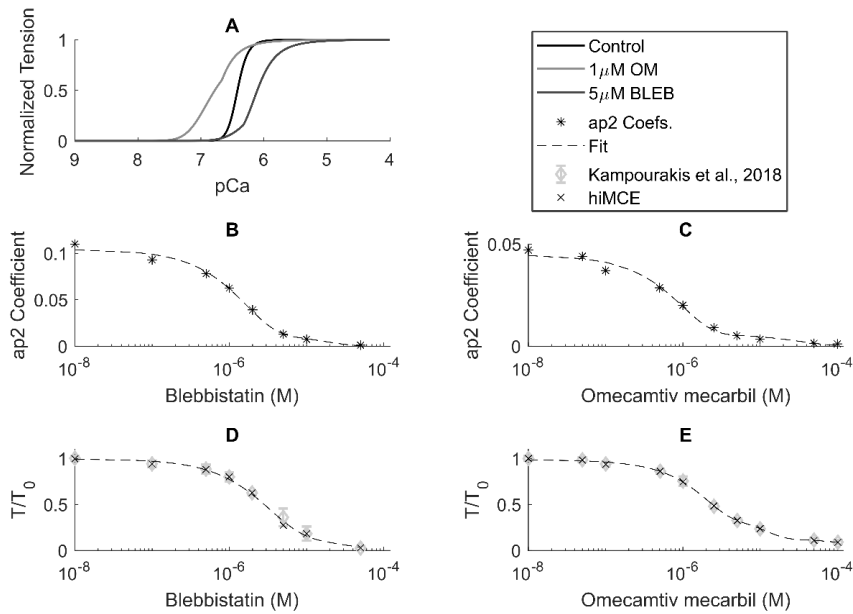


Figure 19 Mapping the dose-dependent inotropy of OM and BLEB onto the governing parameter in the hiMCE model. Isometric Ca^{2+} -tension relationships in control and drug-induced conditions (A), ap2 coefficients obtained for various concentrations of BLEB and OM (B and C), dose-dependent isometric tension- Ca^{2+} relationships of BLEB (D) and OM (E). The *in vitro* data from (Kampourakis et al., 2018). T_0 represents the isometric force in control condition.

5.4 The results of hiMCES model

5.4.1 Simulation of ischemia

During the process of I/R, the SERCA submodel experiences alterations in metabolite levels that have a significant impact on both the sensitivity of Ca^{2+} and the amplitude of Ca^{2+} uptake, as depicted in Figure 20. The hiMCES model, when implemented with the original SERCA parameters, did not exhibit any abnormalities in AP CaT during ischemia/reperfusion. In order to identify a distinct set of parameters for the SERCA model that can accurately simulate the hiMCES model and produce APs while also capturing abnormalities in AP/CaT, I performed a reparameterization of the SERCA submodel (as outlined in Table 11). This reparameterization was guided by the results of sensitivity tests conducted on the pump rate amplitude and Ca^{2+} sensitivity, as illustrated in Figures S3-S10 of Study

IV. Additionally, Ca^{2+} sensitivity of SERCA pump rates at various pH levels is depicted in Figure S11 of Study IV. This figure serves to validate that the calibrated SERCA pump utilized for ischemic simulations accurately reproduces the acidic response, as observed in prior studies conducted by (Ji et al., 1999; Tran et al., 2009).

To clarify, the selection of parameters was determined through a deliberate manual tuning procedure based on informed decision-making. In summary, a range of increments, such as 10%, 20%, and 50%, was employed, commencing with an initial estimate within the range of 5/100 to 5 times the baseline values. The objective of the optimization was to achieve the highest possible pump rate while ensuring that the pump rate-pCa curve remained within the acidic region, as depicted in Figure S11 of Study IV. The range of values considered for this optimization fell between 5% and 500% of the baseline values.

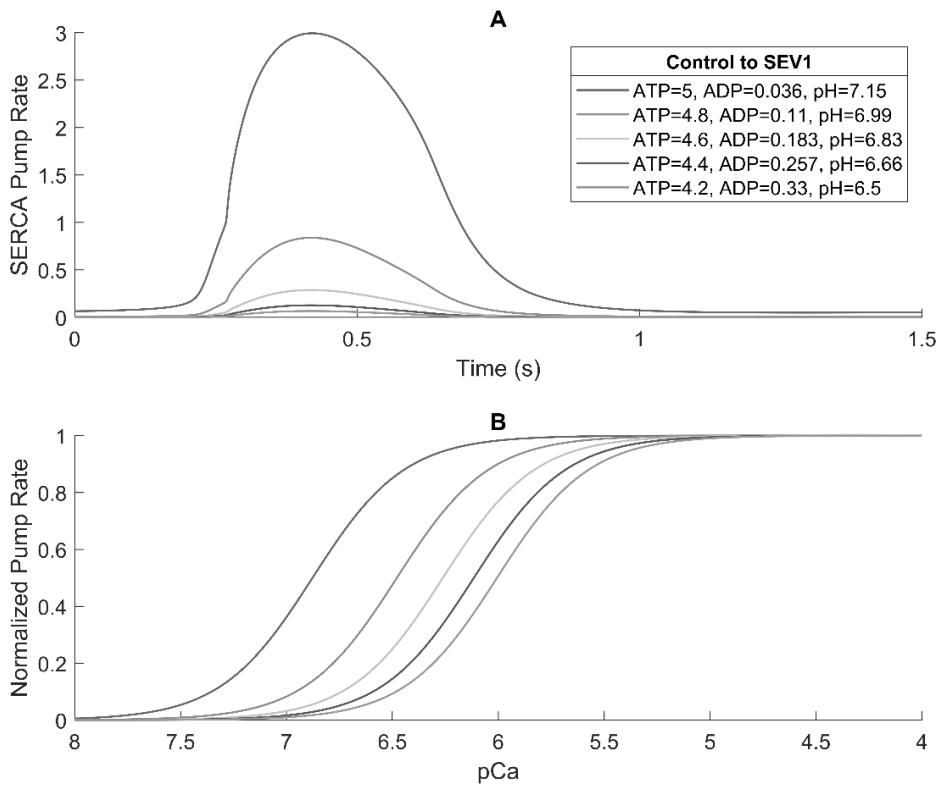


Figure 20 The impact of alterations in metabolite levels on the behavior of the SERCA model is examined. The SERCA submodel predicts significant modifications in both the amplitude (A) of the SERCA pump rate and the sensitivity to Ca^{2+} (B). The inclusion of the metabolite-sensitive SERCA submodel in the whole-cell model in Study IV was motivated by the SERCA response to ischemic-induced metabolite changes.

Table 11 The parameters of the SERCA model, both in standard and reparametrized forms, are examined. The second column was sourced directly from (Tran et al., 2009).

Parameter	Control	Ischemia (SEV1 & SEV2)
k_1^+ (mM ⁻¹ s ⁻¹)	25900	2 × 25900
k_2^+ (s ⁻¹)	2540	2 × 2540
k_3^+ (s ⁻¹)	20.5	5 × 20.5
k_1^- (mM ⁻¹ s ⁻¹)	2	2
k_2^- (mM ⁻¹ s ⁻¹)	67200	0.1 × 67200
k_3^- (mM ⁻¹ s ⁻¹)	149	149
$K_{d,CaI}$ (mM)	0.91	0.1 × 0.91
$K_{d,CaSR}$ (mM)	2.24	2.24
$K_{d,H1}$ (mM)	1.09 × 10 ⁻⁵	1.09 × 10 ⁻⁵
$K_{d,Hi}$ (mM ²)	3.54 × 10 ⁻³	3.54 × 10 ⁻³
$K_{d,Hsr}$ (mM ²)	1.05 × 10 ⁻⁸	0.1 × 1.05 × 10 ⁻⁸
$K_{d,H}$ (mM)	7.24 × 10 ⁻⁵	5 × 7.24 × 10 ⁻⁵
n_H	2	0.97 × 2

The model results were assessed for two levels of ischemic severity, namely SEV1 and SEV2, as depicted in Figure 21. The durations of APs exhibited a decrease, while the depolarization time demonstrated an increase in response to ischemic conditions at two different levels of severity, as depicted in Figure 21A. These findings align consistently with the observations made in previous *in vitro* studies involving hiPSC-CMs exposed to hypoxic conditions (Häkli et al., 2021b, 2022). The observed decrease in potassium currents (Figure 21B&G) during ischemia, which leads to an elevation in resting membrane voltage, aligns with the findings from hiPSC-CMs experiments conducted under hypoxic conditions (Deo et al., 2020). Moreover, the model demonstrated a noteworthy decrease in I_{to} (as depicted in Figure 21D&E SEV2), which plays a crucial role in the repolarization phase of hiPSC-CMs (Koivumäki et al., 2018). The hiMCES model successfully reproduced the observed direct relationship between I_{CaL} and AP plateau height, as documented in the experimental study on ischemia by (Rogers et al., 2021) (Figure 21E&A). The observed elevation in intracellular Na⁺ concentration during ischemic conditions (as depicted in Figure 21C) aligns with the findings reported by (Gaballah et al., 2022) regarding hypoxic conditions in hiPSC-CMs. In SEV2 condition, the hiMCES model accurately replicated the elevation of the CaT baseline, consistent with the notable rise in the diastolic concentration of Ca²⁺ observed in isolated rabbit and rat ischemic hearts (Eberli et al., 2000) (Figure 21F). At SEV2, the model demonstrated a

simulated decrease of 17.4% in CaT tDecay_{90,10} (from 317 to 262 ms). This reduction is consistent with the experimentally reported range of 15.2-36.3% decrease in CaT tDecay_{90,10} in hiPSC-CMs under hypoxic conditions, as reported by (Gaballah et al., 2022).

Lastly, I compared the simulated alterations in APD₉₀ with the *in vitro* findings derived from human CMs (Sutton, 2000) (after 3minutes), cat (Kimura et al., 1990) (after 10-15 minutes), and guinea pig (Penny & Sheridan, 1983) (after 10-15 minutes) as presented in Figure 21H. Analogously, the changes in APD₉₀ were also juxtaposed with other *in silico* models of ischemia as reported in Figure 21H. An ischemic study conducted by (Weiss et al., 2009) utilized the TenTusscher 2006 (TT06) model developed by (Ten Tusscher & Panfilov, 2006). The study examined severities of 5 and 10 minutes and incorporated the I_{KATP} formulation from (Ferrero et al., 1996). The qualitative agreement between the observed trend and the simulated changes in APD₉₀ is illustrated in Figure 21H.

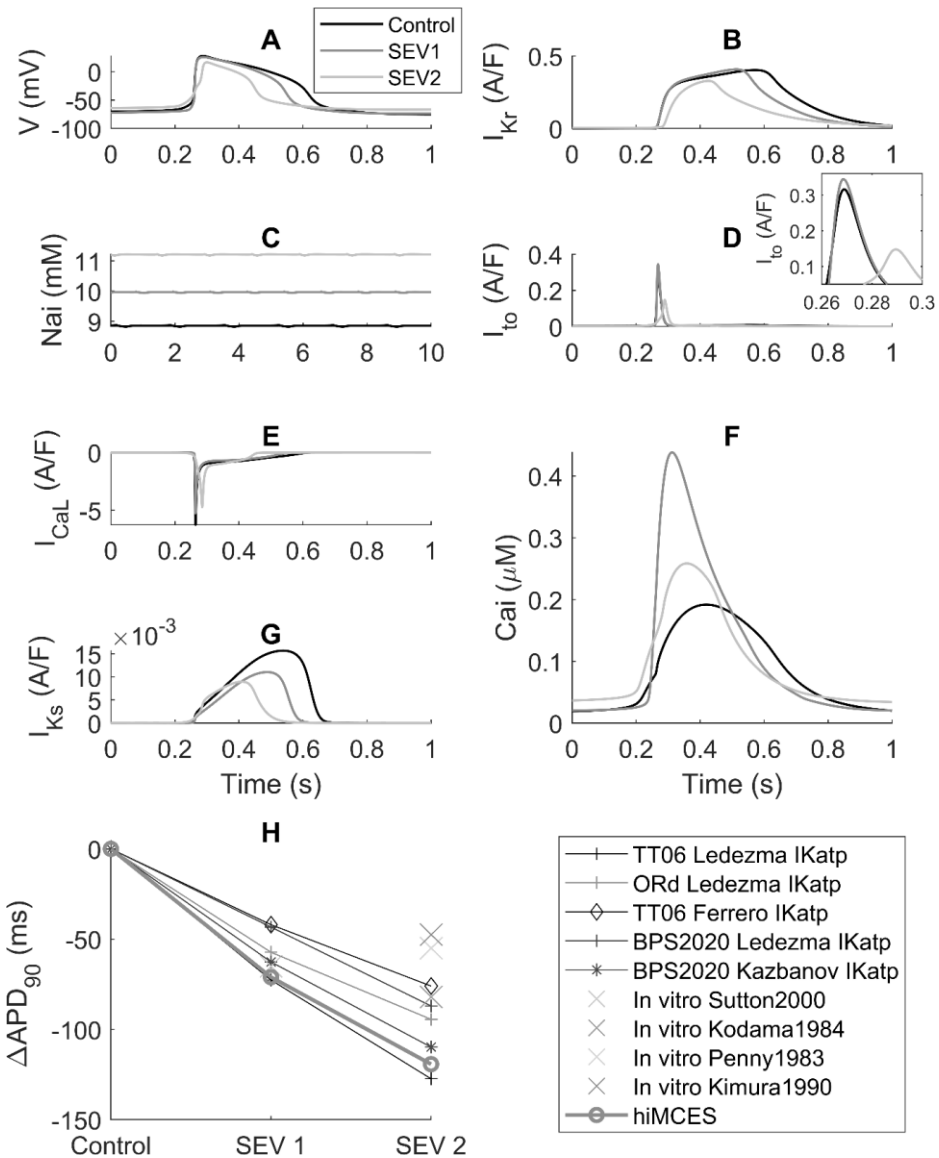


Figure 21 The hiMCES model simulates the various degrees of ischemia: Action potentials (AP) (A), rapid delayed rectified K⁺ current (I_{kr}) (B), intracellular Na⁺ concentration (C), transient outward K⁺ current (I_{to}) (D), L-type Ca²⁺ current (I_{CaL}) (E), Ca²⁺ transients (F), slow delayed rectified K⁺ current (I_{ks}) (G), and changes in AP duration at 90% of repolarization (APD₉₀) (H). In silico data: TT06 Ledezma (Ledezma et al., 2019), ORd (Ledezma et al., 2019), TT06 Ferrero (Weiss et al., 2009), BPS2020 (Forouzandehmehr, Bartolucci, et al., 2021). In vitro data: Sutton (Sutton, 2000), Kodama (KODAMA et al., 1984), Penny (Penny & Sheridan, 1983), Kimura (Kimura et al., 1990).

5.4.2 Simulation of Levosimendan mechanism of action

The current inhibitions were calculated based on the IC50 values and Hill coefficients for Levo, as reported by (Passini et al., 2019), using the channel blocking formalism. Moreover, Levo is a pharmacological agent that acts as a positive inotropic modulator by enhancing the sensitivity of troponin C to Ca²⁺. This is achieved through the augmentation of troponin C affinity for Ca²⁺ ions and the stabilization of its conformation (Gaballah et al., 2022). The developed tension was simulated and the corresponding values of K_{on} scaling coefficients were calculated based on the dose-dependent inotropic data reported for Levo by (Haikala, 1997), I simulated the developed tension and calculated the corresponding values of K_{on} scaling coefficients (Figure 22A). K_{on} governs the transition between troponin to Ca²⁺-bound troponin state (Rice et al., 2008) (Figure 13). In Study IV, I also took into consideration the impact of Levo as an I_{KATP} activator, as discussed in the works of (Gaballah et al., 2022; Parissis et al., 2007; Pathak et al., 2013). The f_{KATP} values that correspond to the augmented currents observed in Figure 22B were determined for the administered doses of Levo, utilizing *in vitro* data from (Yokoshiki et al., 1997). The Levo model of action mechanism is detailed in Table 12.

Table 12 Parameters adopted to model the effect of Levosimendan . I_{Na}: fast Na⁺ current, I_{CaL}: L-type Ca²⁺ current, I_{Kr}: Rapid delayed rectified K⁺ current, K_{on}: rate constant for Ca²⁺ to troponin C binding affinity (Rice et al., 2008; Tran et al., 2010), f_{KATP}: fraction of open I_{KATP} channels (Ferrero et al., 1996; Kazbanov et al., 2014).

Dose (μM)	I _{Na} block (%)	I _{CaL} block (%)	I _{Kr} block (%)	K _{on} coefs.	f _{KATP} activation (%)
0.3	0.35	1.04	5.11	1.1	0.2385
2	2.28	6.57	16.38	1.32	11.8538
10	10.45	26.01	36.91	1.88	84.3903

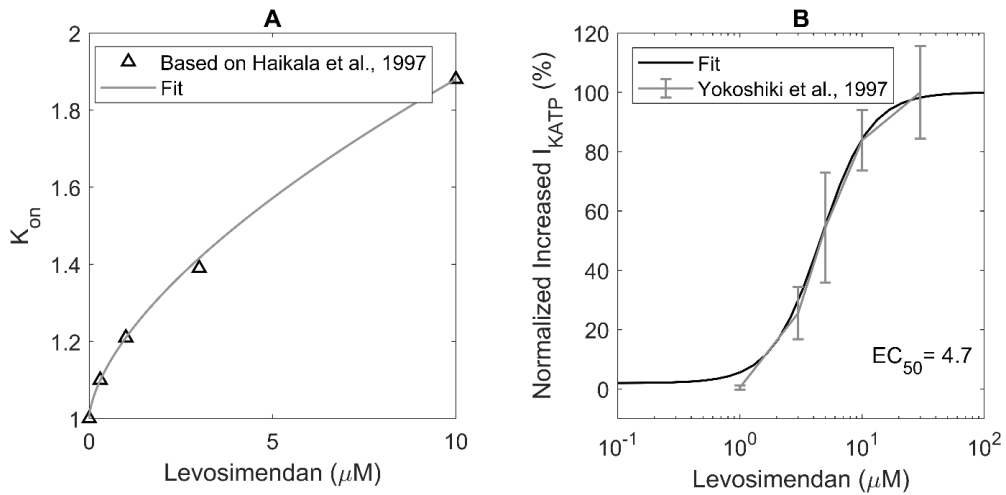


Figure 22 The new model of Levo action mechanism accounts for Ca^{2+} -sensitizing and I_{KATP} modulation. Scaling coefficients of K_{on} calculated for each different Levo concentrations based on (Haikala, 1997) (A), Normalized increased I_{KATP} in response to different doses of Levo from (Yokoshiki et al., 1997) (B).

5.4.3 Ischemic-induced arrhythmia simulation and I_{Ks}

Commencing from an equilibrium state under control conditions, the model was executed for a duration of 250 seconds. During the transition phase from the 250th to the 350th second, the parameters were adjusted to simulate the ischemic mode. Subsequently, the complete ischemic phase was executed over a duration of 500 seconds, spanning from the 350th to the 850th second. The transition, denoting the onset of reperfusion, commenced at the 850th second and continued until the 950th second. Lastly, the model was simulated for an additional 200 seconds subsequent to the final transition, as depicted in Figure 23A&B and Figure 14B. The I/R outcomes, as depicted in Figures 23-25, were acquired using the hiMCES model version, employing optimized maximum conductances and currents (SET coefficient, as described in section 4.6.2).

The hiMCES I/R model effectively simulated ischemic-induced arrhythmia, specifically EADs, and abnormalities in CaTs (Figure 23C&D). These results align consistently with the experimental data obtained from hiPSC-CMs subjected to hypoxia, as reported by (Gaballah et al., 2022). The experimental findings of (Gaballah et al., 2022) corroborate the simulated occurrence of double-peaks and CaT plateau abnormalities, as depicted in Figure 23D, in hiPSC-CMs during

ischemia. Furthermore, the computed dV/dt_{max} during the ischemic phase, before the occurrence of EADs, exhibited a decrease to approximately one-fourth of the dV/dt_{max} value observed in the control condition (34.9 to 9.6 V/s). Maximum upstroke velocity, dV/dt_{max} , exhibits an inverse relationship with the depolarization time, and the simulated change quantitatively agree with the experimentally reported elevation in the depolarization time for hiPSC-CMs in I/R (Häkli et al., 2022).

Furthermore, I investigated the impact of I_{Ks} activation on the outcomes of the model in I/R. The AP and CaT abnormalities were consistently abolished by I_{Ks} activation, as demonstrated in Figure 23E&F, in accordance with the I/R model of rabbit cardiomyocytes (X. Guo et al., 2012). As a consequence, the abolition of ischemic-induced aftercontractions was observed (Figure 23G).

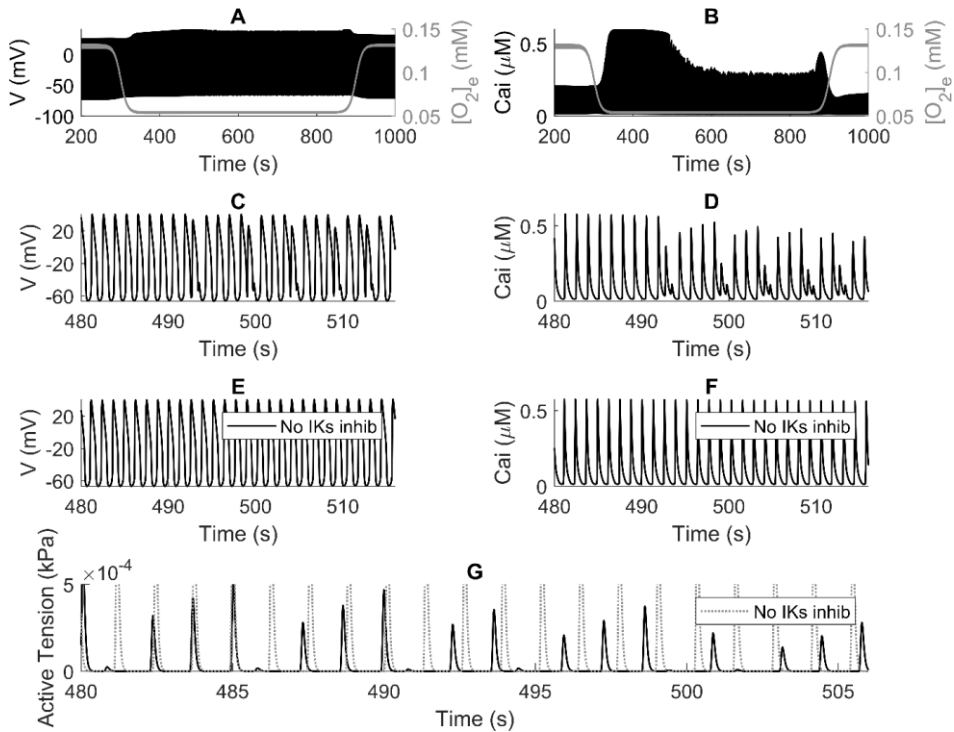


Figure 23 The Ischemia/Reperfusion results of hiMCES model in Study IV. The ischemic-induced abnormalities (A&B) and simulated cardioprotective effect of slow delayed rectified K^+ current (I_{Ks}) in action potential (C&E), Ca^{2+} transients (D&F), and active tension (G).

5.4.4 Simulation of Levosimendan in ischemia and reperfusion

In order to comprehend the recently documented antiarrhythmic impact of Levo, as reported by (Gaballah et al., 2022), I investigated the effect of a $2\mu\text{M}$ dose of Levo on AP, CaT, and active tension generated during I/R simulations. The results presented in Figure 24A-D demonstrate the abolition of EADs and a significant reduction in CaT plateau abnormalities. These findings are consistent with the administration of $2\mu\text{M}$ Levo in an *in vitro* study conducted on hypoxic hiPSC-CMs, as reported by (Gaballah et al., 2022). Consequently, this resulted in a cardioprotective impact on the contractility as a result of the elimination of aftercontractions (Figure 24E).

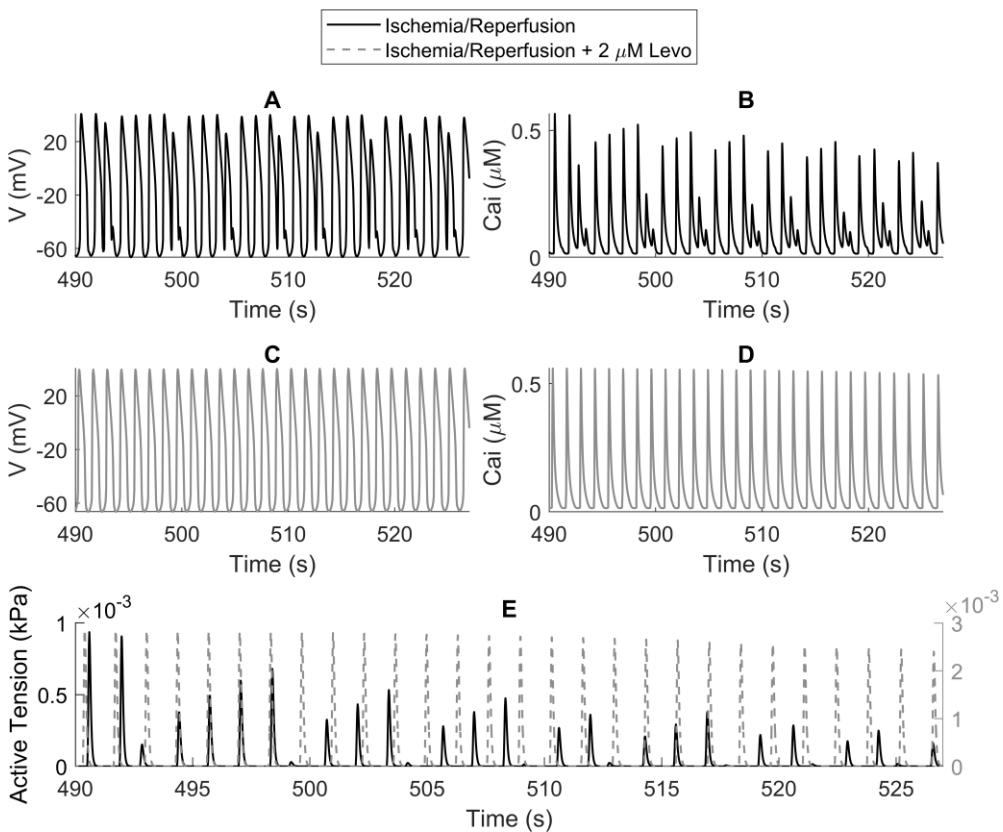


Figure 24 The Ischemia/Reperfusion (I/R) model of hiMCES in response to $2\mu\text{M}$ Levo. Action potential and CaT in I/R (A&B), action potential and CaT in I/R + $2\mu\text{M}$ Levo (C&D), and active tension in I/R vs I/R + $2\mu\text{M}$ Levo (E).

Figure 25 presents the primary model outcomes and their reaction to a Levo concentration of $2\mu\text{M}$ both during and after the reperfusion transition. The results of the study indicate that the model accurately predicted an increase in active tension (Figure 25A) and contractile ATPase rate (Figure 25C) in response to Levo, despite observing a decrease in CaT during the late reperfusion phase (Figure 25B). Correspondingly, a negligible alteration in OCR was simulated during the reperfusion and postreperfusion stages (Figure 25G), aligning with the documented impact of Levo on Ca^{2+} sensitization during ischemia in human research (Ng, 2004). In the reperfusion, when considering the alterations in active tension and ATPase rate (Figure 25A&C), it can be inferred that the administration of Levo results in an improvement in the cardiac energy consumption, similar to its impact during the ischemic phase (Fig. S13G of Study IV). This favorable energetic result observed in this study aligns with previous findings that demonstrate the regenerative effects of Levo on the contractile function and impaired cardiac energetics in various subjects, including human subjects (Ng, 2004), hiPSC-CMs (Gaballah et al., 2022), and Langendorff guinea-pig hearts (Haikala, 1997) during ischemic conditions. The simulation of Levo effect during I/R demonstrates a biphasic pattern in CaT and CaSR starting at the initiation of reperfusion, as depicted in Figure 25B&D. Additionally, there is a notable decrease in the duration of SERCA phosphorylation, as illustrated in Figure 25H. Significantly, the administration of Levo did not contribute to the restoration of CaT and CaSR to normoxic levels, as depicted in Figure 25B&D. Additionally, Levo did not have an impact on the AP profile observed 50 seconds after the transition phase of reperfusion, as illustrated in Figure 25E. The simulation results (Figure 25F) indicate that there was a modest decrease in the impaired SERCA uptake pump function as a result of the presence of $2\mu\text{M}$ Levo.

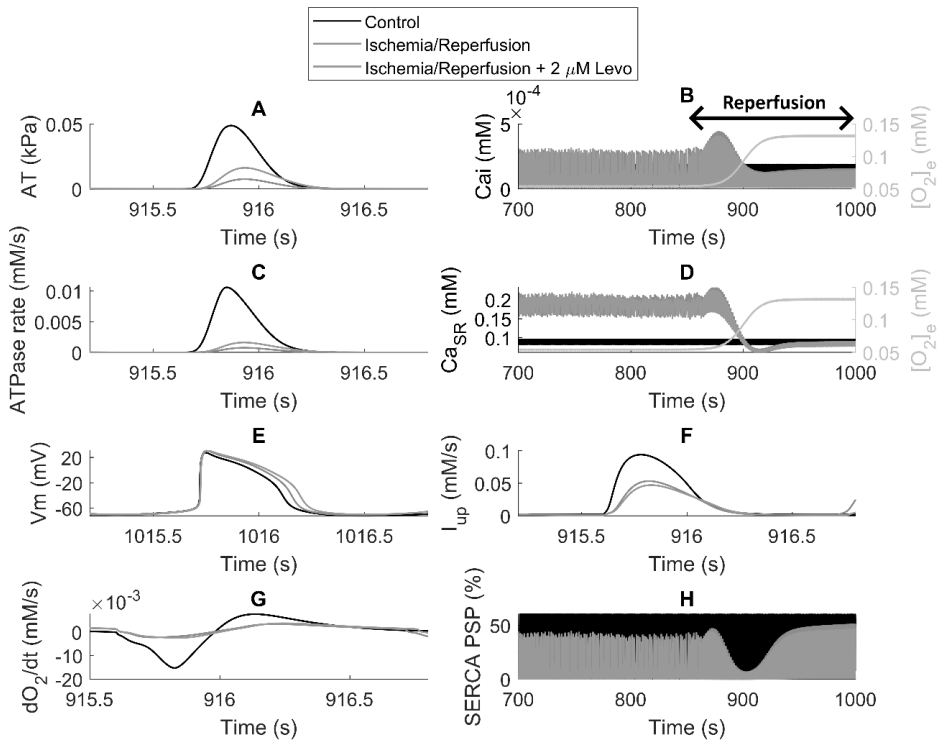


Figure 25 The ischemia/reperfusion results of hiMCEs model and the effect of 2 μM Levo: Active tensions (A), Ca^{2+} transients (B), contractile ATPase rate (C), sarcoplasmic Reticulum Ca^{2+} concentrations (D), action potentials shown 50 s postreperfusion transition (E), Ca^{2+} uptake flux via SERCA pump (F), oxygen consumption rate (G), and percent SERCA of phosphorylation (H).

6 DISCUSSION

6.1 The model of hiPSC-CMs electromechanics

Aside from a successful integration of a contractile mechanism into a dynamic model of cardiac electrophysiology, Study I significance was in proposing the first balanced contractile and electrophysiological structures of calibration-validation for the dawn of *in silico* cell level electromechanical researches. The feature which was matured in the hiPSC-CM-CE model (Study II) that presents an electromechanical representation of hiPSC-CMs, achieved by integrating the Paci2020 ionic model and the reparametrized Rice2008 CE model. Additionally, a novel passive force mechanism was incorporated. The mechanical characteristics of the model were verified through independent validation using contraction protocols that were previously reported in experimental studies involving hiPSC-CMs. The hiPSC-CM-CE model successfully predicted the inotropic effect of various multichannel action reference drugs and their arrhythmogenic effects, specifically in relation to aftercontractions. The simulations accurately anticipated the dynamics of the involvement of non-cardiomyocytes in hiPSC-CM tissues. In general, Studies I and II have established a dependable mechanistic framework that can guide future investigations on functionalities of hiPSC-CMs.

The ability to replicate essential *in vitro* AP and CaT biomarkers is imperative for computational models of CMs. The hiPSC-CM-CE model successfully reproduces all the AP and CaT biomarkers within the experimental ranges as documented in the studies conducted by (Paci et al., 2018, 2020). Moreover, the significance of CE integration and reparameterization in relation to the electrophysiological biomarkers is demonstrated in Table 8. It is worth mentioning that the reparameterization of the CE has the potential to rectify the deviation of four electrophysiological biomarkers from their optimal range, which occurred when the original Rice CE was employed instead of the reparametrized version.

The accurate representation of biochemical XB-related phenomena can be achieved through the utilization of mathematical myofilament models that encompass multiple states. However, it is important to note that the computational

cost associated with these models is substantial. The primary objective of contemporary myofilament dynamic models is to achieve a balance between biophysical accuracy and computational efficiency. In light of this, the Rice CE model (Rice et al., 2008) was chosen for Study II due to its inclusion of crucial Ca^{2+} -based activation and sarcomere length-based sensitivity mechanisms within its contractile machinery. A comprehensive examination of this topic has been previously provided (Trayanova & Rice, 2011). My primary impetus for reparametrizing the initial Rice computational model of cardiac electrophysiology was to facilitate the model's ability to faithfully reproduce a diverse array of electrophysiological and mechanical measurements, a capability that was lacking in the Paci2020+original Rice CE model (see Figure S4 and Table 3 in (Forouzandehmehr, Koivumäki, et al., 2021)).

The evaluation of contractility plays a pivotal role in the construction of a mathematical cellular model for cardiac electromechanics (Campbell et al., 2008; Forouzandehmehr et al., 2020; Margara et al., 2020; Margara, Wang, et al., 2021; Negroni et al., 2015; Pioner et al., 2020; Rice et al., 2008; Tran et al., 2017; Zile & Trayanova, 2017). Within this particular context, an important mechanical indicator to consider is FCS (as depicted in Figure 15G), which is commonly regarded as a reliable measure of contractile capacity (Pioner et al., 2020). The hiPSC-CM-CE achieved the development of a percentage of FCS within the specified experimental parameters at 1 Hz pacing, 1.8 mM extracellular Ca^{2+} concentration, and a temperature of 37 °C. Additionally, the simulated durations from the point of maximum contraction to 50% and 25% of relaxation (referred to as RT50 and RT25, respectively), which serve as indicators of relaxation kinetics, indicate that the model falls within the validation target range in terms of mechanical outputs and sarcomere dynamics. Additionally, it should be noted that the hiPSC-CM-CE model accurately replicated the tension magnitude observed in hiPSC-CMs within the experimental range *in vitro*, at a concentration of 1.8 mM of extracellular Ca^{2+} and a temperature of 37 °C (Figure 15E) (Ruan et al., 2016). The aforementioned properties lend support to the model's suitability as a robust mathematical foundation for future research on the modeling of contractility and associated dysfunctions.

In addition, an important measure of contractility commonly observed in experimental studies on single cell hiPSC-CMs is known as the motion waveform or contraction-relaxation velocity (Hayakawa et al., 2014; Rodriguez et al., 2014). In recent times, there has been significant research activity focused on investigating the role of reduced relaxation velocity and extended relaxation duration in the characterization of diastolic dysfunction (Hayakawa et al., 2014). Furthermore, the

examination of cardiac pathologies, including ischaemic diseases, hypertension, and rare genetic disorders, has been found to be linked to the velocity and duration of contraction and relaxation (Hayakawa et al., 2014). The hiPSC-CM-CE model accurately reproduces the velocity profiles of physiological contraction and relaxation, as demonstrated in Figure 2E in (Forouzandehmehr, Koivumäki, et al., 2021) and Figure 17B. These findings are in agreement with previous experimental studies on hiPSC-CMs conducted by (Hayakawa et al., 2014; Rodriguez et al., 2014). Hence, the findings of Study II demonstrate that the model exhibited accuracy and robustness in simulating the effects of the aforementioned disorders, specifically on the profiles of contraction-relaxation velocity.

The hiPSC-CM-CE model also helped exploring the impact and action mechanism of two inotropic drugs, Verapamil and Bay-K 8644, at ion channel level. The validated simulated effects of 90 nM of Verapamil and 1 μ M of Bay-K8644 on AP morphology were mapped onto change in ICaL profiles (Figure 16B) providing insights into potential targets for future drug development with negative and positive inotropy.

The study conducted by (Iseoka et al., 2018) has provided evidence regarding the essential contribution of non-cardiomyocytes to the electromechanics, functionality, and therapeutic applications of hiPSC-CMs tissues. It is important to highlight that the presence of non-CMs plays a crucial role in the production of functional hiPSC-EHTs for use in cardiac regeneration therapy. According to (Iseoka et al., 2018), the hiPSC-CM EHTs, which consist of approximately 50-70% cardiomyocytes, have demonstrated both structural stability and enhanced therapeutic capabilities. The hiPSC-CM-CE, functioning as an inter-scale capability, effectively replicated the observed contraction-relaxation velocity and cell shortening trends in experimental studies (Forouzandehmehr, Koivumäki, et al., 2021; Iseoka et al., 2018). Furthermore, the inclusion of the new passive force in the CE allowed for an accurate categorization of the inotropic effects of non-CMs in hiPSC-CM tissues during simulation. Moreover, the simulated variations in the positive and negative inotropic effects for FCS and motion waveform, as depicted in Figure 17A and Figure 17B respectively, align with hiPSC-CMs experimental findings reported in (Iseoka et al., 2018). The model accurately predicts the lowest contractile potential consistent with the biophysical principles underlying the non-CM effects, which exhibit the greatest inhibition of electrical propagation at a ctn value of 25% (Iseoka et al., 2018).

6.2 Electro-mechano-energetics in HCM and drug mechanism

Cardiomyocytes, which lack the ability to regenerate, are responsible for generating approximately two billion contractions over an average lifespan. This demanding task necessitates a substantial energy supply, specifically six kilograms of ATP per day (Ingwall, 2002). Notably, approximately 50% of total energy consumption can be attributed to the operation of sarcomeres during contraction. (McDougal & Dewey, 2017). Hence, it is imperative to investigate the contractile function of CMs in relation to cardiac metabolism in order to better understand the pathological conditions that arise from sarcomeric mutations, such as MYH7^{R403Q/+} HCM. The findings of our analysis indicate that the inclusion of the metabolite-sensitive CE scheme effectively captures the observed impairment in tension relaxation, which is approximately 33%, resulting from the presence of the R403Q mutation. It is worth noting that the inclusion of energetics in the analysis rendered the proposed extra feedback from XB cycling to the thin filaments, as previously suggested by (Margara, Rodriguez, et al., 2021), unnecessary for reproducing the observed changes in relaxation dynamics. This emphasizes the significance of incorporating metabolite-sensitive computational models that are constrained by (patho)physiological considerations in the study of sarcomeric cardiomyopathies.

The investigation of contractile energetics assumes great significance in the examination of potential pharmaceutical interventions documented in (pre)clinical trials for HCM, including MAVA, BLEB, and OM. The findings of Study III indicate that achieving a quantitatively accurate simulation of the impact of MAVA, BLEB, and OM, either in a single dose or in a dose-dependent manner, necessitates the calibration of parameters within the CE that directly or indirectly influence the energetics. This calibration process is detailed in Table 6 and Tables 3, 4, S1, and S2 of (Forouzandehmehr et al., 2022)). Significantly, a key observation in Study III arises from the parameters utilized in calibrating the model for simulating a concentration of 0.5 μM MAVA. The MAVA modeling approach was extended by calibrating the parameters related to CE alteration that influence the Pi-dependent transition between the permissive binding state on the thin filament (P) and the strongly bound XBs prior to the isomerized rotation (XB_A). Furthermore, I adjusted the modulation of Ca^{2+} binding and sensitivity in the CE, as well as the MgATP-dependent transitions between the P and XB states in the strongly bound post-isomerized rotation state (XB_B). These adjustments align with the findings reported in relevant metabolic studies conducted by (Alsulami & Marston, 2020; Awinda et

al., 2020; Green et al., 2016). In order to better understand the specific mechanism of action of the drug, Study III suggests several modulations (presented in Table 6) to explain the observed effects of MAVA. These modulations suggest that, in addition to altering the disrupted ratio of DRX to SRX, MAVA may also induce a new equilibrium between interfilaments. This modulation would affect tension-producing and energetic factors that directly impact the reverse transition between XB_A and XB_B , which in turn influences the strain-dependent isomerization of myosin heads. The potential pharmacological insight derived from the hiMCE model is intriguing due to the inherent ability of the MAVA mechanism of action to restore normal regulation of impaired metabolism caused by the R403Q variant. This restoration involves addressing the impaired proton-dependent transition in the R403Q variant, as discussed by (Toepfer et al., 2020).

The calibrations pertaining to drugs and HCM discussed in this study align with the suggested structure-function relationships of the OM and BLEB as outlined in the work by (Kampourakis et al., 2018). In their study, Kampourakis et al. suggested that myosin heads bound to OM induce the repositioning of tropomyosin into its activated (ON) state upon binding to actin, even in the absence of Ca^{2+} bound to troponin. Significantly, the stabilization of the ON state of thick filaments has been largely attributed to the activation of XB , which is a result of the influence of OM. Additionally, the stabilization of ON positions in thick filaments has been postulated to facilitate the maintenance of an activated state in thin filaments by inhibiting the reversion of tropomyosin to its off positions (Kampourakis et al., 2018). The translation of this was accomplished using the hiMCE model, which involved the modification of k_{off} constants. These constants are responsible for the rate at which Ca^{2+} is released from both low and high affinity locations on troponin. The transition rates have an impact on the regulatory sites located on cardiac troponin, resulting in the activation of the XB cycle (Iran et al., 2010).

Conversely, within the physiological range of intermediate Ca^{2+} concentrations (pCa 9 to 4.3), the activation of actins in conjunction with the thick filaments is facilitated by OM, as demonstrated by (Kampourakis et al., 2018). The hiMCE model incorporates modifications to the K_{on} , K_{np} , and K_{pn} rate constants, which are responsible for the binding of Ca^{2+} to troponin. Additionally, the model adjusts the forward and backward transition rates between the P and N configurations. These modifications are detailed in Table 4 of the study III (Forouzandehmehr et al., 2022). Moreover, the parameters that govern the regulation of thin filaments by Ca^{2+} bound troponin, namely K_{on} , n_{perm} , k_{offL} , k_{offH} , k_{pn} , k_{np} , and $k_{offmode}$, have only been calibrated for the activation of OM. These parameters have not been calibrated for

BLEB, as BLEB does not activate both filaments to their ON states, as noted by (Kampourakis et al., 2018). Moreover, the adjustment of the coefficient of the Troppreg variable, which represents the proportion of actins bound to Ca^{2+} , as described in (Rice et al., 2008), is in line with the documented impact of these medications. Both OM and BLEB calibrations typically result in a significant reduction in the co-operativity of Ca^{2+} activation, as reported by (Kampourakis et al., 2018).

The observed elevation in Pi concentration in the HCM variant of the hiMCE model aligns with the experimental findings on metabolic changes associated with HCM R403Q and R92Q mutations in mouse models (Abraham et al., 2013; Spindler et al., 1998). Furthermore, it has been observed that the compromised blood flow in the coronary arteries caused by HCM is associated with an abnormal energy production process that leads to an increase in ADP and Pi levels (Sequeira et al., 2019). This finding aligns with the principle of phosphate and creatine conservation in the body (Tran et al., 2010). Similarly, the alterations in myofilament kinetics induced by the HCM mutation result in an increase in ADP-mediated products (van der Velden et al., 2018). Consequently, I elevated the concentration of MgADP within the physiological ranges (Tran et al., 2010). It is worth mentioning that the activation of myofilaments in HCM and dilated cardiomyopathy is affected in a similar manner by the influence of OM and BLEB, as demonstrated by (Spudich, 2014). This suggests that the development of HCM involves a disruption in actomyosin signaling. Furthermore, the elucidation of the underlying mechanism of hypercontractility induced by HCM, specifically the R403Q HCM variant, has been expounded upon in relation to structural changes in the thick filament and the generation of tension (Alamo et al., 2017; Nag et al., 2017; Trivedi et al., 2018). With this in mind, since the alteration of the ap_2 coefficient (as shown in Table 5) allows the XB cycling machinery to accurately replicate the behavior observed in HCM (as depicted in Figure 18), the hiMCE model proposes that the disrupted interfilament signaling associated with HCM is potentially caused by a distortion-dependent forward transition from the A state to the B state of the XB complex. This is followed by the subsequent impact resulting from the presence of strongly bound XB states population in the steady-state condition. This observation suggests that the disrupted actomyosin signaling observed in HCM may be attributed to an aberrant regulation of the isomerization process, whereby myosin heads transition from a pre-rotated (XB_A) to a post-rotated (XB_B) state, consequently impacting the strain experienced in the myosin neck region. Analogously, it is plausible that the aforementioned process could elucidate the mechanisms through which OM, BLEB,

and MAVA collectively contribute to the establishment of a novel interfilament balance, thereby facilitating the restoration of normal tension generation during XB cycling. The insights provided by this hypothesis, which is derived from the predictions of the hiMCE model, have the potential to expedite the progress of pharmaceutical interventions for sarcomere cardiomyopathies and mutation-dependent HCM.

In Study III, focusing on ap2 regulatory effect, a mechanistic approach was proposed to integrate the dose-dependent impact of BLEB and OM, as depicted in Figure 19. This approach aligns with the experimental findings of (Kampourakis et al., 2018). The dose-dependent effects of OM and BLEB, as observed in (Kampourakis et al., 2018), exhibit an inverse Hill function trend. This trend is also reflected in the values of the ap2 coefficients in hiMCE model, obtained for the concentrations examined, as depicted in Figure 19B-E. Furthermore, Study III indicates that the alterations in F2, hf, and ap2 (Table 4 in (Forouzandehmehr et al., 2022)) imply that OM also promotes the swift dissociation of XBs. This finding adds to the understanding of how OM disrupts the coupling between actin and myosin, which is a key aspect of its mechanism of action. Moreover, the precise replication of reduced APD resulting from 1 μ M OM and the heightened basal ATPase rate values, as depicted in Figure 5 of (Forouzandehmehr et al., 2022), serves as additional evidence that the incorporation of metabolite-sensitive alterations in the XB cycling of the cardiac CE system cannot be disregarded in the context of precision medicine. This is particularly crucial when simulating the effects of medications that primarily affect ATPases.

6.3 Electro-mechano-energetics in ischemia/reperfusion

Myocardial infarction (MI) is recognized as the leading cause of mortality on a global scale, as stated by (Nowbar et al., 2019). The optimization of treatments aimed at restoring normal cardiomyocyte homeostasis and metabolism following an ischemic insult is of significant importance (He et al., 2022). The pathophysiological mechanisms that contribute to I/R injuries, such as disrupted cytosolic Ca²⁺ transients, oxidative stress, rapid pH correction, and phosphate overload (He et al., 2022) are interconnected and intricate. Consequently, comprehensive quantitative investigations are required to fully understand these mechanisms. In order to achieve this objective, the utilization of *in vitro*-matching computational protocols and

biophysically detailed mathematical models pertaining to cellular electro-mechano-energetic coupling holds significant significance.

In order to examine the pathophysiological mechanisms and effects of drugs related to I/R, my primary objective was to enhance our existing *in silico* model of hiPSC-CMs from Study III (Forouzandehmehr et al., 2022). This enhancement involved incorporating a metabolite-sensitive SERCA pump and an oxygen dynamic formulation that establishes a connection between cellular energetics and extracellular oxygen concentration ($[O_2]_e$). It is worth mentioning that the proposed dynamic oxygen formulation incorporates the contraction ATPase rate, which I had anticipated would have a significant impact especially on the study of I/R (Bo et al., 2021; Laslett et al., 1985; McDougal & Dewey, 2017). I did not take I_{KATP} into account in the oxygen dynamic formulation due to its reported insignificant effect on myocardial oxygen consumption rate in the context of I/R, as documented by (Offstad et al., 1994).

In Study IV, the IC_{50} -based inhibition drug simulation formalism was extended by accounting for the role of I_{KATP} and troponin C affinity for Ca^{2+} in Levo action mechanism model. This was done to obtain a more accurate simulation of Levo effect consistently with (Gaballah et al., 2022). Consistently with the *in vitro* findings of hiPSC-CMs in hypoxia (Gaballah et al., 2022), the hiMCES model successfully replicated the significant decrease in AP amplitude and the occurrence of CaT abnormalities caused by the administration of 2 μ M Levo. This phenomenon may be linked to the impact of Levo on the constituents contributing to the repolarization reserve of the hiPSC-CM model, as depicted in Figures S13A-C of Study IV. This observation aligns with previous findings that demonstrate the prolongation of the QT interval in both healthy individuals and patients with heart failure following administration of Levo, as reported by (Ng, 2004).

Moreover, it is worth mentioning that the model made a noteworthy prediction regarding a substantial rise in the Ca^{2+} flux toward the myofilament as a result of Levo during SEV1 ischemia (refer to Figure S13F in Study IV). This finding suggests that Levo has the ability to regulate the transition of significantly increased CaT levels during ischemia, as well as the impaired CaT caused by the rapid restoration of metabolites during the reperfusion phase (Figure 25B). The simulations suggest that Levo has the potential to extend the reperfusion transitions, particularly in relation to SERCA phosphorylation (Figure 25H). The aforementioned observation exhibits a noteworthy correlation with a recent computational investigation, conducted by (Grass et al., 2022) which proposed a two-step reperfusion protocol as a potential means of reducing cellular damage in contrast to a swift return to physioxia. In

addition, Study IV findings indicate that Levo is a unique inotrope that does not seem to enhance contractility by increasing myocardial oxygen demand (refer to Figure 25G and Figure S13G in Study IV), which is consistent with previous *in vitro* studies (Ng, 2004). The question of whether Levo corrects the impaired contractile relaxation through augmentation of SERCA phosphorylation or other mechanisms has been the subject of previous research (Ng, 2004). The predictions made by the hiMCES model indicate that the constructive impact of Levo in improving the compromised contractile and energetic relaxation is likely attributed to its ability to enhance the affinity of troponin C for Ca^{2+} binding, thereby intensifying the JCB. This impact is not primarily a result of inhibiting SERCA phosphorylation, which would increase the removal of cytosolic Ca^{2+} .

According to the findings presented in (Tran et al., 2009) and simulated in Figure 20, a decrease in pH leads to a reduction in the Ca^{2+} sensitivity of SERCA. Study IV posits that the observed rise in metabolic proton and acidic residues in the I/R, as reported by (Grass et al., 2022), could potentially impact the functioning of SERCA through a pathological competitive proton binding. Acidic residues involved in proton and Ca^{2+} binding (Tran et al., 2009) demonstrate a greater affinity of proton for the Ca^{2+} binding sites in the SERCA luminal orientation. Conversely, they show a lower affinity of proton binding to cytosol-facing Ca^{2+} binding docks (Tran et al., 2009). As these factors gain higher influence in the acidic environment of ischemia, the reduction in $K_{d,\text{Hsr}}$ in the reparameterization (Table 11), increasing the distance between $K_{d,\text{Hi}}$ and $K_{d,\text{Hsr}}$, suggests that ischemia may enhance the competitive proton binding for the luminal oriented Ca^{2+} binding sites of SERCA, ultimately leading to an elevation in SR Ca^{2+} , as demonstrated in Figure 25D. Significantly, the aforementioned findings indicate that the increase in proton leak has a dual effect: firstly, it disrupts cellular metabolism, resulting in heightened oxidative stress during I/R (Grass et al., 2022); and secondly, it may exacerbate an already perturbed competitive proton binding process, leading to a pathological alteration in SERCA function. This is imperative as a new insight into the interconnected nature of oxidative stress elevation and Ca^{2+} overload as the primary mechanisms underlying I/R injuries (He et al., 2022).

The hiMCES model demonstrates the ability to predict diastolic relaxation dysfunction in calcium transient (Ca^{2+}) as shown in Figure 21F. Additionally, it accurately predicts the impairment of contractile machinery (Figure S13J in Study IV) and the alteration of energetics in the cardiac environment (Figure S13I in Study IV) under ischemic conditions. In a previous study, (Joulin et al., 2009) documented the presence of contractile relaxation dysfunction in mouse hearts induced by sepsis-

related heart failure. The authors proposed that this impairment in diastolic function is a result of inhibited phosphorylation of SERCA. It is noteworthy that hiMCES model in Study IV also predicts an inhibition of SERCA phosphorylation activity during the reperfusion phase, as depicted in Figure 25H. Significantly, within the context of I/R, this inhibition may suggest a mechanism that contributes to the augmentation of the already elevated levels of phosphate groups, which are known to be associated with I/R injuries (Ng, 2004).

Notably, the increased contraction ATPase rate in response to CE transition to hypoxic metabolite concentrations (Table 8) elevated the simulated OCR at the onset of ischemia (Figure 4D in Study IV). In the context of I/R treatment, mapping the abnormal oxygen dynamic at the onset of ischemia onto the abnormally elevated contractile ATPase rate is indicative of the therapeutic significance of targeting the CE compared to other ionic factors affecting the OCR. Furthermore, these data highlight the importance of troponin C-affiliated Ca^{2+} sensitizing inotropes like Levo in restoring the cardiac contractile functionality independent of oxygen consumption (Ng, 2004).

6.4 Limitations and future perspectives

The models presented in this study effectively capture several important electromechanical outcomes of hiPSC-CMs. However, further investigation and simulation are required to study the inherent heterogeneity of myofilaments, which may vary across different morphologies of hiPSC-CMs. Moreover, it should be noted that all the models described in this thesis have been implemented using ODEs. In other words, the explicit incorporation of spatial aspects has not been taken into account. In order to uphold a practical system of ODEs, the CE submodel incorporates approximations. Nevertheless, in order to account for spatial scales and local interactions that cannot be explicitly modeled by mean-field approaches, approximations are made in Ca^{2+} -based myofilament activation and the utilization of mean XB strains. Other essential limitations affecting the translational power of such studies include hiPSC-CMs immaturity, strong dependence of ischemic *in vitro* studies on O_2 and insufficient data on other energetic mechanisms such as mitochondria, and translational challenges between *in vitro* studies and *in vivo* conditions. Another inherent limitation shared in all Studies I-IV might arise from the methodology itself, i.e., choosing the sets of *in vitro* data for

calibrations/validations coupled with the *in vitro* data quality and protocol discrepancies. In the next sections, I detail the limitations and future research potentials for each model developed in this thesis.

6.4.1 The hiPSC-CM-CE model (Study II)

Study II (Forouzandehmehr, Koivumäki, et al., 2021) demonstrates that the hiPSC-CM-CE model effectively predicts the inotropic effects of non-CMs in hiPSC-CMs tissues as an inter-scale analysis. However, it is important to note that this model is a simplified representation of the actual system. To achieve a more comprehensive understanding, future research should consider incorporating the influence of heterogeneous hiPSC-CMs substrates, EHT sarcomere alignments, and myosin expression into the modelling framework.

It would be of interest to investigate the impact of incorporating the reparametrized CE into other hiPSC-CMs electrophysiology models such as Kernik2019 and Koivumäki2018 models (Kernik et al., 2019; Koivumäki et al., 2018). In (Paci, T Koivumäki, et al., 2021), authors have compared the three models in terms of their responses to drugs. However, I deemed it beyond the purview of this thesis due to the following rationales. The complexity of integrating the CE in the Koivumäki2018 study is greatly influenced by the intracellular compartmentalization. In contrast, the Kernik2019 model exhibits a comparable compartmentalization approach as observed in the Paci2020 model. Nevertheless, the integration of the CE models would pose certain challenges, primarily stemming from variations in the handling of Ca^{2+} ions between the Paci2020 and Kernik2019 models. The latter model replicates a CaT peak that is 2.5 times higher and an I_{CaL} amplitude that is 50% greater. Given the nonlinearity observed in Ca^{2+} cooperation and sensitivity in the CE, it becomes necessary to employ a distinct reparameterization approach. The integration of the current reparameterization of the Rice CE into the Kernik2019 model would yield an electromechanical model that lacks consistency with experimental ranges in terms of its simulated results.

6.4.2 The hiMCE model (Study III)

I postulated that the administration of $0.5 \mu\text{M}$ MAVA has the potential to normalize the heightened levels of MgADP and Pi in the HCM model variant, bringing them back to their original baseline values as documented in Table 5. While this assumption aligns with the proposed mechanism of action of MAVA as described

by (Green et al., 2016), it still represents a simplification. Additionally, a primary limitation of hiPSC-CMs is their dependence on glycolytic metabolism, which differs from the fatty acid-based metabolism observed in native hV-CMs. Another factor that contributes to variations in energy levels is the disparity between the surrounding medium *in vitro* and *in vivo* settings. As hiMCE model does not incorporate the energy production process, we deem it appropriate to exclude the discussion of metabolic differences from the scope of this study. As the availability of comprehensive *in vitro* data on hiPSC-CM metabolism increases, the modeling endeavors outlined in this thesis provide a robust foundation for the subsequent development of cardiomyocyte models that incorporate energy production.

The structural immaturity of hiPSC-CMs, as well as their distinctive sarcomere alignment and performance, and their impact on HCM and drug-induced studies are noteworthy. The fundamental basis for the model HCM variant and MAVA calibration lies in the utilization of *in vitro* data from hiPSC-CMs at day 30 following differentiation, which provides evidence of cardiomyocyte maturation (Toepfer et al., 2020). To validate the hiPSC-CMs findings in relation to *in vivo* data, (Toepfer et al., 2020) performed comparative analyses on both a mouse model of HCM and human cardiac tissues affected by HCM. The analysis demonstrated that both the HCM variant in mice and the HCM variant in hiPSC-CMs exhibited increased contractility compared to their respective WT models, as depicted in Figure 3 C&I of (Toepfer et al., 2020). In addition, an extended contractile relaxation was also noted in both mouse CMs and hiPSC-CMs as illustrated in Figure 3D&J of (Toepfer et al., 2020). Furthermore, (Toepfer et al., 2020) demonstrated a reduction in hypercontractility and myosin population in mouse CMs and hiPSC-CMs as a result of MAVA treatment. This dose-dependent decrease was observed in Figure 3, panels E and K of the aforementioned study. Overall, the findings presented in Figure 3 of (Toepfer et al., 2020) demonstrate that the effects of HCM and drug-induced changes on hiPSC-CMs align with the observed patterns in mouse WT and R403Q cardiomyocyte variants. The primary focus of this thesis was to prioritize the utilization of *in vitro* data from hiPSC-CMs for the calibration and validation of results. However, it is important to note that the aforementioned points suggest that the validation of and calibration for MYH7^{R403Q/+} and drug-induced outcomes using cell lines other than hiPSC-CMs remain valid and acceptable methodologies.

Moreover, due to its 0D nature, the hiMCE computational model does not explicitly incorporate the characteristic sarcomere disorganization observed in hiPSC-CMs. As additional experimental data becomes accessible, exploring this

potential avenue for computational studies in HCM holds promise for its potential significance and interest.

6.4.3 The hiMCES model (Study IV)

Study IV does not incorporate the energetic component due to the scarcity of available data on hiPSC-CM mitochondrial dynamics. Moreover, it should be noted that the hiMCES model lacks an ATP-sensitive I_{NaK} formulation. Consequently, the representation of the I_{NaK} in the OCR formulation is a simplified approximation. Future research endeavors could potentially derive significant advantages by enhancing the level of detail regarding crossbridge cycling in the CE model. This enhancement could facilitate a comprehensive characterization of the relaxation dysfunction associated with I/R and shed light on the underlying mechanism of action of Levo.

Another limitation affecting Study IV was the limitations of the *in vitro* research (Gaballah et al., 2022) I used to validate the results and also justify the methodology. Namely, not distinguishing hiPSC-CMs subtypes (atrial, ventricular, and nodal), absence of metabolic profile measurements giving information on ATP, ADP, and phosphorylation states, and randomness in Ca^{2+} video imaging. In addition, the maladaptive reduction of the cell culture oxygen level provided the time-window for the hiPSC-CMs to adopt to the new condition which is dissimilar to *in vivo* acute ischemia where the temporal events are usually sudden (Gaballah et al., 2022). Moreover, the metabolic resemblance of the hiPSC-CMs *in vitro* to fetal CMs, specifically, their dependence on glycolysis rather than FA-based oxidative pathway was another limitation affecting also Study IV structure.

Finally, similar to Studies I-III, Study IV also face the structural limitation imposed by using ODEs for such biological environment, i.e., lacking explicit description of spatial aspects of hiPSC-CMs at cell level, especially in the CE submodel (details are given in (Rice et al., 2008)).

7 CONCLUSION

7.1 Biophysical modeling development and calibration maps

Meeting the accurate FCS, CRT₅₀, and AT amplitude were introduced as the optimization goals of the CM electromechanical calibrations. The sensitivity analysis and dynamics of the CE machinery studied in Studies I&II offer a robust reparameterization roadmap specifically from animal-based computational myofilament submodels to hiPSC-CMs contractile phenotype. A correct categorization of inotropic effects of non-CMs was recapitulated in accord with hiPSC-CMs experimental reports. The offered formulation as a passive force can be a basis for future advanced machine learning algorithms targeting classifications of such. Finally, the initial iteration of the *in silico* hiPSC-CMs electromechanics model underwent testing using a protocol that involved inducing arrhythmogenic and inotropic effects through drug administration. This model successfully replicated the occurrence of aftercontractions resulting from triggered EADs, in alignment with experimental data. The model demonstrates proficiency in facilitating the expansion and interpretation of the findings in the realms of computational simulations and *in vitro* experiments conducted on tissue and organ levels.

Building upon hiPSC-CM-CE model, deep-phenotyping MYH7^{R403Q/+}-HCM pathophysiology and MAVA effect with regard to the metabolite contractile machinery was offered in Study III. The metabolite-sensitivity in the CE played a key role in capturing the contractile dysfunction, in terms of hypercontractility and irregular CRT₅₀, in R403-HCM and the cardioprotective effect of MAVA. Explicitly, the model could map the disturbed interfilament kinetics in HCM onto optimization of CE parameters affecting XB state transitions and Pi, MgATP, and MgADP.

Ultimately, Study IV offers the most complete model of cell-biophysics and calibration setup as it includes a metabolite-sensitive model of SERCA pump in tandem with a metabolite-sensitive CE particularly optimized to capture the ischemic-induced effects, importantly, AP and Ca^T abnormalities.

7.2 Extending the orthodox drug modeling formalism

In traditional channel-blocking formalism (based on IC50s and Hill coeffs.), the first model developed in this thesis, hiPSC-CM-CE (Study II), simulated the drug-induced effects on the electrophysiology and contractility consistently. The therapeutic compounds investigated in Study III were sarcomere targeting molecules; MAVA, BLEB, and OM. Therefore, their mechanism of action was modeled by CE optimizations accordingly, and the XB parameter governing the dose-dependence of OM and BLEB inotropic effect was identified. In Study IV, in accord with dose-dependent inotropic data of Levo, the increase in the troponin C affinity for Ca^{2+} in presence of Levo was modeled by change in the transition rate between troponin and Ca-bound troponin states (K_{on}) in XB cycling. Furthermore, the dose-dependent effect of Levo as an I_{KATP} agonist was included in the drug-induced calibration besides the channel-blockings for I_{Na} , I_{CaL} , and I_{Kr} , leading to more reliable predictions of drug effects in I/R.

7.3 Discovering cellular crosstalks in ischemia/reperfusion

Extending the biophysics of the model by inclusion of metabolite-sensitivity, oxygen dynamics, and optimizations helped in deep-phenotyping hiPSC-CMs in I/R. Explicitly, introducing an oxygen dynamic formulation with a contractile ATPase rate was a first step toward linking the cellular energetics to OCR.

Of note, the SERCA calibration provided insight into the abnormal competitive proton binding for SR during I/R. Explicitly, increased affinity of proton binding for luminal-oriented Ca^{2+} docking sites was suggested as a mechanism of SERCA response to I/R condition that leads to increased Ca^{2+} concentration in SR.

Furthermore, the power of Ca^{2+} removal in ischemia is important as CaT is elevated. Our model predicted the upper hand of Ca^{2+} flux to the myofilament in comparison with SERCA Ca^{2+} uptake, also confirming that Levo does not increase the inotropy at the expense of elevated oxygen demand.

Our findings suggest that, mechanistically, SERCA contributes similarly in I/R and sepsis-induced heart failure conditions which may be significant in the rationale for future drug development, specifically, in terms of SERCA contribution to the diastolic impairment in contractile relaxation and energetic function. Furthermore, hiMCES model suggested that the increase in proton leak in I/R, which results in

elevated oxidative stress, may also contribute to the ischemic Ca^{2+} overload through disrupted competitive proton binding in SERCA, a step toward establishing the connection between the elevation of oxidative stress and Ca^{2+} overload as the two main mechanisms of I/R injuries. Finally, Levo simulations linked the drug's ameliorative effect of the compound on contractile relaxation dysfunction to the drug's specific Ca^{2+} sensitizing mechanism, which involves Ca^{2+} -bound troponin C and Ca^{2+} flux to the myofilament rather than SERCA phosphorylation inhibition. To summarize, Study IV introduced a novel and robust computational framework of electro-mechano-energetic coupling in hiPSC-CMs, leveraging recent advances in human-based *in vitro* data acquisition. Ultimately, the model can serve as a platform to test I/R treatment ideas according to the temporal evolution of metabolites and molecular mechanisms in cardiomyocytes.

In summary, this thesis presents innovative and reliable computational frameworks for studying the interplay between electro-mechanical and energetic processes in hiPSC-CMs. Besides guiding the optimization of *in vitro* trials, these computational frameworks help increase the translational capacity of the latest advancements in human-based *in vitro* analyses.

REFERENCES

- Abraham, M. R., Bottomley, P. A., Dimaano, V. L., Pinheiro, A., Steinberg, A., Traill, T. A., Abraham, T. P., & Weiss, R. G. (2013). Creatine Kinase Adenosine Triphosphate and Phosphocreatine Energy Supply in a Single Kindred of Patients With Hypertrophic Cardiomyopathy. *The American Journal of Cardiology*, *112*(6), 861–866. <https://doi.org/10.1016/j.amjcard.2013.05.017>
- Ahmed, R. E., Anzai, T., Chanthra, N., & Uosaki, H. (2020). A Brief Review of Current Maturation Methods for Human Induced Pluripotent Stem Cells-Derived Cardiomyocytes. *Frontiers in Cell and Developmental Biology*, *8*. <https://www.frontiersin.org/articles/10.3389/fcell.2020.00178>
- Alamo, L., Ware, J. S., Pinto, A., Gillilan, R. E., Seidman, J. G., Seidman, C. E., & Padrón, R. (2017). Effects of myosin variants on interacting-heads motif explain distinct hypertrophic and dilated cardiomyopathy phenotypes. *eLife*, *6*. <https://doi.org/10.7554/eLife.24634>
- Alsulami, K., & Marston, S. (2020). Small Molecules Acting on Myofilaments as Treatments for Heart and Skeletal Muscle Diseases. *International Journal of Molecular Sciences*, *21*(24), 9599. <https://doi.org/10.3390/ijms21249599>
- Ambrose, J. A., & Singh, M. (2015). Pathophysiology of coronary artery disease leading to acute coronary syndromes. *F1000Prime Rep*, *7*(8). <https://connect.h1.co/prime/reports/m/7/8/>
- Awinda, P. O., Bishaw, Y., Watanabe, M., Guglin, M. A., Campbell, K. S., & Tanner, B. C. W. (2020). Effects of mavacamten on Ca²⁺ sensitivity of contraction as sarcomere length varied in human myocardium. *British Journal of Pharmacology*, *177*(24), 5609–5621. <https://doi.org/10.1111/bph.15271>
- Bakkehaug, J. P., Kildal, A. B., Engstad, E. T., Boardman, N., Næsheim, T., Rønning, L., Aasum, E., Larsen, T. S., Myrmel, T., & How, O.-J. (2015). Myosin Activator Omecamtiv Mecarbil Increases Myocardial Oxygen Consumption and Impairs Cardiac Efficiency Mediated by Resting Myosin ATPase Activity. *Circulation. Heart Failure*, *8*(4), 766–775. <https://doi.org/10.1161/CIRCHEARTFAILURE.114.002152>

- Bartolucci, C., Passini, E., Hyttinen, J., Paci, M., & Severi, S. (2020). Simulation of the Effects of Extracellular Calcium Changes Leads to a Novel Computational Model of Human Ventricular Action Potential With a Revised Calcium Handling. *Frontiers in Physiology*, *11*, 314. <https://doi.org/10.3389/fphys.2020.00314>
- Bo, B., Li, S., Zhou, K., & Wei, J. (2021). The Regulatory Role of Oxygen Metabolism in Exercise-Induced Cardiomyocyte Regeneration. *Frontiers in Cell and Developmental Biology*, *9*. <https://doi.org/10.3389/fcell.2021.664527>
- Botti, Sofia. (2022). *Mathematical modeling of Human Induced Pluripotent Stem Cell-Derived Cardiomyocytes (hiPSC-CMs): From ionic currents to 3D ventricle models*. <https://hdl.handle.net/11571/1467309>
- Brunello, E., Fusi, L., Ghisleni, A., Park-Holohan, S.-J., Ovejero, J. G., Narayanan, T., & Irving, M. (2020). Myosin filament-based regulation of the dynamics of contraction in heart muscle. *Proceedings of the National Academy of Sciences*, *117*(14), 8177–8186. <https://doi.org/10.1073/pnas.1920632117>
- BUTT, A. N., TENNANT, B. P., GILLINGWATER, S. D., SHEPHERD, P. S., & SWAMINATHAN, R. (2000). Binding of Ouabain and Human Ouabainlike Substance to Different Na⁺, K⁺-ATPase Isoforms. *Hypertension Research*, *23*(Supplement), S45–S50. https://doi.org/10.1291/hypres.23.Supplement_S45
- Campbell, S. G., Flaim, S. N., Leem, C. H., & McCulloch, A. D. (2008). Mechanisms of transmurally varying myocyte electromechanics in an integrated computational model. *Philosophical Transactions of the Royal Society A: Mathematical, Physical and Engineering Sciences*. <https://doi.org/10.1098/rsta.2008.0088>
- Campbell, S. G., Lionetti, F. V., Campbell, K. S., & McCulloch, A. D. (2010). Coupling of adjacent tropomyosins enhances cross-bridge-mediated cooperative activation in a markov model of the cardiac thin filament. *Biophysical Journal*. <https://doi.org/10.1016/j.bpj.2010.02.004>
- Chang, J. C., Brennan, K. C., He, D., Huang, H., Miura, R. M., Wilson, P. L., & Wylie, J. J. (2013). A Mathematical Model of the Metabolic and Perfusion Effects on Cortical Spreading Depression. *PLoS ONE*, *8*(8), e70469. <https://doi.org/10.1371/journal.pone.0070469>

- Chen, S., & Li, S. (2012). The Na⁺/Ca²⁺ exchanger in cardiac ischemia/reperfusion injury. *Medical Science Monitor*, 18(11), RA161–RA165. <https://doi.org/10.12659/MSM.883533>
- Chen, Y., Yin, C., Yang, Y., Fan, Z., Shang, J., & Tan, W. (2017). Inhibition of rapid delayed rectifier potassium current (I_{Kr}) by ischemia/reperfusion and its recovery by vitamin E in ventricular myocytes. *Journal of Electrocardiology*, 50(4), 437–443. <https://doi.org/10.1016/j.jelectrocard.2017.03.007>
- Clark, J. A., Sewanan, L. R., Schwan, J., Kluger, J., Campbell, K. S., & Campbell, S. G. (2021). Fast-relaxing cardiomyocytes exert a dominant role in the relaxation behavior of heterogeneous myocardium. *Archives of Biochemistry and Biophysics*, 697, 108711. <https://doi.org/10.1016/j.abb.2020.108711>
- Coppini, R., Ferrantini, C., Yao, L., Fan, P., Del Lungo, M., Stillitano, F., Sartiani, L., Tosi, B., Suffredini, S., Tesi, C., Yacoub, M., Olivotto, I., Belardinelli, L., Poggesi, C., Cerbai, E., & Mugelli, A. (2013). Late Sodium Current Inhibition Reverses Electromechanical Dysfunction in Human Hypertrophic Cardiomyopathy. *Circulation*, 127(5), 575–584. <https://doi.org/10.1161/CIRCULATIONAHA.112.134932>
- Coppini, R., Ho, C. Y., Ashley, E., Day, S., Ferrantini, C., Girolami, F., Tomberli, B., Bardi, S., Torricelli, F., Cecchi, F., Mugelli, A., Poggesi, C., Tardiff, J., & Olivotto, I. (2014). Clinical Phenotype and Outcome of Hypertrophic Cardiomyopathy Associated With Thin-Filament Gene Mutations. *Journal of the American College of Cardiology*, 64(24), 2589–2600. <https://doi.org/10.1016/j.jacc.2014.09.059>
- Cressman, J. R., Ullah, G., Ziburkus, J., Schiff, S. J., & Barreto, E. (2009). The influence of sodium and potassium dynamics on excitability, seizures, and the stability of persistent states: I. Single neuron dynamics. *Journal of Computational Neuroscience*, 26(2), 159–170. <https://doi.org/10.1007/s10827-008-0132-4>
- Crocini, C., & Gotthardt, M. (2021). Cardiac sarcomere mechanics in health and disease. *Biophysical Reviews*, 13(5), 637–652. <https://doi.org/10.1007/s12551-021-00840-7>
- Daley, G. Q. (2015). Stem cells and the evolving notion of cellular identity. *Philosophical Transactions of the Royal Society B: Biological Sciences*, 370(1680), 20140376. <https://doi.org/10.1098/rstb.2014.0376>

- de Tombe, P. P. (2003). Cardiac myofilaments: Mechanics and regulation. *Journal of Biomechanics*, 36(5), 721–730. [https://doi.org/10.1016/S0021-9290\(02\)00450-5](https://doi.org/10.1016/S0021-9290(02)00450-5)
- De Vuyst, E., Boengler, K., Antoons, G., Sipido, K. R., Schulz, R., & Leybaert, L. (2011). Pharmacological modulation of connexin-formed channels in cardiac pathophysiology. *British Journal of Pharmacology*, 163(3), 469–483. <https://doi.org/10.1111/j.1476-5381.2011.01244.x>
- Deo, M., Akwaboah, A., Tsevi, B., Treat, J. A., & Cordeiro, J. M. (2020). Role of the rapid delayed rectifier K⁺ current in human induced pluripotent stem cells derived cardiomyocytes. *Archives of Stem Cell and Therapy*, 1(1), 14–18. <https://doi.org/10.46439/stemcell.1.003>
- Dutta, S., Mincholé, A., Quinn, T. A., & Rodriguez, B. (2017). Electrophysiological properties of computational human ventricular cell action potential models under acute ischemic conditions. *Progress in Biophysics and Molecular Biology*, 129, 40–52. <https://doi.org/10.1016/j.pbiomolbio.2017.02.007>
- Eberli, F. R., Strömer, H., Ferrell, M. A., Varma, N., Morgan, J. P., Neubauer, S., & Apstein, C. S. (2000). Lack of Direct Role for Calcium in Ischemic Diastolic Dysfunction in Isolated Hearts. *Circulation*, 102(21), 2643–2649. <https://doi.org/10.1161/01.CIR.102.21.2643>
- Eisner, D. A., Caldwell, J. L., Kistamás, K., & Trafford, A. W. (2017). Calcium and Excitation-Contraction Coupling in the Heart. *Circulation Research*, 121(2), 181–195. <https://doi.org/10.1161/CIRCRESAHA.117.310230>
- Endeward, V. (2012). The rate of the deoxygenation reaction limits myoglobin- and hemoglobin-facilitated O₂ diffusion in cells. *Journal of Applied Physiology*, 112(9), 1466–1473. <https://doi.org/10.1152/jappphysiol.00835.2011>
- Fabbri, A., Fantini, M., Wilders, R., & Severi, S. (2017). Computational analysis of the human sinus node action potential: Model development and effects of mutations. *The Journal of Physiology*, 595(7), 2365–2396. <https://doi.org/10.1113/JP273259>
- Ferrandi, M., Manunta, P., Balzan, S., Hamlyn, J. M., Bianchi, G., & Ferrari, P. (1997). Ouabain-like Factor Quantification in Mammalian Tissues and Plasma. *Hypertension*, 30(4), 886–896. <https://doi.org/10.1161/01.HYP.30.4.886>

- Ferrantini, C., Pioner, J. M., Mazzoni, L., Gentile, F., Tosi, B., Rossi, A., Belardinelli, L., Tesi, C., Palandri, C., Matucci, R., Cerbai, E., Olivotto, I., Poggesi, C., Mugelli, A., & Coppini, R. (2018). Late sodium current inhibitors to treat exercise-induced obstruction in hypertrophic cardiomyopathy: An in vitro study in human myocardium. *British Journal of Pharmacology*, *175*(13), 2635–2652. <https://doi.org/10.1111/bph.14223>
- Ferrero, J. M., Sáiz, J., Ferrero, J. M., & Thakor, N. V. (1996). Simulation of Action Potentials From Metabolically Impaired Cardiac Myocytes. *Circulation Research*, *79*(2), 208–221. <https://doi.org/10.1161/01.RES.79.2.208>
- Forouzandehmehr, M., Bartolucci, C., Hyttinen, J., Koivumaki, J. T., & Paci, M. (2021). Sensitivity of the Human Ventricular BPS2020 Action Potential Model to the In Silico Mechanisms of Ischemia. *2021 Computing in Cardiology (CinC)*, 1–4. <https://doi.org/10.23919/CinC53138.2021.9662800>
- Forouzandehmehr, M., Cogno, N., Koivumäki, J., Hyttinen, J., & Paci, M. (2020). The Comparison Between Two Mathematical Contractile Elements Integrated into an hiPSC-CM In-silico Model. *Computing in Cardiology*, *47*. <https://doi.org/10.22489/CinC.2020.055>
- Forouzandehmehr, M., Koivumäki, J. T., Hyttinen, J., & Paci, M. (2021). A mathematical model of hiPSC cardiomyocytes electromechanics. *Physiological Reports*, *9*(22). <https://doi.org/10.14814/phy2.15124>
- Forouzandehmehr, M., Paci, M., Koivumäki, J. T., & Hyttinen, J. (2022). Altered contractility in mutation-specific hypertrophic cardiomyopathy: A mechano-energetic in silico study with pharmacological insights. *Frontiers in Physiology*, *13*. <https://doi.org/10.3389/fphys.2022.1010786>
- Gaballah, M., Penttinen, K., Kreutzer, J., Mäki, A.-J., Kallio, P., & Aalto-Setälä, K. (2022). Cardiac Ischemia On-a-Chip: Antiarrhythmic Effect of Levosimendan on Ischemic Human-Induced Pluripotent Stem Cell-Derived Cardiomyocytes. *Cells*, *11*(6), 1045. <https://doi.org/10.3390/cells11061045>
- Garcia-Dorado, D., Ruiz-Meana, M., Inserte, J., Rodriguez-Sinovas, A., & Piper, H. M. (2012). Calcium-mediated cell death during myocardial reperfusion. *Cardiovascular Research*, *94*(2), 168–180. <https://doi.org/10.1093/cvr/cvs116>
- Gartzonikas, I. K., Naka, K. K., & Anastasakis, A. (2023). Current and emerging perspectives on pathophysiology, diagnosis, and management of

- hypertrophic cardiomyopathy. *Hellenic Journal of Cardiology*, 70, 65–74.
<https://doi.org/10.1016/j.hjc.2022.11.002>
- Gollapudi, S. K., Yu, M., Gan, Q.-F., & Nag, S. (2021). Synthetic thick filaments: A new avenue for better understanding the myosin super-relaxed state in healthy, diseased, and mavacamten-treated cardiac systems. *Journal of Biological Chemistry*, 296, 100114.
<https://doi.org/10.1074/jbc.RA120.016506>
- Gomes, A. V., Potter, J. D., & Szczesna-Cordary, D. (2002). The Role of Troponins in Muscle Contraction. *IUBMB Life*, 54(6), 323–333.
<https://doi.org/10.1080/15216540216037>
- Grandi, E., Pasqualini, F. S., & Bers, D. M. (2010). A novel computational model of the human ventricular action potential and Ca transient. *Journal of Molecular and Cellular Cardiology*. <https://doi.org/10.1016/j.yjmcc.2009.09.019>
- Grandi, E., Pasqualini, F. S., Pes, C., Corsi, C., Zaza, A., & Severi, S. (2009). Theoretical investigation of action potential duration dependence on extracellular Ca²⁺ in human cardiomyocytes. *Journal of Molecular and Cellular Cardiology*, 46(3), 332–342. <https://doi.org/10.1016/j.yjmcc.2008.12.002>
- Grass, M., McDougal, A. D., Blazeski, A., Kamm, R. D., García-Cardena, G., & Dewey, C. F. (2022). A computational model of cardiomyocyte metabolism predicts unique reperfusion protocols capable of reducing cell damage during ischemia/reperfusion. *Journal of Biological Chemistry*, 298(5), 101693.
<https://doi.org/10.1016/j.jbc.2022.101693>
- Green, E. M., Wakimoto, H., Anderson, R. L., Evanchik, M. J., Gorham, J. M., Harrison, B. C., Henze, M., Kawas, R., Oslob, J. D., Rodriguez, H. M., Song, Y., Wan, W., Leinwand, L. A., Spudich, J. A., McDowell, R. S., Seidman, J. G., & Seidman, C. E. (2016). A small-molecule inhibitor of sarcomere contractility suppresses hypertrophic cardiomyopathy in mice. *Science*, 351(6273), 617–621. <https://doi.org/10.1126/science.aad3456>
- Gunaseeli, I., Doss, M., Antzelevitch, C., Hescheler, J., & Sachinidis, A. (2010). Induced Pluripotent Stem Cells as a Model for Accelerated Patient- and Disease-specific Drug Discovery. *Current Medicinal Chemistry*, 17(8), 759–766.
<https://doi.org/10.2174/092986710790514480>
- Guo, X., Gao, X., Wang, Y., Peng, L., Zhu, Y., & Wang, S. (2012). IKs Protects from Ventricular Arrhythmia during Cardiac Ischemia and Reperfusion in Rabbits

by Preserving the Repolarization Reserve. *PLoS ONE*, 7(2), e31545. <https://doi.org/10.1371/journal.pone.0031545>

Guo, Y., & Pu, W. T. (2020). Cardiomyocyte Maturation. *Circulation Research*, 126(8), 1086–1106. <https://doi.org/10.1161/CIRCRESAHA.119.315862>

Habecker, B. A., Anderson, M. E., Birren, S. J., Fukuda, K., Herring, N., Hoover, D. B., Kanazawa, H., Paterson, D. J., & Ripplinger, C. M. (2016). Molecular and cellular neurocardiology: Development, and cellular and molecular adaptations to heart disease. *The Journal of Physiology*, 594(14), 3853–3875. <https://doi.org/10.1113/JP271840>

Haikala, H. (1997). The role of cAMP- and cGMP-dependent protein kinases in the cardiac actions of the new calcium sensitizer, levosimendan. *Cardiovascular Research*, 34(3), 536–546. [https://doi.org/10.1016/S0008-6363\(97\)00057-6](https://doi.org/10.1016/S0008-6363(97)00057-6)

Häkli, M., Kreutzer, J., Mäki, A.-J., Välimäki, H., Cherian, R. M., Kallio, P., Aalto-Setälä, K., & Pekkanen-Mattila, M. (2022). Electrophysiological Changes of Human-Induced Pluripotent Stem Cell-Derived Cardiomyocytes during Acute Hypoxia and Reoxygenation. *Stem Cells International*, 2022, 1–15. <https://doi.org/10.1155/2022/9438281>

Häkli, M., Kreutzer, J., Mäki, A.-J., Välimäki, H., Lappi, H., Huhtala, H., Kallio, P., Aalto-Setälä, K., & Pekkanen-Mattila, M. (2021a). Human induced pluripotent stem cell-based platform for modeling cardiac ischemia. *Scientific Reports*, 11(1), 4153. <https://doi.org/10.1038/s41598-021-83740-w>

Häkli, M., Kreutzer, J., Mäki, A.-J., Välimäki, H., Lappi, H., Huhtala, H., Kallio, P., Aalto-Setälä, K., & Pekkanen-Mattila, M. (2021b). Human induced pluripotent stem cell-based platform for modeling cardiac ischemia. *Scientific Reports*, 11(1), 4153. <https://doi.org/10.1038/s41598-021-83740-w>

Hausenloy, D. J., & Yellon, D. M. (2013). Myocardial ischemia-reperfusion injury: A neglected therapeutic target. *The Journal of Clinical Investigation*, 123(1), 92–100. <https://doi.org/10.1172/JCI62874>

Hayakawa, T., Kunihiro, T., Ando, T., Kobayashi, S., Matsui, E., Yada, H., Kanda, Y., Kurokawa, J., & Furukawa, T. (2014). Image-based evaluation of contraction-relaxation kinetics of human-induced pluripotent stem cell-derived cardiomyocytes: Correlation and complementarity with extracellular electrophysiology. *Journal of Molecular and Cellular Cardiology*. <https://doi.org/10.1016/j.yjmcc.2014.09.010>

- He, J., Liu, D., Zhao, L., Zhou, D., Rong, J., Zhang, L., & Xia, Z. (2022). Myocardial ischemia/reperfusion injury: Mechanisms of injury and implications for management (Review). *Experimental and Therapeutic Medicine*, 23(6), 430. <https://doi.org/10.3892/etm.2022.11357>
- Ho, C. Y., Charron, P., Richard, P., Girolami, F., Van Spaendonck-Zwarts, K. Y., & Pinto, Y. (2015). Genetic advances in sarcomeric cardiomyopathies: State of the art. *Cardiovascular Research*, 105(4), 397–408. <https://doi.org/10.1093/cvr/cvz025>
- Ho, C. Y., Day, S. M., Ashley, E. A., Michels, M., Pereira, A. C., Jacoby, D., Cirino, A. L., Fox, J. C., Lakdawala, N. K., Ware, J. S., Caleshu, C. A., Helms, A. S., Colan, S. D., Girolami, F., Cecchi, F., Seidman, C. E., Sajeev, G., Signorovitch, J., Green, E. M., & Olivotto, I. (2018). Genotype and Lifetime Burden of Disease in Hypertrophic Cardiomyopathy. *Circulation*, 138(14), 1387–1398. <https://doi.org/10.1161/CIRCULATIONAHA.117.033200>
- Ho, C. Y., Olivotto, I., Jacoby, D., Lester, S. J., Roe, M., Wang, A., Waldman, C. B., Zhang, D., Sehnert, A. J., & Heitner, S. B. (2020). Study Design and Rationale of EXPLORER-HCM. *Circulation: Heart Failure*. <https://doi.org/10.1161/CIRCHEARTFAILURE.120.006853>
- Hong, T., & Shaw, R. M. (2017). Cardiac T-Tubule Microanatomy and Function. *Physiological Reviews*, 97(1), 227–252. <https://doi.org/10.1152/physrev.00037.2015>
- Hooijman, P., Stewart, M. A., & Cooke, R. (2011). A New State of Cardiac Myosin with Very Slow ATP Turnover: A Potential Cardioprotective Mechanism in the Heart. *Biophysical Journal*, 100(8), 1969–1976. <https://doi.org/10.1016/j.bpj.2011.02.061>
- Hoskins, A. C., Jacques, A., Bardswell, S. C., McKenna, W. J., Tsang, V., Remedios, C. G. dos, Ehler, E., Adams, K., Jalilzadeh, S., Avkiran, M., Watkins, H., Redwood, C., Marston, S. B., & Kentish, J. C. (2010). Normal passive viscoelasticity but abnormal myofibrillar force generation in human hypertrophic cardiomyopathy. *Journal of Molecular and Cellular Cardiology*, 49(5), 737–745. <https://doi.org/10.1016/j.yjmcc.2010.06.006>
- Hu, D., Linders, A., Yamak, A., Correia, C., Kijlstra, J. D., Garakani, A., Xiao, L., Milan, D. J., van der Meer, P., Serra, M., Alves, P. M., & Domian, I. J. (2018). Metabolic Maturation of Human Pluripotent Stem Cell-Derived Cardiomyocytes by Inhibition of HIF1 α and LDHA. *Circulation Research*, 123(9), 1066–1079. <https://doi.org/10.1161/CIRCRESAHA.118.313249>

- Huebsch, N., Charrez, B., Neiman, G., Siemons, B., Boggess, S. C., Wall, S., Charwat, V., Jäger, K. H., Cleres, D., Telle, Å., Lee-Montiel, F. T., Jeffreys, N. C., Deveshwar, N., Edwards, A. G., Serrano, J., Snuderl, M., Stahl, A., Tveito, A., Miller, E. W., & Healy, K. E. (2022). Metabolically driven maturation of human-induced-pluripotent-stem-cell-derived cardiac microtissues on microfluidic chips. *Nature Biomedical Engineering*, 6(4), Article 4. <https://doi.org/10.1038/s41551-022-00884-4>
- Ingwall, J. S. (2002). *ATP and the Heart*. Springer US. <https://doi.org/10.1007/978-1-4615-1093-2>
- Iseoka, H., Miyagawa, S., Fukushima, S., Saito, A., Masuda, S., Yajima, S., Ito, E., Sougawa, N., Takeda, M., Harada, A., Lee, J.-K., & Sawa, Y. (2018). Pivotal Role of Non-cardiomyocytes in Electromechanical and Therapeutic Potential of Induced Pluripotent Stem Cell-Derived Engineered Cardiac Tissue. *Tissue Engineering Part A*, 24(3–4), 287–300. <https://doi.org/10.1089/ten.tea.2016.0535>
- Ji, Y., Loukianov, E., Loukianova, T., Jones, L. R., & Periasamy, M. (1999). SERCA1a can functionally substitute for SERCA2a in the heart. *American Journal of Physiology-Heart and Circulatory Physiology*, 276(1), H89–H97. <https://doi.org/10.1152/ajpheart.1999.276.1.H89>
- Joulin, O., Marechaux, S., Hassoun, S., Montaigne, D., Lancel, S., & Neviere, R. (2009). Cardiac force-frequency relationship and frequency-dependent acceleration of relaxation are impaired in LPS-treated rats. *Critical Care*, 13(1), R14. <https://doi.org/10.1186/cc7712>
- Kalogeris, T., Baines, C. P., Krenz, M., & Korthuis, R. J. (2016). Ischemia/Reperfusion. In *Comprehensive Physiology* (pp. 113–170). John Wiley & Sons, Ltd. <https://doi.org/10.1002/cphy.c160006>
- Kampourakis, T., Zhang, X., Sun, Y.-B., & Irving, M. (2018). Omecamtiv mercabil and blebbistatin modulate cardiac contractility by perturbing the regulatory state of the myosin filament. *The Journal of Physiology*, 596(1), 31–46. <https://doi.org/10.1113/JP275050>
- Karakikes, I., Ameen, M., Termglinchan, V., & Wu, J. C. (2015). Human induced pluripotent stem cell-derived cardiomyocytes: Insights into molecular, cellular, and functional phenotypes. *Circulation Research*, 117(1), 80–88. <https://doi.org/10.1161/CIRCRESAHA.117.305365>

- Kaur, J., Tilkins, M. L., Eckert, R., & Boucher, S. (2013). Methods for Culturing Human Embryonic Stem Cells in a Xeno-Free System. In U. Lakshmiopathy & M. C. Vemuri (Eds.), *Pluripotent Stem Cells: Methods and Protocols* (pp. 115–126). Humana Press. https://doi.org/10.1007/978-1-62703-348-0_9
- Kawana, M., Sarkar, S. S., Sutton, S., Ruppel, K. M., & Spudich, J. A. (2017). Biophysical properties of human β -cardiac myosin with converter mutations that cause hypertrophic cardiomyopathy. *Science Advances*, *3*(2), e1601959. <https://doi.org/10.1126/sciadv.1601959>
- Kawas, R. F., Anderson, R. L., Ingle, S. R. B., Song, Y., Sran, A. S., & Rodriguez, H. M. (2017). A small-molecule modulator of cardiac myosin acts on multiple stages of the myosin chemomechanical cycle. *Journal of Biological Chemistry*, *292*(40), 16571–16577. <https://doi.org/10.1074/jbc.M117.776815>
- Kazbanov, I. V., Clayton, R. H., Nash, M. P., Bradley, C. P., Paterson, D. J., Hayward, M. P., Taggart, P., & Panfilov, A. V. (2014). Effect of Global Cardiac Ischemia on Human Ventricular Fibrillation: Insights from a Multi-scale Mechanistic Model of the Human Heart. *PLoS Computational Biology*, *10*(11), e1003891. <https://doi.org/10.1371/journal.pcbi.1003891>
- Keizer, J., & Levine, L. (1996). Ryanodine receptor adaptation and Ca^{2+} (-)-induced Ca^{2+} release-dependent Ca^{2+} oscillations. *Biophysical Journal*, *71*(6), 3477–3487. [https://doi.org/10.1016/S0006-3495\(96\)79543-7](https://doi.org/10.1016/S0006-3495(96)79543-7)
- Kennedy, A., Finlay, D. D., Guldenring, D., Bond, R., Moran, K., & McLaughlin, J. (2016). The Cardiac Conduction System: Generation and Conduction of the Cardiac Impulse. *Critical Care Nursing Clinics of North America*, *28*(3), 269–279. <https://doi.org/10.1016/j.cnc.2016.04.001>
- Kernik, D. C., Morotti, S., Wu, H., Garg, P., Duff, H. J., Kurokawa, J., Jalife, J., Wu, J. C., Grandi, E., & Clancy, C. E. (2019). A computational model of induced pluripotent stem-cell derived cardiomyocytes incorporating experimental variability from multiple data sources. *The Journal of Physiology*, *597*(17), 4533–4564. <https://doi.org/10.1113/JP277724>
- Khan, M. A., Hashim, M. J., Mustafa, H., Baniyas, M. Y., Suwaidi, S. K. B. M. A., AlKatheeri, R., Alblooshi, F. M. K., Almatrooshi, M. E. A. H., Alzaabi, M. E. H., Darmaki, R. S. A., Lootah, S. N. A. H., Khan, M. A., Hashim, M. J., Mustafa, H., Baniyas, M. Y., Suwaidi, S. K. B. M. A., AlKatheeri, R., Alblooshi, F. M. K., Almatrooshi, M. E. A. H., ... Lootah, S. N. A. H. (2020). Global Epidemiology of Ischemic Heart Disease: Results from the Global

Burden of Disease Study. *Cureus*, 12(7).
<https://doi.org/10.7759/cureus.9349>

- Kimura, S., Bassett, A. L., Furukawa, T., Cuevas, J., & Myerburg, R. J. (1990). Electrophysiological properties and responses to simulated ischemia in cat ventricular myocytes of endocardial and epicardial origin. *Circulation Research*, 66(2), 469–477. <https://doi.org/10.1161/01.RES.66.2.469>
- Klabunde, R. E. (2017). Cardiac electrophysiology: Normal and ischemic ionic currents and the ECG. *Advances in Physiology Education*, 41(1), 29–37. <https://doi.org/10.1152/advan.00105.2016>
- Kockskämper, J. (2016). Excitation–Contraction Coupling of Cardiomyocytes. In K.-D. Schlüter (Ed.), *Cardiomyocytes – Active Players in Cardiac Disease* (pp. 67–96). Springer International Publishing. https://doi.org/10.1007/978-3-319-31251-4_3
- KODAMA, I., WILDE, A., JANSE, M., DURRER, D., & YAMADA, K. (1984). Combined effects of hypoxia, hyperkalemia and acidosis on membrane action potential and excitability of guinea-pig ventricular muscle*. *Journal of Molecular and Cellular Cardiology*, 16(3), 247–259. [https://doi.org/10.1016/S0022-2828\(84\)80591-X](https://doi.org/10.1016/S0022-2828(84)80591-X)
- Koivumäki, J. T., Naumenko, N., Tuomainen, T., Takalo, J., Oksanen, M., Puttonen, K. A., Lehtonen, Š., Kuusisto, J., Laakso, M., Koistinaho, J., & Tavi, P. (2018). Structural Immaturity of Human iPSC-Derived Cardiomyocytes: In Silico Investigation of Effects on Function and Disease Modeling. *Frontiers in Physiology*, 9. <https://doi.org/10.3389/fphys.2018.00080>
- Koivumäki, J. T., Seemann, G., Maleckar, M. M., & Tavi, P. (2014). In Silico Screening of the Key Cellular Remodeling Targets in Chronic Atrial Fibrillation. *PLOS Computational Biology*, 10(5), e1003620. <https://doi.org/10.1371/journal.pcbi.1003620>
- Kolwicz, S. C., Purohit, S., & Tian, R. (2013). Cardiac Metabolism and its Interactions With Contraction, Growth, and Survival of Cardiomyocytes. *Circulation Research*, 113(5), 603–616. <https://doi.org/10.1161/CIRCRESAHA.113.302095>
- Kramer, J., Obejero-Paz, C. A., Myatt, G., Kuryshev, Y. A., Bruening-Wright, A., Verducci, J. S., & Brown, A. M. (2013). MICE Models: Superior to the HERG Model in Predicting Torsade de Pointes. *Scientific Reports*, 3(1), 2100. <https://doi.org/10.1038/srep02100>

- Land, S., & Niederer, S. A. (2015). A Spatially Detailed Model of Isometric Contraction Based on Competitive Binding of Troponin I Explains Cooperative Interactions between Tropomyosin and Crossbridges. *PLoS Computational Biology*. <https://doi.org/10.1371/journal.pcbi.1004376>
- Land, S., Niederer, S. A., Louch, W. E., Sejersted, O. M., & Smith, N. P. (2013). Integrating multi-scale data to create a virtual physiological mouse heart. *Interface Focus*. <https://doi.org/10.1098/rsfs.2012.0076>
- Land, S., Park-Holohan, S. J., Smith, N. P., dos Remedios, C. G., Kentish, J. C., & Niederer, S. A. (2017). A model of cardiac contraction based on novel measurements of tension development in human cardiomyocytes. *Journal of Molecular and Cellular Cardiology*. <https://doi.org/10.1016/j.yjmcc.2017.03.008>
- Laslett, L. J., Paumer, L., & Amsterdam, E. A. (1985). Increase in myocardial oxygen consumption indexes by exercise training at onset of ischemia in patients with coronary artery disease. *Circulation*, *71*(5), 958–962. <https://doi.org/10.1161/01.CIR.71.5.958>
- Ledezma, C. A., Zhou, X., Rodríguez, B., Tan, P. J., & Díaz-Zuccarini, V. (2019). A modeling and machine learning approach to ECG feature engineering for the detection of ischemia using pseudo-ECG. *PLOS ONE*, *14*(8), e0220294. <https://doi.org/10.1371/journal.pone.0220294>
- Lester, R. M., Paglialunga, S., & Johnson, I. A. (2019). QT Assessment in Early Drug Development: The Long and the Short of It. *International Journal of Molecular Sciences*, *20*(6), Article 6. <https://doi.org/10.3390/ijms20061324>
- Li, X., Liu, M., Sun, R., Zeng, Y., Chen, S., & Zhang, P. (2016). Protective approaches against myocardial ischemia reperfusion injury. *Experimental and Therapeutic Medicine*, *12*(6), 3823–3829. <https://doi.org/10.3892/etm.2016.3877>
- Libby, P., & Theroux, P. (2005). Pathophysiology of Coronary Artery Disease. *Circulation*, *111*(25), 3481–3488. <https://doi.org/10.1161/CIRCULATIONAHA.105.537878>
- Limongelli, G., Monda, E., D'Aponte, A., Caiazza, M., Rubino, M., Esposito, A., Palmiero, G., Moscarella, E., Messina, G., Calabro', P., Scudiero, O., Pacileo, G., Monda, M., Bossone, E., Day, S. M., & Olivotto, I. (2021). Combined Effect of Mediterranean Diet and Aerobic Exercise on Weight Loss and Clinical Status in Obese Symptomatic Patients with Hypertrophic

- Cardiomyopathy. *Heart Failure Clinics*, 17(2), 303–313.
<https://doi.org/10.1016/j.hfc.2021.01.003>
- Liu, J., Gong, Y., Xia, L., & Zhao, X. (2016). In Silico Investigation into Cellular Mechanisms of Cardiac Alternans in Myocardial Ischemia. *Computational and Mathematical Methods in Medicine*, 2016, 1–9.
<https://doi.org/10.1155/2016/4310634>
- Liu, J., Zhao, X., Gong, Y., Zhang, J., Zang, Y., & Xia, L. (2019). Exploring Impaired SERCA Pump-Caused Alternation Occurrence in Ischemia. *Computational and Mathematical Methods in Medicine*, 2019, 1–10.
<https://doi.org/10.1155/2019/8237071>
- Lowey, S., Bretton, V., Joel, P. B., Trybus, K. M., Gulick, J., Robbins, J., Kalganov, A., Cornachione, A. S., & Rassier, D. E. (2018). Hypertrophic cardiomyopathy R403Q mutation in rabbit β -myosin reduces contractile function at the molecular and myofibrillar levels. *Proceedings of the National Academy of Sciences*, 115(44), 11238–11243.
<https://doi.org/10.1073/pnas.1802967115>
- Ma, J., Guo, L., Fiene, S. J., Anson, B. D., Thomson, J. A., Kamp, T. J., Kolaja, K. L., Swanson, B. J., & January, C. T. (2011). High purity human-induced pluripotent stem cell-derived cardiomyocytes: Electrophysiological properties of action potentials and ionic currents. *American Journal of Physiology-Heart and Circulatory Physiology*, 301(5), H2006–H2017.
<https://doi.org/10.1152/ajpheart.00694.2011>
- Mahmoodzadeh, S., & Dworatzek, E. (2019). The Role of 17β -Estradiol and Estrogen Receptors in Regulation of Ca^{2+} Channels and Mitochondrial Function in Cardiomyocytes. *Frontiers in Endocrinology*, 10.
<https://www.frontiersin.org/articles/10.3389/fendo.2019.00310>
- Makinose, M. (1973). Possible functional states of the enzyme of the sarcoplasmic calcium pump. *FEBS Letters*, 37(2), 140–143.
[https://doi.org/10.1016/0014-5793\(73\)80443-0](https://doi.org/10.1016/0014-5793(73)80443-0)
- Maltsev, V. A., & Lakatta, E. G. (2009). Synergism of coupled subsarcolemmal Ca^{2+} clocks and sarcolemmal voltage clocks confers robust and flexible pacemaker function in a novel pacemaker cell model. *American Journal of Physiology. Heart and Circulatory Physiology*, 296(3), H594–615.
<https://doi.org/10.1152/ajpheart.01118.2008>

- Mannhardt, I., Breckwoldt, K., Letuffe-Brenière, D., Schaaf, S., Schulz, H., Neuber, C., Benzin, A., Werner, T., Eder, A., Schulze, T., Klampe, B., Christ, T., Hirt, M. N., Huebner, N., Moretti, A., Eschenhagen, T., & Hansen, A. (2016). Human Engineered Heart Tissue: Analysis of Contractile Force. *Stem Cell Reports*, 7(1), 29–42. <https://doi.org/10.1016/j.stemcr.2016.04.011>
- Manning, A. S., & Hearse, D. J. (1984). Reperfusion-induced arrhythmias: Mechanisms and prevention. *Journal of Molecular and Cellular Cardiology*, 16(6), 497–518. [https://doi.org/10.1016/S0022-2828\(84\)80638-0](https://doi.org/10.1016/S0022-2828(84)80638-0)
- Margara, F., Psaras, Y., Wang, Z. J., Schmid, M., Doste, R., Garfinkel, A. C., Repetti, G. G., Seidman, J. G., Seidman, C. E., Rodriguez, B., Toepfer, C. N., & Bueno-Orovio, A. (2022). Mechanism based therapies enable personalised treatment of hypertrophic cardiomyopathy. *Scientific Reports*, 12(1), 22501. <https://doi.org/10.1038/s41598-022-26889-2>
- Margara, F., Rodriguez, B., Toepfer, C. N., & Bueno-Orovio, A. (2021). Mavacamten Efficacy in Mutation-specific Hypertrophic Cardiomyopathy: An In Silico Approach to Inform Precision Medicine. *2021 Computing in Cardiology (CinC)*, 48, 1–4. <https://doi.org/10.23919/CinC53138.2021.9662736>
- Margara, F., Wang, Z. J., Bueno-Orovio, A., & Rodriguez, B. (2020). Human Ventricular Modelling and Simulation of Drug Action on Electrophysiology and Contraction. *2020 Computing in Cardiology*, 1–4. <https://doi.org/10.22489/CinC.2020.386>
- Margara, F., Wang, Z. J., Levrero-Florencio, F., Santiago, A., Vázquez, M., Bueno-Orovio, A., & Rodriguez, B. (2021). In-silico human electro-mechanical ventricular modelling and simulation for drug-induced pro-arrhythmia and inotropic risk assessment. *Progress in Biophysics and Molecular Biology*, 159, 58–74. <https://doi.org/10.1016/j.pbiomolbio.2020.06.007>
- María Sofía Martínez, Andrés García, Eliana Luzardo, Mervin Chávez-Castillo, Luis Carlos Olivar, Juan Salazar, Manuel Velasco, Joselyn Joanna Rojas Quintero, & Valmore Bermúdez. (2017). Energetic metabolism in cardiomyocytes: Molecular basis of heart ischemia and arrhythmogenesis. *Energetic Metabolism in Cardiomyocytes: Molecular Basis of Heart Ischemia and Arrhythmogenesis*, 1, 130–141. <https://doi.org/10.20517/2574-1209.2017.34>
- Maron, B. J., Gardin, J. M., Flack, J. M., Gidding, S. S., Kurosaki, T. T., & Bild, D. E. (1995). Prevalence of Hypertrophic Cardiomyopathy in a General Population of Young Adults. *Circulation*, 92(4), 785–789. <https://doi.org/10.1161/01.CIR.92.4.785>

- Maron, B. J., Maron, M. S., & Semsarian, C. (2012). Genetics of Hypertrophic Cardiomyopathy After 20 Years: Clinical Perspectives. *Journal of the American College of Cardiology*, *60*(8), 705–715. <https://doi.org/10.1016/j.jacc.2012.02.068>
- Maron, B. J., Spirito, P., Roman, M. J., Paranicas, M., Okin, P. M., Best, L. G., Lee, E. T., & Devereux, R. B. (2004). Prevalence of hypertrophic cardiomyopathy in a Population-Based sample of American Indians aged 51 to 77 years (the Strong Heart Study)**The opinions expressed in this report are those of the authors and do not necessarily reflect the views of the Indian Health Service. *The American Journal of Cardiology*, *93*(12), 1510–1514. <https://doi.org/10.1016/j.amjcard.2004.03.007>
- McDougal, A. D., & Dewey, C. F. (2017). Modeling oxygen requirements in ischemic cardiomyocytes. *Journal of Biological Chemistry*, *292*(28), 11760–11776. <https://doi.org/10.1074/jbc.M116.751826>
- McNamara, J. W., Li, A., Lal, S., Bos, J. M., Harris, S. P., van der Velden, J., Ackerman, M. J., Cooke, R., & Dos Remedios, C. G. (2017). MYBPC3 mutations are associated with a reduced super-relaxed state in patients with hypertrophic cardiomyopathy. *PloS One*, *12*(6), e0180064. <https://doi.org/10.1371/journal.pone.0180064>
- McNamara, J. W., Li, A., Smith, N. J., Lal, S., Graham, R. M., Kooiker, K. B., van Dijk, S. J., Remedios, C. G. D., Harris, S. P., & Cooke, R. (2016). Ablation of cardiac myosin binding protein-C disrupts the super-relaxed state of myosin in murine cardiomyocytes. *Journal of Molecular and Cellular Cardiology*, *94*, 65–71. <https://doi.org/10.1016/j.yjmcc.2016.03.009>
- Meis, L., & Vianna, A. L. (1979). Energy Interconversion by the Ca²⁺-Dependent ATPase of the Sarcoplasmic Reticulum. *Annual Review of Biochemistry*, *48*(1), 275–292. <https://doi.org/10.1146/annurev.bi.48.070179.001423>
- Michailova, A., Saucerman, J., Ellen Belik, M., & McCulloch, A. D. (2005). Modeling Regulation of Cardiac KATP and L-type Ca²⁺ Currents by ATP, ADP, and Mg²⁺. *Biophysical Journal*, *88*(3), 2234–2249. <https://doi.org/10.1529/biophysj.104.046284>
- Moore, J. R., Leinwand, L., Warshaw, D. M., Robbins, J., Seidman, C., & Watkins, H. (2012). Understanding Cardiomyopathy Phenotypes Based on the Functional Impact of Mutations in the Myosin Motor. *Circulation Research*, *111*(3), 375–385. <https://doi.org/10.1161/CIRCRESAHA.110.223842>

- Mosqueira, D., Mannhardt, I., Bhagwan, J. R., Lis-Slimak, K., Katili, P., Scott, E., Hassan, M., Prondzynski, M., Harmer, S. C., Tinker, A., Smith, J. G. W., Carrier, L., Williams, P. M., Gaffney, D., Eschenhagen, T., Hansen, A., & Denning, C. (2018). CRISPR/Cas9 editing in human pluripotent stem cell-cardiomyocytes highlights arrhythmias, hypocontractility, and energy depletion as potential therapeutic targets for hypertrophic cardiomyopathy. *European Heart Journal*, *39*(43), 3879–3892. <https://doi.org/10.1093/eurheartj/ehy249>
- Murata, M., Tohyama, S., & Fukuda, K. (2010). Impacts of recent advances in cardiovascular regenerative medicine on clinical therapies and drug discovery. *Pharmacology & Therapeutics*, *126*(2), 109–118. <https://doi.org/10.1016/j.pharmthera.2010.01.010>
- Musuamba, F. T., Skottheim Rusten, I., Lesage, R., Russo, G., Bursi, R., Emili, L., Wangorsch, G., Manolis, E., Karlsson, K. E., Kulesza, A., Courcelles, E., Boissel, J., Rousseau, C. F., Voisin, E. M., Alessandrello, R., Curado, N., Dall'ara, E., Rodriguez, B., Pappalardo, F., & Geris, L. (2021). Scientific and regulatory evaluation of mechanistic in silico drug and disease models in drug development: Building model credibility. *CPT: Pharmacometrics & Systems Pharmacology*, *10*(8), 804–825. <https://doi.org/10.1002/psp4.12669>
- Nag, S., Sommesse, R. F., Ujfalusi, Z., Combs, A., Langer, S., Sutton, S., Leinwand, L. A., Geeves, M. A., Ruppel, K. M., & Spudich, J. A. (2015a). Contractility parameters of human β -cardiac myosin with the hypertrophic cardiomyopathy mutation R403Q show loss of motor function. *Science Advances*, *1*(9). <https://doi.org/10.1126/sciadv.1500511>
- Nag, S., Sommesse, R. F., Ujfalusi, Z., Combs, A., Langer, S., Sutton, S., Leinwand, L. A., Geeves, M. A., Ruppel, K. M., & Spudich, J. A. (2015b). Contractility parameters of human β -cardiac myosin with the hypertrophic cardiomyopathy mutation R403Q show loss of motor function. *Science Advances*, *1*(9). <https://doi.org/10.1126/sciadv.1500511>
- Nag, S., & Trivedi, D. V. (2021). To lie or not to lie: Super-relaxing with myosins. *eLife*, *10*. <https://doi.org/10.7554/eLife.63703>
- Nag, S., Trivedi, D. V., Sarkar, S. S., Adhikari, A. S., Sunitha, M. S., Sutton, S., Ruppel, K. M., & Spudich, J. A. (2017). The myosin mesa and the basis of hypercontractility caused by hypertrophic cardiomyopathy mutations. *Nature Structural & Molecular Biology*, *24*(6), 525–533. <https://doi.org/10.1038/nsmb.3408>

- Negroni, J. A., Morotti, S., Lascano, E. C., Gomes, A. V., Grandi, E., Puglisi, J. L., & Bers, D. M. (2015). β -adrenergic effects on cardiac myofilaments and contraction in an integrated rabbit ventricular myocyte model. *Journal of Molecular and Cellular Cardiology*.
<https://doi.org/10.1016/j.yjmcc.2015.02.014>
- Nerbonne, J. M., & Kass, R. S. (2005). Molecular Physiology of Cardiac Repolarization. *Physiological Reviews*, 85(4), 1205–1253.
<https://doi.org/10.1152/physrev.00002.2005>
- Ng, T. M. H. (2004). Levosimendan, a New Calcium-Sensitizing Inotrope for Heart Failure. *Pharmacotherapy*, 24(10), 1366–1384.
<https://doi.org/10.1592/phco.24.14.1366.43145>
- Nguyen, N., Nguyen, W., Nguyenton, B., Ratchada, P., Page, G., Miller, P. E., Ghetti, A., & Abi-Gerges, N. (2017). Adult Human Primary Cardiomyocyte-Based Model for the Simultaneous Prediction of Drug-Induced Inotropic and Proarrhythmia Risk. *Frontiers in Physiology*, 8, 1073.
<https://doi.org/10.3389/fphys.2017.01073>
- Niederer, S. A., Lumens, J., & Trayanova, N. A. (2019). Computational models in cardiology. *Nature Reviews Cardiology*, 16(2), 100–111.
<https://doi.org/10.1038/s41569-018-0104-y>
- Nowbar, A. N., Gitto, M., Howard, J. P., Francis, D. P., & Al-Lamee, R. (2019). Mortality From Ischemic Heart Disease. *Circulation: Cardiovascular Quality and Outcomes*, 12(6). <https://doi.org/10.1161/CIRCOUTCOMES.118.005375>
- Offstad, J., Kirkeboen, K. A., Ilebekk, A., & Downing, S. E. (1994). ATP gated potassium channels in acute myocardial hibernation and reperfusion. *Cardiovascular Research*, 28(6), 872–880.
<https://doi.org/10.1093/cvr/28.6.872>
- O'Hara, T., Virág, L., Varró, A., & Rudy, Y. (2011). Simulation of the Undiseased Human Cardiac Ventricular Action Potential: Model Formulation and Experimental Validation. *PLoS Computational Biology*, 7(5), e1002061.
<https://doi.org/10.1371/journal.pcbi.1002061>
- Olivotto, I., Cecchi, F., & Yacoub, M. H. (2009). Myocardial bridging and sudden death in hypertrophic cardiomyopathy: Salome drops another veil. *European Heart Journal*, 30(13), 1549–1550.
<https://doi.org/10.1093/eurheartj/ehp216>

- Ommen, S. R., Mital, S., Burke, M. A., Day, S. M., Deswal, A., Elliott, P., Evanovich, L. L., Hung, J., Joglar, J. A., Kantor, P., Kimmelstiel, C., Kittleson, M., Link, M. S., Maron, M. S., Martinez, M. W., Miyake, C. Y., Schaff, H. V., Semsarian, C., & Sorajja, P. (2020). 2020 AHA/ACC Guideline for the Diagnosis and Treatment of Patients With Hypertrophic Cardiomyopathy: A Report of the American College of Cardiology/American Heart Association Joint Committee on Clinical Practice Guidelines. *Journal of the American College of Cardiology*, 76(25), e159–e240. <https://doi.org/10.1016/j.jacc.2020.08.045>
- Paci, M., Hyttinen, J., Aalto-Setälä, K., & Severi, S. (2013). Computational models of ventricular-and atrial-like human induced pluripotent stem cell derived cardiomyocytes. *Annals of Biomedical Engineering*. <https://doi.org/10.1007/s10439-013-0833-3>
- Paci, M., Hyttinen, J., Rodriguez, B., & Severi, S. (2015). Human induced pluripotent stem cell-derived versus adult cardiomyocytes: An in silico electrophysiological study on effects of ionic current block. *British Journal of Pharmacology*. <https://doi.org/10.1111/bph.13282>
- Paci, M., Koivumäki, J. T., Lu, H. R., Gallacher, D. J., Passini, E., & Rodriguez, B. (2021). Comparison of the Simulated Response of Three in Silico Human Stem Cell-Derived Cardiomyocytes Models and in Vitro Data Under 15 Drug Actions. *Frontiers in Pharmacology*, 12. <https://doi.org/10.3389/fphar.2021.604713>
- Paci, M., Passini, E., Klimas, A., Severi, S., Hyttinen, J., Rodriguez, B., & Entcheva, E. (2020). All-Optical Electrophysiology Refines Populations of In Silico Human iPSC-CMs for Drug Evaluation. *Biophysical Journal*. <https://doi.org/10.1016/j.bpj.2020.03.018>
- Paci, M., Pölönen, R. P., Cori, D., Penttinen, K., Aalto-Setälä, K., Severi, S., & Hyttinen, J. (2018). Automatic optimization of an in silico model of human iPSC derived cardiomyocytes recapitulating calcium handling abnormalities. *Frontiers in Physiology*. <https://doi.org/10.3389/fphys.2018.00709>
- Paci, M., Koivumäki, J., Lu, H. R., Gallacher, D. J., Passini, E., & Rodriguez, B. (2021). Comparison of the simulated response of three in silico human stem cell-derived cardiomyocytes models and in vitro data under 15 drug actions. *Frontiers in Pharmacology*.
- Parissis, J. T., Andreadou, I., Markantonis, S. L., Bistola, V., Louka, A., Pyriochou, A., Paraskevaidis, I., Filippatos, G., Iliodromitis, E. K., & Kremastinos, D.

- Th. (2007). Effects of Levosimendan on circulating markers of oxidative and nitrosative stress in patients with advanced heart failure. *Atherosclerosis*, *195*(2), e210–e215. <https://doi.org/10.1016/j.atherosclerosis.2007.07.011>
- Passini, E., Trovato, C., Morissette, P., Sannajust, F., Bueno-Orovio, A., & Rodriguez, B. (2019). Drug-induced shortening of the electromechanical window is an effective biomarker for in silico prediction of clinical risk of arrhythmias. *British Journal of Pharmacology*, *176*(19), 3819–3833. <https://doi.org/10.1111/bph.14786>
- Pathak, A., Lebrin, M., Vaccaro, A., Senard, J. M., & Despas, F. (2013). Pharmacology of levosimendan: Inotropic, vasodilatory and cardioprotective effects. *Journal of Clinical Pharmacy and Therapeutics*, *38*(5), 341–349. <https://doi.org/10.1111/jcpt.12067>
- PENNY, W. J., & SHERIDAN, D. J. (1983). Arrhythmias and cellular electrophysiological changes during myocardial “ischaemia” and reperfusion. *Cardiovascular Research*, *17*(6), 363–372. <https://doi.org/10.1093/cvr/17.6.363>
- Petrushanko, I. Yu., Bogdanov, N. B., Lapina, N., Boldyrev, A. A., Gassmann, M., & Bogdanova, A. Yu. (2007). Oxygen-induced Regulation of Na/K ATPase in Cerebellar Granule Cells. *Journal of General Physiology*, *130*(4), 389–398. <https://doi.org/10.1085/jgp.200709783>
- Pioner, J. M., Guan, X., Klaiman, J. M., Racca, A. W., Pabon, L., Muskheli, V., Macadangdang, J., Ferrantini, C., Hoopmann, M. R., Moritz, R. L., Kim, D. H., Tesi, C., Poggesi, C., Murry, C. E., Childers, M. K., Mack, D. L., & Regnier, M. (2020). Absence of full-length dystrophin impairs normal maturation and contraction of cardiomyocytes derived from human-induced pluripotent stem cells. *Cardiovascular Research*. <https://doi.org/10.1093/cvr/cvz109>
- Rice, J. J., Wang, F., Bers, D. M., & De Tombe, P. P. (2008). Approximate model of cooperative activation and crossbridge cycling in cardiac muscle using ordinary differential equations. *Biophysical Journal*. <https://doi.org/10.1529/biophysj.107.119487>
- Richard Conti, C. (1991). The stunned and hibernating myocardium: A brief review. *Clinical Cardiology*, *14*(9), 708–712. <https://doi.org/10.1002/clc.4960140903>

- RODRIGUEZ, B., TRAYANOVA, N., & NOBLE, D. (2006). Modeling Cardiac Ischemia. *Annals of the New York Academy of Sciences*, 1080(1), 395–414. <https://doi.org/10.1196/annals.1380.029>
- Rodriguez, M. L., Graham, B. T., Pabon, L. M., Han, S. J., Murry, C. E., & Sniadecki, N. J. (2014). Measuring the Contractile Forces of Human Induced Pluripotent Stem Cell-Derived Cardiomyocytes With Arrays of Microposts. *Journal of Biomechanical Engineering*, 136(5). <https://doi.org/10.1115/1.4027145>
- Rogers, A. J., Selvalingam, A., Alhousseini, M. I., Krummen, D. E., Corrado, C., Abuzaid, F., Baykaner, T., Meyer, C., Clopton, P., Giles, W., Bailis, P., Niederer, S., Wang, P. J., Rappel, W.-J., Zaharia, M., & Narayan, S. M. (2021). Machine Learned Cellular Phenotypes in Cardiomyopathy Predict Sudden Death. *Circulation Research*, 128(2), 172–184. <https://doi.org/10.1161/CIRCRESAHA.120.317345>
- Rohde, J. A., Roopnarine, O., Thomas, D. D., & Muretta, J. M. (2018). Mavacamten stabilizes an autoinhibited state of two-headed cardiac myosin. *Proceedings of the National Academy of Sciences*, 115(32), E7486–E7494. <https://doi.org/10.1073/pnas.1720342115>
- Rolfe, D. F., & Brown, G. C. (1997). Cellular energy utilization and molecular origin of standard metabolic rate in mammals. *Physiological Reviews*, 77(3), 731–758. <https://doi.org/10.1152/physrev.1997.77.3.731>
- Romero, L., Carbonell, B., Trenor, B., Rodríguez, B., Saiz, J., & Ferrero, J. M. (2011). Systematic characterization of the ionic basis of rabbit cellular electrophysiology using two ventricular models. *Progress in Biophysics and Molecular Biology*, 107(1), 60–73. <https://doi.org/10.1016/j.pbiomolbio.2011.06.012>
- Rosano, G. M. C., Fini, M., Caminiti, G., & Barbaro, G. (n.d.). Cardiac Metabolism in Myocardial Ischemia. *Current Pharmaceutical Design*, 14(25), 2551–2562.
- Ruan, J. L., Tulloch, N. L., Razumova, M. V., Saiget, M., Muskheli, V., Pabon, L., Reinecke, H., Regnier, M., & Murry, C. E. (2016). Mechanical Stress Conditioning and Electrical Stimulation Promote Contractility and Force Maturation of Induced Pluripotent Stem Cell-Derived Human Cardiac Tissue. *Circulation*. <https://doi.org/10.1161/CIRCULATIONAHA.114.014998>

- Sager, P. T., Gintant, G., Turner, J. R., Pettit, S., & Stockbridge, N. (2014). Rechanneling the cardiac proarrhythmia safety paradigm: A meeting report from the Cardiac Safety Research Consortium. *American Heart Journal*, *167*(3), 292–300. <https://doi.org/10.1016/j.ahj.2013.11.004>
- Sanada, S., Komuro, I., & Kitakaze, M. (2011). Pathophysiology of myocardial reperfusion injury: Preconditioning, postconditioning, and translational aspects of protective measures. *American Journal of Physiology-Heart and Circulatory Physiology*, *301*(5), H1723–H1741. <https://doi.org/10.1152/ajpheart.00553.2011>
- Sarantitis, I., Papanastasopoulos, P., Manousi, M., Baikoussis, N. G., & Apostolakis, E. (2012). The cytoskeleton of the cardiac muscle cell. *Hellenic Journal of Cardiology: HJC = Hellenike Kardiologike Epitheorese*, *53*(5), 367–379.
- Sarkar, S. S., Trivedi, D. V., Morck, M. M., Adhikari, A. S., Pasha, S. N., Ruppel, K. M., & Spudich, J. A. (2020). The hypertrophic cardiomyopathy mutations R403Q and R663H increase the number of myosin heads available to interact with actin. *Science Advances*, *6*(14). <https://doi.org/10.1126/sciadv.aax0069>
- Sartiani, L., Bettioli, E., Stillitano, F., Mugelli, A., Cerbai, E., & Jaconi, M. E. (2007). Developmental changes in cardiomyocytes differentiated from human embryonic stem cells: A molecular and electrophysiological approach. *Stem Cells (Dayton, Ohio)*, *25*(5), 1136–1144. <https://doi.org/10.1634/stemcells.2006-0466>
- Schmid, M., & Toepfer, C. N. (2021). Cardiac myosin super relaxation (SRX): A perspective on fundamental biology, human disease and therapeutics. *Biology Open*, *10*(2). <https://doi.org/10.1242/bio.057646>
- Schotten, U., Voss, S., Wiederin, T. B., Voss, M., Schoendube, F., Hanrath, P., & Schumacher, C. (1999). Altered force-frequency relation in hypertrophic obstructive cardiomyopathy. *Basic Research in Cardiology*, *94*(2), 120–127. <https://doi.org/10.1007/s003950050134>
- Sepp, M., Sokolova, N., Jugai, S., Mandel, M., Peterson, P., & Vendelin, M. (2014). Tight Coupling of Na⁺/K⁺-ATPase with Glycolysis Demonstrated in Permeabilized Rat Cardiomyocytes. *PLoS ONE*, *9*(6), e99413. <https://doi.org/10.1371/journal.pone.0099413>

- Sequeira, V., Bertero, E., & Maack, C. (2019). Energetic drain driving hypertrophic cardiomyopathy. *FEBS Letters*, *593*(13), 1616–1626. <https://doi.org/10.1002/1873-3468.13496>
- Sewanian, L. R., Schwan, J., Kluger, J., Park, J., Jacoby, D. L., Qyang, Y., & Campbell, S. G. (2019). Extracellular Matrix From Hypertrophic Myocardium Provokes Impaired Twitch Dynamics in Healthy Cardiomyocytes. *JACC: Basic to Translational Science*, *4*(4), 495–505. <https://doi.org/10.1016/j.jacbts.2019.03.004>
- Shannon, T. R., Wang, F., Puglisi, J., Weber, C., & Bers, D. M. (2004). A mathematical treatment of integrated Ca dynamics within the ventricular myocyte. *Biophysical Journal*, *87*(5), 3351–3371. <https://doi.org/10.1529/biophysj.104.047449>
- Shattock, M. J., Ottolia, M., Bers, D. M., Blaustein, M. P., Boguslavskyi, A., Bossuyt, J., Bridge, J. H. B., Chen-Izu, Y., Clancy, C. E., Edwards, A., Goldhaber, J., Kaplan, J., Lingrel, J. B., Pavlovic, D., Philipson, K., Sipido, K. R., & Xie, Z.-J. (2015). Na⁺/Ca²⁺ exchange and Na⁺/K⁺-ATPase in the heart. *The Journal of Physiology*, *593*(6), 1361–1382. <https://doi.org/10.1113/jphysiol.2014.282319>
- Sheikh, F., Ouyang, K., Campbell, S. G., Lyon, R. C., Chuang, J., Fitzsimons, D., Tangney, J., Hidalgo, C. G., Chung, C. S., Cheng, H., Dalton, N. D., Gu, Y., Kasahara, H., Ghassemian, M., Omens, J. H., Peterson, K. L., Granzier, H. L., Moss, R. L., McCulloch, A. D., & Chen, J. (2012). Mouse and computational models link Mlc2v dephosphorylation to altered myosin kinetics in early cardiac disease. *Journal of Clinical Investigation*. <https://doi.org/10.1172/JCI61134>
- Sicouri, S., Timothy, K. W., Zygmunt, A. C., Glass, A., Goodrow, R. J., Belardinelli, L., & Antzelevitch, C. (2007). Cellular basis for the electrocardiographic and arrhythmic manifestations of Timothy syndrome: Effects of ranolazine. *Heart Rhythm*, *4*(5), 638–647. <https://doi.org/10.1016/j.hrthm.2006.12.046>
- Skibsbye, L., Jespersen, T., Christ, T., Maleckar, M. M., Brink, J. van den, Tavi, P., & Koivumäki, J. T. (2016). Refractoriness in human atria: Time and voltage dependence of sodium channel availability. *Journal of Molecular and Cellular Cardiology*, *101*, 26–34. <https://doi.org/10.1016/j.yjmcc.2016.10.009>
- Smith, A. S. T., Macadangdang, J., Leung, W., Laflamme, M. A., & Kim, D.-H. (2017). Human iPSC-derived cardiomyocytes and tissue engineering

- strategies for disease modeling and drug screening. *Biotechnology Advances*, 35(1), 77–94. <https://doi.org/10.1016/j.biotechadv.2016.12.002>
- Smith, G. L., & Eisner, D. A. (2019). Calcium Buffering in the Heart in Health and Disease. *Circulation*, 139(20), 2358–2371. <https://doi.org/10.1161/CIRCULATIONAHA.118.039329>
- Sneyd, J., & Dufour, J.-F. (2002). A dynamic model of the type-2 inositol trisphosphate receptor. *Proceedings of the National Academy of Sciences of the United States of America*, 99(4), 2398–2403. <https://doi.org/10.1073/pnas.032281999>
- Sommese, R. F., Sung, J., Nag, S., Sutton, S., Deacon, J. C., Choe, E., Leinwand, L. A., Ruppel, K., & Spudich, J. A. (2013). Molecular consequences of the R453C hypertrophic cardiomyopathy mutation on human β -cardiac myosin motor function. *Proceedings of the National Academy of Sciences*, 110(31), 12607–12612. <https://doi.org/10.1073/pnas.1309493110>
- Spindler, M., Saupe, K. W., Christe, M. E., Sweeney, H. L., Seidman, C. E., Seidman, J. G., & Ingwall, J. S. (1998). Diastolic dysfunction and altered energetics in the alphaMHC403/+ mouse model of familial hypertrophic cardiomyopathy. *Journal of Clinical Investigation*, 101(8), 1775–1783. <https://doi.org/10.1172/JCI1940>
- Spudich, J. A. (2014). Hypertrophic and Dilated Cardiomyopathy: Four Decades of Basic Research on Muscle Lead to Potential Therapeutic Approaches to These Devastating Genetic Diseases. *Biophysical Journal*, 106(6), 1236–1249. <https://doi.org/10.1016/j.bpj.2014.02.011>
- Spudich, J. A. (2019). Three perspectives on the molecular basis of hypercontractility caused by hypertrophic cardiomyopathy mutations. *Pflügers Archiv - European Journal of Physiology*, 471(5), 701–717. <https://doi.org/10.1007/s00424-019-02259-2>
- Strauss, D. G., Gintant, G., Li, Z., Wu, W., Blinova, K., Vicente, J., Turner, J. R., & Sager, P. T. (2019). Comprehensive In Vitro Proarrhythmia Assay (CiPA) Update from a Cardiac Safety Research Consortium / Health and Environmental Sciences Institute / FDA Meeting. *Therapeutic Innovation and Regulatory Science*. <https://doi.org/10.1177/2168479018795117>
- Sutton, P. M. I. (2000). Repolarisation and refractoriness during early ischaemia in humans. *Heart*, 84(4), 365–369. <https://doi.org/10.1136/heart.84.4.365>

- Szentandrassy, N., Horvath, B., Vaczi, K., Kistamas, K., Masuda, L., Magyar, J., Banyasz, T., Papp, Z., & Nanasi, P. P. (2016). Dose-dependent electrophysiological effects of the myosin activator omecamtiv mecarbil in canine ventricular cardiomyocytes. *Journal of Physiology and Pharmacology: An Official Journal of the Polish Physiological Society*, 67(4), 483–489.
- Takahashi, K., Tanabe, K., Ohnuki, M., Narita, M., Ichisaka, T., Tomoda, K., & Yamanaka, S. (2007). Induction of Pluripotent Stem Cells from Adult Human Fibroblasts by Defined Factors. *Cell*, 131(5), 861–872. <https://doi.org/10.1016/j.cell.2007.11.019>
- Takahashi, K., & Yamanaka, S. (2006). Induction of Pluripotent Stem Cells from Mouse Embryonic and Adult Fibroblast Cultures by Defined Factors. *Cell*. <https://doi.org/10.1016/j.cell.2006.07.024>
- Tanaka, A., Yuasa, S., Node, K., & Fukuda, K. (2015). Cardiovascular Disease Modeling Using Patient-Specific Induced Pluripotent Stem Cells. *International Journal of Molecular Sciences*, 16(8), Article 8. <https://doi.org/10.3390/ijms160818894>
- Tardiff, J. C., Carrier, L., Bers, D. M., Poggesi, C., Ferrantini, C., Coppini, R., Maier, L. S., Ashrafian, H., Huke, S., & van der Velden, J. (2015). Targets for therapy in sarcomeric cardiomyopathies. *Cardiovascular Research*, 105(4), 457–470. <https://doi.org/10.1093/cvr/cvv023>
- ten Tusscher, K. H. W. J., Noble, D., Noble, P. J., & Panfilov, A. V. (2004). A model for human ventricular tissue. *American Journal of Physiology-Heart and Circulatory Physiology*, 286(4), H1573–H1589. <https://doi.org/10.1152/ajpheart.00794.2003>
- ten Tusscher, K. H. W. J., & Panfilov, A. V. (2006). Alternans and spiral breakup in a human ventricular tissue model. *American Journal of Physiology. Heart and Circulatory Physiology*, 291(3), H1088-1100. <https://doi.org/10.1152/ajpheart.00109.2006>
- Ten Tusscher, K. H. W. J., & Panfilov, A. V. (2006). Alternans and spiral breakup in a human ventricular tissue model. *American Journal of Physiology - Heart and Circulatory Physiology*. <https://doi.org/10.1152/ajpheart.00109.2006>
- Toepfer, C. N., Garfinkel, A. C., Venturini, G., Wakimoto, H., Repetti, G., Alamo, L., Sharma, A., Agarwal, R., Ewoldt, J. F., Cloonan, P., Letendre, J., Lun, M., Olivotto, I., Colan, S., Ashley, E., Jacoby, D., Michels, M., Redwood, C. S.,

- Watkins, H. C., ... Seidman, C. E. (2020). Myosin Sequestration Regulates Sarcomere Function, Cardiomyocyte Energetics, and Metabolism, Informing the Pathogenesis of Hypertrophic Cardiomyopathy. *Circulation*, *141*(10). <https://doi.org/10.1161/CIRCULATIONAHA.119.042339>
- Toepfer, C. N., Wakimoto, H., Garfinkel, A. C., McDonough, B., Liao, D., Jiang, J., Tai, A. C., Gorham, J. M., Lunde, I. G., Lun, M., Lynch, T. L., McNamara, J. W., Sadayappan, S., Redwood, C. S., Watkins, H. C., Seidman, J. G., & Seidman, C. E. (2019). Hypertrophic cardiomyopathy mutations in MYBPC3 dysregulate myosin. *Science Translational Medicine*, *11*(476). <https://doi.org/10.1126/scitranslmed.aat1199>
- Tomek, J., Bueno-Orovio, A., Passini, E., Zhou, X., Mincholé, A., Britton, O., Bartolucci, C., Severi, S., Shrier, A., Virag, L., Varro, A., & Rodriguez, B. (2019). Development, calibration, and validation of a novel human ventricular myocyte model in health, disease, and drug block. *eLife*, *8*. <https://doi.org/10.7554/eLife.48890>
- Tran, K., Han, J.-C., Crampin, E. J., Taberner, A. J., & Loiselle, D. S. (2017). Experimental and modelling evidence of shortening heat in cardiac muscle. *The Journal of Physiology*, *595*(19), 6313–6326. <https://doi.org/10.1113/JP274680>
- Tran, K., Smith, N. P., Loiselle, D. S., & Crampin, E. J. (2009). A Thermodynamic Model of the Cardiac Sarcoplasmic/Endoplasmic Ca²⁺ (SERCA) Pump. *Biophysical Journal*, *96*(5), 2029–2042. <https://doi.org/10.1016/j.bpj.2008.11.045>
- Tran, K., Smith, N. P., Loiselle, D. S., & Crampin, E. J. (2010). A Metabolite-Sensitive, Thermodynamically Constrained Model of Cardiac Cross-Bridge Cycling: Implications for Force Development during Ischemia. *Biophysical Journal*, *98*(2). <https://doi.org/10.1016/j.bpj.2009.10.011>
- Trayanova, N. A., & Rice, J. J. (2011). Cardiac Electromechanical Models: From Cell to Organ. *Frontiers in Physiology*, *2*. <https://doi.org/10.3389/fphys.2011.00043>
- Trivedi, D. V., Adhikari, A. S., Sarkar, S. S., Ruppel, K. M., & Spudich, J. A. (2018). Hypertrophic cardiomyopathy and the myosin mesa: Viewing an old disease in a new light. *Biophysical Reviews*, *10*(1), 27–48. <https://doi.org/10.1007/s12551-017-0274-6>

- Turer, A. T., & Hill, J. A. (2010). Pathogenesis of Myocardial Ischemia-Reperfusion Injury and Rationale for Therapy. *American Journal of Cardiology*, *106*(3), 360–368. <https://doi.org/10.1016/j.amjcard.2010.03.032>
- Uchida, K., Matsuyama, K., Tanaka, K., & Doi, K. (1992). Diffusion coefficient for O₂ in plasma and mitochondrial membranes of rat cardiomyocytes. *Respiration Physiology*, *90*(3), 351–362. [https://doi.org/10.1016/0034-5687\(92\)90114-C](https://doi.org/10.1016/0034-5687(92)90114-C)
- Ulmer, B. M., & Eschenhagen, T. (2020). Human pluripotent stem cell-derived cardiomyocytes for studying energy metabolism. *Biochimica et Biophysica Acta (BBA) - Molecular Cell Research*, *1867*(3), 118471. <https://doi.org/10.1016/j.bbamcr.2019.04.001>
- Utter, M. S., Ryba, D. M., Li, B. H., Wolska, B. M., & Solaro, R. J. (2015). Omecamtiv Mecarbil, a Cardiac Myosin Activator, Increases Ca²⁺ Sensitivity in Myofilaments With a Dilated Cardiomyopathy Mutant Tropomyosin E54K. *Journal of Cardiovascular Pharmacology*, *66*(4).
- van der Sanden, B., Dhobb, M., Berger, F., & Wion, D. (2010). Optimizing stem cell culture. *Journal of Cellular Biochemistry*, *111*(4), 801–807. <https://doi.org/10.1002/jcb.22847>
- van der Velden, J., Tocchetti, C. G., Varricchi, G., Bianco, A., Sequeira, V., Hilfiker-Kleiner, D., Hamdani, N., Leite-Moreira, A. F., Mayr, M., Falcão-Pires, I., Thum, T., Dawson, D. K., Balligand, J.-L., & Heymans, S. (2018). Metabolic changes in hypertrophic cardiomyopathies: Scientific update from the Working Group of Myocardial Function of the European Society of Cardiology. *Cardiovascular Research*, *114*(10), 1273–1280. <https://doi.org/10.1093/cvr/cvy147>
- Veerman, C. C., Kosmidis, G., Mummery, C. L., Casini, S., Verkerk, A. O., & Bellin, M. (2015). Immaturity of Human Stem-Cell-Derived Cardiomyocytes in Culture: Fatal Flaw or Soluble Problem? *Stem Cells and Development*, *24*(9), 1035–1052. <https://doi.org/10.1089/scd.2014.0533>
- Wan Ab Naim, W. N., Mohamed Mokhtarudin, M. J., Bakir, A. A., Alia Nasuha Mohd Nor, P. N., & Nik Mohamed, N. A. (2021). Study of Oxygen Deprivation on Cardiomyocyte using Electro-chemical Coupled Mathematical Model. *2020 IEEE-EMBS Conference on Biomedical Engineering and Sciences (IECBES)*, 142–146. <https://doi.org/10.1109/IECBES48179.2021.9398825>

- Wan Ab Naim, W. N., Mohamed Mokhtarudin, M. J., Chan, B. T., Lim, E., Ahmad Bakir, A., & Nik Mohamed, N. A. (2021). The study of myocardial ischemia-reperfusion treatment through computational modelling. *Journal of Theoretical Biology*, *509*, 110527. <https://doi.org/10.1016/j.jtbi.2020.110527>
- Wang, R., Wang, M., He, S., Sun, G., & Sun, X. (2020). Targeting Calcium Homeostasis in Myocardial Ischemia/Reperfusion Injury: An Overview of Regulatory Mechanisms and Therapeutic Reagents. *Frontiers in Pharmacology*, *11*. <https://www.frontiersin.org/articles/10.3389/fphar.2020.00872>
- Wei, Y., Ullah, G., Ingram, J., & Schiff, S. J. (2014). Oxygen and seizure dynamics: II. Computational modeling. *Journal of Neurophysiology*, *112*(2), 213–223. <https://doi.org/10.1152/jn.00541.2013>
- Weiss, D. L., Iffland, M., Sachse, F. B., Seemann, G., & Dössel, O. (2009). Modeling of cardiac ischemia in human myocytes and tissue including spatiotemporal electrophysiological variations / Modellierung kardialer Ischämie in menschlichen Myozyten und Gewebe. *Biomedizinische Technik/Biomedical Engineering*, *54*(3), 107–125. <https://doi.org/10.1515/BMT.2009.016>
- Yang, K.-C., Breitbart, A., De Lange, W. J., Hofsteen, P., Futakuchi-Tsuchida, A., Xu, J., Schopf, C., Razumova, M. V., Jiao, A., Boucek, R., Pabon, L., Reinecke, H., Kim, D.-H., Ralphe, J. C., Regnier, M., & Murry, C. E. (2018). Novel Adult-Onset Systolic Cardiomyopathy Due to MYH7 E848G Mutation in Patient-Derived Induced Pluripotent Stem Cells. *JACC: Basic to Translational Science*, *3*(6), 728–740. <https://doi.org/10.1016/j.jacbts.2018.08.008>
- Yin, C., Chen, Y., Wu, H., Xu, D., & Tan, W. (2017). Attenuation of ischemia/reperfusion-induced inhibition of the rapid component of delayed rectifier potassium current by Isosteviol through scavenging reactive oxygen species. *Biochimica et Biophysica Acta (BBA) - Biomembranes*, *1859*(12), 2447–2453. <https://doi.org/10.1016/j.bbamem.2017.09.003>
- Yin, P. T., Han, E., & Lee, K.-B. (2016). Engineering Stem Cells for Biomedical Applications. *Advanced Healthcare Materials*, *5*(1), 10–55. <https://doi.org/10.1002/adhm.201400842>
- Yokoshiki, H., Katsube, Y., Sunagawa, M., & Sperelakis, N. (1997). The novel calcium sensitizer levosimendan activates the ATP-sensitive K⁺ channel in rat ventricular cells. *The Journal of Pharmacology and Experimental Therapeutics*, *283*(1), 375–383.

- Ytrehus, K. (2006). Models of myocardial ischemia. *Drug Discovery Today: Disease Models*, 3(3), 263–271. <https://doi.org/10.1016/j.ddmod.2006.10.013>
- Zile, M. A., & Trayanova, N. A. (2017). Myofilament protein dynamics modulate EAD formation in human hypertrophic cardiomyopathy. *Progress in Biophysics and Molecular Biology*, 130, 418–428. <https://doi.org/10.1016/j.pbiomolbio.2017.06.015>
- Zile, M. A., & Trayanova, N. A. (2018). Increased thin filament activation enhances alternans in human chronic atrial fibrillation. *American Journal of Physiology-Heart and Circulatory Physiology*, 315(5), H1453–H1462. <https://doi.org/10.1152/ajpheart.00658.2017>
- Zou, Y., Song, L., Wang, Z., Ma, A., Liu, T., Gu, H., Lu, S., Wu, P., Zhang, †, Ying, Shen, †, Li, Cai, Y., Zhen, ‡, Yisong, Liu, Y., & Hui, R. (2004). Prevalence of idiopathic hypertrophic cardiomyopathy in China: A population-based echocardiographic analysis of 8080 adults. *The American Journal of Medicine*, 116(1), 14–18. <https://doi.org/10.1016/j.amjmed.2003.05.009>

PUBLICATION I

The Comparison Between Two Mathematical Contractile Elements Integrated into an hiPSC-CM *In-silico* Model

Mohamadamin Forouzandehmehr, Nicolo Cogno, Jussi T Koivumäki, Jari
Hytinen, Michelangelo Paci

Computing in Cardiology 2020; Vol 47. doi: 10.22489/CinC.2020.055.

**Publication reprinted under the terms of the Creative Commons Attribution
License (CC BY 4.0).**

The Comparison Between Two Mathematical Contractile Elements Integrated into an hiPSC-CM *In-silico* Model

Mohamadamin Forouzandehmehr¹, Nicolò Cogno², Jussi T Koivumäki¹, Jari Hyttinen¹, Michelangelo Paci¹

¹Faculty of Medicine and Health Technology, Tampere University, Tampere, Finland

²Institut für Festkörperphysik, Technische Universität Darmstadt, Darmstadt, Germany

Abstract

Human induced pluripotent stem cell-derived cardiomyocytes (hiPSC-CMs) are a valuable tool for *in vitro* drug testing and disease studies. As contractility has become one of the main experimental outputs, hiPSC-CMs in *silico* models should also feature the mechanisms of force generation. Thus, we integrated two contractile elements (CE), Rice2008 and Negroni2015, into Paci2020 hiPSC-CM model. The simulated force-Ca²⁺ relationships from skinned versions of the CEs revealed rather close pCa₅₀ values for both CEs: 6.17 and 6.10, respectively for Rice2008 and Negroni2015. However, Hill's coefficients for the two curves were 7.30 and 3.6. The relationships agreed with *in vitro* data from human engineered heart tissues. Most of the biomarkers measured from simulated spontaneous action potentials (APs) and Ca²⁺ transients (CaTs) showed good agreement with *in vitro* data for both CEs. The active peak force observed in paced conditions (1 Hz) and at extracellular Ca²⁺ concentration ([Ca²⁺]_o) of 1.8 mM was 0.011 mN/mm² for Paci2020+Rice2008 and 0.57 mN/mm² for Paci2020+Negroni2015. These values match, qualitatively with the 0.26 mN/mm² peak force reported previously *in vitro* at [Ca²⁺]_o=1.8 mM. Our results set an opening to develop more sophisticated hiPSC-CM models featuring both electrophysiology and biomechanics.

1. Introduction

The role of computer-based modeling in cardiac pathophysiology investigations in a variety of scopes (from the arterial network to cell electrophysiological *in silico* models) through different approaches (finite element analysis to machine learning algorithm), has become increasingly important in recent years [1]–[7].

As a valuable modeling tool, human induced pluripotent stem cell-derived cardiomyocytes (hiPSC-CM) have been considered a promising structure for drug testing and disease studies, since they retain the same genetic information as the donor. Notably, the need for

prediction of drug effects and cardiotoxicity highlights the importance of developing *in silico* methods as well as use of hiPSC-CMs; the fact which also has made it essentially supported by the Comprehensive *In Vitro* Proarrhythmia Assay (CiPA) initiative [8]–[10].

Biomarkers calculated from Ca²⁺ transients (CaTs) are as valuable as the ones measured from action potential (AP), due to the vital role of Ca²⁺ cycling in cell functions and the increasing access to hiPSC-CM Ca²⁺ data. Notably, Ca²⁺ is fundamental in the heart excitation-contraction (EC) coupling, i.e., how the electrical and the mechanical properties of the heart are linked together and how the AP leads to the cardiomyocyte contraction. Indeed, the association of cardiac electrical and mechanical properties is shaped in view of Ca²⁺ cycling. Controversially, in previously developed cardiac muscle mechanical models, the contractile part, in effect, has been divorced from the electrophysiology formalism [11]. While this gap has started to be filled by a number of studies which have addressed the length and force-dependent relationships of Ca²⁺ and crossbridge construction, yet the majority has not gone beyond the cardiomyocyte ion handling and electrophysiological indices [12].

Improvement in understanding of the EC coupling, as the key player in generating sequential contraction of cardiac muscles, and the pro-arrhythmic risk assessments, highlight the need for a comprehensive mathematical hiPSC-CM model, specifically in mechanical terms. Here, two well-established mathematical contractile element (CE) models, namely Rice2008 [13] and Negroni2015 [14], have been integrated into the recently published Paci2020 hiPSC-CM *in silico* model [15]. We assessed the CE's impact on hiPSC-CM electrophysiology in terms of AP and CaT biomarkers and proposed a preliminary comparison of the capabilities of the two CEs in recapitulating *in vitro* hiPSC-CM force-Ca²⁺ data. As future steps, it is noteworthy that such findings can be validated against novel *in vitro* measurements reported previously on hiPSC-CMs [16].

2. Materials and methods

2.1. Contractile element and integration

In Negroni2015 machinery, myosin heads attach to actin in the overlapping area of thin and thick filaments. This zone emerges following their sliding past each other and enables cross bridges (XB) to form and as a result generates the force. XBs are assumed as elastic components which have a mobile end and a fixed end secured to the free end of thick filament (Fig.1).

Similarly, in Rice2008 CE structure, the action of cycling XBs is responsible for the development of the active force. Explicitly, the fraction of myosin heads in the overlap zone initiates the force development. However, the contributions of the passive force and the viscoelastic component must be considered to simulate a more comprehensive myofilament response. In our simulations, the muscle length of $2.1 \mu\text{m}$ was assumed as the rest length at which there is no passive force. The optional series elastic element in Rice2008 is suitable for simulation of protocols which the internal sarcomere can shorten owing to the stretch in the compliant end. Also, we assumed the myofilament in the Rice CE has a Newtonian viscosity set to 0.3% of $F_{\text{max}} \mu\text{m}^{-1} \text{s}^{-1}$ based on an experimental mean value [17].

The Ca^{2+} binding to troponin system is the main conception underlying the two CEs which were integrated to Paci2020 model. While the two CEs significantly differ from how they handle the states of troponin system, the crossbridge mechanism, and the Ca^{2+} bindings, both use the cytosolic Ca^{2+} to run their multiple states of troponin regulations and simulate the dynamic flux of Ca^{2+} towards the myofilament as the feedback. The detail of Ca^{2+} binding to troponin can be found in [13], [14].

3. Results and discussion

3.1. Force- Ca^{2+} relationship

The simulated force- Ca^{2+} relationships showed a rather close pCa_{50} values for both CEs: 6.17 and 6.10 for Rice2008 and Negroni2015, respectively. Whereas, Hill's coefficients for the two curves were 7.30 and 3.60. As can be seen in Fig. 2, the relationships were in qualitative agreement with *in vitro* data obtained from human engineered heart tissues [18].

3.2. Force development and Ca^{2+} transients after integration

The active peak force observed in paced conditions (1 Hz) and at extracellular Ca^{2+} concentration ($[\text{Ca}^{2+}]_o$) of 1.8 mM was 0.011 mN/mm^2 for Paci2020+Rice2008 and 0.57 mN/mm^2 for Paci2020+Negroni2015. As can be observed also in Fig. 3, these values match, qualitatively,

the 0.26 mN/mm^2 the *in vitro* peak force reported previously by Stoehr et al. at $[\text{Ca}^{2+}]_o = 1.8 \text{ mM}$ [18].

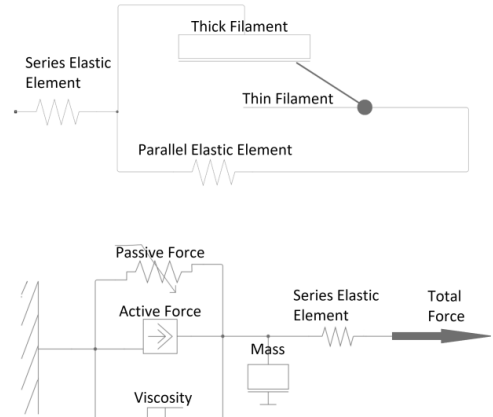


Figure 1. The mechanical schematic illustrations of the Negroni2015 (upper panel) and Rice2008 (lower panel).

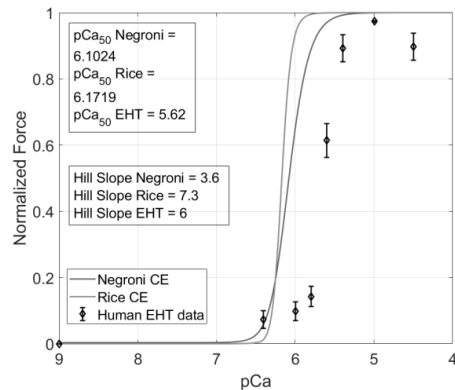


Figure 2. Simulated force- Ca^{2+} relationships of skinned versions of the Negroni model (blue), Rice model (orange), and recorded on engineered heart tissues (EHT) (*in vitro* data from [18]).

3.3. Force-SL relationship

As the developed force is directly influenced by the Sarcomere Length (SL), we studied the effect of change in SL on the developed active force in 1 Hz paced condition (Fig. 4). As can be seen, the increase in SL resulted in the elevation of peak force. Furthermore, the trend of simulated results follows its corresponding *in vitro* data reported for cat trabeculae [19].

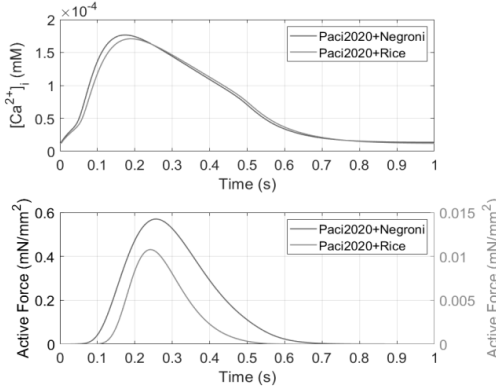


Figure 3. CaTs (upper panel) and the developed active force (lower panel) simulated for the Pac2020+Rice2008 and Pac2020+Negroni2015 models for $[Ca^{2+}]_o = 1.8$ mM and 1 Hz pacing.

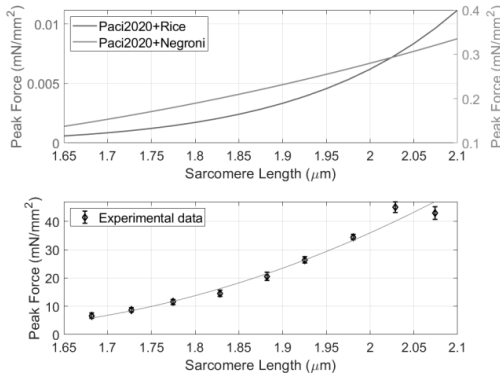


Figure 4. Calculated developed peak force of the two integrated hiPSC-CM model with respect to change in Sarcomere Length (SL) (upper panel). *In vitro* data of force-SL relationship measured in cat cardiac trabeculae from [19] (lower panel).

3.4. Evaluation of biomarkers

The ability to replicate key AP and CaT biomarkers was studied for the two integrated models. These simulations were done in spontaneous beating condition. In both hiPSC-CM models with integrated CEs, most of the biomarkers measured from simulated spontaneous APs and CaTs showed good agreement with the corresponding *in vitro* data. Notably, unlike the Pac2020+Negroni2015, the model with the Rice2008 CE replicated also the AP triangulation factor (AP Tri) of ventricular like hiPSC-CMs within the experimental range. Tables 1 and 2 show the biomarkers values for each model and indicate whether they have successfully recapitulated experimental results.

Table 1. Biomarker evaluation for Pac2020+Negroni2015. WER: within experimental range.

Biomarker	Simulated Value	Exp. Value (Mean±SD)	WER
APA (mV)	104.6	104±6	true
MDP (mV)	-75.3	-75.6±6.6	true
AP CL (ms)	1504.9	1700±548	true
dV/dt max (V/s)	13.5	27.8±26.3	true
APD ₁₀ (ms)	92.3	74.1±26.3	true
APD ₃₀ (ms)	230.7	180±59	true
APD ₉₀ (ms)	377.3	415±119	true
AP Tri	3.69	2.5±1.1	false
CaT DURATION (ms)	641.3	805±188	true
CaT tRise _{10, peak} (ms)	131.4	270±108	false
Cat tRise _{10,50} (ms)	38.3	82.9±50.5	true
CaT tRise _{10,90} (ms)	82.4	167±70	false
CaT tDecay _{90,10} (ms)	331	410±100	true

Table 2. Biomarker evaluation for Pac2020+Rice2008.

Biomarker	Simulated Value	Exp. Value (Mean±SD)	WER
APA (mV)	104.7	104±6	true
MDP (mV)	-75.3	-75.6±6.6	true
AP CL (ms)	1558.6	1700±548	true
dV/dt max (V/s)	14.0	27.8±26.3	true
APD ₁₀ (ms)	93.4	74.1±26.3	true
APD ₃₀ (ms)	234.5	180±59	true
APD ₉₀ (ms)	384.9	415±119	true
AP Tri	3.57	2.5±1.1	true
CaT DURATION (ms)	680.4	805±188	true
CaT tRise _{10, peak} (ms)	136.3	270±108	false
Cat tRise _{10,50} (ms)	39.4	82.9±50.5	true
CaT tRise _{10,90} (ms)	86.2	167±70	false
CaT tDecay _{90,10} (ms)	348.7	410±100	true

To elucidate, AP biomarkers assessed are listed as: APA (AP amplitude), MDP (maximum diastolic potential), CL (cycle length), dV/dt max (maximum upstroke velocity), APD₁₀ and APD₃₀ and APD₉₀ (AP duration at 10, 30, 90% of repolarization), AP Tri (AP triangulation factor). Also, CaT biomarkers are DURATION (duration of the transient), tRise_{10, peak} (time to peak), tRise_{10, 50} and tRise_{10, 90} (rise time from 10 to 50% and 90% of maximum threshold), and tDecay_{90,10} (decay time from 90 to 10%).

4. Conclusion

The role of hiPSC-CMs and their mathematical modelling, has become increasingly prevalent in fundamental studies of electrophysiological and contractile function, as well as, pharmacological tests.

Here, two established CE models, namely Rice2008 and Negroni2015, have been integrated into Paci2020 hiPSC-CM model. Our work represents a first attempt to move beyond electrophysiology in *in silico* descriptions of hiPSC-CMs, through evaluating two of CE models. Our results show a qualitative agreement with *in vitro* data from hiPSC-CMs and represent a starting point to develop more refined hiPSC-CM models combining both electrophysiology and contractility. This new generation of *in silico* models will be able to simulate the effects of diseases affecting not only the electrophysiology (e.g. channelopathies), but also the contractile machinery (e.g. hypertrophic or dilated cardiomyopathy).

Acknowledgments

Mohamadamin Forouzandehmehr was supported by Faculty of Medicine and Health Technology, Tampere University. Dr. Michelangelo Paci was supported by the Academy of Finland (project CardSiPop, decision number 307967). Dr. Koivumäki was supported by Academy of Finland Centre of Excellence in Body-on-Chip Research and Pirkanmaa regional fund of the Finnish Cultural Foundation (grant numbers 50171514 and 50201322).

References

- [1] M. Forouzandehmehr and A. Shamloo, "Margination and adhesion of micro- and nanoparticles in the coronary circulation: A step towards optimised drug carrier design," *Biomech. Model. Mechanobiol.*, 2018.
- [2] A. Shamloo, A. Amani, M. Forouzandehmehr, and I. Ghoytasi, "In silico study of patient-specific magnetic drug targeting for a coronary LAD atherosclerotic plaque," *Int. J. Pharm.*, 2019.
- [3] E. Passini *et al.*, "Human in silico drug trials demonstrate higher accuracy than animal models in predicting clinical pro-arrhythmic cardiotoxicity," *Front. Physiol.*, 2017.
- [4] M. C. Lancaster and E. A. Sobie, "Improved prediction of drug-induced torsades de pointes through simulations of dynamics and machine learning algorithms," *Clin. Pharmacol. Ther.*, 2016.
- [5] A. Shamloo and M. Forouzandehmehr, "Personalised deposition maps for micro- and nanoparticles targeting an atherosclerotic plaque: attributions to the receptor-mediated adsorption on the inflamed endothelial cells," *Biomech. Model. Mechanobiol.*, 2019.
- [6] D. Shah *et al.*, "hiPSC-derived cardiomyocyte model of LQT2 syndrome derived from asymptomatic and symptomatic mutation carriers reproduces clinical differences in aggregates but not in single cells," *Cells*, 2020.
- [7] J. Parikh, V. Gurev, and J. J. Rice, "Novel two-step classifier for Torsades de Pointes risk stratification from direct features," *Front. Pharmacol.*, 2017.
- [8] A. Muszkiewicz *et al.*, "Variability in cardiac electrophysiology: Using experimentally-calibrated populations of models to move beyond the single virtual physiological human paradigm," *Prog. Biophys. Mol. Biol.*, 2016.
- [9] O. J. Britton *et al.*, "Experimentally calibrated population of models predicts and explains intersubject variability in cardiac cellular electrophysiology," *Proc. Natl. Acad. Sci. U. S. A.*, 2013.
- [10] D. G. Strauss *et al.*, "Comprehensive In Vitro Proarrhythmia Assay (CiPA) Update from a Cardiac Safety Research Consortium / Health and Environmental Sciences Institute / FDA Meeting," *Ther. Innov. Regul. Sci.*, 2019.
- [11] L. Chin, P. Yue, J. J. Feng, and C. Y. Seow, "Mathematical simulation of muscle cross-bridge cycle and force-velocity relationship," *Biophys. J.*, 2006.
- [12] A. R. Soltis and J. J. Saucerman, "Synergy between CaMKII substrates and β -adrenergic signaling in regulation of cardiac myocyte Ca₂ handling," *Biophys. J.*, 2010.
- [13] J. J. Rice, F. Wang, D. M. Bers, and P. P. De Tombe, "Approximate model of cooperative activation and crossbridge cycling in cardiac muscle using ordinary differential equations," *Biophys. J.*, 2008.
- [14] J. A. Negroni *et al.*, " β -adrenergic effects on cardiac myofilaments and contraction in an integrated rabbit ventricular myocyte model," *J. Mol. Cell. Cardiol.*, 2015.
- [15] M. Paci *et al.*, "All-Optical electrophysiology refines populations of in silico human iPSC-CMs for drug evaluation," *Biophys. J.*, 2020.
- [16] A. Ahola, R. P. Pölonen, K. Aalto-Setälä, and J. Hyttinen, "Simultaneous measurement of contraction and calcium transients in stem cell derived cardiomyocytes," *Ann. Biomed. Eng.*, 2018.
- [17] P. P. de Tombe and H. E. ter Keurs, "An internal viscous element limits unloaded velocity of sarcomere shortening in rat myocardium," *J. Physiol.*, 1992.
- [18] A. Stoehr *et al.*, "Automated analysis of contractile force and Ca₂⁺ transients in engineered heart tissue," *Am. J. Physiol. - Hear. Circ. Physiol.*, 2014.
- [19] P. P. De Tombe and H. E. D. J. Ter Keurs, "Sarcomere dynamics in cat cardiac trabeculae," *Circ. Res.*, 1991.

Address for correspondence:
 Mohamadamin Forouzandehmehr.
 Arvo Ylpön katu 34, (Arvo building, 2nd floor), D224
 33520 Tampere, Finland.
 mohamadamin.forouzandehmehr@tuni.fi

PUBLICATION II

A Mathematical model of hiPSC Cardiomyocytes Electromechanics

Mohamadamin Forouzandehmehr, Jussi T. Koivumäki, Jari Hyttinen, Michelangelo Paci

Physiol. Rep. 9 (2021). doi:10.14814/phy2.15124.

Publication reprinted under the terms of the Creative Commons Attribution License (CC BY 4.0).

A mathematical model of hiPSC cardiomyocytes electromechanics

Mohamadamin Forouzandehmehr  | Jussi T. Koivumäki | Jari Hyttinen | Michelangelo Paci

Faculty of Medicine and Health Technology, Tampere University, Tampere, Finland

Correspondence

Mohamadamin Forouzandehmehr, Arvo Ylpön katu 34, FI-33520 Tampere, Finland.

Email: mohamadamin.forouzandehmehr@tuni.fi

Funding information

Tampere University; Finnish Cultural Foundation, Grant/Award Number: 160735, 210813, 50171514 and 50201322

Abstract

Human induced pluripotent stem cell-derived cardiomyocytes (hiPSC-CMs) are becoming instrumental in cardiac research, human-based cell level cardiotoxicity tests, and developing patient-specific care. As one of the principal functional readouts is contractility, we propose a novel electromechanical hiPSC-CM computational model named the hiPSC-CM-CE. This model comprises a reparametrized version of contractile element (CE) by Rice et al., 2008, with a new passive force formulation, integrated into a hiPSC-CM electrophysiology formalism by Paci et al. in 2020. Our simulated results were validated against *in vitro* data reported for hiPSC-CMs at matching conditions from different labs. Specifically, key action potential (AP) and calcium transient (CaT) biomarkers simulated by the hiPSC-CM-CE model were within the experimental ranges. On the mechanical side, simulated cell shortening, contraction–relaxation kinetic indices (RT_{50} and RT_{25}), and the amplitude of tension fell within the experimental intervals. Markedly, as an inter-scale analysis, correct classification of the inotropic effects due to non-cardiomyocytes in hiPSC-CM tissues was predicted on account of the passive force expression introduced to the CE. Finally, the physiological inotropic effects caused by Verapamil and Bay-K 8644 and the aftercontractions due to the early afterdepolarizations (EADs) were simulated and validated against experimental data. In the future, the presented model can be readily expanded to take in pharmacological trials and genetic mutations, such as those involved in hypertrophic cardiomyopathy, and study arrhythmia trigger mechanisms.

KEYWORDS

action potential, contractility, drug test, human stem cell-derived cardiomyocyte, immature cardiomyocytes, in silico modeling

This is an open access article under the terms of the Creative Commons Attribution License, which permits use, distribution and reproduction in any medium, provided the original work is properly cited.

© 2021 The Authors. *Physiological Reports* published by Wiley Periodicals LLC on behalf of The Physiological Society and the American Physiological Society.

1 | INTRODUCTION

The rapid development of engineered heart tissue approaches opens novel avenues for drug trials and investigating heart diseases, building on the recent advancements in producing hiPSC-CMs. Furthermore, by holding the same genetic information as the donor, hiPSC-CM-based methods hold great promise for developing patient-specific treatment options. As the interest in investigating the contractile indices of hiPSC-CMs grows, *in vitro* measurements of contractility, such as video microscopy (Ahola et al., 2018), are becoming a standard alongside the more classical electrophysiological studies, such as patch-clamp experiments. Accordingly, there is a great need for developing comprehensive computational models of hiPSC-CMs that describe the biomechanical function, in addition to electrophysiology. Aside from the chance to better understand the underlying physiology, the more advanced models would answer the pressing need for drug effect calculations and cardiotoxicity predictions. The idea has also been advocated by the Comprehensive In Vitro Proarrhythmia Assay (CiPA) initiative (Strauss et al., 2019).

Mathematical models in cardiology, developed on different scales, have been growing in complexity, thanks to the progress in the predictive power of computer-based frameworks (Amani et al., 2021; Forouzanmehr & Shamloo, 2018, 2021; Hossain et al., 2014; Muller et al., 2014; Paci et al., 2013; Shamloo et al., 2019; Shamloo & Forouzanmehr, 2019; Zile & Trayanova, 2018). The dominating focus in the mathematical modeling of cardiac or muscle cells has been the electrophysiology (Bartolucci et al., 2020; Grandi et al., 2010; Kernik et al., 2019; O'Hara et al., 2011; Paci, Pölonen, et al., 2018; Tomek et al., 2019; Tusscher & Panfilov, 2006), and the electromechanical aspect has received much less attention. In some non-human multi-scale mathematical models, especially for the mouse and rat, elements of myofilament contraction are at play with a detailed biophysical formalism (Rice et al., 2008; Campbell et al., 2010; Land et al., 2013; Land & Niederer, 2015; Sheikh et al., 2012). The alterations in intracellular properties can be associated with entire organ mechanical outcomes using such models. Moreover, based on modifications to channels or the proteins involved in Ca^{2+} and contractile regulations, these models were successful in the prediction of key cardiac function indices. To include the mechanical aspects of cardiomyocytes, there have been efforts to establish human biophysical models of tension production capable of integration into a whole organ contraction assembly (Land et al., 2017). Furthermore, some models of human ventricular cardiomyocyte (hV-CM) electromechanics simulating active tensions and sarcomere dynamics (Margara et al., 2020, 2021) have also been

introduced. However, there is a lack of biophysical models of whole hiPSC-CM electromechanics, which can predict active tension, cell shortening, and particularly inotropic effect of non-cardiomyocytes (Iseoka et al., 2018).

This study aimed to develop a comprehensive computational model of hiPSC-CMs to capture the essential cellular electromechanics and finally validate the model against hiPSC-CMs *in vitro* data. Accordingly, a reparametrized version of a cardiac myofilament model proposed by Rice et al. (2008), with a new passive force formulation, has been integrated into a hiPSC-CM electrophysiology model by Paci et al. (2020). We explored and validated the capability of our model through simulations of AP and CaT biomarkers, the key electrophysiological currents and intracellular concentrations, the contraction-relaxation velocity, fractional cell shortening, generated active tension, aftercontractions, as well as drug-induced and non-cardiomyocyte mechanical effects.

2 | METHODS

2.1 | The electrophysiology model

Figure S1 in the Supplementary Materials shows the schematics of the hiPSC-CM-CE model, outlining cell compartments, ion channels and pumps, and the CE. The model comprises two cellular compartments, which are cytosol and sarcoplasmic reticulum (SR). In Paci2020, both I_f and the pre-upstroke inward component of Na^+/Ca^{2+} exchanger (I_{NCX}) sustain the spontaneous electrical activity. The underlying electrophysiology is described by the classical Hodgkin & Huxley formalism, giving the membrane potential as follows:

$$C \frac{dV}{dt} = -(I_{Na} + I_{NaL} + I_{CaL} + I_f + I_{K1} + I_{Kr} + I_{Ks} + I_{to} + I_{NaCa} + I_{NaK} + I_{pCa} + I_{bNa} + I_{bCa} - I_{stim}) \quad (1)$$

where C denotes cell capacitance, I_{stim} is the stimulus current, and V represents membrane potential. All simulations have been done assuming the temperature at 37°C and with extracellular concentrations of 151, 5.4, and 1.8 mM for Na, K, and Ca^{2+} , respectively.

2.2 | The contractile model

Figure S2 shows a schematic diagram of the CE (Rice et al., 2008), which takes in an adequate cellular machinery while maintaining an admirable balance between mechanistic detail and model parsimony. In Rice CE, to simulate the experimental protocols of internal sarcomere shortening, a series elastic element

is considered to enable stretch in the compliant end. Ultimately, to improve the model stability and circumvent sudden changes in sarcomere length velocity, a mass term has been considered.

The development of myofibrillar active force results from the fraction of cross-bridges (XBs) which can bind strongly. To elucidate, this process hinges upon the overlap of the thick filament (myosin) and the thin filament (actin). In the hiPSC-CM-CE model, the rest length of the sarcomere, at which no passive force exists, has been set 1.9 μm in accord with experimental reports for hiPSC-CMs (Pioner et al., 2020). Correspondingly, the Newtonian viscosity of the myofibrillar was set to 0.3% of $F_{\text{max}} \mu\text{m}^{-1} \text{s}^{-1}$ in line with experimental data (de Tombe & ter Keurs, 1992). In non-isosarcometric scenarios, the change in sarcomere length follows:

$$\frac{d}{dt}SL = \frac{\text{Integral}_{\text{Force}} + (SL_0 - SL) \times \text{vsc}}{m} \quad (2)$$

where SL is the sarcomere length, Frc denotes the developed active force, vsc is the viscosity, and m is mass. The integral force has been defined by Equation S4 in the supplementary materials.

Importantly, a distinct feature of Rice2008 CE is how the calcium–troponin binding system and thus the XB machinery is handled. There are two types of calcium binding: the regulatory Ca^{2+} binding, which only affects thin-filament activation, and the apparent Ca^{2+} binding, which influences the cytosolic CaT , in other words, the Ca binding sensed by the cell. Here, we integrated the CE into Paci2020 electrophysiology by (A) subtracting the total troponin concentration from the total buffered Ca^{2+} concentration and (B) subtracting the Ca^{2+} flux toward the myofibrils from the cytosolic Ca^{2+} (the apparent Ca^{2+} binding). The latter is described by:

$$\frac{d}{dt} [\text{Trop}_{\text{Apr}}\text{Ca}] = [\text{Troponin}] \times \frac{d}{dt} \text{Trop}_{\text{Apr}}(s) \quad (3)$$

$$\begin{aligned} \frac{d}{dt} \text{Trop}_{\text{Apr}}(s) = & -\frac{d}{dt} \text{SOVF}_{\text{thin}}(s) \times \text{Trop}_L \\ & + (1 - \text{SOVF}_{\text{thin}}(s)) \times \frac{d}{dt} \text{Trop}_L + \frac{d}{dt} \text{SOVF}_{\text{thin}}(s) \\ & \times (\text{Frct}_{\text{SBXB}} \times \text{Trop}_L + (1 - \text{Frct}_{\text{SBXB}}) \times \text{Trop}_L) \\ & + \text{SOVF}_{\text{thin}}(s) \times \left(\frac{d}{dt} \text{Frct}_{\text{SBXB}} \times \text{Trop}_L + \text{Frct}_{\text{SBXB}} \right) \\ & \times \frac{d}{dt} \text{Trop}_H - \frac{d}{dt} \text{Frct}_{\text{SBXB}} \times \text{Trop}_L + (1 - \text{Frct}_{\text{SBXB}}) \times \frac{d}{dt} \text{Trop}_L \end{aligned} \quad (4)$$

As given in Equation (3), the time rate of apparent Ca^{2+} binding to troponin, Trop_{Apr} is multiplied by the total buffer concentration of troponin, $[\text{Troponin}]$, which is 70 μM in our simulations. Also, the flux from cytosolic Ca^{2+} toward the myofibrillar is given by Equation (4). Here, $\text{SOVF}_{\text{thin}}(s)$ is the thin filament overlap, which is a

function of sarcomere length s . Trop_L and Trop_H denote the Ca^{2+} binding to low and high affinity troponin, respectively. Finally, $\text{Frct}_{\text{SBXB}}$ is the fraction of strongly attached XBs. The equations and details of the CE used in the hiPSC-CM-CE have been fully given in Rice et al. (2008).

Recently, the role of cardiomyocytes to non-cardiomyocytes ratio has been proven critical in electro-mechanics of engineered heart tissues (EHTs) derived from hiPSC-CMs. Similarly, it plays a vital role in the structure/function and therapeutic potentials of hiPSC-CMs (Iseoka et al., 2018). Notably, the quantity of non-cardiomyocytes is crucial in generating functional iPSC-derived EHTs as grafts in cardiac-regeneration therapy. The EHTs containing 50–70% of cardiomyocytes exhibited stable structures and increased therapeutic potential (Iseoka et al., 2018). To include the effect of the non-cardiomyocyte components in the model and according to the biphasic trend in contraction–relaxation velocities observed for different cardiomyocyte ratios in EHTs (Figure S7), we introduced a piecewise function as the passive force (Equation 5). We used an exponential first guess for the curve fitting regarding the trends observed in Figure S7 and minimized the error manually, so maximums of simulated contraction–relaxation velocities best replicate the data in Figure S7. Here, the passive force represents the effect of the non-cardiomyocyte components on the sarcomere dynamics and cell contractions which is defined as follows:

$$F_{\text{passive}}(x) = \begin{cases} F_{\text{titin}}(x), & \text{ctn} = 100 \\ \frac{1}{0.54 \times (4.66 \times e^{-3.05c^{4.9}}) \times (F_{\text{titin}}(x) + F_{\text{collagen}}(x))}, & 100 > \text{ctn} \geq 70 \\ \frac{1}{(6 \times e^{-6.17c^{2.91}}) \times (F_{\text{titin}}(x) + F_{\text{collagen}}(x))}, & 70 > \text{ctn} > 0 \end{cases} \quad (5)$$

where c is equal to $\text{ctn}/100$ and ctn indicates the percent of CMs in the EHT, x denotes the sarcomere length, and CM is cardiomyocyte.

2.3 | Reparameterization of the contractile element

The foundation of the development of the Rice et al. CE was *in vitro* rabbit data. Therefore, by adapting XB cycling and calcium-based thin filament activation parameters, the CE was adjusted to match the literature-based hiPSC-CM Ca^{2+} and tension data. The main strategy in reparameterizing the CE was finding a set of parameters with which the model can simulate key contraction-related hiPSC-CMs protocols in the reported experimental ranges in 37°C and extracellular Ca^{2+} concentration of 1.8 mM (see Section 2.4). Namely, % of cell shortening at 1 Hz pacing and contraction RT_{50} (the time from contraction peak

to half of the relaxation) from Pioner et al. (2020), and the amplitude of developed active tension from Ruan et al. (2016).

The tuned parameters of the CE mainly govern the Ca^{2+} binding to troponin, except for m (mass), in Equation (2), which is essentially a tuning parameter related to improving the model response times, and $xbmodsp$, which is the species-dependent parameter influencing the thin filament regulation and XB cycling and inversely correlates with the size of the organism (Rice et al., 2008). Table 1 gives the modified and original values of the parameters in the CE.

In this work, we tuned the CE parameters manually, following the adjustments reported in (Zile & Trayanova, 2018), in order to simulate the available experimental data. According to the equations handling the troponin and XB regulations, we first investigated the effect of the changes in the parameters listed in Figure 1 on the mechanical outputs we aimed to simulate. The green and black texts denote the positive and negative effects on the mechanical outputs selected for validation, respectively. We highlight that the effects presented in Figure 1 do not come from a sensitivity analysis, but from the manual tuning of the parameters performed in a sequential manner. We considered $\pm 25\%$ of the CE baseline values as the constraints for the parameter tuning, except for K_{offmod} , m , and kxb . K_{offmod} is a species-dependent parameter (inversely correlating with the organism's size) and contributes to the total rate for unbinding rate in the high- and low-affinity conditions in regulatory Ca^{2+} binding. The mass, denoted by m in Equation (2), improves the stability of the integration of the model equations and avoids rapid changes in muscle shortening velocity in fast muscle release protocols. It is also a parameter to tune and improve the model response

times (Rice et al., 2008). Markedly, similar limitations and assumptions considered in this work have been reported previously for Rice CE reparameterizations (Campbell et al., 2008; Zile & Trayanova, 2017).

Furthermore, we changed the value of kxb , the tension scaling parameter in the reparameterization. In the hiPSC-CM-CE model, tension is scaled to obtain the final simulated tension from the normalized active tension as follows:

$$Tension = kxb \times F_{active} \quad (6)$$

where F_{active} is calculated by Equation 35 in Rice et al. (2008), and kxb is the scaling constant that corresponds to the total number of XBs and the fraction of cycling XBs in the force-generating state at any time, as also reported in Land et al. (2012).

In the literature, this scaling constant has been treated either as an original experimental value or a model-based parameter whose value depends upon other experimental values. As an example of the latter, in the Niederer-Hunter-Smith (NHS) model (Niederer et al., 2006), the equivalent parameter is 56.2 kPa. However, the value is set to 100 kPa in later whole-organ models (Niederer & Smith, 2009). In Rice original CE model, $kxb \approx 120$ kPa. Also, Land et al. set this scaling constant at 120 kPa consistently with previous models and with the higher end values for maximum tension and twitches (Land et al., 2012).

The values reported experimentally for the kxb in the literature range within multiple orders of magnitudes. Blanchard et al. reported maximum tension in mouse muscle strips to be 12.96 kPa (Blanchard et al., 1999). Stuyvers et al. indicated the maximal stress is around 17 kPa for mouse muscle with 1.9 μm of sarcomere length (Stuyvers et al., 2002). Palmer et al. also reported comparable maximum activated tension for mice isometric analysis around 14 kPa (Palmer et al., 2004). However, some twitch transient data peak at 50 kPa (Stull et al. 2002) and other results go up to 112 kPa for maximum developed tension (Kreutziger et al., 2011).

Peak active tensions experimentally reported for hiPSC-CMs range from ~ 1.2 to ~ 45 kPa (Pioner et al., 2020; Yang et al., 2018). Specifically, Pioner et al. have reported 18.6 ± 2.5 as the maximal developed tension for in hiPSC-CM myofilaments (Pioner et al., 2020). However, there are other studies that report an order of magnitude lower peak twitches for hiPSC-CM-CEs (Rodriguez et al., 2014; Ruan et al., 2016). In line with these findings, we set $kxb = 12$ kPa, placing the peak tension within the experimental data range for hiPSC-CMs and thus resulting in the final simulated 0.055 kPa active tension.

TABLE 1 Baseline (Rice et al., 2008) and the modified values of the parameters changed in the CE

Parameter	Baseline value	The hiPSC-CM-CE	% of change
K_{on} ($\text{s}^{-1} \text{mM}^{-1}$)	50×10^3	62.5×10^3	25
K_{offL} (s^{-1})	250	200	-20
K_{offH} (s^{-1})	25	25	0
Perm_{50}	0.5	0.6	20
n_{perm}	15	11.28	-24.8
K_{n-p} (s^{-1})	500	550	10
K_{p-n} (s^{-1})	50	50	0
K_{offmod}	1	0.5	-50
m ($\text{s}^2 \mu\text{m}^{-1}$)	5×10^{-5}	2×10^{-5}	-60
kxb	120	12	—
$xbmodsp$	0.2, 1, 1.33	0.2	—

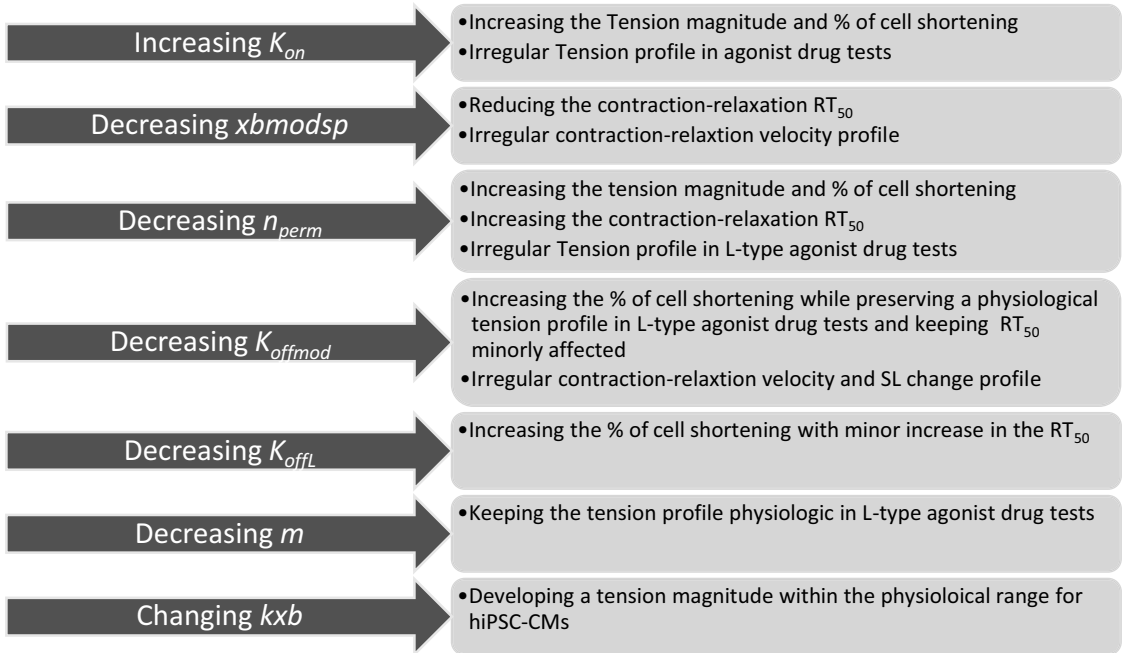


FIGURE 1 Tuning parameters of the CE and their effect on the hiPSC-CM-CE. The green and black texts highlight the positive and negative effects on the mechanical outputs selected for validation, respectively

Lastly, we performed the sensitivity analysis (Figure S3) to investigate the hiPSC-CM-CE behavior regarding the mechanical biomarkers following the method detailed in Romero et al. (2011). For each biomarker, b , and model parameter, p , the percentage of change $D_{c,p,a}$, sensitivity $S_{c,p}$, and relative sensitivity $r_{c,p}$, are defined as follows:

$$D_{b,p,m} = \frac{(b_{p,m} - b_{ctl})}{b_{ctl}} \times 100 \quad (7)$$

$$S_{b,p} = \frac{\Delta D_{b,p,m}}{\Delta m} = \frac{D_{b,p,+15\%} - D_{b,p,-15\%}}{0.3} \quad (8)$$

$$r_{b,p} = \frac{S_{b,p}}{|S_{b,p}|_{max,b}} \quad (9)$$

2.4 | In vitro data for the contractile element reparameterization

The experimental ranges obtained from hiPSC-CMs based on which the CE of the model has been reparameterized were the percent of cell shortening (preserved cell contractility) (Pioner et al., 2020), the contraction-relaxation RT_{50} (Pioner et al., 2020), and the tension magnitude (Ruan et al., 2016).

In Pioner et al. (2020), the supplementary materials detail the process of obtaining the differentiated cardiomyocytes and their long-term maturation as single cells on nanotopographic (nanopattern) substrata. An inverted microscope integrated into a video-based edge detection system has been used for visualization of single hiPSC-CMs fractional shortening (% of cell shortening). The cells were paced at 0.5, 1, or 2 Hz using field stimulation and were perfused at 37°C, with Tyrode solution.

In Ruan et al. (2016), undifferentiated hiPSCs were obtained from a lung fibroblast cell line. After trypsinization of the hiPSC-derived cardiomyocytes into single cells, engineered heart tissue structures were made of a collagen-based three-dimensional scaffold encapsulating the single cells. The 2-mm-long sections constructs were attached to a force transducer and a length controller. Using LabView software, length and force signals of spontaneously contracting constructs were digitally recorded. The authors assumed a circular cross-section for the preparations and normalized the force to the cross-sectional area of the constructs. The diameter was measured at non-strained lengths, and the area was calculated accordingly. The *in vitro* data were obtained when the solution temperature was maintained at 37°C.

In Iseoka et al. (2018), using magnetic-activated cell sorting, the scaffold-free hiPSC-CM EHTs at different

#	Experimental paper	[Ca ²⁺] _e	Temperature (°C)	Biomarkers used for the reparameterization
1	(Pioner et al., 2020)	1.8 mM	37	% of cell shortening,
2	(Clark et al., 2021)	1.8 mM	37	Contraction RT ₅₀
3	(Yang et al., 2018)	1.8 mM	37	% of cell shortening, contraction RT ₂₅ ,
4	(Ruan et al., 2016)	1.8 mM	Mechanical measurements and drug tests at 37, Histological measurements and microscopy at room temp.	Active tension amplitude and inotropic effects of Verapamil and Bay-K 8644
5	(Iseoka et al., 2018)	N/A	37	Inotropic effects of non-cardiomyocytes on the mechanical outputs of hiPSC-CMs
6	(Hayakawa et al., 2014)	N/A	37	Contraction velocity profile
7	(Rodriguez et al., 2014)	N/A	37	Contraction velocity profile

Note: [Ca²⁺]_e denotes the extracellular Ca²⁺ concentration.

ratios of cardiomyocytes (25%, 50%, 70%, or 90%) were generated. Using a camera-based motion analysis setup, the contractile features of the EHTs were investigated. Table 2 gives a concise map of the model reparameterization with attention to the hiPSC-CMs experimental results reported in the cited papers.

2.5 | Drug tests protocols

The occurrence of aftercontractions (Nguyen et al., 2017; Novak et al., 2012) is caused by abnormalities in the electrophysiology, e.g. delayed (DADs) and early afterdepolarizations (EADs). To trigger EADs, we blocked I_{Kr} by 95%. Since the Paci2020 model responds to a strong I_{Kr} block with a remarkable APD prolongation but does not develop EADs (Paci, Koivumäki, et al., 2021), to evaluate the occurrence of aftercontractions, we tested I_{Kr} block on few illustrative model variants capable of generating EADs for strong I_{Kr} block. These models were extracted from an *in silico* population previously generated using the Paci2020 model as a baseline and modulating maximum conductances/currents of I_{Na^+} , I_{NaL} , I_{CaL} , I_f , I_{to} , I_{Kr} , I_{Ks} , I_{K1} , I_{NaCa} , I_{NaK} and I_{pCa} in the range [0.5, 2], as done in Paci, Pölonen, et al. (2018).

Furthermore, the drug-induced inotropic effects were investigated by simulating the effect of 90 nM of

Verapamil (as the I_{CaL} inhibitor) and 1 μ M of Bay-K8644 (the I_{CaL} agonist). We simulated Verapamil administration with a simple pore-block model, setting the IC_{50} and Hill coefficients of the involved blockers as given in Table S1 in the supplementary materials. Similarly, the effect of 1 μ M of Bay-K8644 on the model was studied, setting 17.3 nM and 1.25 as the EC_{50} and Hill coefficient of I_{CaL} blocker, respectively (Bechem & Hoffmann, 1993; Rae & Calixto, 1989).

3 | RESULTS

3.1 | Reparameterization: contractility

The main results of integrating original Rice CE into the Paci2020 electrophysiology are shown in Figure S4. The uncalibrated version failed to simulate the main mechanical results within the *in vitro* ranges. We also studied the role of mechanical feedback (Figure S5). Results indicate that the strong coupling has a significant effect on the cytosolic Ca²⁺ concentration. Compared with the weakly coupled condition, the CaT peak was decreased by 20.3%, and the simulated active tension consequently by 52.2%. This behavior is consistent with the results of the mechanical feedback study done by a hV-CM ionic model integrated into Rice CE (Zile & Trayanova, 2016).

TABLE 2 hiPSC-CM experimental papers used for the reparameterization of the model

The strong coupling term comes against weak coupling, where there is no mechanical feedback. In other words, by strong coupling, we mean incorporating myofilament feedback on calcium dynamics which was done using a dynamic term for troponin buffering of intracellular calcium (Equation 4) using the approach in Rice et al. (2008). Of note, the profile and magnitude of JCaBMyo (Figure 2d) are consistent with the corresponding simulations by other mathematical CE models (Negroni & Lascano, 2008; Negroni et al., 2015).

For the skinned version of the CE, the steady-state tension vs. sarcomere length (SL) relationship is one of the experimental characterizations that significantly influences the model development. As can be seen in Figure 2a, in comparison with the original CE, there is an improvement in the physiologic behavior in the reparametrized version in terms of fitting to the reference experimental data obtained from cat trabeculae (De Tombe & Ter Keurs, 1991).

In line with cell shortening data obtained for hiPSC-CMs in Pioner et al. (2020), our model simulates the cell shortening within experimental range at 1 Hz pacing (Figure 2b). Also, at 1 Hz pacing, RT_{50} was simulated 161 ms, which is in the experimental range reported for

hiPSC-CMs (145.9–170.1 ms (Clark et al., 2021)). Figure 2c shows the tension amplitude simulated by the hiPSC-CM-CE, in spontaneous condition, which locates within the experimental range reported for hiPSC-CMs at matching conditions of 1.8 mM extracellular Ca^{2+} and 37°C (Figure 2c) (Ruan et al., 2016). Figure 2d shows the flux of Ca^{2+} toward the myofilament and the corresponding CaT trace. Furthermore, Figure 2e illustrates the normalized contraction velocity curve, which recapitulates the standard shape and the experimental records for hiPSC-CMs obtained via traction force microscopy in Hayakawa et al. (2014).

Figure S3 in the supplementary material shows a sensitivity analysis map of the hiPSC-CM-CE model regarding the target mechanical outputs. The relative sensitivity of the biomarkers (fractional cell shortening, active tension peak, and RT_{50}) is shown on a 0–1 scale as a response to 15% of change of the parameters on the y-axis. For example, n_{perm} has the most intense inverse effect on ATpeak and RT_{50} , meaning, by decreasing n_{perm} the biomarker values increase. The results indicate that each simulated contractile biomarker, specifically % of cells shortening (Figure S4d), is heavily influenced by n_{perm} ; the parameter that

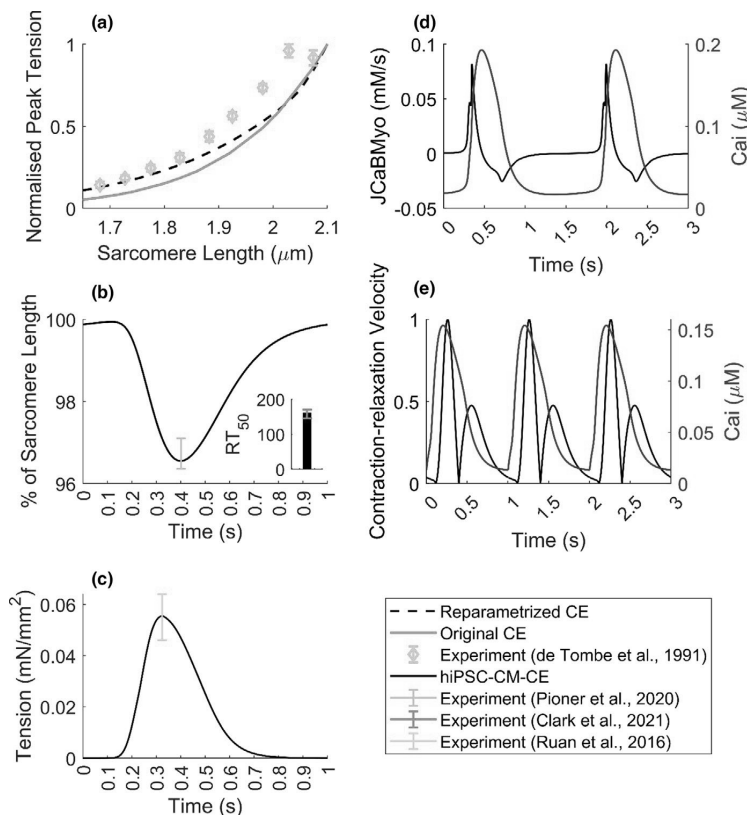


FIGURE 2 Mechanical biomarkers simulated by the hiPSC-CM-CE model. (a) Normalized peak tensions vs. SL. (b) % of cell shortening and contraction RT_{50} (time from peak contraction to 50% relaxation) at 1 Hz pacing. (c) The simulated tension profile at spontaneous beating. (d) The binding flux of Ca^{2+} toward the myofilament (JCaBMyo) and the CaT. (e) Normalized motion waveform (contraction–relaxation velocity) and the CaT at 1 Hz pacing

represents the non-linear function of nearest-neighbor cooperativity in myofilament Ca^{2+} -based activation in cycling XBs in Rice CE.

3.2 | Electrophysiological properties of the hiPSC-CM-CE model

In Table 3, we reported the biomarkers simulated by the Paci2020 + the original Rice CE (i.e. before the CE calibration) model and the hiPSC-CM-CE model, together with the experimental biomarkers previously summarized in Paci, Pölonen, et al. (2018). The simulations were done in the spontaneous beating condition until the steady-state.

Table 3 presents that the integration of the original CE into the ionic model moved 4/13 biomarkers out of the range and the reparameterization of the CE restored them (column Paci2020 + Original Rice CE vs. hiPSC-CM-CE). Since the hiPSC-CM-CE model inherits its electrophysiology from the Paci2020 model, which does not simulate the contractile function of hiPSC-CMs, we compared the simulated AP, CaT, and ionic current traces of the two models (Figure 3).

3.3 | Validation: fractional shortening, drug-induced, and arrhythmogenic effects

To validate the hiPSC-CM-CE model, we compared the simulated contraction with *in vitro* data from Yang et al. (2018) that was not used in the model parameterization process. Furthermore, the effects of 90 nM of Verapamil (antiarrhythmic drug class IV) and 1 μM of Bay-K 8644 (L-type Ca^{2+} channel agonist) on the model outputs were simulated.

As Figure 4 shows, the hiPSC-CM-CE mechanical results at 1.5 Hz pacing place within the ranges of experimental contraction biomarkers reported for hiPSC-CM single cell lines at 1.8 mM extracellular Ca^{2+} and 37°C (Yang et al., 2018). The simulated fractional cell shortening and the contraction RT_{25} are 1.86% and 89 ms, located within the reported *in vitro* intervals of $2.04 \pm 0.2\%$ and 75.2–90.3 ms, respectively.

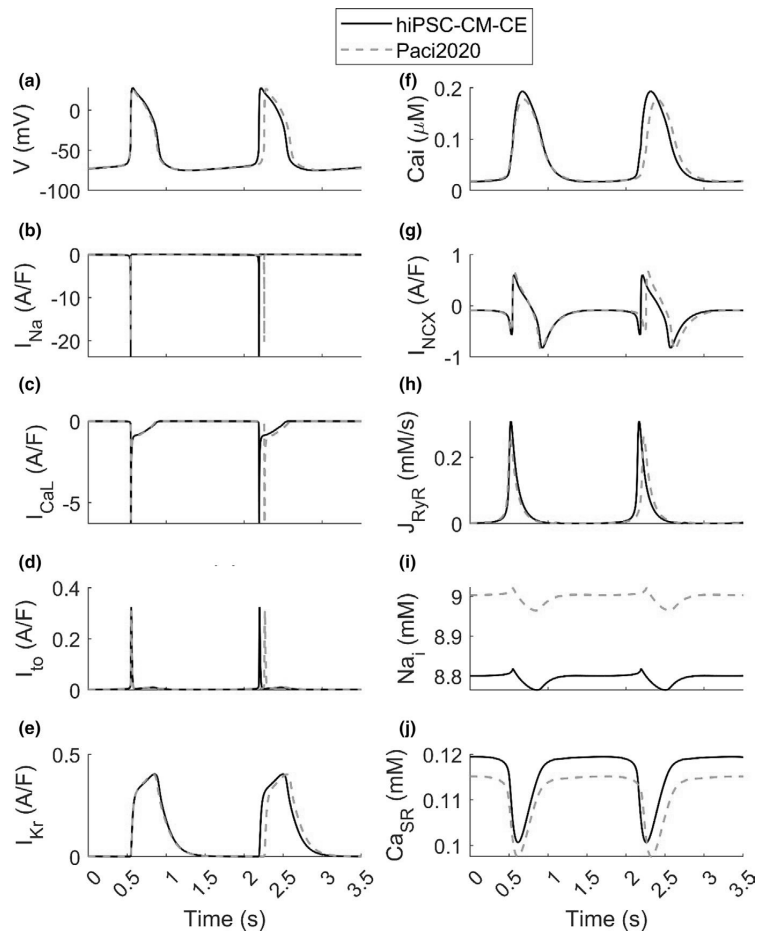
The effect of 90 nM Verapamil was simulated as a multichannel action reference compound, which was selected according to human-based data (Kramer et al., 2013). On the other hand, the effect of 1 μM of Bay-K 8644, for which we expect a positive inotropic effect as in Ruan et al. (2016), has been simulated as an agonist drug compound that influences only I_{CaL} .

No.	Biomarker	Paci2020	Paci2020 + Original Rice CE	hiPSC-CM-CE	Exp. value (Mean \pm SD)
1	APA (mV)	102	105	103	104 \pm 6
2	MDP (mV)	-74.9	-75.3	-75.0	-75.6 \pm 6.6
3	AP CL (ms)	1712	1559	1644	1700 \pm 548
4	dV/dt max (V/s)	20.5	14.0	23.9	27.8 \pm 26.3
5	APD ₁₀ (ms)	87.0	109.5	95.0	74.1 \pm 26.3
6	APD ₃₀ (ms)	224	259	238	180 \pm 59
7	APD ₉₀ (ms)	390	421	403	415 \pm 119
8	AP Tri	2.8	3.2	2.9	2.5 \pm 1.1
9	CaT DURATION (ms)	691	681	693	805 \pm 188
10	CaT tRise _{10, peak} (ms)	184	136	163	270 \pm 108
11	CaT tRise _{10,50} (ms)	54.9	39.2	46.2	82.9 \pm 50.5
12	CaT tRise _{10,90} (ms)	118	86	102	167 \pm 70
13	CaT tDecay _{90,10} (ms)	341	349	343	410 \pm 100

Note: AP biomarkers listed are: APA (AP amplitude), MDP (maximum diastolic potential), CL (cycle length), dV/dt max (maximum upstroke velocity), APD₁₀ and APD₃₀ and APD₉₀ (AP duration at 10, 30, 90% of repolarization, respectively), AP Tri (AP triangulation index). And CaT biomarkers are DURATION (duration of the transient), tRise_{10, peak} (time to peak), tRise_{10,50} and tRise_{10,90} (rise time from 10 to 50% and 90% of maximum threshold, respectively), and tDecay_{90,10} (decay time from 90 to 10%). The out-of-range values are in italics. The third column is taken directly from the original Paci2020 publication (Paci et al., 2020).

TABLE 3 Biomarkers computed on simulated spontaneous APs and CaTs and their comparison with Paci2020 model, Paci2020 + Original rice CE model (i.e. before the calibration of the contractile element) and the experimental values (Paci et al., 2020; Paci, Pölonen, et al., 2018)

FIGURE 3 Simulated action potentials and ionic currents of the hiPSC-CM-CE model vs. Paci2020 (Paci et al., 2020) in spontaneous beating in the steady-state condition. (a) Membrane potential. (b) Fast Na^+ current (I_{Na}). (c) L-type Ca^{2+} current (I_{CaL}). (d) Transient outward K^+ current (I_{to}). (e) Rapid delayed rectifier K^+ current (I_{Kr}). (f) Cytosolic Ca^{2+} concentration (Ca_i). (g) $\text{Na}^+/\text{Ca}^{2+}$ exchanger (I_{NCX}). (h) Ca^{2+} release from sarcoplasmic reticulum (J_{RyR}). (i) Cytosolic Na^+ concentration (Na_i). (j) Sarcoplasmic Ca^{2+} concentration (Ca_{SR})



The hiPSC-CM-CE simulation results show that Bay-K 8644 prolongs the AP (Figure 5a) and brings an increase in cytosolic Ca^{2+} (Figure 5c), and thus an elevated active tension (Figure 5d). These findings are in line with the AP prolongation (Sicouri et al., 2007) and positive inotropic effect reported *in vitro* for Bay-K 8644 (Ruan et al., 2016).

As is observable in Figure 5d, in accord with reports classifying Verapamil as a negative inotropic drug in hiPSC-CMs (Ruan et al., 2016) and hV-CMs (Nguyen et al., 2017), our results correctly replicate Verapamil-induced effects on the mechanical outputs. Finally, the relaxation kinetics of the hiPSC-CM-CE model, analyzed using RT_{80} (time from peak contraction to 80% of relaxation), follows the experimental trends and ranges reported for commercial and lab-based hiPSC-CMs as illustrated in Figure 5e.

Concurring with experimental results, the induction of abnormalities in electrical repolarization (EADs) can occur due to the use of drugs known to block the I_{Kr} current, namely, the class III antiarrhythmic Dofetilide (Guo et al., 2011) and the abnormalities in diastolic depolarization

(DADs) can occur due to Isoproterenol (Novak et al., 2012). Those arrhythmogenic phenomena can also lead to contractile irregularities detectable in the form of aftercontractions, as has been shown previously in hV-CMs (Nguyen et al., 2017) and hiPSC-CMs (Novak et al., 2012). Figure 6 shows selected electrophysiologic and mechanical traces simulated by the hiPSC-CM-CE after we tuned its maximum conductances and currents with two different coefficient sets, namely SET1 and SET2, that had triggered EADs in the Paci2020 model, as response to 95% I_{Kr} block. Of note, the original Paci2020 model (as its predecessor Paci2018) responds to a strong I_{Kr} block with an extreme APD prolongation but no EADs (Paci, Koivumäki, et al., 2021; Paci, Pölonen, et al., 2018). However, experimentally calibrated populations of models generated by using Paci2020 or Paci2018 models contain models that can produce EAD as a response to I_{Kr} block or more in general during *in silico* tests of multichannel drugs with a substantial effect on hERG (Paci et al., 2018, 2020). As shown in Figure 6, 95% I_{Kr} block triggers EADs in SET1

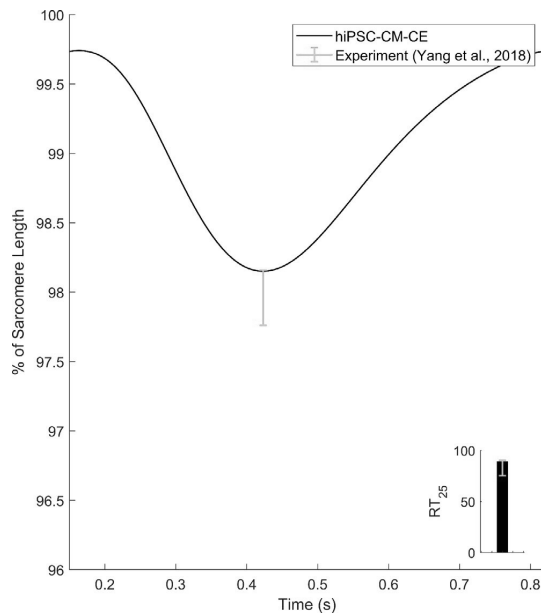


FIGURE 4 Percent of cell shortening and the contraction RT_{25} (time from peak contraction to 50% of relaxation) simulated by the hiPSC-CM-CE model

and SET2 and the consequent aftercontractions. In Figure 6, both in SET1 and SET2, we observe APD prolongation due to the I_{Kr} block and the subsequent alterations in CaTs due to anomalous Ca^{2+} releases from SR (see the arrows in J_{RyR}). On the one hand, these releases increase the cytosolic Ca^{2+} concentration, thus triggering aftercontractions. On the other hand, they activate the inward I_{NCX} that depolarizes the membrane potential during its repolarization, which triggers EADs (Paci et al., 2021; Priori & Corr, 1990; Szabo et al., 1994). In SET2, we even observe consecutive EADs and aftercontractions. In this case, the first inward I_{NCX} activation is so strong that triggers almost a full anticipated AP (blue arrows). Then, a second I_{NCX} activation triggers the second EADs, where we observe an I_{CaL} reactivation up to -0.22 A/F (green arrows). Furthermore, we replicated the Verapamil and Bay-K 8644 tests also on SET1 and SET2 (Figure S6), observing in both cases a negative inotropic effect for Verapamil and a positive inotropic effect for Bay-K 8644 consistent with the results in Figure 5.

3.4 | Exploring the impact of non-cardiomyocytes

The pivotal role of non-cardiomyocytes in the electromechanics of hiPSC-CMs, expressly the mechanical outputs,

has been confirmed previously (Iseoka et al., 2018). Here, following the biphasic trend in contraction–relaxation velocities observed for different ctn ratios in EHTs (Figure S7), we defined the CE passive force as a piecewise function (Equation 5). The implementation of a new passive force to the CE led to a correct categorization of the inotropic effects of non-cardiomyocytes (Figure 7). This is considered as an inter-scale analysis of the behavior of the hiPSC-CM tissues provided by the hiPSC-CM-CE simulations. In detail, inter-scale means that simulations were done based on a single cell (0D) framework simulating and predicting in a simple way the behavior of a multicellular (1D or 2D) domain.

When changing the ctn, the model simulated positive and negative inotropic effects according to the *in vitro* data reported in Iseoka et al. (2018) for contraction–relaxation velocity and cell deformation. The highest deformation distance, which also can represent the contractile force, was simulated for EHTs comprising 70% of cardiomyocytes (Figure 7a). Moreover, our results show that the contraction–relaxation velocities increase by increasing the cardiomyocyte portion (Figure 7b). Velocities simulated at 90% of ctn were smaller than those simulated for EHTs comprising 70% cardiomyocytes, as reported experimentally in Iseoka et al. (2018). Importantly, the model predicts the lowest contractile performance in accord with the reported non-cardiomyocyte effects indicating the highest inhibition of electrical propagation for ctn = 25% (Iseoka et al., 2018).

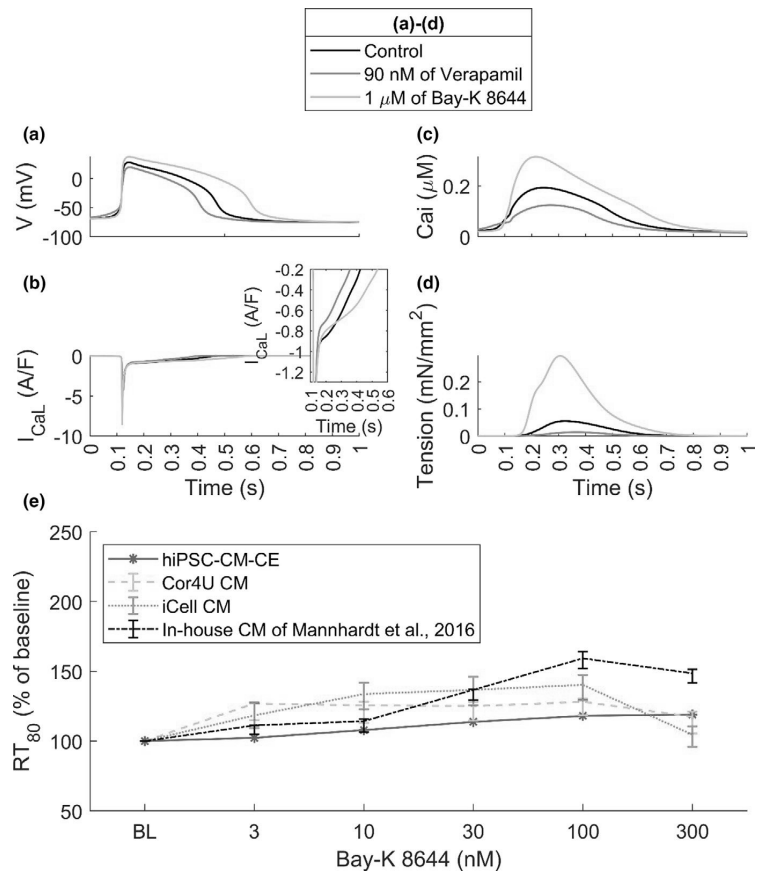
4 | DISCUSSION

This work proposes an electromechanical hiPSC-CM model obtained by coupling the Paci2020 ionic model, and the reparametrized Rice2008 CE model, while also adding a new passive force handling. The mechanical behavior of the model has been independently validated by key contraction protocols reported experimentally for hiPSC-CMs. Notably, the inotropic effect of different multichannel action reference drugs and arrhythmogenic effects, in terms of aftercontractions, have been accurately predicted by the hiPSC-CM-CE model. The simulations also correctly predicted the dynamics of the contribution of non-cardiomyocytes to hiPSC-CM tissues. Overall, this study provides a reliable mechanistic framework for future studies on hiPSC-CMs and the functions of immature cardiac cells.

4.1 | hiPSC-CM-CE electromechanics

The capability to simulate key *in vitro* AP and CaT biomarkers is necessary for *in silico* cardiomyocyte models.

FIGURE 5 Electrophysiology and contractility of the hiPSC-CM-CE in control and drug modes. (a) Action potentials. (b) L-type Ca^{2+} currents. (c) Cytosolic Ca^{2+} transients. (d) Active tensions. (e) RT_{80} (time from peak contraction to 80% of relaxation) results of the model in response to different concentrations of Bay-K 8644 and the in vitro data obtained from different hiPSC-CMs. Cor4U and iCell are commercial cardiomyocytes the data of which have been acquired from Mannhardt et al. (2016). Cases (a–d) show data at spontaneous condition, and case (e) shows the model results at 1.5 Hz pacing. BL: Baseline. Of note, the same tests presented in panels (a–d) were also performed in paced conditions (1 Hz), without observing noteworthy differences with the results presented in this figure



The hiPSC-CM-CE model recapitulates all the AP and CaT biomarkers within the experimental ranges reported in (Paci et al., 2020; Paci, Pöhlönen, et al., 2018). Furthermore, Table 3 signifies the impact of CE integration and reparameterization regarding the electrophysiological biomarkers. Notably, the reparameterization of the CE could restore the four electrophysiological biomarkers that were out-of-range when the original Rice CE was used instead of the reparameterized one.

The biochemical XB-related phenomena can be represented more accurately by the mathematical myofilament models consisting of many states, yet the computational cost is significant as well. Thus, maintaining a balance between biophysical accuracy and computational efficiency is the primary goal of current myofilament dynamic models. Given this, we selected Rice et al. (2008) model for this research as the essential calcium-based activation and sarcomere length-based sensitivity mechanisms are incorporated by this contractile machinery. A thorough review on this subject has been given earlier (Trayanova & Rice, 2011). Correspondingly, our main motivation to reparameterize the original Rice CE was enabling the model to

accurately recapitulate a broad range of electrophysiological and mechanical readouts as the Paci2020 + original Rice CE could not (Figure S4 and Table 3).

The assessment of the contractility is crucial when developing a mathematical cell model of cardiac electromechanics (Campbell et al., 2008; Forouzanmehr et al., 2020; Margara et al., 2020, 2021; Negroni et al., 2015; Pioner et al., 2020; Rice et al., 2008; Tran et al., 2017; Zile & Trayanova, 2017). In that context, the tension–SL relationship is not only a standard experimental protocol in myofilament studies (Negroni et al., 2015; Rice et al., 2008) but also serves as a measure for evaluating the CE mathematical models. The tension–SL relationship in Figure 2a shows that the reparameterized CE was able to replicate an improved tension–SL curve regarding the experimental ranges obtained for cat trabeculae.

Correspondingly, another key mechanical index here is fractional cell shortening (Figure 2b), which often is considered as a representative of the contractile capacity (Pioner et al., 2020). At 1 Hz pacing, the hiPSC-CM-CE has successfully developed % of cell shortening within the experimental range reported for hiPSC-CMs at 1.8 mM of

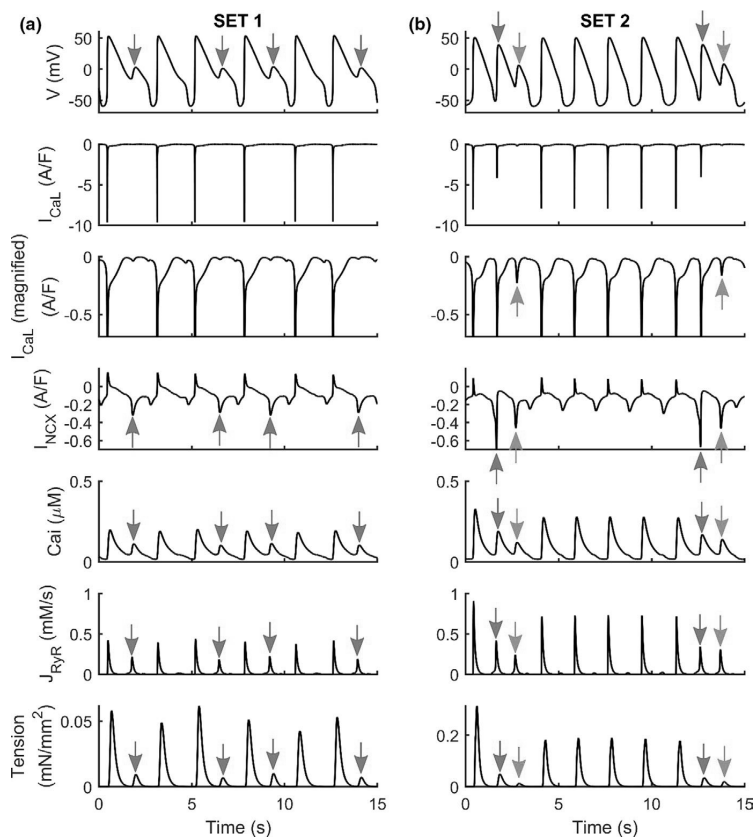


FIGURE 6 Action potentials, L-type Ca^{2+} currents (I_{CaL}), $\text{Na}^+/\text{Ca}^{2+}$ exchangers (I_{NCX}), Calcium Transients, Ca^{2+} releases from the sarcoplasmic reticulum (J_{RyR}), and active tensions simulated for two sets of parameters (SET1 and SET2) used to generate models which develop EADs (a) and (b), using hiPSC-CM-CE as baseline. Blue arrows show almost full anticipated APs due to the strong first inward I_{NCX} activation. Then, a second I_{NCX} activation triggers the second EADs where we observe an I_{CaL} reactivation up to -0.22 pA/pF (green arrows). The scales of tensions are different. In the third line, we show a magnification of the I_{CaL} traces, highlighting I_{CaL} reactivation

extracellular Ca^{2+} and 37. Also, the simulated times from peak contraction to 50 and 75% of relaxation (RT_{50} and RT_{25} , respectively), as measures for relaxation kinetics, show that the model sits within a desirable domain in terms of mechanical outputs and sarcomere dynamics. It is also worth mentioning that the hiPSC-CM-CE model simulates the tension magnitude within the hiPSC-CMs experimental range at 1.8 mM of extracellular Ca^{2+} and 37 (Figure 2c) (Ruan et al., 2016). These properties endorse the model as a capable mathematical base for future works on modeling contractility and the relevant dysfunctions.

Finally, another essential contractility index routinely reported in experimental myofilament studies (Hayakawa et al., 2014; Rodriguez et al., 2014) is referred to as motion waveform or contraction-relaxation velocity. Lately, the role of decreased relaxation velocity and prolonged relaxation duration in the characterization of diastolic dysfunction has been actively investigated (Hayakawa et al., 2014). Also, the study of cardiac pathologies such as ischaemic diseases, hypertension, and rare genetic disorders are associated with the contraction-relaxation velocity and duration (Hayakawa et al., 2014). The hiPSC-CM-CE replicates physiological contraction-relaxation

velocity profiles (Figure 2e) consistent with the experimental findings for hiPSC-CMs (Hayakawa et al., 2014; Rodriguez et al., 2014). Therefore, our model is suitable for simulating the effects of the aforementioned disorders as mentioned above on the contraction-relaxation velocity profiles.

The fundamental role of non-cardiomyocytes in the electromechanics, function, and therapeutic potential of hiPSC-CMs tissues has been proved (Iseoka et al., 2018). Notably, in producing functional hiPSC-derived EHTs as platforms in cardiac-regeneration therapy, the quantity of non-cardiomyocytes is vital. The hiPSC-CM EHTs comprising 50–70% of cardiomyocytes have shown stable structures and augmented the therapeutic potential (Iseoka et al., 2018). As an inter-scale capability, the hiPSC-CM-CE featuring this passive force simulated the contraction-relaxation velocity and cell shortening trends observed experimentally (Figure S7). This also indicates a correct classification of the inotropic effects of non-cardiomyocytes in hiPSC-CM tissues simulated on account of the new passive force introduced to the CE. Furthermore, the ctn-based variations in the simulated positive and negative inotropic effects for motion waveform

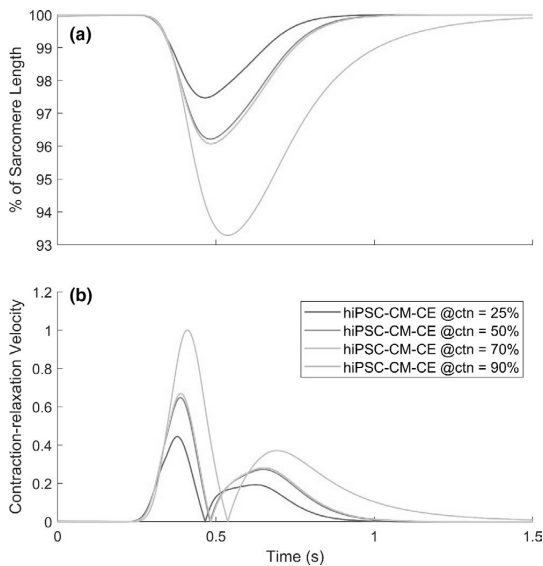


FIGURE 7 Simulated percent of cell shortenings (a) and (b) contraction–relaxation velocities at different percents of cardiomyocytes in the engineered heart tissue (ctns), normalized over the maximum value simulated for ctn = 70%

(Figure 7b) and fractional cell shortening (Figure 7a) are consistent with the corresponding experimental data reported in Iseoka et al. (2018). The model fittingly predicts the lowest contractile potential according to the underlying biophysics behind the non-cardiomyocyte effects demonstrating the highest inhibition of electrical propagation for ctn = 25% (Iseoka et al., 2018).

4.2 | hiPSC-CM-CE and drug-induced effects

The pharmaceutical industry and research consider the inotropic and pro-arrhythmic liabilities as their main concerns (Laverty et al., 2011). Congruently, evaluating the potentials of new drug candidates designed to target cardiac electromechanics is a must in the early phases of drug discovery (Nguyen et al., 2017). Computational approaches have been proved to be a promising opportunity for fast and inexpensive drug screenings and accurate prediction of clinical hazards (Li et al., 2019). Nevertheless, the inotropic risk assessments based on *in silico* approaches are greatly missing. To study the drug-induced influences on hiPSC-CMs electromechanics, we have presented a model validated against experimental data reported for relevant drugs. The correct classification of negative and positive inotropic outcomes for the selected reference compounds and the mechanism

behind the observed final contractility are captured by hiPSC-CM-CE simulations.

The chosen drugs in this study are reference compounds having different pro-arrhythmic profiles and distinguished clinical results. Verapamil is not classified by CredibleMeds (Woosley et al., 2021), and it is included in the “No TdP risk” category in the *in silico* model-based ranking by Passini et al. (2017) (Paci et al., 2020). Bay-K 8644 prolongs action potential duration resulting in prolongation of the QT interval (Sicouri et al., 2007) and is connected with an increase in TdP risk (Sicouri et al., 2010).

The electromechanical coupling correctly replicates the APD prolongation induced by Bay-K 8644. Consequently, an increase in cytosolic Ca^{2+} , and therefore an elevated active tension (Figure 5d) has also been correctly predicted by the model. These results are consistent with positive inotropic results reported for Bay-K 8644 (Ruan et al., 2016; Sicouri et al., 2007). Markedly, the hiPSC-CM-CE accurately predicts the prolonged relaxation due to Bay K-8644 (negative lusitropic effect). Of note, an essential indicator for proarrhythmic cardiotoxicity is the drug-induced upsurge in APD_{90} , the action potential duration at 90% of its repolarization (Mannhardt et al., 2016). The Bay K-8644 results simulated here, which follows the traces reported *in vitro* (Figure 5e), confirm that relaxation time RT_{80} of hiPSC-CMs might be a fit replacement parameter for repolarization time or APD_{90} , as also suggested earlier (Mannhardt et al., 2016).

Verapamil is a multichannel action compound blocking a number of currents, namely I_{Kr} , I_{CaL} , and I_{NaF} (Kramer et al., 2013). Markedly, the CaT is mainly affected by the I_{CaL} block (Figure 5b,c), leading to a negative inotropic effect (Figure 5d) which is consistent with experimental reports of inotropic effects of Verapamil in hiPSC-CMs (Ruan et al., 2016) and hV-CMs (Nguyen et al., 2017). Notably, the depressant effect of Verapamil on myocardial contractility pose a potential risk of using it for subjects having severe left ventricular dysfunction and, therefore, it is generally prohibited in such cases (Margara et al., 2021). The simulated Verapamil negative inotropic effect (Figure 5d and Figure S6) confirms this risk.

After contractions appear in cardiac tissues and trabeculae following dofetilide administration (Nguyen et al., 2017), as well as, in myocardial slices containing titin and collagen administered with isoproterenol (Watson et al., 2019). The EAD/DAD-induced mechanical response predicted by our model (Figure 6) closely matches the experimental findings reported for hV-CMs (Nguyen et al., 2017) and hiPSC-CMs (Novak et al., 2012). This makes hiPSC-CM-CE suitable to be the baseline for population-based studies aimed to assess

drug cardiotoxic effects on contractility, in addition to electrophysiology.

4.3 | Limitations and future works

While the model presented here captures some of the key electromechanical results of hiPSC-CMs, studying the intrinsic heterogeneity of myofilaments, which may differ in different known morphologies of hiPSC-CMs, needs further studies and simulations. Furthermore, the whole system has been implemented with ordinary differential equations (ODEs), i.e., the explicit considerations of spatial aspects have not been considered. To maintain an implementable system of ODEs, the CE model involves approximations. However, the approximations considered in Ca^{2+} -based myofilament activation and mean XB strains are used to fill the gap due to spatial scales, including local interactions, which are important but cannot be explicitly modeled by mean-field approaches. The tension–SL relationship of the skinned version of CE was the only result that has been compared against the experimental data of cat trabeculae due to the lack of corresponding data for hiPSC-CMs.

Although our inter-scale analysis shows that the hiPSC-CM-CE model accurately predicts the inotropic effects of non-cardiomyocytes in hiPSC-CMs tissues, it is still a simplification of the actual system as accounting for the effect of heterogeneous hiPSC-CMs substrates, and myosin expression in tissues requires a more comprehensive modeling framework.

There are other recent ionic models of hiPSC-CMs (Kernik et al., 2019; Koivumäki et al., 2018) for which observing the effect of integrating the novel CE would be of interest, as the three models were already compared for their responses to drugs in Paci, Koivumäki, et al. (2021). However, we consider it out of the scope of this paper because of the following reasons. The intracellular compartmentalization of the Koivumäki2018 would make the CE integration extremely complex. Conversely, the Kernik2019 model shares the same compartmentalization of the Paci2020 model. However, the CE integration would still present specific challenges due to differences in the Ca^{2+} handling between the Paci2020 and the Kernik2019 models. The latter simulates a 2.5 times higher CaT peak and a 50% greater I_{CaL} amplitude. Considering the non-linearity of Ca^{2+} cooperation and sensitivity in the CE, a different reparameterization would be needed. Simply adding the current reparameterization of the Rice CE to the Kernik2019 model would just result in an electromechanical model whose simulated results are not consistent with experimental ranges.

5 | CONCLUSIONS

Throughout the literature, the bulk of research in mathematical modeling for cardiomyocytes has been focused on electrophysiology. Specifically, excitation–contraction coupling in the myocardium or the association of the electrical and the mechanical parties has garnered less attention. hiPSC-CMs are instrumental in developing patient-specific models and cardiotoxicity tests at the cell level. Therefore, we have proposed a genuine electromechanical hiPSC-CM model named hiPSC-CM-CE. Notably, fractional cell shortening, contraction RT_{50} , the amplitude of tension, and the inotropic effect of non-cardiomyocytes have been recapitulated within experimental ranges by the hiPSC-CM-CE. Lastly, the drug-induced arrhythmogenic and inotropic effects and the aftercontractions due to triggered EADs have been simulated and validated against experimental data. The current model is a capable tool for extensions and translations of the findings toward *in silico* and *in vitro* in tissue- and organ-level.


ACKNOWLEDGMENTS

Mohamadamin Forouzandehmehr was supported by the graduate school of Faculty of Medicine and Health Technology, Tampere University. Dr. Michelangelo Paci was supported by the Finnish Cultural Foundation (decisions 160735 and 210813). Dr. Jussi Koivumäki was supported by Academy of Finland Centre of Excellence in Body-on-Chip Research and Pirkanmaa regional fund of the Finnish Cultural Foundation (grant numbers 50171514 and 50201322).

CONFLICT OF INTEREST

The authors declare no conflict of interests.

ORCID

Mohamadamin Forouzandehmehr  <https://orcid.org/0000-0001-7568-3860>

REFERENCES

- Ahola, A., Pölonen, R. P., Aalto-Setälä, K., & Hyttinen, J. (2018). Simultaneous measurement of contraction and calcium transients in stem cell derived cardiomyocytes. *Annals of Biomedical Engineering*, 46(1), 148–158. <https://doi.org/10.1007/s10439-017-1933-2>
- Amani, A., Shamlou, A., Barzegar, S., & Forouzandehmehr, M. (2021). Effect of material and population on the delivery of nanoparticles to an atherosclerotic plaque: A patient-specific *In Silico* Study. *Langmuir*, 37, 1551–1562. <https://doi.org/10.1021/acs.langmuir.0c03158>
- Bartolucci, C., Passini, E., Hyttinen, J., Paci, M., & Severi, S. (2020). Simulation of the effects of extracellular calcium changes leads to a novel computational model of human ventricular

- action potential with a revised calcium handling. *Frontiers in Physiology*, *11*, 314. <https://doi.org/10.3389/fphys.2020.00314>
- Bechem, M., & Hoffmann, H. (1993). The molecular mode of action of the Ca agonist (-) BAY K 8644 on the cardiac Ca channel. *Pflügers Archiv European Journal of Physiology*, *424*, 343–353. <https://doi.org/10.1007/BF00384362>
- Blanchard, E., Seidman, C., Seidman, J. G., LeWinter, M., & Maughan, D. (1999). Altered crossbridge kinetics in the α MHC 403/+ mouse model of familial hypertrophic cardiomyopathy. *Circulation Research*, *84*, 475–483.
- Campbell, S. G., Flaim, S. N., Leem, C. H., & McCulloch, A. D. (2008). Mechanisms of transmurally varying myocyte electromechanics in an integrated computational model. *Philosophical Transactions of the Royal Society A: Mathematical, Physical and Engineering Sciences*, *366*(1879), 3361–3380. <https://doi.org/10.1098/rsta.2008.0088>
- Campbell, S. G., Lionetti, F. V., Campbell, K. S., & McCulloch, A. D. (2010). Coupling of adjacent tropomyosins enhances cross-bridge-mediated cooperative activation in a markov model of the cardiac thin filament. *Biophysical Journal*, *98*, 2254–2264. <https://doi.org/10.1016/j.bpj.2010.02.004>
- Clark, J. A., Sewanan, L. R., Schwan, J., Kluger, J., Campbell, K. S., & Campbell, S. G. (2021). Fast-relaxing cardiomyocytes exert a dominant role in the relaxation behavior of heterogeneous myocardium. *Archives of Biochemistry and Biophysics*, *697*, 108711. <https://doi.org/10.1016/j.abb.2020.108711>
- De Tombe, P. P., & Ter Keurs, H. E. D. J. (1991). Sarcomere dynamics in cat cardiac trabeculae. *Circulation Research*, *68*(2), 588–596. <https://doi.org/10.1161/01.RES.68.2.588>
- de Tombe, P. P., & ter Keurs, H. E. (1992). An internal viscous element limits unloaded velocity of sarcomere shortening in rat myocardium. *Journal of Physiology*, *454*(1), 619–642. <https://doi.org/10.1113/jphysiol.1992.sp019283>
- Forouzandehmehr, M., Cogno, N., Koivumäki, J., Hyttinen, J., & Paci, M. (2020). *The Comparison Between Two Mathematical Contractile Elements Integrated into an hiPSC-CM In-silico Model*. In *Computing in Cardiology*. <http://www.cinc.org/archives/2020/pdf/CinC2020-055.pdf>
- Forouzandehmehr, M., & Shamloo, A. (2018). Margination and adhesion of micro- and nanoparticles in the coronary circulation: A step towards optimised drug carrier design. *Biomechanics and Modeling in Mechanobiology*, *17*(1), 205–221. <https://doi.org/10.1007/s10237-017-0955-x>
- Forouzandehmehr, M., & Shamloo, A. (2021). High haematocrit blood flow and adsorption of micro- and nanoparticles on an atherosclerotic plaque: An in-silico study. *Current Drug Delivery*, *18*. <https://doi.org/10.2174/156720181866621031611458>
- Grandi, E., Pasqualini, F. S., & Bers, D. M. (2010). A novel computational model of the human ventricular action potential and Ca transient. *Journal of Molecular and Cellular Cardiology*, *48*(1), 112–121. <https://doi.org/10.1016/j.yjmcc.2009.09.019>
- Guo, D., Liu, Q., Liu, T., Elliott, G., Gingras, M., Kowey, P. R., & Yan, G. X. (2011). Electrophysiological properties of HBI-3000: A new antiarrhythmic agent with multiple-channel blocking properties in human ventricular myocytes. *Journal of Cardiovascular Pharmacology*, *57*(1), 79–85. <https://doi.org/10.1097/FJC.0b013e3181ffe8b3>
- Hayakawa, T., Kunihiro, T., Ando, T., Kobayashi, S., Matsui, E., Yada, H., Kanda, Y., Kurokawa, J., & Furukawa, T. (2014). Image-based evaluation of contraction-relaxation kinetics of human-induced pluripotent stem cell-derived cardiomyocytes: Correlation and complementarity with extracellular electrophysiology. *Journal of Molecular and Cellular Cardiology*, *77*, 178–191. <https://doi.org/10.1016/j.yjmcc.2014.09.010>
- Hossain, S. S., Hughes, T. J., & Decuzzi, P. (2014). Vascular deposition patterns for nanoparticles in an inflamed patient-specific arterial tree. *Biomechanics and Modeling in Mechanobiology*, *13*, 585–597.
- Iseoka, H., Miyagawa, S., Fukushima, S., Saito, A., Masuda, S., Yajima, S., Ito, E., Sougawa, N., Takeda, M., Harada, A., Lee, J.-K., & Sawa, Y. (2018). Pivotal role of non-cardiomyocytes in electromechanical and therapeutic potential of induced pluripotent stem cell-derived engineered cardiac tissue. *Tissue Engineering Part A*, *24*, 287–300. <https://doi.org/10.1089/ten.tea.2016.0535>
- Kernik, D. C., Morotti, S., Wu, H., Garg, P., Duff, H. J., Kurokawa, J., Jalife, J., Wu, J. C., Grandi, E., & Clancy, C. E. (2019). A computational model of induced pluripotent stem-cell derived cardiomyocytes incorporating experimental variability from multiple data sources. *Journal of Physiology*, *597*, 4533–4564. <https://doi.org/10.1113/JP277724>
- Koivumäki, J. T., Naumenko, N., Tuomainen, T., Takalo, J., Oksanen, M., Puttonen, K. A., Lehtonen, Š., Kuusisto, J., Laakso, M., Koistinaho, J., & Tavi, P. (2018). Structural immaturity of human iPSC-derived cardiomyocytes: In silico investigation of effects on function and disease modeling. *Frontiers in Physiology*, *9*. <https://doi.org/10.3389/fphys.2018.00080>
- Kramer, J., Obejero-Paz, C. A., Myatt, G., Kuryshev, Y. A., Bruening-Wright, A., Verducci, J. S., & Brown, A. M. (2013). MICE models: Superior to the HERG model in predicting torsade de pointes. *Scientific Reports*, *3*, 2100. <https://doi.org/10.1038/srep02100>
- Kreutziger, K. L., Piroddi, N., McMichael, J. T., Tesi, C., Poggesi, C., & Regnier, M. (2011). Calcium binding kinetics of troponin C strongly modulate cooperative activation and tension kinetics in cardiac muscle. *Journal of Molecular and Cellular Cardiology*, *50*, 165–174. <https://doi.org/10.1016/j.yjmcc.2010.10.025>
- Land, S., & Niederer, S. A. (2015). A Spatially detailed model of isometric contraction based on competitive binding of troponin I explains cooperative interactions between tropomyosin and crossbridges. *PLoS Computational Biology*, *11*(8), e1004376. <https://doi.org/10.1371/journal.pcbi.1004376>
- Land, S., Niederer, S. A., Aronsen, J. M., Espe, E. K. S., Zhang, L., Louch, W. E., Sjaastad, I., Sejersted, O. M., & Smith, N. P. (2012). An analysis of deformation-dependent electromechanical coupling in the mouse heart. *Journal of Physiology*, *590*(18), 4553–4569. <https://doi.org/10.1113/jphysiol.2012.231928>
- Land, S., Niederer, S. A., Louch, W. E., Sejersted, O. M., & Smith, N. P. (2013). Integrating multi-scale data to create a virtual physiological mouse heart. *Interface Focus*, *3*(2), 20120076. <https://doi.org/10.1098/rsfs.2012.0076>
- Land, S., Park-Holohan, S. J., Smith, N. P., dos Remedios, C. G., Kentish, J. C., & Niederer, S. A. (2017). A model of cardiac contraction based on novel measurements of tension development in human cardiomyocytes. *Journal of Molecular and Cellular Cardiology*, *106*, 68–83. <https://doi.org/10.1016/j.yjmcc.2017.03.008>
- Lavery, H. G., Benson, C., Cartwright, E. J., Cross, M. J., Garland, C., Hammond, T., Holloway, C., McMahon, N., Milligan, J., Park, B. K., Pirmohamed, M., Pollard, C., Radford, J., Roome,

- N., Sager, P., Singh, S., Suter, T., Suter, W., Trafford, A., ... Valentin, J. P. (2011). How can we improve our understanding of cardiovascular safety liabilities to develop safer medicines? *British Journal of Pharmacology*, *163*, 675–693. <https://doi.org/10.1111/j.1476-5381.2011.01255.x>
- Li, Z., Ridder, B. J., Han, X., Wu, W. W., Sheng, J., Tran, P. N., Wu, M., Randolph, A., Johnstone, R. H., Mirams, G. R., Kuryshv, Y., Kramer, J., Wu, C., Crumb, W. J., & Strauss, D. G. (2019). Assessment of an in silico mechanistic model for proarrhythmia risk prediction under the Ci PA initiative. *Clinical Pharmacology and Therapeutics*, *105*, 466–475.
- Mannhardt, I., Breckwoldt, K., Letuffe-Brenière, D., Schaaf, S., Schulz, H., Neuber, C., Benzin, A., Werner, T., Eder, A., Schulze, T., Klampe, B., Christ, T., Hirt, M. N., Huebner, N., Moretti, A., Eschenhagen, T., & Hansen, A. (2016). Human engineered heart tissue: Analysis of contractile force. *Stem Cell Reports*, *7*, 29–42. <https://doi.org/10.1016/j.stemcr.2016.04.011>
- Margara, F., Wang, Z. J., Bueno-Orovio, A., & Rodriguez, B. (2020). Human ventricular modelling and simulation of drug action on electrophysiology and contraction. (pp. 1–4). In *2020 computing in cardiology*.
- Margara, F., Wang, Z. J., Levrero-Florencio, F., Santiago, A., Vázquez, M., Bueno-Orovio, A., & Rodriguez, B. (2021). In-silico human electro-mechanical ventricular modelling and simulation for drug-induced pro-arrhythmia and inotropic risk assessment. *Progress in Biophysics and Molecular Biology*, *159*, 58–74. <https://doi.org/10.1016/j.pbiomolbio.2020.06.007>
- Muller, K., Fedosov, D. A., & Gompper, G. (2014). Margination of micro- and nano-particles in blood flow and its effect on drug delivery. *Scientific Reports*, *4*, 4871.
- Negróni, J. A., & Lascano, E. C. (2008). Simulation of steady state and transient cardiac muscle response experiments with a Huxley-based contraction model. *Journal of Molecular and Cellular Cardiology*, *45*, 300–312. <https://doi.org/10.1016/j.yjmcc.2008.04.012>
- Negróni, J. A., Morotti, S., Lascano, E. C., Gomes, A. V., Grandi, E., Puglisi, J. L., & Bers, D. M. (2015). β -adrenergic effects on cardiac myofilaments and contraction in an integrated rabbit ventricular myocyte model. *Journal of Molecular and Cellular Cardiology*, *81*, 162–175. <https://doi.org/10.1016/j.yjmcc.2015.02.014>
- Nguyen, N., Nguyen, W., Nguyenton, B., Ratchada, P., Page, G., Miller, P. E., Ghetti, A., & Abi-Gerges, N. (2017). Adult human primary cardiomyocyte-based model for the simultaneous prediction of drug-induced inotropic and pro-arrhythmia risk. *Frontiers in Physiology*, *8*, 1073. <https://doi.org/10.3389/fphys.2017.01073>
- Niederer, S. A., Hunter, P. J., & Smith, N. P. (2006). A quantitative analysis of cardiac myocyte relaxation: A simulation study. *Biophysical Journal*, *90*, 1697–1722.
- Niederer, S. A., & Smith, N. P. (2009). The role of the Frank–Starling law in the transduction of cellular work to whole organ pump function: A computational modeling analysis. *PLoS Computational Biology*, *5*(4), e1000371. <https://doi.org/10.1371/journal.pcbi.1000371>
- Novak, A., Barad, L., Zeevi-Levin, N., Shick, R., Shtrichman, R., Lorber, A., Itskovitz-Eldor, J., & Binah, O. (2012). Cardiomyocytes generated from CPVT307H patients are arrhythmogenic in response to β -adrenergic stimulation. *Journal of Cellular and Molecular Medicine*, *16*, 468–482. <https://doi.org/10.1111/j.1582-4934.2011.01476.x>
- O'Hara, T., Virág, L., Varró, A., & Rudy, Y. (2011). Simulation of the undiseased human cardiac ventricular action potential: Model formulation and experimental validation. *PLoS Computational Biology*, *7*(5), e1002061. <https://doi.org/10.1371/journal.pcbi.1002061>
- Paci, M., Casini, S., Bellin, M., Hyttinen, J., & Severi, S. (2018). Large-scale simulation of the phenotypical variability induced by loss-of-function long QT mutations in human induced pluripotent stem cell cardiomyocytes. *International Journal of Molecular Sciences*, *19*, 3583. <https://doi.org/10.3390/ijms19113583>
- Paci, M., Hyttinen, J., Aalto-Setälä, K., & Severi, S. (2013). Computational models of ventricular-and atrial-like human induced pluripotent stem cell derived cardiomyocytes. *Annals of Biomedical Engineering*, *41*(11), 2334–2348. <https://doi.org/10.1007/s10439-013-0833-3>
- Paci, M., Koivumäki, J. T., Lu, H. R., Gallacher, D. J., Passini, E., & Rodriguez, B. (2021). Comparison of the simulated response of three in silico human stem cell-derived cardiomyocytes models and in vitro data under 15 drug actions. *Frontiers in Pharmacology*, *12*. <https://doi.org/10.3389/fphar.2021.604713>
- Paci, M., Passini, E., Klimas, A., Severi, S., Hyttinen, J., Rodriguez, B., & Entcheva, E. (2020). All-optical electrophysiology refines populations of in silico human iPSC-CMs for drug evaluation. *Biophysical Journal*, *118*(10), 2596–2611. <https://doi.org/10.1016/j.bpj.2020.03.018>
- Paci, M., Penttinen, K., Pekkanen-Mattila, M., & Koivumäki, J. T. (2021). Arrhythmia mechanisms in human induced pluripotent stem cell-derived cardiomyocytes. *Journal of Cardiovascular Pharmacology*, *77*, 300–316. <https://doi.org/10.1097/FJC.0000000000000972>
- Paci, M., Pölonen, R. P., Cori, D., Penttinen, K., Aalto-Setälä, K., Severi, S., & Hyttinen, J. (2018). Automatic optimization of an in silico model of human iPSC derived cardiomyocytes recapitulating calcium handling abnormalities. *Frontiers in Physiology*, *9*. <https://doi.org/10.3389/fphys.2018.00709>
- Palmer, B. M., Fishbaugher, D. E., Schmitt, J. P., Wang, Y., Alpert, N. R., Seidman, C. E., Seidman, J. G., VanBuren, P., & Maughan, D. W. (2004). Differential cross-bridge kinetics of FHC myosin mutations R403Q and R453C in heterozygous mouse myocardium. *American Journal of Physiology-Heart and Circulatory Physiology*, *287*, H91–H99. <https://doi.org/10.1152/ajpheart.01015.2003>
- Passini, E., Britton, O. J., Lu, H. R., Rohrbacher, J., Hermans, A. N., Gallacher, D. J., Greig, R. J. H., Bueno-Orovio, A., & Rodriguez, B. (2017). Human in silico drug trials demonstrate higher accuracy than animal models in predicting clinical proarrhythmic cardiotoxicity. *Frontiers in Physiology*, *8*. <https://doi.org/10.3389/fphys.2017.00668>
- Pioner, J. M., Guan, X., Klaiman, J. M., Racca, A. W., Pabon, L., Muskheili, V., Macadangdang, J., Ferrantini, C., Hoopmann, M. R., Moritz, R. L., Kim, D. H., Tesi, C., Poggesi, C., Murry, C. E., Childers, M. K., Mack, D. L., & Regnier, M. (2020). Absence of full-length dystrophin impairs normal maturation and contraction of cardiomyocytes derived from human-induced pluripotent stem cells. *Cardiovascular Research*, *116*(2), 368–382. <https://doi.org/10.1093/cvr/cvz109>
- Priori, S. G., & Corr, P. B. (1990). Mechanisms underlying early and delayed afterdepolarizations induced by catecholamines. *American Journal of Physiology-Heart and Circulatory*

- Physiology*, 258, H1796–H1805. <https://doi.org/10.1152/ajpheart.1990.258.6.H1796>
- Rae, G. A., & Calixto, J. B. (1989). Interactions of calcium antagonists and the calcium channel agonist Bay K 8644 on neurotransmission of the mouse isolated vas deferens. *British Journal of Pharmacology*, 96, 333–340. <https://doi.org/10.1111/j.1476-5381.1989.tb11822.x>
- Rice, J. J., Wang, F., Bers, D. M., & De Tombe, P. P. (2008). Approximate model of cooperative activation and crossbridge cycling in cardiac muscle using ordinary differential equations. *Biophysical Journal*, 95(5), 2368–2390. <https://doi.org/10.1529/biophysj.107.119487>
- Rodriguez, M. L., Graham, B. T., Pabon, L. M., Han, S. J., Murry, C. E., & Sniadecki, N. J. (2014). Measuring the contractile forces of human induced pluripotent stem cell-derived cardiomyocytes with arrays of microposts. *Journal of Biomechanical Engineering*, 136(5). <https://doi.org/10.1115/1.4027145>
- Romero, L., Carbonell, B., Trenor, B., Rodriguez, B., Saiz, J., & Ferrero, J. M. (2011). Systematic characterization of the ionic basis of rabbit cellular electrophysiology using two ventricular models. *Progress in Biophysics and Molecular Biology*, 107, 60–73. <https://doi.org/10.1016/j.pbiomolbio.2011.06.012>
- Ruan, J. L., Tulloch, N. L., Razumova, M. V., Saiget, M., Muskheli, V., Pabon, L., Reinecke, H., Regnier, M., & Murry, C. E. (2016). Mechanical stress conditioning and electrical stimulation promote contractility and force maturation of induced pluripotent stem cell-derived human cardiac tissue. *Circulation*, 134(20), 1557–1567. <https://doi.org/10.1161/CIRCULATIONAHA.114.014998>
- Shamloo, A., Amani, A., Forouzandehmehr, M., & Ghoytasi, I. (2019). In silico study of patient-specific magnetic drug targeting for a coronary LAD atherosclerotic plaque. *International Journal of Pharmaceutics*, 559, 113–129. <https://doi.org/10.1016/j.ijpharm.2018.12.088>
- Shamloo, A., & Forouzandehmehr, M. (2019). Personalised deposition maps for micro- and nanoparticles targeting an atherosclerotic plaque: Attributions to the receptor-mediated adsorption on the inflamed endothelial cells. *Biomechanics and Modeling in Mechanobiology*, 18(3), 813–828. <https://doi.org/10.1007/s10237-018-01116-y>
- Sheikh, F., Ouyang, K., Campbell, S. G., Lyon, R. C., Chuang, J., Fitzsimons, D., Tangney, J., Hidalgo, C. G., Chung, C. S., Cheng, H., Dalton, N. D., Gu, Y., Kasahara, H., Ghassemian, M., Omens, J. H., Peterson, K. L., Granzier, H. L., Moss, R. L., McCulloch, A. D., & Chen, J. U. (2012). Mouse and computational models link Mlc2v dephosphorylation to altered myosin kinetics in early cardiac disease. *Journal of Clinical Investigation*, 122(4), 1209–1221. <https://doi.org/10.1172/JCI61134>
- Sicouri, S., Glass, A., Ferreiro, M., & Antzelevitch, C. (2010). Transseptal dispersion of repolarization and its role in the development of torsade de pointes arrhythmias. *Journal of Cardiovascular Electrophysiology*, 21, 441–447. <https://doi.org/10.1111/j.1540-8167.2009.01641.x>
- Sicouri, S., Timothy, K. W., Zygmunt, A. C., Glass, A., Goodrow, R. J., Belardinelli, L., & Antzelevitch, C. (2007). Cellular basis for the electrocardiographic and arrhythmic manifestations of Timothy syndrome: Effects of ranolazine. *Hear Rhythm*, 4, 638–647. <https://doi.org/10.1016/j.hrthm.2006.12.046>
- Strauss, D. G., Gintant, G., Li, Z., Wu, W., Blinova, K., Vicente, J., Turner, J. R., & Sager, P. T. (2019). Comprehensive In vitro proarrhythmia assay (CiPA) update from a Cardiac Safety Research Consortium/Health and Environmental Sciences Institute/FDA Meeting. *Therapeutic Innovation & Regulatory Science*, 53(4), 519–525. <https://doi.org/10.1177/2168479018795117>
- Stuyvers, B. D., McCulloch, A. D., Guo, J., Duff, H. J., & Keurs, H. E. D. J. (2002). Effect of stimulation rate, sarcomere length and Ca²⁺ on force generation by mouse cardiac muscle. *Journal of Physiology*, 544, 817–830.
- Szabo, B., Sweidan, R., Rajagopalan, C. V., & Lazzara, R. (1994). Role of Na⁺: Ca²⁺ exchange current in Cs⁺-induced early afterdepolarizations in purkinje fibers. *Journal of Cardiovascular Electrophysiology*, 5, 933–944.
- Ten Tusscher, K. H. W. J., & Panfilov, A. V. (2006). Alternans and spiral breakup in a human ventricular tissue model. *American Journal of Physiology-Heart and Circulatory Physiology*, 291(3), H1088–H1100. <https://doi.org/10.1152/ajpheart.00109.2006>
- Tomek, J., Bueno-Orovio, A., Passini, E., Zhou, X., Mincholé, A., Britton, O., Bartolucci, C., Severi, S., Shrier, A., Virag, L., Varro, A., & Rodriguez, B. (2019). Development, calibration, and validation of a novel human ventricular myocyte model in health, disease, and drug block. *Elife*, 8. <https://doi.org/10.7554/eLife.48890>
- Tran, K., Han, J.-C., Crampin, E. J., Taberner, A. J., & Loiselle, D. S. (2017). Experimental and modelling evidence of shortening heat in cardiac muscle. *Journal of Physiology*, 595, 6313–6326. <https://doi.org/10.1113/JP274680>
- Trayanova, N. A., & Rice, J. J. (2011). Cardiac electromechanical models: From cell to organ. *Frontiers in Physiology*, 2. <https://doi.org/10.3389/fphys.2011.00043>
- Watson, S. A., Duff, J., Bardi, I., Zabielska, M., Atanur, S. S., Jabbour, R. J., Simon, A., Tomas, A., Smolenski, R. T., Harding, S. E., Perbellini, F., & Terracciano, C. M. (2019). Biomimetic electromechanical stimulation to maintain adult myocardial slices in vitro. *Nature Communications*, 10, 2168. <https://doi.org/10.1038/s41467-019-10175-3>
- Woolsey, R. L., Heise, C. W., & Romero, K. A. (2021). QTdrugs List. <https://crediblemeds.org/>
- Yang, K.-C., Breitbart, A., De Lange, W. J., Hofsteen, P., Futakuchi-Tsuchida, A., Xu, J., Schopf, C., Razumova, M. V., Jiao, A., Boucek, R., Pabon, L., Reinecke, H., Kim, D.-H., Ralphe, J. C., Regnier, M., & Murry, C. E. (2018). Novel adult-onset systolic cardiomyopathy due to MYH7 E848G mutation in patient-derived induced pluripotent stem cells. *JACC Basic to Translational Science*, 3, 728–740.
- Zile, M. A., & Trayanova, N. A. (2016). Rate-dependent force, intracellular calcium, and action potential voltage alternans are modulated by sarcomere length and heart failure induced-remodeling of thin filament regulation in human heart failure: A myocyte modeling study. *Progress in Biophysics and Molecular Biology*, 120, 270–280. <https://doi.org/10.1016/j.pbiomolbio.2015.12.012>
- Zile, M. A., & Trayanova, N. A. (2017). Myofilament protein dynamics modulate EAD formation in human hypertrophic cardiomyopathy. *Progress in Biophysics and Molecular Biology*, 130, 418–428. <https://doi.org/10.1016/j.pbiomolbio.2017.06.015>
- Zile, M. A., & Trayanova, N. A. (2018). Increased thin filament activation enhances alternans in human chronic atrial fibrillation. *American Journal of Physiology-Heart and Circulatory*

Physiology, 315, H1453–H1462. <https://doi.org/10.1152/ajpheart.00658.2017>

SUPPORTING INFORMATION

Additional supporting information may be found in the online version of the article at the publisher's website.

How to cite this article: Forouzandehmehr, M., Koivumäki, J. T., Hyttinen, J., & Paci, M. (2021). A mathematical model of hiPSC cardiomyocytes electromechanics. *Physiological Reports*, 9, e15124. <https://doi.org/10.14814/phy2.15124>

PUBLICATION III

Altered contractility in mutation-specific hypertrophic cardiomyopathy: A mechano-energetic *in silico* study with pharmacological insights

Mohamadamin Forouzandehmehr, Michelangelo Paci, Jussi T. Koivumäki, Jari Hyttinen,

Front. Physiol. 13 (2022). doi:10.3389/fphys.2022.1010786.

Publication reprinted under the terms of the Creative Commons Attribution License (CC BY 4.0).



OPEN ACCESS

EDITED BY

Simone Scacchi,
University of Milan, Italy

REVIEWED BY

Serdar Göktepe,
Middle East Technical University, Turkey
Guido Caluori,
INSERM Institut de Rythmologie et
Modélisation Cardiaque (IHU-Liryc),
France

*CORRESPONDENCE

Mohamadamin Forouzandehmehr,
mohamadamin.forouzandehmehr@
tuni.fi

SPECIALTY SECTION

This article was submitted to
Computational Physiology and
Medicine,
a section of the journal
Frontiers in Physiology

RECEIVED 03 August 2022

ACCEPTED 14 October 2022

PUBLISHED 31 October 2022

CITATION

Forouzandehmehr M, Paci M,
Koivumäki JT and Hyttinen J (2022),
Altered contractility in mutation-
specific hypertrophic cardiomyopathy:
A mechano-energetic *in silico* study
with pharmacological insights.
Front. Physiol. 13:1010786.
doi: 10.3389/fphys.2022.1010786

COPYRIGHT

© 2022 Forouzandehmehr, Paci,
Koivumäki and Hyttinen. This is an
open-access article distributed under
the terms of the Creative Commons
Attribution License (CC BY). The use,
distribution or reproduction in other
forums is permitted, provided the
original author(s) and the copyright
owner(s) are credited and that the
original publication in this journal is
cited, in accordance with accepted
academic practice. No use, distribution
or reproduction is permitted which does
not comply with these terms.

Altered contractility in mutation-specific hypertrophic cardiomyopathy: A mechano-energetic *in silico* study with pharmacological insights

Mohamadamin Forouzandehmehr*, Michelangelo Paci,
Jussi T Koivumäki and Jari Hyttinen

Faculty of Medicine and Health Technology, Tampere University, Tampere, Finland

Introduction: Mavacamten (MAVA), Blebbistatin (BLEB), and Omecamtiv mecarbil (OM) are promising drugs directly targeting sarcomere dynamics, with demonstrated efficacy against hypertrophic cardiomyopathy (HCM) in (pre) clinical trials. However, the molecular mechanism affecting cardiac contractility regulation, and the diseased cell mechano-energetics are not fully understood yet.

Methods: We present a new metabolite-sensitive computational model of human induced pluripotent stem cell-derived cardiomyocytes (hiPSC-CMs) electromechanics to investigate the pathology of R403Q HCM mutation and the effect of MAVA, BLEB, and OM on the cell mechano-energetics.

Results: We offer a mechano-energetic HCM calibration of the model, capturing the prolonged contractile relaxation due to R403Q mutation (~33%), without assuming any further modifications such as an additional Ca^{2+} flux to the thin filaments. The HCM model variant correctly predicts the negligible alteration in ATPase activity in R403Q HCM condition compared to normal hiPSC-CMs. The simulated inotropic effects of MAVA, OM, and BLEB, along with the ATPase activities in the control and HCM model variant agree with *in vitro* results from different labs. The proposed model recapitulates the tension- Ca^{2+} relationship and action potential duration change due to $1\mu M$ OM and $5\mu M$ BLEB, consistently with *in vitro* data. Finally, our model replicates the experimental dose-dependent effect of OM and BLEB on the normalized isometric tension.

Conclusion: This work is a step toward deep-phenotyping the mutation-specific HCM pathophysiology, manifesting as altered interfilament kinetics. Accordingly, the modeling efforts lend original insights into the MAVA, BLEB, and OM contributions to a new interfilament balance resulting in a cardioprotective effect.

KEYWORDS

in silico modeling, human stem cell-derived cardiomyocyte, action potential, immature cardiomyocytes, cardiac metabolism, hypertrophic cardiomyopathy, pharmacology

Introduction

With a prevalence ranging from 1/500 to 1/200 (Semsarian et al., 2015; Malhotra and Sharma, 2017), HCM represents the most prevalent genetic cardiac disorder mainly associated with pathogenic variants in sarcomere protein genes (Santini et al., 2020). Pathologies such as myocardium hypercontractility (Sarkar et al., 2020), impaired relaxation (Toepfer et al., 2020), elevated cardiac energy consumption, diastolic dysfunction, arrhythmogenesis, and heart failure (Sarkar et al., 2020) manifest due to such variants. The driver of the cyclic interactions between thin and thick filaments is the ATP hydrolysis by myosin—the enzymatic motor of sarcomere (Spudich, 2014). In HCM, myosin binding protein C and adult cardiac myosin isoforms (primarily encoded by MYBPS3 and MYH7 genes, respectively) host most of these pathogenic variants in sarcomere (Ho et al., 2018; Toepfer et al., 2019; Schmid and Toepfer, 2021).

Mavacamten (MAVA), Blebbistatin (BLEB), and Omecamtiv mecarbil (OM) are compounds directly modulating myofilament dynamics with promising effectiveness in treatment of sarcomeric cardiomyopathies. MAVA is an allosteric inhibitor of cardiac myosin ATPase with a negative inotropic effect and demonstrating efficacy in R403Q HCM clinical trials (Green et al., 2016; Santini et al., 2020). BLEB, a well characterized ATPase inhibitor, alters the Ca^{2+} sensitivity of the myofilament and has been widely used in trials (Kampourakis et al., 2018; Rahman et al., 2018; Wang et al., 2018; Gyimesi et al., 2021). OM is a recently developed myosin ATPase activator with a positive inotropic effect enhancing cardiac contractility (Tsukamoto, 2019).

The mechanisms of action of these drugs and their effects on cardiomyocyte electro-mechano-energetics are still to be fully known and under active research (Tsukamoto, 2019; Santini et al., 2020). Accordingly, computational studies on the effects of these drugs are mostly lacking. Focusing on R403Q HCM mutation, Margara et al. (2021) investigated the efficacy of MAVA, simulating the tension- Ca^{2+} relationship and active tension curves. They hypothesized that the impaired tension relaxation phase is caused by feedback from crossbridge (XB) cycling to the thin filament. Although this assumption results in consistent simulated impaired tension relaxation, the proposed MAVA mechanism of action coupled with a lack of a metabolite-sensitive mechanism in the contractile element (CE) urged us to investigate further the cause of this impairment. On the other hand, *in silico* models have been employed to probe the effect of BLEB beside animal muscle fibre experiments (Rahman et al., 2018), highlighting the role of BLEB in shifting the rate-limiting momentum from weakly to strongly bound states in XB cycling (Rahman et al., 2018). Finally, as an ion channel study, the effect of OM has been simulated using an *in silico* model of human ventricular action potential (AP) focusing on pro-arrhythmic assessments (Qu et al., 2021). Of note, Qu et al. report an IC_{50} of

125.5 μM highlighting the significance of OM influence on the CE in 1–10 μM of OM compared with channel blocking formalism (Qu et al., 2021). In summary, to the best of our knowledge, no computational study has reported experimentally validated drug-induced Ca^{2+} sensitivity, ATPase dynamics, and dose-dependent effect of MAVA, BLEB, and OM on the tension- Ca^{2+} relationship, regarding the HCM pathophysiology. This coupled with the facts that these compounds are essentially myosin ATPase activators/inhibitors necessitate studying the drug effects using advanced metabolite-sensitive models. In addition, HCM mutations misregulate sarcomere function and cardiac energy consumption (van der Velden et al., 2018). This further highlights the need for a model that enables capturing the electro-mechano-energetics in pathophysiological investigations.

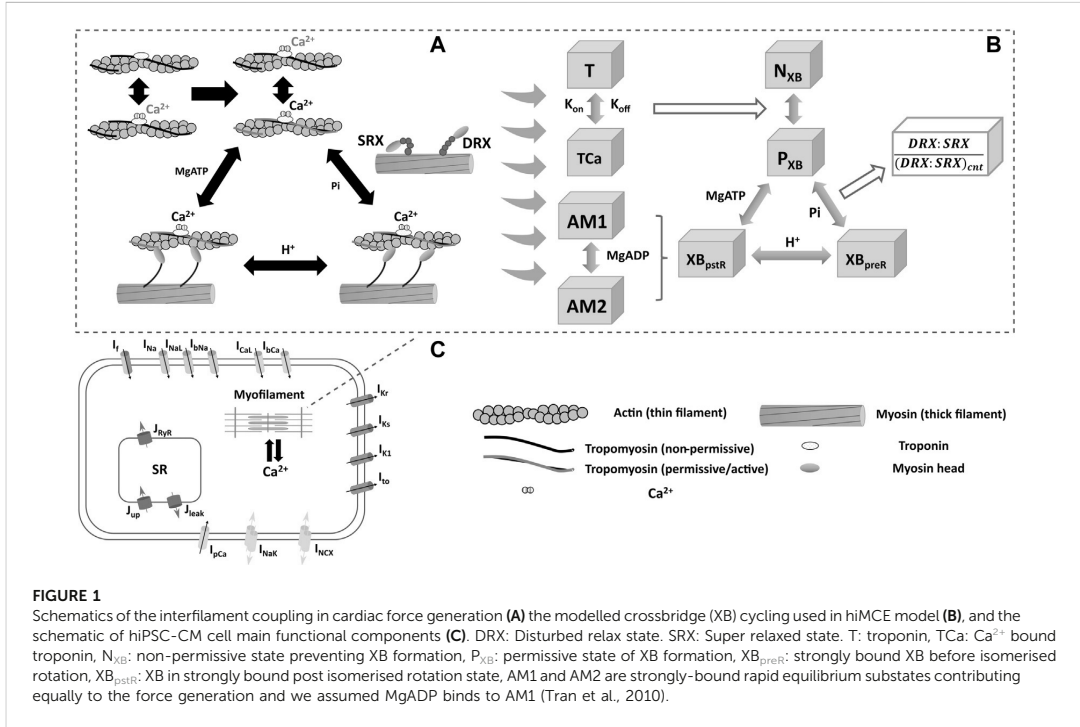
Here, we investigate the pathophysiology of HCM R403Q myosin mutation using a computational metabolite-sensitive model of hiPSC-CMs electromechanics developed based on ordinary differential equations (ODEs). This model, named hiMCE, is an update of our previous model of hiPSC-CM electromechanics (Forouzandehmehr et al., 2021) capturing ATPase activity and accounting for metabolite-sensitive kinetics (Figure 1) in the XB cycling and extending the capacity of models of the molecular mechanism of contraction and the drug effect predictions. The drugs studied here are modulators of myofilament dynamics, we reparametrized the CE of the model using available experimental data and presented novel mechanistic methods to simulate the effect of MAVA, OM, and BLEB on the Ca^{2+} sensitivity, contractility, and energetics of the hiPSC-CMs.

Methods

Extension to a metabolite-sensitive contractile element

We previously integrated a reparametrized mathematical model of the CE by Rice et al. (2008) with a new passive force handling into the hiPSC-CM model of electrophysiology by Paci et al. (2020) and studied the inotropic effect of different compounds (Forouzandehmehr et al., 2021). Based on (Rice et al. (2008) CE, Tran et al. (2017) introduced a mathematical model of a CE that incorporated metabolic-sensitivity. This was achieved by extending the model by Rice et al. (2008), with new parameters that account for the competitive binding of metabolic protons (H^+) to the binding sites of Ca^{2+} on troponin C, and incorporates the binding kinetics of MgADP in the XB cycling (Figure 1). The extended mechanistic description divides the strongly bound state post isomerized rotation (XB_{pstr}) into two substates in rapid equilibrium, AM1 and AM2, to capture MgADP binding kinetics in the XBs (Figure 1).

The thermodynamically constrained model of XB kinetics and Ca^{2+} activation is divided into four states including a non-permissive



(N_{XB}), a permissive (P_{XB}), a pre power stroke state (XB_{preR}), and a post power stroke state (XB_{pstR}) (Figure 1) (Tran et al., 2017). XB_{preR} and XB_{pstR} states both denote the state of strongly bound myosin heads to the actins (Rice et al., 2008; Tran et al., 2017). In diastole, XBs are in N_{XB} state and when activated by Ca²⁺ XBs enter P_{XB} state where they can participate in the binding and unbinding of myosin heads and processes of tension generation (Figure 1) (Tran et al., 2017). The active tension produced as the result of the process is equal to the product of myosin head strain and strongly bound states fractional occupancy (Tran et al., 2017).

In the present work, we have taken this metabolite-sensitive CE model proposed by Tran et al. (2017), and modified it to incorporate active contraction mechanisms integrated with the Paci2020 model of hiPSC-CMs electrophysiology (Paci et al., 2020). This extended CE model was manually tuned using the information from a previous sensitivity analysis of the contractile machinery (Forouzandehmehr et al., 2021) (Table 1). We calibrated the model to capture the AP, CaT, and contractile experimental biomarkers measured in hiPSC-CMs in control conditions, listed in Table 6.

This calibrated control/healthy model variant was then modified to describe an HCM mutation and the effect of pharmaceutical mechanical modulators, and in sections 2.2 and 2.3, we explain the tuning of the relevant CE parameters for each scenario. To enlighten

the role of these parameters, we describe the XB kinetics (Tran et al., 2010) as follows in relation to Figure 1:

$$\frac{d}{dt}P_{XB} = k_{npt} \times N_{XB} + ap3 \times XB_{pstR} + am1 \times XB_{preR} - (k_{pnt} + ap1 + am3) \times P_{XB} \tag{1}$$

$$\frac{d}{dt}XB_{preR} = ap1 \times F1 \times P_{XB} - am1 \times F2 \times XB_{preR} - ap2 \times XB_{preR} + am2 \times XB_{pstR} \tag{2}$$

$$\frac{d}{dt}XB_{pstR} = am3 \times P_{XB} + ap2 \times XB_{preR} - (am2 + ap3) \times XB_{pstR} \tag{3}$$

$$N_{XB} = 1 - (P_{XB} + XB_{preR} + XB_{pstR}) \tag{4}$$

where k_{npt} and k_{pnt} are transition rates between N_{XB} and P_{XB} and responsible for XB cycling activation (Rice et al., 2008). $am1$ takes into account the Pi-dependent transition rate in the XB and has been defined in (Tran et al., 2010). $ap1$ is equal to the attachment rate to XB_{preR} (Tran et al., 2010) which is given as:

$$f_{ap} \times xbmodsp \times Qf_{ap}^{((T_{mpc}-37)/10)} \tag{5}$$

TABLE 1 The values of the contractile element parameters for hiPSC-CM-CE (Forouzandehmehr et al., 2021) and hiMCE. F1 and F2 represent DRX:SRX/(DRX:SRX)_{control} ratio in the XB cycling. K_{onR} , K_{np} and K_{off} are rate constants for Ca^{2+} binding to troponin, the forward and backward transition rates between Pxb and Nxb states, respectively (Rice et al., 2008). n_{perm} and $perm_{50}$ denote the Hill coefficient and the half-activation constant, respectively, describing the nonlinearity of the cooperativity in Ca^{2+} activation of XBs (Rice et al., 2008). K_{offL} and K_{offH} represent the rate constants affecting Ca^{2+} unbinding from low and high affinity sites on troponin, respectively (Rice et al., 2008). M denotes the mass term in the model of sarcomere by Rice et al. (Rice et al., 2008). K_{xb} represents the tension scaler detailed in (Forouzandehmehr et al., 2021). $Xbmodsp$ is a species-dependent XB cycling rate scaler (Rice et al., 2008). h_f denotes the rate constant in the forward transition between XB_{preR} and XB_{pstR} (Rice et al., 2008).

#	Parameter	hiPSC-CM-CE	hiMCE (control mode)
1	F1	1	1
2	F2	1	1
3	K_{on} ($s^{-1} mM^{-1}$)	62.5×10^3	62.5×10^3
4	K_{offL} (s^{-1})	200	200
5	K_{offH} (s^{-1})	25	25
6	$perm_{50}$	0.6	0.6
7	n_{perm}	11.28	11.55
8	K_{np} (s^{-1})	550	550
9	K_{ps} (s^{-1})	50	50
10	K_{offmod}	0.5	0.5
11	m ($s^2 \mu m^{-1}$)	2×10^{-5}	2×10^{-5}
12	k_{xb}	12	13.1
14	$xbmodsp$	0.2	0.2
15	h_f (s^{-1})	2000	2000

TABLE 2 The parameter used in the HCM model variant. Pi_{ref} denotes the reference value for inorganic phosphate (Pi) in the simulations. $ap2$ is a variable influencing detachment of crossbridges. F1 and F2 are coefficients affecting pre-rotational states in XB cycling as also used in (Margara et al., 2021).

#	Parameter	Control value	Value in HCM model variant
1	Pi_{ref} (mM)	2	18.9
2	MgADP (mM)	36×10^{-3}	72×10^{-3}
3	$ap2$ coef	1	0.315
4	F1	1	1.3
5	F2	1	1.3

f_{ap} value is set to $500 s^{-1}$ and Qf_{ap} is the temperature-dependence set to 6.25 (Rice et al., 2008), in this work. $xbmodsp$ (species-dependent XB cycling rate scaler (Rice et al., 2008)) value is given in Table 1. $am3$ denotes a thermodynamically constrained transition rate from P_{XB} to XB_{pstR} state accounting for MgATP release when the myosin heads transit from weakly to

TABLE 3 Modifications to the model parameters to simulate the effect of Mavacamten. A, B, C, D, and E are coefficients in Eqs 15–19 affecting P_{XB} - XB_{preR} regulation, Pi-dependent transition in P_{XB} - XB_{preR} , XB_{preR} - XB_{postR} regulation, Proton-dependent transition in XB_{postR} - XB_{preR} , and MgATP-dependent transition from XB_{postR} - P_{XB} , respectively. BL is the baseline value given in Table 1. Default values of A-E, $ap1$ and $ap3$ coefs., F1 and F2 are equal to 1.

#	Parameter	Values in 0.5 μM MAVA
1	K_{on} ($mM^{-1} s^{-1}$)	BL \times 1.048
2	n_{perm}	BL \times 0.688
3	A	0.26
4	B	0.4
5	C	5.4
6	D	0.4
7	E	2.39
8	$ap1$ coef	1.45
9	$ap3$ coef	0.28
10	F1	0.1
11	F2	0.1

TABLE 4 The modifications to the parameters to simulate the effects of BLEB and OM. BL: Baseline values of hiMCE model given in Table 1.

#	Parameter	Modifications for 5 μM BLEB	Modifications for 1 μM OM
1	F1	5.015	4.1
2	F2	0.1	0.1
3	Tropreg coef	0.2	0.2
4	$ap2$ coef	0.012	0.02
5	$ap3$ coef	0.03	0.03
6	$am2$ coef	0.25	0.15
7	K_{on} ($mM^{-1} s^{-1}$)	-	BL \times 1.28
8	n_{perm}	-	BL \times 1.182
9	$perm_{50}$	BL \times 1.33	BL \times 1.33
10	K_{ps} (s^{-1})	-	BL \times 0.2
11	K_{np} (s^{-1})	-	BL \times 1.182
12	K_{offmod}	-	BL \times 0.52
13	K_{offL} (s^{-1})	-	BL \times 1.75
14	K_{offH} (s^{-1})	-	BL \times 0.6
15	h_f (s^{-1})	-	BL \times 2

strongly attached XB states detailed in (Tran et al., 2010). $ap3$ is the MgADP and MgATP-sensitive transition rate from XB_{pstR} to P_{XB} (Tran et al., 2010) and is calculated as:

$$ap3 = [MgATP] \times g_{xbt} \times \left(\frac{k_{dADP} + MgADP^*}{k_{dADP} + [MgADP]} \right) \quad (6)$$

Where $MgADP^*$ denotes the reference (physiological) concentration of MgADP of $36 \mu M$ and k_{dADP} is the MgADP

TABLE 5 The experimental data used for calibration of the model and validation of the simulated results.

Type	Experiment	Cell/tissue type	Observation	Figure/ Table	Preparation data
Calibration	Toefer et al. (2020)	hiPSC-CMs	33% increase of tension relaxation in R403Q Corrected tension relaxation due to MAVA in R403Q	Figure 3C	hiPSC-CM cell lines at day 30 post-differentiation
	(Green et al. (2016); Toefer et al. (2020))	hiPSC-CMs, Murine	The fractional cell shortening in R403Q	Figure 3F	
	(Green et al. (2016); Awinda et al. (2020))	Murine, Human	Reduction in fractional cell shortening due to MAVA	Figure 3F	hiPSC-CM cell lines at day 30 post-differentiation, isolated adult rat ventricular cardiomyocytes treated with increasing concentrations of MAVA
	Kampourakis et al. (2018)	Rat	Reduction in maximum tension due to MAVA Change in pCa50, Hill coefficient, and maximum tension due to OM and BLEB OM and BLEB dose-dependent contractile response	Figure 3C Table 7 and Figure 4A Figures 4D,E	Isolated adult rat ventricular cardiomyocytes, skinned human myocardial strips Demembrated rat ventricular trabeculae
Validation	Sewanani et al. (2019)	hiPSC-CMs	The unaffected CaT in R403Q	Figure 3B	Engineered heart tissues made of hiPSC-CMs on decellularized porcine left ventricular tissue blocks
	(Nag et al. (2015); Sarkar et al. (2020))	Human, hiPSC-CMs	Negligible change in ATPase in R403Q	Figure 3D	Human β -cardiac myosin
	Green et al. (2016)	Murine	Unchanged CaT and pCa ₅₀ in Tension-pCa curve due to MAVA	Figure 3B, Fig. S1	Isolated adult rat ventricular cardiomyocytes
	Rohde et al. (2018) Kawas et al. (2017)	Human, Porcine, Bovine, and Murine	Reduction in ATPase rate due to MAVA	Figure 3D	Human β -cardiac myosin, Porcine and Bovine ventricular myosin, mouse cardiac myofibrils
	Green et al. (2016)				
	Gollapudi et al. (2021)				
	Kawas et al. (2017)	Human & Bovine	Slowed relaxation in ATPase rate due to MAVA	Figure 3D	Human and bovine cardiac myosins
	Szentandrassy et al. (2016)	Canine	Change in APD due to 1 μ M OM	Figure 5A	Left ventricular single canine myocytes
(Bakkehaug et al. (2015); Utter et al. (2015))	Murine Porcine	ATPase basal value increase due to OM	Figure 5B	<i>Ex vivo</i> mouse and <i>in vivo</i> pig hearts	

dissociation constant detailed in (Tran et al., 2010). g'_{XB} denotes a first order rate constant tuned by Tran et al. (2010) to maintain the validity of original Rice CE model (Rice et al., 2008) under physiological metabolic conditions regarding MgADP kinetics detailed in. $am2$ is equal to the transition from XB_{pstR} to XB_{preR} which is proton and MgADP-sensitive (Tran et al., 2010):

$$am2 = h'_{br} \times [H^+] \times \left(\frac{k_{dADP} + MgADP^*}{MgADP^*} \times \frac{[MgATP]}{k_{dADP} + [MgADP]} \right) \tag{7}$$

Again, h'_{br} represents the adjustment of the rate constant affecting the transition between XB_{preR} and XB_{pstR} states to include physiological proton and MgADP dependent effects further detailed in (Tran et al., 2010). Following the method proposed in (Margara et al., 2021), we defined F1 and F2 (Eq. (2)) as modulators of the transition between permissive binding state on actin (P_{XB}) and strongly bound XBs before isomerized rotation

(XB_{preR}). In our model, F1 and F2 represent the $(DRX:SRX)/(DRX:SRX)_{control}$ ratio (=1 in control mode) and indirectly affect the ATPase dynamics (Figure 1). $ap2$ is equal to the forward transition rate between XB_{preR} and XB_{pstR} , which is defined as (Rice et al., 2008):

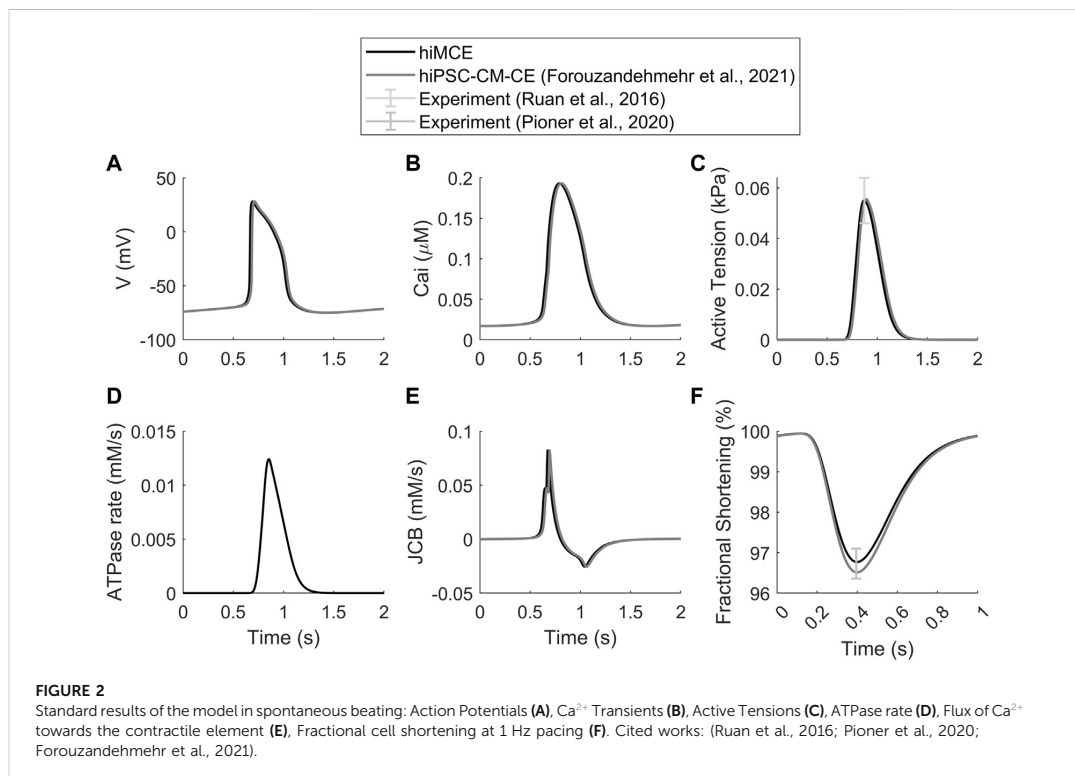
$$h_f \times h_{fmd} \times xbmodsp \times Q_{hf}^{((T_{mpc}-37)/10)} \tag{8}$$

$$h_{fmd} = e^{\left(-sign(xXB_{preR}) \times hfmdc \times \left(\frac{xXB_{preR}}{x_0} \right)^2 \right)} \tag{9}$$

The value for h_f is given in Table 1. Q_{hf} represents the temperature dependence, here set to 6.25. h_{fmd} incorporates strain dependence into the forward transition rate, h_{fT} . $hfmdc$ is set to five and specifies the extent to which the isomerization rate is influenced by the mean strain of XB_{preR} (xXB_{preR}). x_0 is the mean strain (distortion) of XB_{pstR} state when the net motion between actin and myosin filaments is absent. Here, x_0 is set to 0.007 μ m.

TABLE 6 Action potential (AP), Ca²⁺ transients (CaT), and active tension (AT) calculated biomarkers in spontaneous condition and their comparison with Paci2020 and hiPSC-CM-CE model (i.e. no metabolite-sensitive CE) and the experimental values (Paci et al., 2018; Paci et al., 2020). APA: AP amplitude, MDP: maximum diastolic potential, CL: cycle length, dV/dt max: maximum upstroke velocity, APD₁₀ and APD₃₀ and APD₉₀: AP duration at 10, 30, 90% of repolarization, respectively, AP Tri: AP triangulation index. The simulated biomarkers of CaT are DURATION: duration of the transient, tRise_{10, peak}: time to peak, tRise_{10, 50} and tRise_{10, 90}: rise time from 10 to 50% and 90% of maximum threshold, respectively, and tDecay_{90, 10}: decay time from 90 to 10%. AT: Active tension, RT₅₀: time from peak contraction to 50% of relaxation, %FS: percent of fractional shortening. The experimental ranges for contraction biomarkers are from (Forouzandehmehr et al., 2021). The third column is taken directly from the original Paci2020 publication (Paci et al., 2020).

No.	Biomarker	Paci2020	hiPSC-CM-CE	hiMCE	Exp. Value (Mean ± SD)
1	APA (mV)	102	103	103	104 ± 6
2	MDP (mV)	-74.9	-75.0	-75.0	-75.6 ± 6.6
3	AP CL (ms)	1712	1644	1644	1700 ± 548
4	dV/dt max (V/s)	20.5	23.9	24.0	27.8 ± 26.3
5	APD10 (ms)	87.0	95.0	95.1	74.1 ± 26.3
6	APD30 (ms)	224	238	238	180 ± 59
7	APD90 (ms)	390	403	403	415 ± 119
8	AP Tri	2.8	2.9	3	2.5 ± 1.1
9	CaT DURATION (ms)	691	693	693	805 ± 188
10	CaT tRise10, peak (ms)	184	163	163	270 ± 108
11	CaT tRise10,50 (ms)	54.9	46.2	45.9	82.9 ± 50.5
12	CaT tRise10,90 (ms)	118	102	102	167 ± 70
13	CaT tDecay90,10 (ms)	341	343	343	410 ± 100
14	AT magnitude (kPa)	-	0.055	0.055	0.055 ± 0.009
15	RT50 (ms)	-	161	158	158 ± 12.1
16	%FS	-	3.45	3.23	3.27 ± 0.37



Furthermore, $ap1$ to $ap3$ and $am1$ to $am3$ also affect the time rate of change in the mean strains, Eqs (10), (11), and the steady-state population of strongly bound XB states Eqs (12)–(14) (Tran et al., 2010):

$$\frac{d}{dt}xXB_{preR} = 0.5 \times \frac{dSL}{dt} + \frac{\varphi}{XB_{preR}^{DFract}} \left[- (ap1 \times xXB_{preR}) + am2 \times (xXB_{pstR} - x_0 - xXB_{preR}) \right] \quad (10)$$

$$\frac{d}{dt}xXB_{pstR} = 0.5 \times \frac{dSL}{dt} + \frac{\varphi}{XB_{pstR}^{DFract}} \left[ap2 \times (xXB_{preR} + x_0 - xXB_{pstR}) \right] \quad (11)$$

$$XB_{preR}^{DFract} = \frac{am3 \times am2 + ap3 \times ap1 + am2 \times ap1}{\sum XB^{DFract}} \quad (12)$$

$$XB_{pstR}^{DFract} = \frac{ap1 \times ap2 + am3 \times ap1 + am3 \times ap2}{\sum XB^{DFract}} \quad (13)$$

$$\sum XB^{DFract} = ap1 \times ap2 + am3 \times am1 + am3 \times ap2 + am3 \times am2 + ap3 \times ap1 + am2 \times ap1 + ap2 \times ap3 + am3 \times am1 + ap3 \times am1 \quad (14)$$

Where $\frac{dSL}{dt}$ denotes the sarcomere length velocity and φ represents an empirical scaler equal to 2 (Rice et al., 2008). For the detailed explanation of the metabolite-sensitive XB cycling we refer the readers to (Tran et al., 2010).

The contractile element calibration for HCM model variant

Our baseline CE inherits the main effects of contractile metabolic products such as MgATP, MgADP, inorganic Phosphate (Pi), and H^+ on the tension development mechanism from the original Tran et al. model (Tran et al., 2010; Tran et al., 2017). We used this baseline model to develop an HCM mutant variant (R403Q) model, with altered myofilament kinetics. This model variant was created by modifying specific metabolic parameters to achieve a simulated state consistent with experimental reports of R403Q HCM (Table 2).

To obtain the HCM model variant, we changed F1 and F2 values following (Margará et al., 2021) and in line with the sensitivity test given in Supplementary Figure S4. We also increased the value of MgADP concentration and the reference value of Pi. Finally, we changed the $ap2$ coefficient regarding the model sensitivity given in Supplementary Figure S2.

The contractile element calibration for drug-induced effects

Previously, (Margará et al. (2021) assumed in their computational study that MAVA mainly influences the

transitions between XB_{preR} and P_{XB} states following the DRX: SRX disturbing theory reported in (Toepfer et al., 2020). This was implemented by introducing F1 and F2 (with default values of 1) coefficients (Eq. (2)) representing DRX:SRX ratios to the time-dependent description of XB_{preR} state.

In addition, we simulated the effect of MAVA not only by altering the values of F1 and F2 but also modifying the parameters listed in Table 1 to obtain a comprehensive and accurate simulation of the effect of 0.5 μM MAVA on our HCM R403Q model variant as given in Table 3. These further modifications, done as a manual parameter tuning, are based on the reported effect of MAVA on Ca^{2+} activation and binding process (Awinda et al., 2020), Pi (Alsulami and Marston, 2020), and ATPase activity (Green et al., 2016). Specifically, changes in K_{on} and n_{perm} values have been made regarding the sensitivity analyses given in (Forouzandehmehr et al., 2021). The F1 and F2 values were changed according to model sensitivity behavior given in Supplementary Figure S4. Further, $ap1$ and $ap3$ coefficients and A-E values were obtained by trial and error.

To indicate, A modulates P_{XB} to XB_{preR} transition, B influences Pi-dependent XB_{preR} to P_{XB} transition, C takes effect on XB_{preR} to XB_{pstR} transition, D affects proton-dependent XB_{pstR} to XB_{preR} transition, and E controls MgATP-dependent transition from XB_{pstR} to P_{XB} states. Correspondingly, the proposed modulations (A to E in Table 3) to Eqs (15)–(19), are in line with a disturbed interfilament signaling that affects the force-producing states of XB suggested in the etiology of R403Q (Nag et al., 2015). Our motivation for the A-E coefficient modifications was the role of $xbmodsp$ parameter in contraction relaxation time observed in the sensitivity study before (Forouzandehmehr et al., 2021). As changing $xbmodsp$ solely could not lead to an accurate simulation of impaired relaxation restored by 0.5 μM MAVA, we used A-E values to optimize the distribution of $xbmodsp$ effect on the XB cycling.

$$f_{apt} = f_{ap} \times A \times xbmodsp \times Q_{f_{ap}}^{((T_{mpc}-37)/10)} \quad (15)$$

$$g_{apt} = g_{ap} \times g_{apslmd} \times B \times xbmodsp \times Q_{g_{ap}}^{((T_{mpc}-37)/10)} \quad (16)$$

$$h_{ft} = h_f \times h_fmd \times C \times xbmodsp \times Q_{h_f}^{((T_{mpc}-37)/10)} \quad (17)$$

$$h_{bt} = h_b \times D \times xbmodsp \times Q_{h_b}^{((T_{mpc}-37)/10)} \quad (18)$$

$$g_{xbt} = g_{xb} \times \max(g_{xbmd}, 1) \times E \times xbmodsp \times Q_{g_{xb}}^{((T_{mpc}-37)/10)} \quad (19)$$

Values of thin filament regulation and XB cycling parameters h_b , g_{ap} , g_{apslmd} and temperature dependences Q_{h_b} , $Q_{g_{xb}}$, $Q_{g_{ap}}$ were directly taken from (Rice et al., 2008). Also, g_{xbmd} is a strain-dependent rate modifier defined in (Rice et al., 2008).

The values of parameters changed in the model to simulate the effects of 5 μM BLEB and 1 μM OM are given in Table 4. F1 and F2 values were obtained with attention to sensitivity plots given in Supplementary Figure S4. Similarly, $ap2$ and $am2$

coefficients were found regarding the model behavior shown in Supplementary Figures S2, S3, and S5. Lastly, values of parameters listed in Table 4 rows 7 to 15 were obtained manually according to the sensitivity reports given in (Forouzandehmehr et al., 2021).

Moreover, to capture the dose-dependent effect of BLEB and OM on the normalized tension, based on model sensitivity tests (Supplementary Figures S2–S5) and previous sensitivity analyses (Forouzandehmehr et al., 2021), we identified the main variable of the CE governing the maximum developed tension, $ap2$, and identified coefficient values accordingly (Supplementary Tables S1 and S2). Supplementary Figures S2–S5 show the sensitivity of tension- Ca^{2+} relationships, active tensions, and ATPase rates to $ap2$, $am2$, and R ($=F1 = F2$) coefficients. Our HCM and drug-induced calibrations are unique sets obtained from an informed manual tuning, with e.g., 10%, 20%, 50% increments, started with a first guess within assumed boundaries (e.g., 1/100 to 5.4 times of baseline values). The examples of the results showing the increments and the model response are given in Supplementary Figures S2–S5. Overall, these sensitivity analyses combined with our previous sensitivity investigations on the CE of our previous model (Forouzandehmehr et al., 2021) were the basis of the informed manual parameter tunings done to obtain HCM- and drug-induced calibrations in this work.

The experimental data for calibrations and validations

Table 5 gives the experimental data using which the results of this work have been calibrated and validated.

Results

The metabolite-sensitive model of hiPSC-CMs

All the equations were solved using ode15s integrator of MATLAB with a maximum step size of 10^{-3} and an initial step size of 2×10^{-5} . To reach the steady state, the results were obtained after 800 beats paced at 1 Hz unless otherwise mentioned.

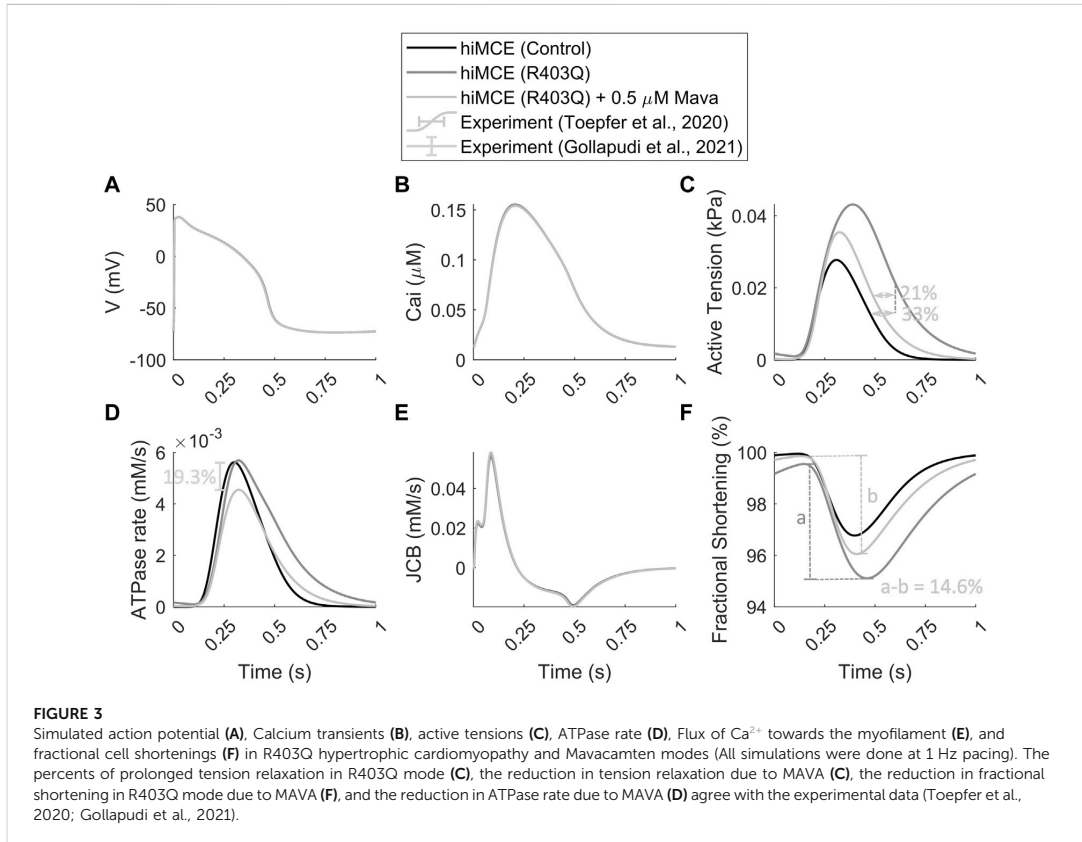
First, we show that our computational model can correctly simulate the main AP, Ca^{2+} transients (CaTs), and active tension (AT) biomarkers as had been simulated by our previous electromechanical hiPSC-CM-CE model (Forouzandehmehr et al., 2021). As Table 6 shows, our new metabolite-sensitive hiMCE model is able to simulate the main biomarkers within the experimental ranges in the validation datasets. The increased thermodynamic detail of the CE did not significantly alter the biomarker values

compared to our previous reparameterization (Forouzandehmehr et al., 2021) and the original Paci et al. hiPSC-CM model (Paci et al., 2020). Also, Figure 2 shows the contractility characteristics simulated using the hiMCE model are consistent with the previously validated results, while also illustrating selected fundamental outputs (Ruan et al., 2016; Pioner et al., 2020).

Hypercontractility in R403Q HCM and mavacamten

In order to simulate the abnormal prolonged relaxation in the developed active tension due to R403Q HCM mutation, Margara et al. (2021) hypothesized a feedback from XB cycling to the thin filament activation. To investigate further, using the parameter values in Table 2 and consistent with the metabolic data detailed in section 2.2, we simulated the active tension and ATPase rate in R403Q HCM model variant. The CaT morphology remains unchanged in the HCM R403Q mode (Figure 3B), consistently with experimental data reported for hiPSC-CMs in (Sewanan et al., 2019). Interestingly, the results in Figure 3C suggest that including energetics in the CE reacts to the pathological changes due to HCM and can correctly predict the prolonged relaxation in the developed active tension (~33%), consistently with *in vitro* hiPSC-CMs data (Toepfer et al., 2020). Moreover, the increased fractional cell shortening (~40%) due to the R403Q mutation is consistent with experimental measurements in (Toepfer et al., 2020). Of note, the model also correctly predicts the negligible change in the ATPase activity (Figure 3D), consistently with the experimental data (Table 5) (Nag et al., 2015; Sarkar et al., 2020).

To simulate the electro-mechano-energetic effect of $0.5 \mu\text{M}$ MAVA, we used the model calibration values listed in Table 3. We have assumed that MAVA would shift the elevated metabolites in the HCM model variant, Pi and MgADP, towards their baseline values. Our model could accurately predict the unaffected CaTs due to MAVA as reported experimentally earlier (Green et al., 2016). Further, the order of reduction in the simulated ATPase rate (19.3%) due to $0.5 \mu\text{M}$ MAVA, Figures 3D, 3is within the reduction range, 17.9–28.5%, reported in previous experimental ATPase activity measurements (Gollapudi et al., 2021). Also, the model consistently predicts the reduction in the relaxation phase in the ATPase rate (Figure 3D) (Kawas et al., 2017). Notably, our simulations quantitatively capture the reduction in the fractional cell shortening and prolonged tension relaxation due to R403Q mutated hiPSC-CMs after $0.5 \mu\text{M}$ MAVA (14.6% and 20.9%, respectively), consistently with recent experimental measurements (Toepfer et al., 2020). Finally as shown in



Supplementary Figure S1, the CE model accurately predicts the unchanged pCa_{50} in the tension- Ca^{2+} relationship consistent with the experimental data for $0.5 \mu\text{M}$ MAVA (Green et al., 2016).

Simulated effects of omecamtiv mecarbil and blebbistatin

Using the CE parameter values listed in Table 4, we simulated the effect of $5 \mu\text{M}$ BLEB and $1 \mu\text{M}$ OM. As Table 7 shows, the drug-induced calibration of the hiMCE model results in accurate predictions of Ca^{2+} sensitive effects of $5 \mu\text{M}$ BLEB and $1 \mu\text{M}$ OM consistent with experimental data (Kampourakis et al., 2018) as also Figure 4A qualitatively confirms. Additionally, the selected values for the coefficients of the tension governing variables in the CE, ap_{2s} (Figures 4B,C and Supplementary Tables S1, S2), leads to the correct dose-dependent prediction for BLEB and OM (Figures 4D,E)

and the expected inverse Hill curves reported experimentally (Kampourakis et al., 2018).

Moreover, our model predicts an insignificant reduction in AP duration (3.4%) due to $1 \mu\text{M}$ OM (Figure 5A), evaluated by calculating APD_{90} values (Figure 5A). This translates to 17 ms reduction in APD_{90} (502–485 ms) which is consistent with the order of APD_{90} reduction due to $1 \mu\text{M}$ OM, 12.2 ms, reported for canine cardiomyocytes at 1 Hz pacing (Szentandrassy et al., 2016). Also, the simulated increase in the basal ATPase rate due to $1 \mu\text{M}$ OM (Figure 5H) is qualitatively consistent with the experimental data reported before (Bakkehaug et al., 2015; Utter et al., 2015).

Our model predicts a 23% increase in the amplitude of the Ca^{2+} flux towards the myofilament, JCB (Figure 5B). The subsequent accumulation of intracellular Ca^{2+} is seen as a 4.5% increase in CaT peak (Figure 5E). Interestingly, the steady-state alterations in sarcolemmal Ca^{2+} transport are very subtle: virtually unchanged I_{CaL} (Figure 5C) and only very slightly increased I_{pCa} (Figure 5F). Whereas there is a

TABLE 7 Experimental data (Kampourakis et al., 2018) and hiMCE results due to the effect of 1 μM OM and 5 μM BLEB. pCa_{50} represents the $-\log$ of the Ca^{2+} concentration associated with 50% of maximum tension. cTnC-E: data from cardiac troponin C (cTnC) E-helix obtained by a rhodamine probe. cRLC-E: Data from a probe connected to the myosin regulatory light chain (RLC).

#	Item	Kampourakis et al., 2018	Hi-MCE model (%)
1	Increase in pCa_{50} due to 1 μM OM	5.4–6.9% (cRLC-E) 3.8–6.4% (cTnC-E)	5.8
2	Decrease in pCa_{50} due to 5 μM BLEB	2.1–5.5% (cRLC-E) 2.6–5.7% (cTnC-E)	4.8
3	Reduction of Hill coef. Due to 1 μM OM	53.2–64.5% (cRLC-E) 57.1–68.1% (cTnC-E)	58.9
4	Reduction of Hill coef. Due to 5 μM BLEB	59.5–73.5% (cRLC-E) 44.8–58.3% (cTnC-E)	49.9
5	Reduction in max tension due to 1 μM OM	0–29% (cRLC-E) 18–47% (cTnC-E)	25.3
6	Reduction in max tension due to 5 μM BLEB	66–90% (cRLC-E) 64–80% (cTnC-E)	76.4

more substantial 17% increase in the amplitude of the I_{NCX} (Figure 5D). The enhanced reverse mode of I_{NCX} causes accumulation of intracellular Na^+ (7.04 vs. 7.43 mM) that promotes a stronger repolarizing I_{NaK} (Figure 5G). This appears to be the mechanism that causes the subtle yet visible 3.4% decrease in the AP duration (Figure 5A), consistently with the reported experiments suggesting OM as a safe compound on cardiac electrophysiology in clinically tolerated doses (Szentandrássy et al., 2016). These predictions can be insightful regarding the consequences of the disturbed interfilament signaling that OM elicits in the XBs.

Discussion

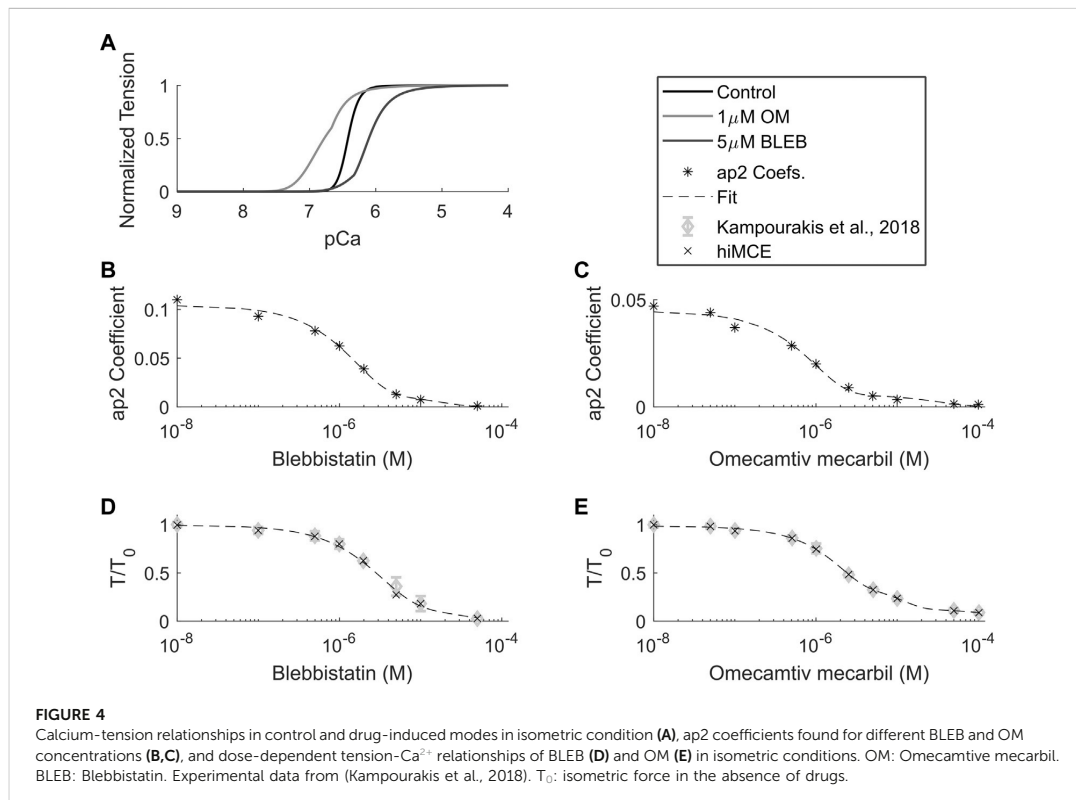
HCM and energetics of contraction

Cardiomyocytes, with no self-renewal capacity, must provide two billion beats during an average lifetime for which the cardiac muscle requires a significant amount of energy, 6 kg of ATP per day (Ingwall, 2002). This energy consumption is predominantly due to the function of sarcomeres in contraction. Therefore, the pathological conditions directly caused by sarcomeric mutations, such as R403Q HCM, necessitate studying contractile function of cardiomyocytes regarding cardiac metabolism. Our analysis demonstrates that the incorporated scheme of the metabolite-sensitive CE is able to capture the impaired (prolonged) tension relaxation, $\sim 33\%$, due to the R403Q mutation. Interestingly, with the energetics included, the additional feedback from XB cycling to the thin filaments, proposed previously by Margara et al. (2021), was not necessary to replicate the altered relaxation. This further highlights the

importance of considering (patho)physiologically constrained metabolite-sensitive computational models in the investigation of sarcomeric cardiomyopathies.

HCM and drug-induced model calibrations

Contractile energetics become highly important when studying promising drugs reported in HCM clinical trials such as MAVA, BLEB, and OM. As our results show, the quantitatively valid simulation of the effect of MAVA, BLEB, and OM, in single dose or dose-dependently, could not be done without the calibration of parameters in the CE that directly or indirectly affect the energetics (Tables 3, 4, S1, and S2). Markedly, one of the important insights of this study stems from the parameters involved in the calibration of the model for the simulation of 0.5 μM MAVA. We took the MAVA modeling one step further by calibrating the CE altering parameters affecting Pi-dependent transition between permissive binding state on actin (P_{XB}) and the strongly bound XBs before isomerized rotation (XB_{preR}) state. Also, we modulated Ca^{2+} binding and sensitivity of the CE, and MgATP-dependent transitions between P_{XB} and XBs in strongly bound post isomerized rotation state (XB_{postR}) in accord with experimental metabolic reports (Green et al., 2016; Alsulami and Marston, 2020; Awinda et al., 2020). Towards decoding the precise drug mechanism of action, the modulations proposed here to explain the effect of MAVA (Table 3) implies that, alongside altering the disturbed DRX:SRX ratio, MAVA might also induce a new interfilament equilibrium, modulating tension-producing and energetic terms that explicitly affect the reverse transition at play between XB_{preR} and XB_{postR} affecting the strain-dependent isomerization of myosin heads. This possible



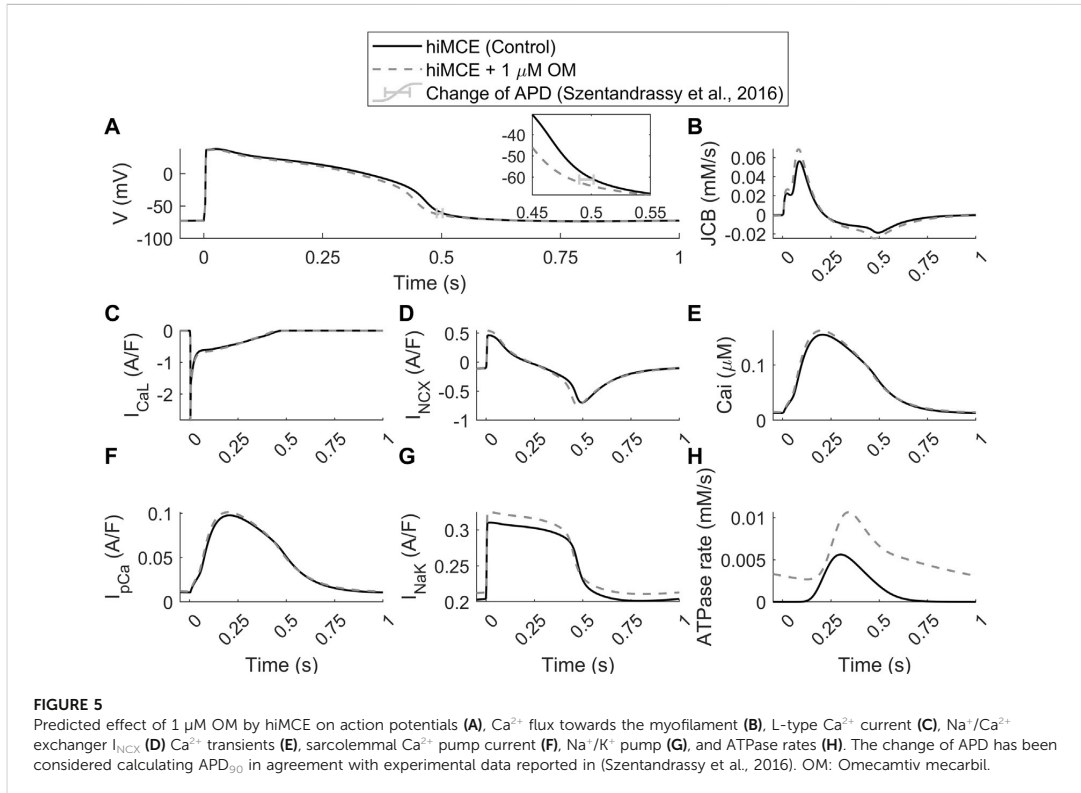
pharmacological insight emerging from our model is interesting as MAVA mechanism of action inherently shifts the R403Q impaired metabolism towards normal regulation and this involves the impaired proton-dependent transition in R403Q mode (Toepfer et al., 2020).

The drug- and HCM-related calibrations presented in this work are in line with the proposed OM and BLEB structure-function relationships detailed in (Kampourakis et al., 2018). To enumerate, Kampourakis et al. (2018) have implied that OM-bound myosin heads relocate the tropomyosin to its on state when binding to actin in the absence of Ca^{2+} bound to troponin. Importantly, the XB activation, which is due to the effect of OM, has been significantly attributed to the stabilizing of the ON state of thick filaments. Further, these stabilized ON positions in thick filaments have been considered to promote an ON thin filament state through preventing tropomyosin returning to their off positions. This has been translated in our model by modifying k_{off} constants which are the rate constants affecting Ca^{2+} unbinding from low and high affinity sites on troponin. These transition rates affect regulatory sites on

cardiac troponin leading to activation of XB cycle (Tran et al., 2010).

On the other hand, at intermediate Ca^{2+} in the physiological range (pCa nine to 4.3), OM activates actins along with the thick filaments. In our model, this has been translated by modifying K_{on} , K_{np} and K_{pn} rate constants for Ca^{2+} binding to troponin, forward and backward transition rates between P_{xb} and N_{xb} states, respectively (Table 4). Further, the constant rates directly affecting Ca^{2+} bound troponin thin filaments regulation induced by Ca^{2+} bound troponin (K_{on} , n_{perm} , k_{offL} , k_{offH} , k_{pn} , k_{np} , and k_{offmode}) have only been calibrated towards activation for OM and they are missing in BLEB calibration as BLEB does not switch both filaments to their ON states (Kampourakis et al., 2018). Further, modification of coefficient of Troprog variable, the fraction of actins with Ca^{2+} bound, detailed in (Rice et al., 2008), in both OM and BLEB calibrations is consistent with the reported effect of these drugs as both OM and BLEB generally decrease the Ca^{2+} activation co-operativity (Kampourakis et al., 2018).

In the HCM variant model, the significant increase in Pi concentration is consistent with the experimental metabolic



reports of HCM R403Q and R92Q mutations in animal mouse models (Spindler et al., 1998; Abraham et al., 2013). Moreover, the impaired coronary perfusion due to HCM has been related to an abnormal energy reproduction that contributes to elevation of ADP and Pi (Sequeira et al., 2019), which is also consistent with conservation of phosphate and creatin reaction (Tran et al., 2010). Congruently, the HCM mutation-induced alterations in myofilament kinetics lead to increase in ADP-mediated products (van der Velden et al., 2018). Therefore, we increased the MgADP concentration within physiological ranges (Tran et al., 2010). Notably, the Ca^{2+} dependence in the activation of myofilaments for HCM and dilated cardiomyopathy has been shown to be altered in a similar fashion due to OM and BLEB influence (Spudich, 2014), implying that the etiology of HCM includes a disturbed actomyosin signaling. In addition, the underlying mechanism of HCM-induced hypercontractility, including R403Q HCM, has been explained in light of thick filament structural alterations and the tension generation (Alamo et al., 2017; Nag et al., 2017; Trivedi et al., 2018). Granted that, since with change in *ap2* coefficient (Table 2) the XB cycling machinery could closely capture the HCM behavior (Figure 3), our model

potentially attributes the HCM-induced disturbed interfilament signaling to a distortion-dependent forward transition from XB_{preR} to XB_{pstR} state and the subsequent effect due to population of strongly bound XB states in the steady-state condition. This could imply that the HCM-induced disturbed actomyosin signaling might stem from a misregulated isomerization of myosin heads from pre-rotated to post-rotated force generating state affecting the strain induced in the myosin neck region. Analogically, the same process might explain how OM, BLEB, and Mava contribute to a new interfilament balance, restoring normal XB cycling tension generation. This hypothesis based on our model predictions could be insightful for accelerating the future drug development for sarcomere cardiomyopathies and mutation-specific HCM.

We have introduced a mechanistic solution to incorporate the dose-dependent effect of Blebbistatin and Omecamtiv mecarbil (Figure 4) consistent with experiments (Kampourakis et al., 2018) focusing on *ap2*. Explicitly, the inverse Hill function trend observed in dose-dependent effects of OM and BLEB (Kampourakis et al., 2018) also reflects in the values of *ap2* coefficients obtained for the

studied concentrations (Figures 4B–E). Moreover, changes in F_2 , hf, and ap_2 (Table 4) suggest that OM also favors the rapid detachment of XBs as another contributor to the disturbed actomyosin coupling involved in OM mechanism of action. Furthermore, the accurate simulation of shortened APD due to 1 μ M OM combined with elevated basal ATPase rate values further signifies that inclusion of metabolite-sensitive transitions in the XB cycling of the CE cannot be ignored in precision medicine, especially when simulating the effects of drugs whose main mechanism of action impacts ATPases.

Limitations and future works

The developed mathematical model naturally has some limitations and potentials for advancements in the future studies. Firstly, as we use ODEs instead of computationally expensive PDEs, the cooperative spatial interactions between regulatory proteins and XB action have been approximated with a mean-field technique (Rice et al., 2008). Secondly, we assumed that 0.5 μ M MAVA restores the elevated MgADP and Pi in HCM model variant to their basal values (listed in Table 2). Although this assumption is consistent with MAVA mechanism of action (Green et al., 2016), it is still a simplification. Thirdly, one fundamental limitation of hiPSC-CMs is that they rely on glycolytic metabolism, in contrast to the fatty acid-based metabolism of native human adult ventricular cardiomyocytes. A further source of energetic dissimilarities is the differences between surrounding medium *in vitro* vs. *in vivo* conditions. Given these and as our model does not include energy production process, we consider the metabolic differences out of the scope of this work. As detailed *in vitro* data on hiPSC-CM metabolism emerges, our modeling efforts serve as a solid basis for the next phase of cardiomyocyte models with energy production included.

The structural immaturity and special sarcomere alignment and performance in hiPSC-CMs and its effect on the HCM and drug-induced studies are important. The core of our HCM variant and MAVA calibration is based on hiPSC-CMs *in vitro* data obtained at day 30 post-differentiation, indicating cardiomyocytes maturation (Toepfer et al., 2020). In this work (Toepfer et al., 2020), to validate the hiPSC-CMs finding regarding *in vivo* data, the authors conducted parallel analyses on mouse HCM model and human HCM cardiac tissues. The comparison revealed that each HCM variant (HCM mice and hiPSC-CMs) caused hypercontractility with respect to its WT model (Figure 3 C&I in (Toepfer et al., 2020)). Furthermore, the prolonged contractile relaxation also was observed in mouse cardiomyocytes and hiPSC-CMs (Figures 3D,J in (Toepfer et al., 2020)). In addition, the dose-dependent decrease in

hypercontractility and myosin population in DRX due to MAVA was observed in mouse cardiomyocytes and hiPSC-CMs (Figures 3E,K in (Toepfer et al., 2020)). All in all, Figure 3 in Toepfer et al. (2020) shows that HCM-induced and drug induced effects on hiPSC-CMs are consistent with the corresponding trend observed in mouse WT and R403Q cardiomyocytes variants. Although, our priority in calibration and validation of our results was using hiPSC-CMs *in vitro* data wherever available, all the abovementioned points imply that validation and calibration of HCM and drug-induced results with cell lines other than hiPSC-CMs are still valid and legitimate approaches.

Furthermore, as our computational model is 0D, it does not explicitly account for the disorganization of sarcomeres typical for hiPSC-CMs. This could be an interesting and valuable future direction for HCM computational studies as more experimental data becomes available.

Finally, the model can benefit from the inclusion of a metabolite-sensitive formulation of the intracellular SERCA pump, as a key ATP-dependent transporter. However, as the focus of this work was sarcomeric cardiomyopathies we have considered it out of scope here.

Conclusion

As cardiac precision medicine arises (Niederer et al., 2019; Paci et al., 2021; Forouzandehmehr et al., 2022), the demand for comprehensive computational models capable of performing high throughput pharmacological investigations heightens. This work proposes a novel metabolite-sensitive computational model of hiPSC-CMs electromechanics with demonstrated capacity to simulate sarcomeric cardiomyopathies and the compounds directly affecting the myosin dynamics considering the metabolic pathways. The mechanistic method offered for simulating the effects of HCM and drugs in this work lends insights upon the molecular interactions in contractile function and advance our pathophysiological understanding of the development of future therapeutics for HCM.

Data availability statement

The original contributions presented in the study are included in the article/supplementary material, further inquiries can be directed to the corresponding author.

Author contributions

MF, MP, JK and JH contributed to conception and design of the study. MF performed the simulations and wrote the first draft

of the manuscript. All authors contributed to manuscript revision, read, and approved the submitted version.

Funding

MF was supported by the graduate school of Faculty of Medicine and Health Technology, Tampere University. MP was supported by the Finnish Cultural Foundation (decision 210813) and by Academy of Finland Centre of Excellence in Body-on-Chip Research. JK was supported by Academy of Finland Centre of Excellence in Body-on-Chip Research, Pirkanmaa regional fund of the Finnish Cultural Foundation (grant number 50201322), and Finnish Foundation for Cardiovascular Research (grant number 200101).

Acknowledgments

The authors wish to thank Samuel Wall for very helpful comments during the preparation of this manuscript.

References

- Abraham, M. R., Bottomley, P. A., Dimaano, V. L., Pinheiro, A., Steinberg, A., Traill, T. A., et al. (2013). Creatine kinase adenosine triphosphate and phosphocreatine energy supply in a single kindred of patients with hypertrophic cardiomyopathy. *Am. J. Cardiol.* 112, 861–866. doi:10.1016/j.amjcard.2013.05.017
- Alamo, L., Ware, J. S., Pinto, A., Gillilan, R. E., Seidman, J. G., Seidman, C. E., et al. (2017). Effects of myosin variants on interacting-heads motif explain distinct hypertrophic and dilated cardiomyopathy phenotypes. *Elife* 6, e24634. doi:10.7554/eLife.24634
- Alsulami, K., and Marston, S. (2020). Small molecules acting on myofilaments as treatments for heart and skeletal muscle diseases. *Int. J. Mol. Sci.* 21, 9599. doi:10.3390/ijms21249599
- Awinda, P. O., Bishaw, Y., Watanabe, M., Guglin, M. A., Campbell, K. S., and Tanner, B. C. W. (2020). Effects of mavacamten on Ca²⁺ sensitivity of contraction as sarcomere length varied in human myocardium. *Br. J. Pharmacol.* 177, 5609–5621. doi:10.1111/bph.15271
- Bakkehaug, J. P., Kildal, A. B., Engstad, E. T., Boardman, N., Næshheim, T., Rønning, L., et al. (2015). Myosin activator omecamtiv mecarbil increases myocardial oxygen consumption and impairs cardiac efficiency mediated by resting myosin ATPase activity. *Circ. Heart Fail.* 8, 766–775. doi:10.1161/CIRCHEARTFAILURE.114.002152
- Forouzandehmehr, M., Ghoytasi, I., Shamloo, A., and Ghosi, S. (2022). Particles in coronary circulation: A review on modelling for drug carrier design. *Mat. Des.* 216, 110511. doi:10.1016/j.matdes.2022.110511
- Forouzandehmehr, M., Koivumäki, J. T., Hyttinen, J., and Paci, M. (2021). A mathematical model of hiPSC cardiomyocytes electromechanics. *Physiol. Rep.* 9, e15124. doi:10.14814/phy2.15124
- Gollapudi, S. K., Yu, M., Gan, Q.-F., and Nag, S. (2021). Synthetic thick filaments: A new avenue for better understanding the myosin super-relaxed state in healthy, diseased, and mavacamten-treated cardiac systems. *J. Biol. Chem.* 296, 100114. doi:10.1074/jbc.RA120.016506
- Green, E. M., Wakimoto, H., Anderson, R. L., Evanchik, M. J., Gorham, J. M., Harrison, B. C., et al. (2016). A small-molecule inhibitor of sarcomere contractility suppresses hypertrophic cardiomyopathy in mice. *Science* 351, 617–621. doi:10.1126/science.1243456
- Gyimesi, M., Rauscher, A. Á., Suthar, S. K., Hamow, K. Á., Oravec, K., Lórinz, I., et al. (2021). Improved inhibitory and absorption, distribution, metabolism, excretion, and toxicology (ADMET) properties of blebbistatin derivatives indicate that blebbistatin scaffold is ideal for drug development targeting myosin-2. *J. Pharmacol. Exp. Ther.* 376, 358–373. doi:10.1124/jpet.120.000167
- Ho, C. Y., Day, S. M., Ashley, E. A., Michels, M., Pereira, A. C., Jacoby, D., et al. (2018). Genotype and lifetime burden of disease in hypertrophic cardiomyopathy: Insights from the sarcomeric human cardiomyopathy registry (SHaRe). *Circulation* 138, 1387–1398. doi:10.1161/CIRCULATIONAHA.117.033200
- Ingwall, J. S. (2002). *ATP and the heart*. Boston, MA: Springer US. doi:10.1007/978-1-4615-1093-2
- Kampourakis, T., Zhang, X., Sun, Y.-B., and Irving, M. (2018). Omecamtiv mecarbil and blebbistatin modulate cardiac contractility by perturbing the regulatory state of the myosin filament. *J. Physiol.* 596, 31–46. doi:10.1111/JP275050
- Kawas, R. F., Anderson, R. L., Ingle, S. R. B., Song, Y., Sran, A. S., and Rodriguez, H. M. (2017). A small-molecule modulator of cardiac myosin acts on multiple stages of the myosin chemomechanical cycle. *J. Biol. Chem.* 292, 16571–16577. doi:10.1074/jbc.M117.776815
- Malhotra, A., and Sharma, S. (2017). Ischemic heart disease in women: Not about religion. *Eur. Cardiol.* 12, 8–9. doi:10.15420/ecr.2017.12.1.GE1
- Margara, F., Rodriguez, B., Toepfer, C. N., and Bueno-Orovio, A. (2021). Mavacamten efficacy in mutation-specific hypertrophic cardiomyopathy: an *in silico* approach to inform precision medicine. *Comput. Cardiol.* 2021, 1–4. doi:10.23919/CinC53138.2021.9662736
- Nag, S., Sommes, R. F., Ujfalusi, Z., Combs, A., Langer, S., Sutton, S., et al. (2015). Contractility parameters of human β -cardiac myosin with the hypertrophic cardiomyopathy mutation R403Q show loss of motor function. *Sci. Adv.* 1, e1500511. doi:10.1126/sciadv.1500511
- Nag, S., V Trivedi, D., Sarkar, S. S., Adhikari, A. S., Sunitha, M. S., Sutton, S., et al. (2017). The myosin mesa and the basis of hypercontractility caused by hypertrophic cardiomyopathy mutations. *Nat. Struct. Mol. Biol.* 24, 525–533. doi:10.1038/nsmb.3408
- Niederer, S. A., Lumens, J., and Trayanova, N. A. (2019). Computational models in cardiology. *Nat. Rev. Cardiol.* 16, 100–111. doi:10.1038/s41569-018-0104-y
- Paci, M., Koivumäki, J. T., Lu, H. R., Gallacher, D. J., Passini, E., and Rodriguez, B. (2021). Comparison of the simulated response of three *in silico* human stem cell-derived cardiomyocytes models and *in vitro* data under 15 drug actions. *Front. Pharmacol.* 12, 604713. doi:10.3389/fphar.2021.604713
- Paci, M., Passini, E., Klimas, A., Severi, S., Hyttinen, J., Rodriguez, B., et al. (2020). All-optical electrophysiology refines populations of *in silico* human iPSC-CMs for drug evaluation. *Biophys. J.* 118, 2596–2611. doi:10.1016/j.bpj.2020.03.018
- Paci, M., Pölonen, R. P., Cori, D., Penttinen, K., Aalto-Setälä, K., Severi, S., et al. (2018). Automatic optimization of an *in silico* model of human iPSC derived

Conflict of interest

The authors declare that the research was conducted in the absence of any commercial or financial relationships that could be construed as a potential conflict of interest.

Publisher's note

All claims expressed in this article are solely those of the authors and do not necessarily represent those of their affiliated organizations, or those of the publisher, the editors and the reviewers. Any product that may be evaluated in this article, or claim that may be made by its manufacturer, is not guaranteed or endorsed by the publisher.

Supplementary material

The Supplementary Material for this article can be found online at: <https://www.frontiersin.org/articles/10.3389/fphys.2022.1010786/full#supplementary-material>

- cardiomyocytes recapitulating calcium handling abnormalities. *Front. Physiol.* 9, 709. doi:10.3389/fphys.2018.00709
- Pioner, J. M., Guan, X., Klaiman, J. M., Racca, A. W., Pabon, L., Muskheili, V., et al. (2020). Absence of full-length dystrophin impairs normal maturation and contraction of cardiomyocytes derived from human-induced pluripotent stem cells. *Cardiovasc. Res.* 116, 368–382. doi:10.1093/cvr/cvz109
- Qu, Y., Gao, B., Arimura, Z., Fang, M., and Vargas, H. M. (2021). Comprehensive *in vitro* pro-arrhythmic assays demonstrate that omecamtiv mecarbil has low pro-arrhythmic risk. *Clin. Transl. Sci.* 14, 1600–1610. doi:10.1111/cts.13039
- Rahman, M. A., Ušaj, M., Rassier, D. E., and Månsson, A. (2018). Blebbistatin effects expose hidden secrets in the force-generating cycle of actin and myosin. *Biophys. J.* 115, 386–397. doi:10.1016/j.bpj.2018.05.037
- Rice, J. J., Wang, F., Bers, D. M., and De Tombe, P. P. (2008). Approximate model of cooperative activation and crossbridge cycling in cardiac muscle using ordinary differential equations. *Biophys. J.* 95, 2368–2390. doi:10.1529/biophysj.107.119487
- Rohde, J. A., Roopnarine, O., Thomas, D. D., and Muretta, J. M. (2018). Mavacamten stabilizes an autoinhibited state of two-headed cardiac myosin. *Proc. Natl. Acad. Sci. U. S. A.* 115, E7486–E7494. doi:10.1073/pnas.1720342115
- Ruan, J. L., Tulloch, N. L., Razumova, M. V., Saiget, M., Muskheili, V., Pabon, L., et al. (2016). Mechanical stress conditioning and electrical stimulation promote contractility and force maturation of induced pluripotent stem cell-derived human cardiac tissue. *Circulation* 134, 1557–1567. doi:10.1161/CIRCULATIONAHA.114.014998
- Santini, L., Palandri, C., Nediani, C., Cerbai, E., and Coppini, R. (2020). Modelling genetic diseases for drug development: Hypertrophic cardiomyopathy. *Pharmacol. Res.* 160, 105176. doi:10.1016/j.phrs.2020.105176
- Sarkar, S. S., Trivedi, D. V., Morck, M. M., Adhikari, A. S., Pasha, S. N., Ruppel, K. M., et al. (2020). The hypertrophic cardiomyopathy mutations R403Q and R663H increase the number of myosin heads available to interact with actin. *Sci. Adv.* 6, eax0069. doi:10.1126/sciadv.aax0069
- Schmid, M., and Toepfer, C. N. (2021). Cardiac myosin super relaxation (SRX): a perspective on fundamental biology, human disease and therapeutics. *Biol. Open* 10, bio057646. doi:10.1242/bio.057646
- Semsarian, C., Ingles, J., Maron, M. S., and Maron, B. J. (2015). New perspectives on the prevalence of hypertrophic cardiomyopathy. *J. Am. Coll. Cardiol.* 65, 1249–1254. doi:10.1016/j.jacc.2015.01.019
- Sequeira, V., Bertero, E., and Maack, C. (2019). Energetic drain driving hypertrophic cardiomyopathy. *FEBS Lett.* 593, 1616–1626. doi:10.1002/1873-3468.13496
- Sewanian, L. R., Schwan, J., Kluger, J., Park, J., Jacoby, D. L., Qyang, Y., et al. (2019). Extracellular matrix from hypertrophic myocardium provokes impaired twitch dynamics in healthy cardiomyocytes. *JACC. Basic Transl. Sci.* 4, 495–505. doi:10.1016/j.jacbs.2019.03.004
- Spindler, M., Saupé, K. W., Christe, M. E., Sweeney, H. L., Seidman, C. E., Seidman, J. G., et al. (1998). Diastolic dysfunction and altered energetics in the alphaMHC403/+ mouse model of familial hypertrophic cardiomyopathy. *J. Clin. Invest.* 101, 1775–1783. doi:10.1172/JCI1940
- Spudich, J. A. (2014). Hypertrophic and dilated cardiomyopathy: four decades of basic research on muscle lead to potential therapeutic approaches to these devastating genetic diseases. *Biophys. J.* 106, 1236–1249. doi:10.1016/j.bpj.2014.02.011
- Szentandrassy, N., Horvath, B., Vaczi, K., Kistamas, K., Masuda, L., Magyar, J., et al. (2016). Dose-dependent electrophysiological effects of the myosin activator omecamtiv mecarbil in canine ventricular cardiomyocytes. *J. Physiol. Pharmacol.* 67, 483–489.
- Toepfer, C. N., Garfinkel, A. C., Venturini, G., Wakimoto, H., Repetti, G., Alamo, L., et al. (2020). Myosin sequestration regulates sarcomere function, cardiomyocyte energetics, and metabolism, informing the pathogenesis of hypertrophic cardiomyopathy. *Circulation* 141, 828–842. doi:10.1161/CIRCULATIONAHA.119.042339
- Toepfer, C. N., Wakimoto, H., Garfinkel, A. C., McDonough, B., Liao, D., Jiang, J., et al. (2019). Hypertrophic cardiomyopathy mutations in MYBPC3 dysregulate myosin. *Sci. Transl. Med.* 11, eaat1199. doi:10.1126/scitranslmed.aat1199
- Tran, K., Han, J.-C., Crampin, E. J., Taberner, A. J., and Loiselle, D. S. (2017). Experimental and modelling evidence of shortening heat in cardiac muscle. *J. Physiol.* 595, 6313–6326. doi:10.1113/jp274680
- Tran, K., Smith, N. P., Loiselle, D. S., and Crampin, E. J. (2010). A metabolite-sensitive, thermodynamically constrained model of cardiac cross-bridge cycling: Implications for force development during ischemia. *Biophys. J.* 98, 267–276. doi:10.1016/j.bpj.2009.10.011
- Trivedi, D. V., Adhikari, A. S., Sarkar, S. S., Ruppel, K. M., and Spudich, J. A. (2018). Hypertrophic cardiomyopathy and the myosin mesa: viewing an old disease in a new light. *Biophys. Rev.* 10, 27–48. doi:10.1007/s12551-017-0274-6
- Tsukamoto, O. (2019). Direct sarcomere modulators are promising new treatments for cardiomyopathies. *Int. J. Mol. Sci.* 21, 226. doi:10.3390/ijms21010226
- Utter, M. S., Ryba, D. M., Li, B. H., Wolska, B. M., and Solaro, R. J. (2015). Omecamtiv mecarbil, a cardiac myosin activator, increases Ca²⁺ sensitivity in myofilaments with a dilated cardiomyopathy mutant tropomyosin E54K. *J. Cardiovasc. Pharmacol.* 66, 347–353. doi:10.1097/FJC.0000000000000286
- van der Velden, J., Tocchetti, C. G., Varricchi, G., Bianco, A., Sequeira, V., Hilfiker-Kleiner, D., et al. (2018). Metabolic changes in hypertrophic cardiomyopathies: scientific update from the working group of myocardial function of the European society of cardiology. *Cardiovasc. Res.* 114, 1273–1280. doi:10.1093/cvr/cvy147
- Wang, L., Kim, K., Parikh, S., Cadar, A. G., Bersell, K. R., He, H., et al. (2018). Hypertrophic cardiomyopathy-linked mutation in troponin T causes myofibrillar disarray and pro-arrhythmic action potential changes in human iPSC cardiomyocytes. *J. Mol. Cell. Cardiol.* 114, 320–327. doi:10.1016/j.yjmcc.2017.12.002

MANUSCRIPT IV

An *in silico* model of hiPSC cardiomyocytes mapping the ionic and subcellular crosstalks onto oxygen deprivation and contractile dysfunction in ischemia/reperfusion

Mohamadamin Forouzandehmehr, Michelangelo Paci, Jari Hyttinen, Jussi T. Koivumäki

(Under Review)

